Failure Analysis
of Engineering Structures

Methodology and Case Histories

V. Ramachandran, A.C. Raghuram,
R.V. Krishnan, and S.K. Bhaumik

Failure Analysis and Accident Investigation Group
National Aerospace Laboratories, Bangalore

With contributions from:
T.A. Bhaskaran, C.R. Kannan, M.A. Parameswara, S. Radhakrishnan, K.N. Raju,
R. Rangaraju, B. Dwarakanath Rao, and M.A. Venkataswamy

ASM International®
Materials Park, Ohio 44073-0002
www.asminternational.org

First printing, October 2005

Comments, criticisms, and suggestions are invited, and should be forwarded to ASM International.

Prepared under the direction of the ASM International Technical Books Committee (2004–2005), Yip-Wah Chung, FASM, Chair.

ASM International staff who worked on this project include Scott Henry, Senior Manager of Product and Service Development; Bonnie Sanders, Manager of Production; Madrid Tramble, Senior Production Coordinator, and Kathryn Muldoon, Production Assistant.

Library of Congress Cataloging-in-Publication Data

Failure analysis of engineering structures : methodology and case histories/ V. Ramachandran . . . [et al.] ; with contributions from T.A. Bhaskaran . . . [et al.].
p. cm.
Includes bibliographical references and index.
1. Structural failures. 2. Structural failures—Case studies. 3. Structural analysis (Engineering). 4. Structural analysis (Engineering)—Case studies. I. Ramachandran, V.

ISBN: 0-87170-820-5
SAN: 204-7586
TA656.F32.2005
624.1′71—dc22 2005040979

ASM International®
Materials Park, OH 44073-0002
www.asminternational.org

Printed in the United States of America

Contents

Foreword

By B.R. Pai

Machines and structures have failed in service without warning and with disastrous consequences. Collapse of bridges and buildings, massive splitting of ships and tankers, explosions in chemical factories, in-flight disintegration of aircraft and space vehicles, and other such major disasters have become history. The consequential damages of these mishaps are humanly unforgivable and can never be forgotten by mankind. Needless it is to emphasize the importance of the prompt investigation of these failures in order to ascertain their causes, inform the public, and to take remedial action to prevent their recurrence.

Investigation of service failures and accidents is a formidable, complex, and challenging task, very startling even to start with. In the case of aviation accidents, location of the wreckage itself is a major task, especially if the wreckage is distributed on a mountainous terrain or on the ocean floor. A wreckage distribution map and an inventory of the pieces recovered from the wreckage and their documentation go a long way in reconstruction of the scene just prior to the mishap. The analytical part of the investigation of the damaged structure and its components is a multidisciplinary activity. It demands tremendous responsibility and coordination on the part of the analyst and a thorough knowledge of materials science supplemented with appreciation and application of related engineering disciplines.

Failures are a fact of life. A failure-free system is more a myth than a reality. The engineering profession and the industries aim at design and manufacture of products with the probability of service failure at the absolute minimum. Realizing the significance of failures, especially in aerospace systems, National Aerospace Laboratories nurtured the failure analysis activity from its inception. The Failure Analysis and Accident Investigation Group in the Materials Science Division of this laboratory has been very active in this field for over four decades. Several hundred investigations have been carried out by this group for various organizations, industries, and institutions and remedial actions suggested. The members of this group have assisted in various commissions of inquiry appointed by the government for investigating failures and accidents that took place in India and elsewhere. The feedback received from the clientele has been very satisfying.

Failure Analysis of Engineering Structures: Methodology and Case Histories, by these scientists, is a culmination of years of their experience in the field. The authors have meticulously compiled lots of information on the subject. Chapters in the book cover, inter alia, the common causes of failures with numerous examples; methodology of failure analysis, including some advanced techniques; various mechanisms of failures; and characteristic macroscopic and microscopic features on failed components, which provide significant clues to their causes. Deliberate damage to structures caused by the use of explosives today is a global threat. The authors have provided useful information on the detection and identification of explosive damages. Treatment of this topic with a detailed description of aircraft accidents due to explosive sabotage is exemplary. The authors' sharing of their personal experiences of the investigation of the major aircraft accident to the Boeing 747 aircraft Kanishka of Air India over the Atlantic Ocean is commendable. Keeping in mind that failures and accidents often lead to serious litigations, the authors have also provided a chapter on forensic failure analysis.

Service failure is the ultimate test for the integrity of a machine, though a very expensive and destructive test. It is now a well-known adage that one learns more from failures than from successes. A detailed and faithful account of service failures and accidents and their in-depth analysis provide very valuable lessons for future designers, manufacturers, users, and maintenance personnel. Failure awareness, anticipation of failures and proactive failure analysis form a good part of successful engineering. It is in this context that the study of case histories of failures assume great importance. The authors of this book have thoughtfully added a complete section on case histories.

This book is a good archive of information for failure analysts, practicing engineers, and students of engineering. I compliment the authors for this effort.

B.R. Pai
Director
National Aerospace Laboratories
Bangalore, India
October, 2004

Foreword

By V.S. Arunachalam

Why does a material fail? There can be only four reasons: the material is subject to an environment beyond its design envelope; it is an inappropriate choice for the design and operating conditions; the material, to start with, is defective; or the design itself is wrong. It is vital to know the reasons as component failures can lead to catastrophic accidents causing heavy loss of life and property. Such accidents can slow down or even temporarily stunt the development of new artifacts and systems that appeared so promising. An inappropriate gasket design, of all things, delayed the space shuttle program by many years.

Every failure leaves its own telltale signs in the macrostructure and microstructure of the failed component. It is not always easy to read those signs because the accident could have destroyed the evidence irreversibly, and the failed component itself could present conflicting evidence. In spite of these difficulties, failure analysis has grown to be an important tool in the design and manufacture of engineering parts.

Materials derive their properties from the structure they exhibit, and when they fail, the structure shows that as well. That is why microscopes have become essential tools in failure analysis. Increasing resolution, improved depth of focus, simultaneous chemical analysis at molecular levels, and imaging of imperfections have now become commonplace, thanks to advances in electron, x-ray, and laser optics. Some of the most recent work in hydrogen embrittlement has been made possible because of the availability of sophisticated analytical tools.

Can we simulate a failure in laboratory conditions? Interestingly, an early account of such a simulation where a failure was recreated came out of Nevil Shute's novel, *No Highway* (Amereon Limited, 1988). Since then, the fiction was made real when the Comet aircraft crash was simulated in a specially built water tank. Nowadays, mechanical, physical, and chemical testing of materials and components, in addition to modeling of parts and simulation of components in service, have become commonplace. Thanks to the availability of powerful computers, large computer memory, and impressive processing speeds, computer simulations today provide the verisimilitude of components in service with realistic operating and environmental conditions—all without actually breaking the component. The ubiquitous computer has given us other tools as well, such as fault tree analysis, information, and data mining of past accidents.

Why is the past so important? Psychologists tell us we learn from experience, especially from failures. Every experience adds more information to memory so that our cognitive skills become less bound, and reasoning becomes more logical. That is why we have to document our experiences properly and derive lessons from them. In spite of such efforts, accidents will unfortunately continue to happen because of deliberate acts such as sabotage, or the lessons learned of the past instances have not diffused well, or even for reasons that are beyond our control and past learning. But their numbers will continue to reduce, making our lives safer and property more secure; look at the earthquake-proof structures or the pressure vessels that engineers have built today.

The Bangalore National Aerospace Laboratories (NAL) Failure Analysis Centre has grown to become India's foremost group for this area of analysis. The scientists and engineers working in this group have built a rich repertoire of experiences in failure analysis. The procedures they follow, the techniques they use, and the inferences they draw from the observations make this book a very useful contribution to the study of failure analysis. They have not limited themselves to run-of-the-mill engineering failures, but share their rich and varied experiences in such areas as sabotage with explosives and also litigations that inevitably follow accidents. I have had the privilege of working with the authors of this book and have marveled often at their professional skills and the commitment they brought to their work. ASM International is to be congratulated for publishing this book and thus enabling the NAL group to share their experiences with the global engineering community.

V.S. Arunachalam
Distinguished Service Professor
Carnegie Mellon University, Pittsburgh, PA, and
CSTEP, Bangalore, India

Preface

Service failures of machines and structures without warning have been experienced in many industries with varying degrees of consequential damages. Systematic analysis of such failures has generated a fund of useful information for designers, manufacturers, and users of industrial hardware. With an understanding of failures and their causes, technical remedies were incorporated at various stages and, thus, recurrence of failures prevented. National Aerospace Laboratories (NAL), Bangalore, has been involved in failure analysis and accident investigations for over four decades. Though initially the clientele was mainly from the aerospace sector, several other organizations have taken advantage of this service. The experience gained over the years has culminated in the compilation of this book, *Failure Analysis of Engineering Structures: Methodology and Case Histories.* The book comprises two parts. The first part is a treatment of various aspects of failure analysis with emphasis on techniques. The second part deals with failure case studies analyzed by the Failure Analysis and Accident Investigation Group in the authors' laboratories.

The introductory chapter cites a few major industrial catastrophes encountered in the last century. The importance, philosophy, and the beneficiaries of failure analysis are covered. The failure rate in the life span of machines is comparable to the geriatric curve, high in the initial and final stages and minimum in between. The philosophy of failure analysis is to bring down the failure rate and to extend the span of minimum failure rate.

Chapter 2 covers the common causes of failures. Various failures encountered in industries could ultimately be attributed to some deficiency introduced, though inadvertently, during the various stages of manufacture and operation. These stages include design, production (which covers materials selection, processing operations, treatments, assembly, and inspection), maintenance, service abnormalities, abuses, and environmental effects. Failure cases are described with examples from various industries such as chemical, mining, aviation, power generation, and so forth to illustrate how the deficiencies ultimately led to serious failures.

The success of failure analysis depends on the use of proper analytical techniques in proper sequence. Chapter 3 describes the techniques with which every analyst should be familiar. The techniques described include collecting background information; survey of wreckage; collection and preservation of samples for further laboratory examination; tests such as chemical analysis at various levels, mechanical tests, nondestructive inspection, microscopy, fractography, simulation tests; and final analysis of results to pinpoint the cause of the failure and the sequence of events. Simulation tests often help in clinching specific issues.

Vital information about failures is provided by microscopic examination of samples at various levels of resolution and magnification. A separate chapter is thus devoted to microscopy in failure analysis. Microstructural examination with the metallurgical microscope reveals structural abnormalities, crack origin, and crack path. Fracture surface examination using optical microscope and scanning electron microscope reveals telltale marks characteristic of such failure modes as tensile overload, shear overload, rapid brittle fracture, fatigue, stress corrosion, and so forth. These are described with illustrations in Chapter 4.

Chapter 5 deals with certain advanced techniques of failure analysis. These techniques evolved in recent times, necessitated by the needs of failure analysis in sophisticated industrial systems. In thermal plants that have been in service for a long time, study of samples taken for biopsy without affecting the integrity of the plant has helped in condition monitoring of the plant and estimating its residual life. Fracture Surface Topography Analysis (FRASTA) is another advanced technique by which the evolution of the fracture process could be studied. The practical applications of this technique are described briefly. Other techniques described in this chapter are fault tree analysis (FTA), failure modes and effects analysis (FMEA), failure experience matrix (FEM), expert systems for failure analysis, study of fractals, and quantitative fractography.

Failures in machines and structures are sometimes deliberately caused by antisocial elements, using explosive devices. When metallic objects deform and fracture under explosive conditions where the strain rates are of the order of $10^6\ s^{-1}$, certain distinct features can be found in the fragments produced by explosions. These features are permanent and they survive subsequent crash impact forces. These features are different from the telltale marks produced under normal static loading conditions. In Chapter 6, the signatures of explosion are catalogued under surface features, edge features, microstructural features, and fragment shapes, with illustrations. These have been extremely helpful in the investigation of aircraft accidents caused by explosive sabotage. Two such accidents are described in detail.

Major catastrophes are invariably followed by serious, prolonged, and expensive litigations in courts. Many of the failures and accidents involve a combination of component malfunction and mismanagement. While routine failure investigations aim at finding the cause of the mishap, investigations in courts attempt also to fix responsibilities and recommend punitive action. These can be extended for several years after the accident. Exact evidence with supporting data of high standard has to be presented in the courts to justify penal action. Some of the major accidents de-

scribed in Chapter 2 were followed by judicial inquiries in which experts provided the required testimony. A few cases of forensic investigations are presented in Chapter 7.

The follow-up actions after failure analysis have indeed resulted in numerous advantages to industries. These advantages are described in Chapter 8. Process modification after failure analysis in a chemical industry significantly reduced the hazards encountered earlier. Choice of better and cleaner materials resulted in increased reliability and safety. Codes and standards have been modified to ensure greater safety in hazardous industries. Certain specific actions also ensured greater security in industries, especially aviation. The numerous advantages accrued after taking remedial measures, following an understanding of failures, more than justified the statement, "Many should benefit from the misfortunes of a few."

Part 2 of the book deals with detailed description of various failure cases investigated by the Failure Analysis and Accident Investigation Group at NAL. The majority of cases deal with aviation machines, while a few cases of industrial failures are also included.

The Failure Analysis activity at NAL was nurtured by senior scientists and Directors of the Laboratory, namely, Dr. S. Ramaseshan, Dr. V.S. Arunachalam, Dr. A.K. Singh, Dr. S.R. Valluri, Dr. R. Narasimha, Dr. K.N. Raju, Dr. T.S. Prahlad, and Dr. B.R. Pai. The members of the Failure Analysis Group, Dr. T.A. Bhaskaran, Mr. C.R. Kannan, Mr. M.A. Parameswara, Mr. S. Radhakrishnan, Mr. R. Rangaraju, Mr. Dwarakanath Rao, and Mr. M.A. Venkataswamy, contributed in no small measure in the investigation of numerous cases described in Part 2.

Because failure analysis is a multidisciplinary activity, expertise from other divisions and sections of the Laboratory was drawn frequently as needed. Significant help was received from Graphic Arts, Chemical Analysis Group, X-ray Laboratory, Fatigue Laboratory, and Engineering Services. The authors are thankful to Mr. K. Venkata Ramaiah for his help in computer graphics. In compiling this book, the authors had very useful discussions with Dr. M.K. Asundi of Bhabha Atomic Research Centre, Bombay; Dr. R. Krishnan of Gas Turbine Research Establishment, Bangalore; and Dr. R. Viswanathan of Electric Power Research Institute, Palo Alto.

Designers, manufacturers, maintenance personnel, and users of machines are the beneficiaries of the results of failure analysis. It is hoped that this book would be of use to students of engineering and practicing engineers.

V. Ramachandran
A.C. Raghuram
R.V. Krishnan
S.K. Bhaumik
Bangalore

ASM International is the society for materials engineers and scientists, a worldwide network dedicated to advancing industry, technology, and applications of metals and materials.

ASM International, Materials Park, Ohio, USA
www.asminternational.org

Publication title	Product code
Failure Analysis of Engineering Structures: Methodology and Case Histories	05127G

To order products from ASM International:

Online Visit www.asminternational.org/bookstore

Telephone 1-800-336-5152 (US) or 1-440-338-5151 (Outside US)

Fax 1-440-338-4634

Mail Customer Service, ASM International
9639 Kinsman Rd, Materials Park, Ohio 44073, USA

Email CustomerService@asminternational.org

In Europe American Technical Publishers Ltd.
27-29 Knowl Piece, Wilbury Way, Hitchin Hertfordshire SG4 0SX, United Kingdom
Telephone: 01462 437933 (account holders), 01462 431525 (credit card)
www.ameritech.co.uk

In Japan Neutrino Inc.
Takahashi Bldg., 44-3 Fuda 1-chome, Chofu-Shi, Tokyo 182 Japan
Telephone: 81 (0) 424 84 5550

Failure Analysis of Engineering Structures: Methodology and Case Histories
V. Ramachandran, A.C. Raghuram, R.V. Krishnan, S.K. Bhaumik, p3-4
DOI:10.1361/faes2005p003

CHAPTER 1

Failure Analysis: Why and for Whom?

SERVICE FAILURES of components and structures have been increasingly experienced in several industries, quite often without any warning. Some failures may be trivial, while others may have serious consequences. Service failures may result in:

- Fatalities
- Injuries to personnel
- Damage to property
- Shutdown of an entire plant
- Loss of production
- Ecological problems such as release of hazardous materials
- Expensive and prolonged litigations affecting the credibility of the manufacturers and the reliability of their products

Thus, failures have a great impact on the society and its economy. Failures of structures can occur at various locations, for instance, at home, on the road, in a machine, in an aircraft, or in a big plant. Failure of an aluminum ladder in a home, which led to personal injuries to a woman and the following litigation between her and the manufacturer of the ladder, is an example where the effect of failure is limited to an individual. In contrast, the failure of a pipe in a chemical plant, carrying an inflammable chemical resulted in the total devastation of the entire factory with extensive damage to the community. As the complexity of our technological systems increases, so do the possible catastrophic consequences of the failure. For understanding failures and their prevention, there is a need for the application of many disciplines of science and technology.

The last century witnessed several catastrophic failures. Some of these failures are described in later sections. One of the most tragic brittle failures was that of a molasses tank that failed in Boston on Jan. 15, 1919 and flooded the city with 2.3 million gallons of molasses, drowning people and horses and knocking over the Boston elevated railway structure. Several rapid brittle failures have occurred in structures such as tanks, pressure vessels, ships, and bridges in the United States, Canada, and Europe. The problem was fully appreciated in the 1940s when out of 5000 merchant ships built during World War II, over 1000 had developed cracks of considerable size. At least nine T-2 tankers and seven Liberty ships had broken completely into two as a result of brittle fractures originating from sharp corners and square cutouts.

There have been some more catastrophes in recent times. The tragedy at Bhopal, India on Dec. 3, 1984, which claimed the lives of over 2000 people and maimed many due to the release of the poisonous methyl isocyanate gas is still fresh in memory. The Boeing 747 aircraft Kanishka of Air India plunged into the Atlantic Ocean on June 23, 1985 without any warning, killing all 329 occupants. On Jan. 2, 1988, a 4 million gallon oil storage tank at Ashland, near Pittsburgh, collapsed while filling. Five hundred thousand gallons of diesel fuel flowed into the Monongahela and Ohio rivers, causing a serious environmental problem. Water supply to the city of Pittsburgh was stopped for two weeks. On April 28, 1988, a Boeing 737 aircraft of Aloha Airlines, while flying over the Hawaiian Islands, suddenly experienced explosive decompression, and a major portion of the upper crown skin and structure in the front portion of the main cabin separated in flight, opening the cabin to the sky and causing a serious accident. On Dec. 24, in the same year, an oil pipeline in Missouri collapsed, spilling 800,000 gallons of crude oil into the Missouri River.

Studies following several mishaps have resulted in an awareness that it is not the yield strength or the ultimate tensile strength of a material that would determine the life of a component but rather the formation of a crack and its rate of growth. Crack initiation and propagation can be influenced by a variety of factors that must be understood and appreciated for failure prevention.

Failure of a component or structure can be defined as an unacceptable gap between its expected and actual performance. It is a condition that makes the structure unable to perform its intended function safely, reliably, and economically. Such an unacceptable difference can be due to many reasons. A later chapter explains that the causes of failures rest in defects of one type or another introduced mostly inadvertently during the various stages of the manufacture of a component and its usage.

These defects could get introduced during the design of a component, its manufacture, assembly, inspection, and maintenance. Manufacture of a component involves materials selection, materials certification, processing operations such as casting, forming, joining, machining, heat treatment, surface treatment, and so forth. Service abnormalities and abuses also play a major role in addition to environmental factors. The personnel responsible for the quality assurance at these various stages would get very useful feedback from a detailed failure analysis so that at each stage appropriate precautions could be taken to avoid introduction of deleterious defects. Hence, when there is a failure in a component or structure, the beneficiaries of failure analysis are many in the system.

The failure rate of a system, be it a component, a machine, or a large structure, can be compared with the mortality rate of human beings. This is depicted in the so-called “bath tub” curve (Fig. 1.1), having three distinct zones. During the early life or the infant stage, the failure rate is high. This is generally due to poor design, defective manufacture, and assembly faults of the system. In the

next zone, representing the useful service life, the failures have a constant rate and are random. As the system ages beyond a certain service life, the failure rate increases again. This is the geriatric stage, after the system has suffered wear and other degradation processes. At this stage, the system can no longer function reliably, safely, and economically. All quality control efforts aim at reducing the failure rate in the first zone and extending the life in the second zone.

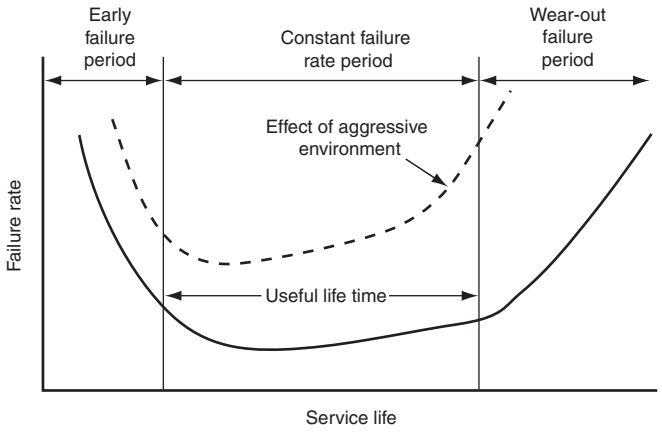

Fig. 1.1 Failure rate during the service life of a system. Source: Ref 1

Failure can be considered a real time test for the integrity of a structure. When a major disaster such as an aircraft accident occurs, it is the manufacturer who is most concerned about investigating the mishap to find out what went wrong and at what stage. Failure is a fact of life. It cannot be totally avoided, as a failure-free system is unattainable or prohibitively expensive. However, when a failure does occur, and if a systematic analysis is carried out, very useful input can be provided to management, engineers, and/or regulatory authorities for taking appropriate corrective actions. Thus, many can benefit from the misfortunes of a few.

REFERENCES

1. A.C. Raghuram and R.V. Krishnan, Failure Analysis—A Real Time Test, *Proceedings of Conference on Advances in Structural Testing, Analysis and Design,* B. Dattaguru et al., Ed., Tata McGraw-Hill, New Delhi, 1980, p 1373

Failure Analysis of Engineering Structures: Methodology and Case Histories
V. Ramachandran, A.C. Raghuram, R.V. Krishnan, S.K. Bhaumik, p5-17
DOI:10.1361/faes2005p005

CHAPTER 2

Common Causes of Failures

IT IS NOW a well-recognized adage that failures do not just happen; they are caused. There are compelling reasons for investigating failures. Unless the true cause of the failure is discovered, no remedial action is possible to prevent its recurrence. Secondly, failure analysis helps considerably in improving the reliability and safety of machinery and structural hardware that form the heart of modern industries. In the last few decades, systematic failure investigations carried out on several failed components have generated a fund of useful information for taking suitable remedial measures to prevent similar incidents. In practice, though failures perhaps cannot be completely eliminated, with experience gained, one can attempt to reduce their probability to a minimum.

Failures can be broadly classified into two categories: those involving fracture and those without fracture. In each category, failures can be further classified depending on whether they are caused by thermal, mechanical, or chemical influences. Further classification is possible to identify the mechanism of failure. Mechanical failures are further studied considering the nature of forces, whether they are by monotonic or repetitive loads. All service failures can ultimately be attributed to defects of various types, introduced mostly inadvertently in the various stages of manufacture of the component. In the following section, some potential causes of service failures are given.

The cause-effect relationship of some defects are also illustrated with appropriate case histories in this chapter. The cases chosen are for illustrating the principles and are by no means exhaustive. Understanding the true causes of failures and documenting them for all concerned is one way to help identify preventive measures.

2.1 Potential Defects Leading to Failures

Imperfection versus Defects as the Root Cause of Failures. One important distinction in failure analysis is the precise usage of the term *defect* in contrast with terms such as *imperfection* or *flaw*. A defect is, by definition, a condition that must be removed or corrected, while an imperfection or flaw is a condition that does not necessarily result in a defective part or failure. This semantic distinction is important in failure analysis because a discontinuity or imperfection may be present, even though it is not directly attributable to the root cause of a failure. A discontinuity, imperfection, or flaw becomes a defect only when it interferes with the intended function and expected life of a part. In the discipline of nondestructive evaluation (NDE), for example, the following definitions are an applicable reference (Ref 1):

- *Discontinuity:* A lack of continuity or cohesion; an intentional or unintentional interruption in the physical structure of configuration of a material or component
- *Imperfection:* A departure of a quality characteristic from its intended condition
- *Flaw:* An imperfection or discontinuity that may be detectable by nondestructive testing and is not necessarily rejectable
- *Defect:* One or more flaws whose aggregate size, shape, orientation, location, or properties do not meet specified acceptance criteria and are rejectable

These NDE-based definitions clearly recognize the reality of some imperfections or discontinuities in most manufactured materials. This distinction is important in failure analysis because a discontinuity or imperfection may be present, even though the failure is attributed to a different root cause. Thus, one basic objective of material failure analysis is determining whether a discontinuity is an actual root-cause (defect) or just an imperfection. Critical engineering assessment of discontinuities is therefore necessary in failure analysis to define whether an imperfection is a defect or simply a harmless discontinuity that does not sacrifice the reliability, intended function, or expected life of a part.

It should also be recognized that the term defect is not always used consistently with the preceding distinctions in mind. In less-than-perfect castings, for example, the term casting defect is sometimes used for general imperfections that do not necessarily contribute to the failures of castings. Many of the common causes of failures of castings occur from one or more aspects of design, materials selection, casting imperfections, faulty processing, improper assembly, or service conditions not initially anticipated. Some casting imperfections have no effect on the function or the service life of cast components but will give an unsatisfactory appearance or will make further processing, such as machining, more costly.

Depending on the context of an investigation, the term defect may also have particular meaning, especially when litigation is involved. For example, the following are some definitions noted in Ref 2:

- *Defect:* An imperfection (deviation from perfection) that can be shown to cause failure by a quantitative analysis and that would not have occurred in the absence of the imperfection
- *Manufacturing defect (Legal)*
  a. Failure to conform to stated specifications
  b. Nonsatisfaction of user requirements
  c. Deviation from the norm

   d. A product leaves the assembly line in substandard condition, differs from the manufacturer's intended result, or differs from other ostensibly identical units of the same product line
- *Design defect (Legal)*
   a. Less safe than expected by the ordinary consumer
   b. Excessive preventable danger
- *Marketing defect (Legal):* Failure to warn or inadequate warning of hazard and risk involved with use of a product

Legal definitions may vary from jurisdiction to jurisdiction, and the preceding legal definitions are cited here only as examples of how a defect may be defined. Just because a part fails does not imply that it contained a defect, and not all defects are a cause for failure. Laws of various jurisdictions may also define what constitutes a defect or defective product.

Improper design

- Underestimate of service stress
- Undesirable geometry
   a. Stress concentrators
   b. Inadequate radii at corners
   c. Inaccessibility for inspection
   d. Difficult to fabricate
- Improper choice of materials
- Improper choice of heat treatment
- Environmental effects
- Ad hoc modifications

Defective manufacture

- Materials
   a. Materials mix-up
   b. Poor quality of material
   c. Nonconformity to specifications
   d. Undesirable phases and nonmetallic inclusions
- Castings
   a. Porosity
   b. Inclusions
   c. Segregation
- Forgings
   a. Folds
   b. Fissures
   c. Unfavorable flow lines
- Welds
   a. Improper fusion
   b. Cracks in heat affected zone
   c. Wrong filler material
- Machined parts
   a. Poor surface finish
   b. Grinding burns
- Heat treatment
   a. Quench cracks
   b. Overheating
   c. Undertempering
- Surface treatment
   a. Improper cleaning
   b. Improper plating
   c. Improper post treatment
- Assembly
   a. Defective joining
   b. Misorientation and misalignment
   c. Inadequate support
   d. Improper tightening
   e. Improper balancing
   f. Damages by tools
   g. Assembly stresses
   h. Distortion

Improper inspection

- Deviations from approved tolerances
- Deviations from acceptance standards
- Wrong techniques
- Nonadherence to schedules of inspection and calibration of inspection tools
- Shortcuts to meet targets

Operation, service abnormalities, and abuses

- Inadequate lubrication
- Improper cleaning
- Nonadherence to operating instructions
   a. Overspeeding
   b. Overloading
   c. Ill-trained operators
- Unexpected service conditions
- Temperature and stress excursions
- Vibrations
- Changes in environment

Environmental effects

- Various types of chemical corrosion
- Stress corrosion
- Corrosion fatigue
- Erosion

Maintenance

- Wrong replacement
- Wrong tools
- Excessive concessions
- Inadequate inspection
- Ad hoc alterations
- Inadequate condition monitoring and preventive maintenance

Combination of the preceding

- Combined action of some of the preceding causes

Sabotage

- Deliberate damage by antisocial acts
- Mechanical damages
- Explosive sabotage

2.2 Examples of Deficiency in Design

Failures in structures can result from inadequacies in design, even with the use of the best material for construction. Such inadequacies can be introduced inadvertently in the original design itself or in any modification carried out during service. Failures of several machine components attributed to faulty design are illustrated in the following examples.

Example: Deficiency in the Original Design: Failure of a Steam Turbine. A 290 mm diameter steam turbine developed excessive noise and vibration and had to be shut down. The nut that locked the two-stage turbine disk in place had worked its way out from the threads and the disk had shifted about 2.5 mm and come off the shaft. The design of the locking mechanism was responsible for the loosening of the nut (Ref 3).

Figure 2.1 shows the two-stage turbine disk and the shaft. The locking nut fitted at the end of the shaft with its two locking pins intact is shown in Fig. 2.2. The locking mechanism is shown in Fig. 2.3. The locking nut with left-handed threads was tightened by rotation in a direction opposite to the rotation of the disk. To retain the nut in this position after tightening, two holes were drilled in situ through the nut and the disk and two pins were inserted.

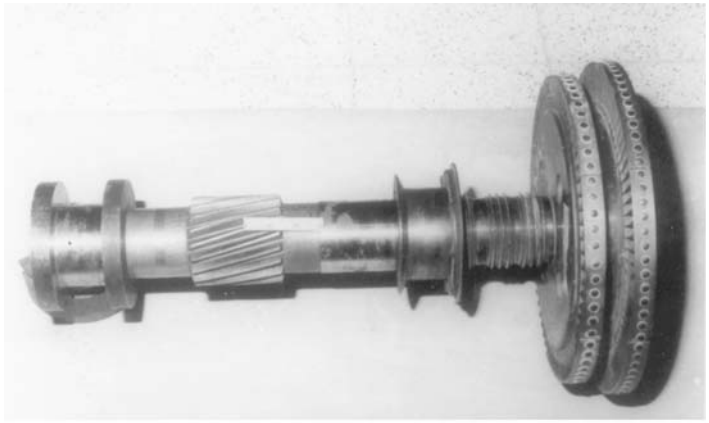

(a)

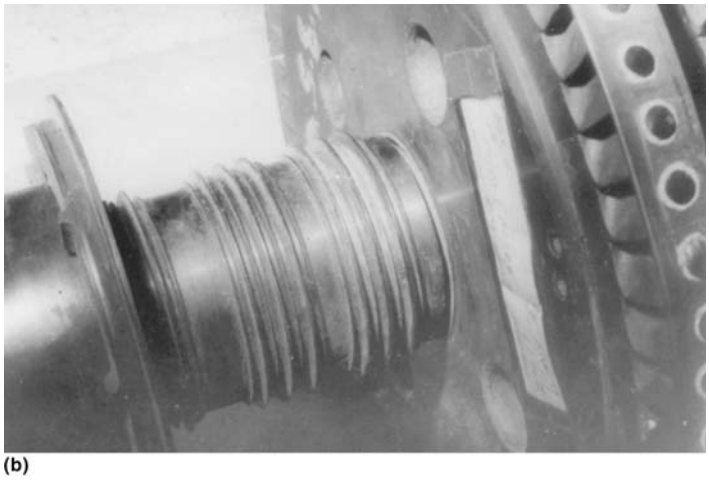

(b)

Fig. 2.1 Turbine disk with the main shaft. (a) Overall view. (b) View showing the lateral shift of the disk from its original position. Source: Ref 3

The locking mechanism did not take into account the slippage of the turbine disk. As can be seen in Fig. 2.4, if the disk slipped, it would automatically loosen the nut. The two locking pins providing the leverage would aid in this loosening. The effect of the slippage is cumulative. Once the loosening was sufficient to clear the locking pins from the holes of the disk, the nut would be completely free and ineffective for locking, thus leading to excessive vibration.

The locking mechanism must be designed to provide positive locking with respect to the disk only.

Example: Deficiency in Ad Hoc Design Modification: A Major Accident in a Chemical Plant. Because attention was not

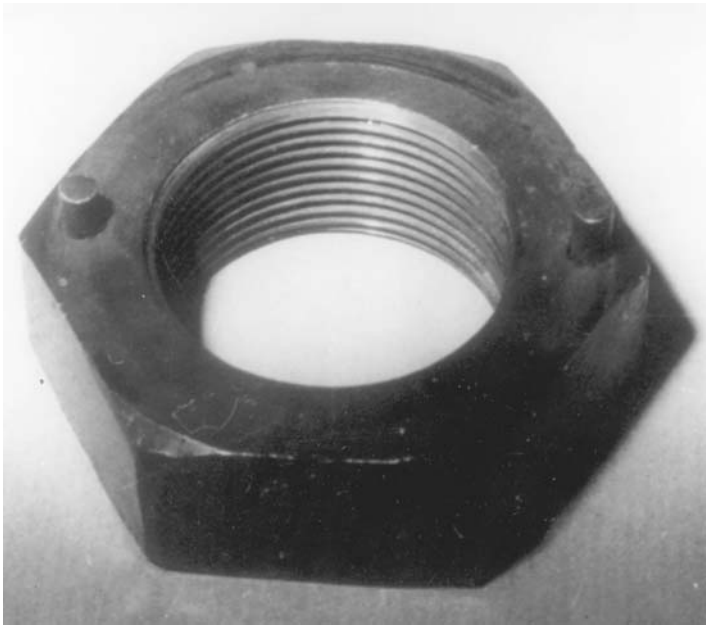

Fig. 2.2 Locking nut with the two pins intact. Source: Ref 3

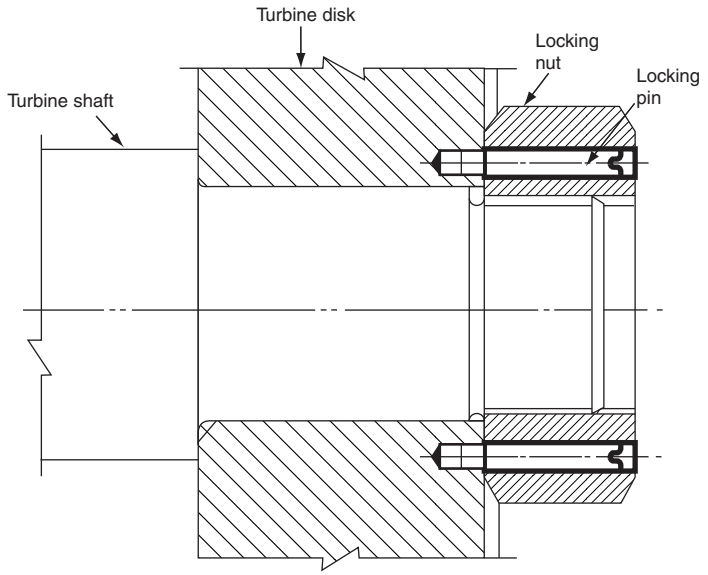

Fig. 2.3 Disk locking arrangement. Source: Ref 3

given to design during an ad hoc modification, a major disaster took place in Flixborough, England, on June 1, 1974 in a chemical plant making caprolactam, a raw material for making nylon. The plant was virtually demolished by an explosion of warlike dimensions (Ref 4). The conflagration associated with the vapor cloud explosion is shown in Fig. 2.5. Twenty-eight people were killed and 36 in the plant injured. Fifty-three members of the public were injured, a few seriously. Hundreds more suffered minor injuries. Property damage extended over a wide area in a 3 km radius, affecting 1821 houses and 167 shops. The cause of the disaster was found by a court of inquiry to be the failure of a bypass pipe introduced into the system during an ad hoc modification.

In one section of the plant, there were six reactors containing the inflammable chemical cyclohexane at a gage pressure of 8.8 kg/cm^2 and 155 °C (310 °F). By introducing air and catalyst, cyclohexane is oxidized to cyclohexanol and cyclohexanone. The products are later separated by distillation and converted to caprolactam. The six reactors are set each 350 mm below the previous one so that the flow from reactor to reactor is by gravity. It was noticed that reactor 5 was missing from the line.

The court inquired into this aspect and gathered the following information. On March 27, 1994, cyclohexane was detected leaking from a vertical crack in reactor 5. In order to restart the production as soon as possible, the cracked reactor 5 was removed and reactors 4 and 6 were connected directly by a 0.5 m (20 in.) bypass pipe as shown in Fig. 2.6. Thus, the scene for the disaster was set. Because the outlet of reactor 4 and the inlet of reactor 6 were at different levels, the two reactors were joined by an inadequately supported bypass assembly consisting of a "dog-leg" pipe of three segments between two expansion bellows at their ends. The fact that bridging the gap with a span of about 6 m (20 ft) presented engineering problems was not immediately appreciated. The pipe was subjected to a bending stress. The court concluded that there was no proper design study, no proper consideration for the need for a support, no safety testing, no reference to the relevant standards, and no reference to the bellow manufacturer's "Designer's Guides." As a result, the assembly as modified was of unknown strength. The bellows were subjected to shear forces for which they were not designed. The pipe was under high and unknown stresses. According to the report, the integrity of a well-designed and constructed plant was thereby destroyed. On the day of the accident, the assembly was perhaps subjected to conditions of pressure and temperature more severe than normal, sufficient to

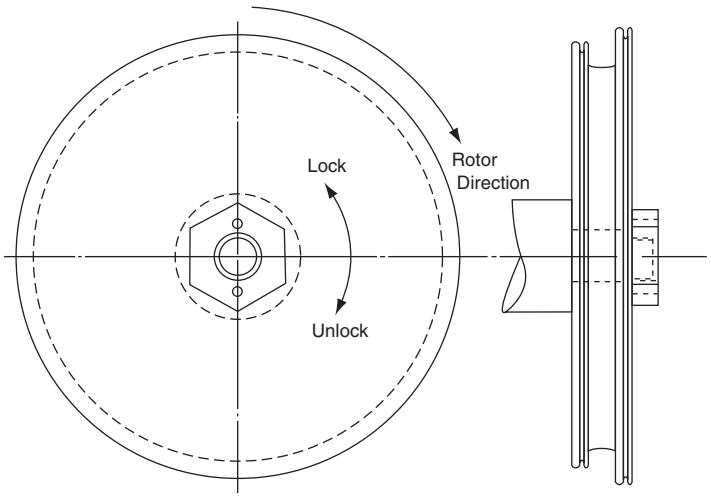

Fig. 2.4 Diagram showing the directions of rotation of the turbine disk and the locking nut. Source: Ref 3

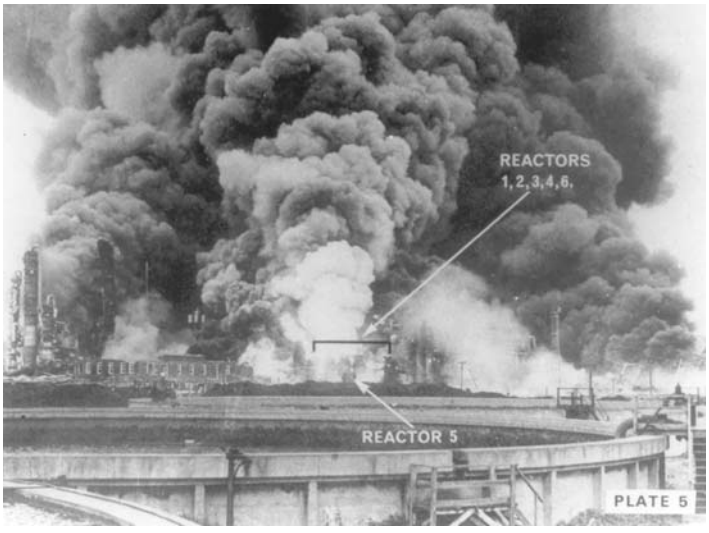

Fig. 2.5 The conflagration. Source: Ref 4. With kind permission of Her Majesty's Stationery Office

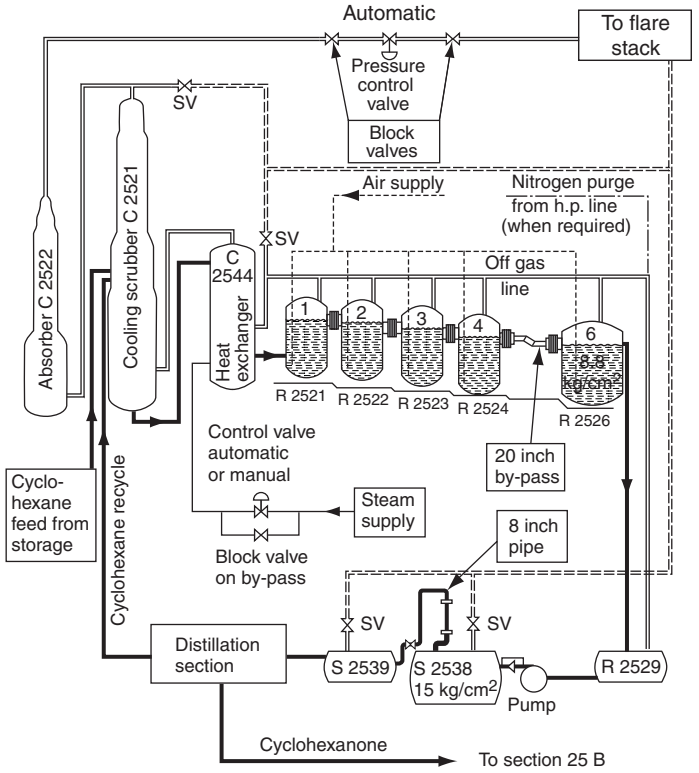

Fig. 2.6 Schematic sketch of the modification in the cyclohexane oxidation plant. Source: Ref 4. With kind permission of Her Majesty's Stationery Office

rupture the assembly. Large quantities of cyclohexane were released as a cloud that exploded with a force equal to 15 to 45 tons of TNT. The control room located nearby and all the personnel and records therein were destroyed. Essential information regarding pressure and temperature of circulating cyclohexane on the day of the accident could not be obtained.

The lesson from the investigation was that any modification in a plant should be designed, constructed, tested, and maintained to the same standards as the original plant. There was also a recommendation that consideration be given to installing devices or systems for recording vital plant operational parameters in a form that would survive the effects of fire and explosion, similar to the black boxes in an aircraft. The Flixborough plant was reconstructed, this time using an entirely different process for making caprolactam, based on hydrogenation of phenol instead of oxidation of the inflammable cyclohexane.

One must recognize that all plants may have hidden design faults. Slackness of management in operation, maintenance, and modification, particularly over a prolonged period, will combine with these weaknesses to produce a disaster, probably unlikely to be repeated, but nevertheless a disaster (Ref 5).

2.3 Examples of Manufacturing Defects

Even with the best design, flaws introduced during the manufacture of components can contribute to failures. As previously listed, such problems can be divided into three major categories dealing with deficiencies in:

- Materials
- Processing that includes operations such as casting, forming, joining, machining, heat treatment, and surface treatment
- Assembling

The following case histories illustrate some of these problems.

2.3.1 Failures due to Materials

The importance of material cleanliness is illustrated in the following example of a machine component. Cleanliness of materials also is extremely important in microelectronics devices. Impurities can poison the surfaces, leading to poor bonding. For example, in gold-coated devices, impurity metal oxides can form during the annealing process and these oxides within the gold layer, though only a few angstroms thick, can lead to poor bonding and malfunctioning of the devices (Ref 6).

Example: Material Defect: Failure of Nimonic Alloy Turbine Blades. The importance of material cleanliness is illustrated in the case where a batch of Nimonic alloy turbine blades failed during a test run of an aircraft engine. Fracture occurred near the root (Fig. 2.7), and fractographic studies indicated that the blades had failed by fatigue (Ref 7).

Sectional metallography was carried out on the failed blades and the path of the propagating crack was followed and documented. The origin of the fatigue crack was found to be the nonmetallic inclusions present in the material. Nonmetallic inclusions in a metallic matrix represent regions of discontinuity and stress concentration. Such inclusions nucleate cracks that propagate by fatigue under service conditions. Figure 2.8 shows a crack associated with one such inclusion.

2.3.2 Failures due to Processing

Defects introduced during the various processing operations can have a serious weakening effect on the component. They can also nucleate cracks that can then propagate by fatigue, leading to premature failures. Several industrial failures due to defective processing and fabrication procedures have been reported in the literature. A few typical cases are reported here.

Example: Microweld Defect: Failure of a Hip Prosthesis. A hip prosthesis, made of a Co-Cr-Mo-C alloy, was implanted in a patient fractured by fatigue in the stem portion (Fig. 2.9). After surgical removal of the prosthesis and failure analysis, it was found that a crack had nucleated on a microweld on the surface of the implant and propagated by fatigue. It was found that the prosthesis had been made by an ordinary casting process and the surface porosity was covered by repair welding. Defective repair welding proved to be detrimental to the patient. It was recommended that rigorous investment casting procedures be adopted for casting orthopedic implants as in the case of aerospace components (Ref 8).

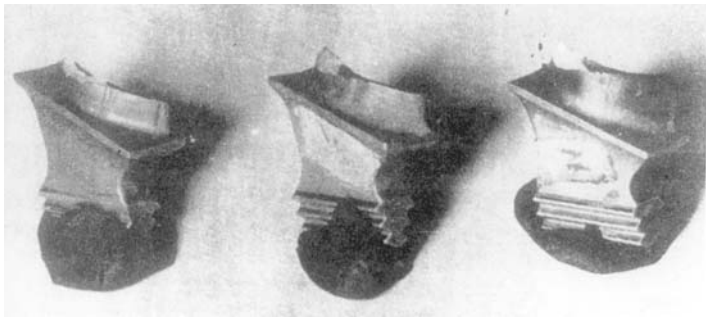

Fig. 2.7 Turbine blades failed near the root. Source: Ref 7

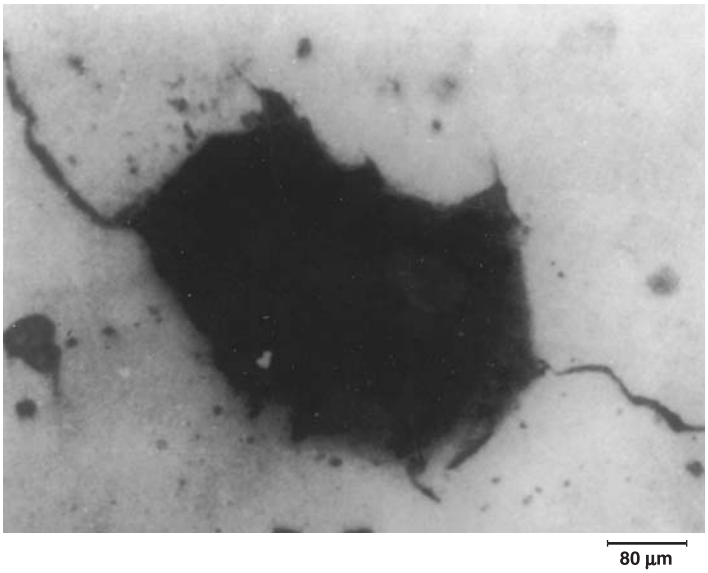

Fig. 2.8 Crack associated with an inclusion. Source: Ref 7

Example: Machining Defect: Failure of Titanium Alloy Compressor Blades. Compressor blades made of an alpha-beta titanium alloy (IMI 550, Ti-4Al-2Sn-4Mo) during routine vibratory fatigue testing were found to have unusually low fatigue life. The reason for this was not immediately apparent. The fatigue cracks were associated with spherical metal beads sticking to the aerofoil surface in each case, the origin being at the point of contact of the bead with the blade surface (Fig. 2.10, 2.11). The beads had a dendritic structure as shown in the scanning electron micrography (SEM) photograph (Fig. 2.12), indicating they had formed by fusion followed by solidification.

In situ x-ray analysis indicated that the beads had the same chemical composition as that of the blade. A study of the operations preceding the fatigue testing revealed that targeting bosses of these forged blades were removed by a grinding operation to facilitate mounting of the blades for fatigue testing. During the grinding operation, particles from the targeting bosses, while still in the molten or semisolid state, must have been thrown onto the blade surface, the impingement causing a localized embrittling effect leading to crack initiation. This theory was confirmed by simulation tests. Extreme care must be exercised during the grinding operation by properly orienting the blades and using suitable suction devices so that the particles are prevented from hitting the blade surface (Ref 9).

Example: Heat Treatment Defect: Cracking of a Nitrided Quill Shaft. This example deals with defects introduced during nitriding of quill shafts for an engine. The quill shafts are subjected to nitriding, but the nitriding operation should be confined only to the quill end, the other regions being suitably masked during heat treatment. By mistake, the entire shaft had been subjected to nitriding. During service, the torsional loads had initiated cracks on the nitrided layer of the shank. Figure 2.13 shows a quill shaft with spiral cracks on the shank portion. This situation is detrimental to

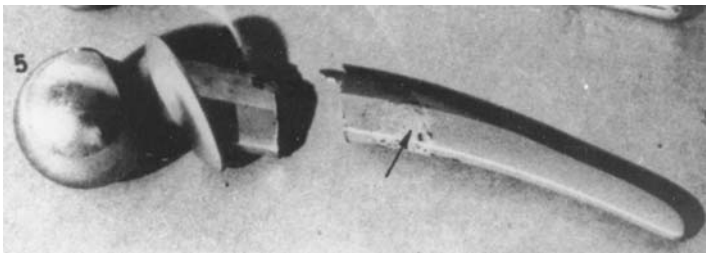

Fig. 2.9 Hip prosthesis failed in the microweld region. Source: Ref 8. With kind permission of Chapman and Hall Limited

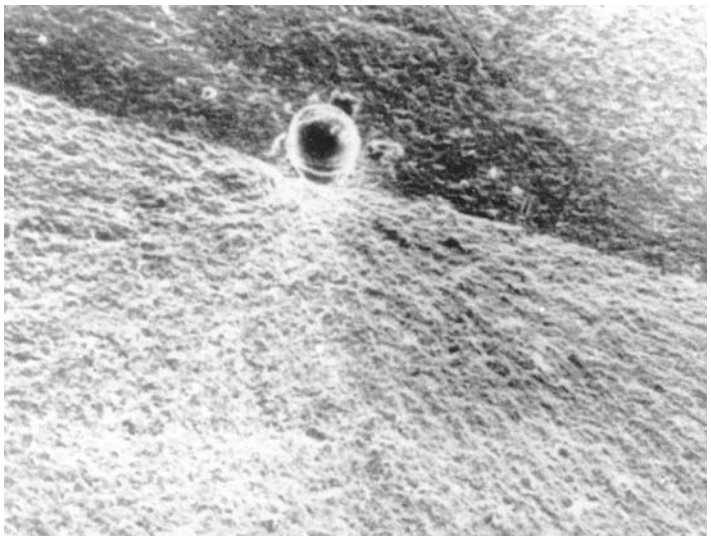

Fig. 2.11 Fatigue crack associated with a bead on the blade surface. Source: Ref 9

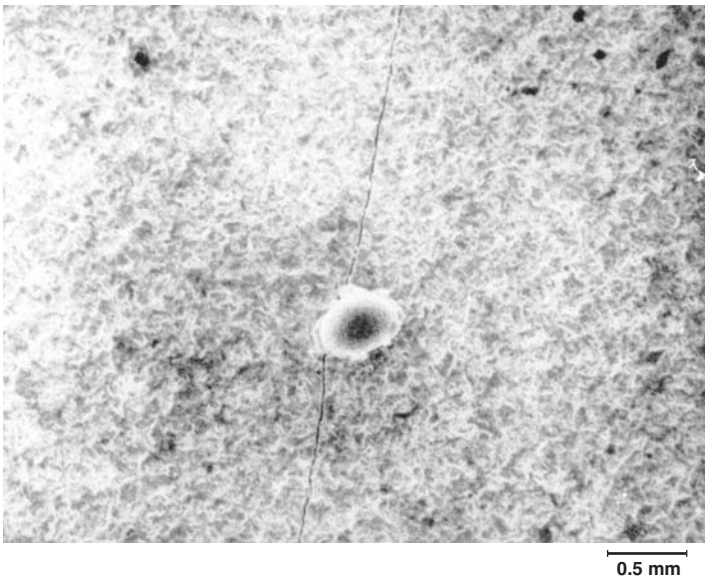

Fig. 2.10 Fractograph showing a metallic bead at the fracture origin. Source: Ref 9

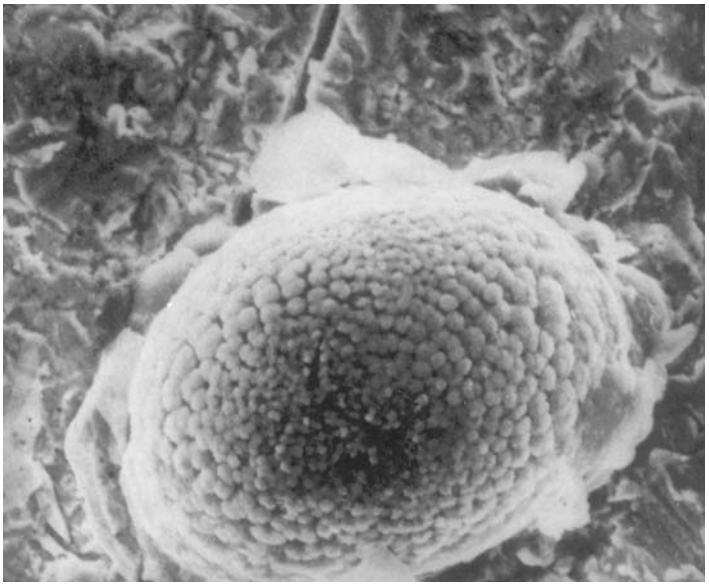

Fig. 2.12 SEM photograph showing the fatigue crack and the dendritic structure of the bead. Source: Ref 9

the continued use of such shafts because these surface cracks can propagate by fatigue during service.

Example: Hydrogen Embrittlement: Failure of a Rocket Suspension Lug. Hydrogen embrittlement is a phenomenon commonly found in high-strength steels after they are exposed to environments in which hydrogen is produced. Cadmium plating is a common surface protection treatment for high-strength steels to guard against corrosion. If proper precautions are not taken, the

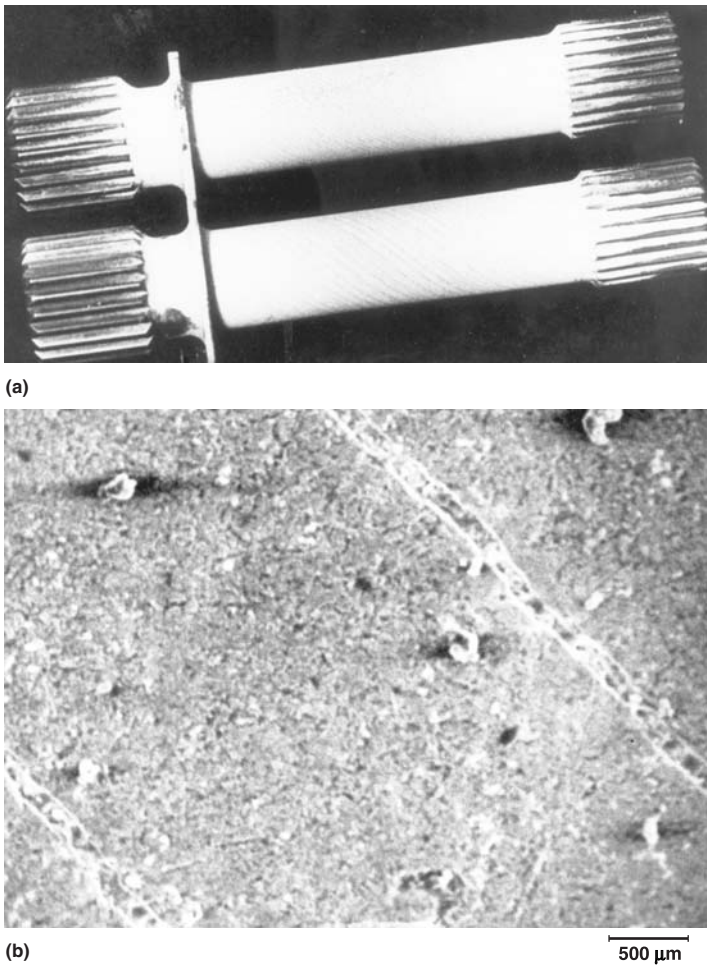

Fig. 2.13 (a) Spiral cracks on the shank surface of a quill shaft and (b) SEM photograph of the cracks

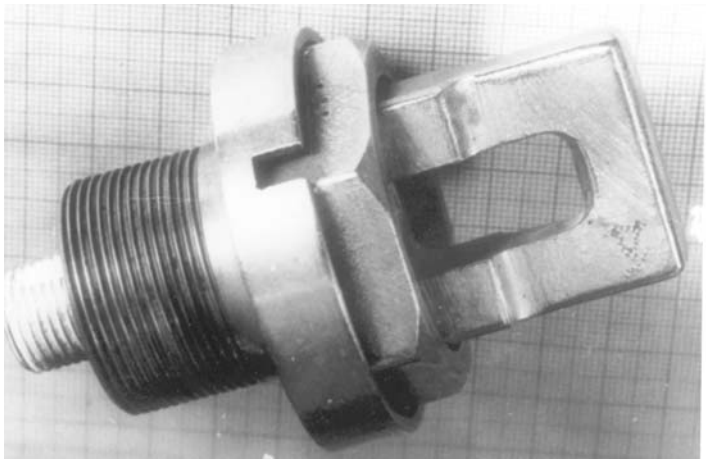

Fig. 2.14 Rocket suspension lug

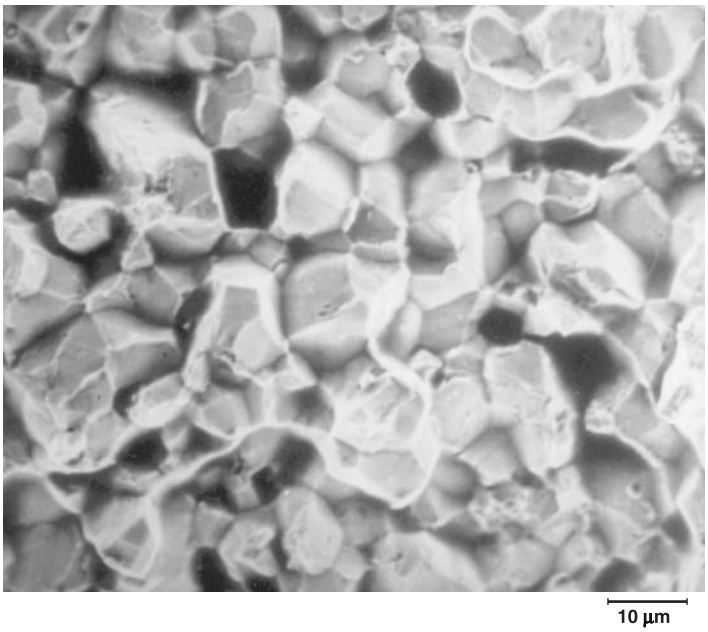

Fig. 2.15 Intergranular fracture of the lug

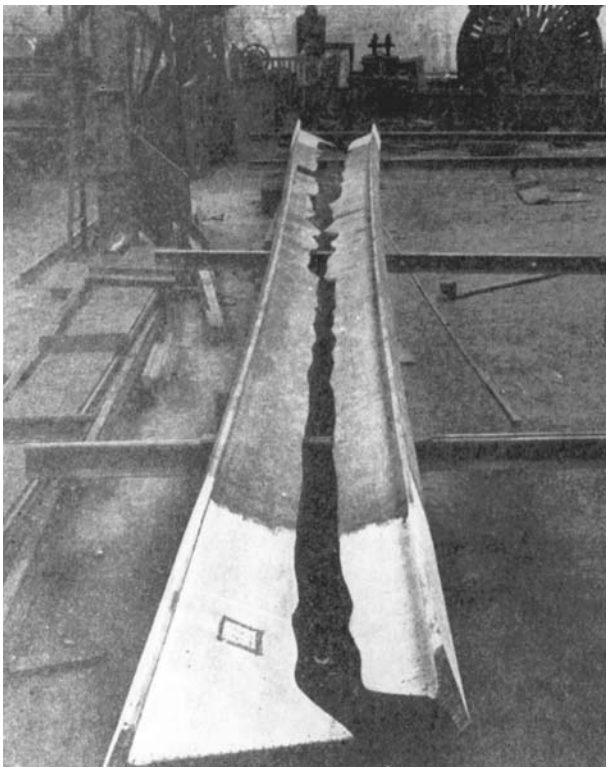

Fig. 2.16 12 m long I-beam split along the web. Source: Ref 10. With kind permission of Reinhold Publishing Company

hydrogen produced during plating can diffuse into the metal and lead to intergranular brittle cracking without warning. A lug for suspending a rocket from an aircraft, made of a high-strength steel, had been cadmium plated. The cadmium plated lug (Fig. 2.14) was kept in the stores in a tightened condition for a length of time. Subsequently, when an attempt was made to loosen the lug for fitting the rocket, it was found cracked inside, with a distinct intergranular fracture, typical of hydrogen embrittlement (Fig. 2.15). Hence, immediately after cadmium plating, it is mandatory to bake such cadmium-plated steel components to expel the hydrogen absorbed by the material during the plating operation. ASTM standard procedures for baking are available.

Fig. 2.17 Broken piston head showing primary failure by fatigue and a secondary crack through two bolt holes

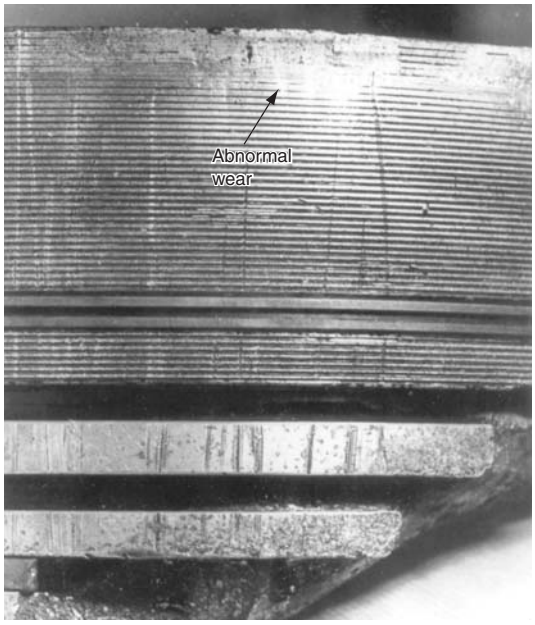

Fig. 2.19 Abnormal wear on one side of the piston head

Example: Residual Stress Relief: Failure of a Long I-beam. When components are manufactured from metals and alloys by the various operations, an important parameter that is overlooked is the residual stress retained during fabrication. Unless adequate precautions are taken to reduce or eliminate them, residual stresses can lead to unexpected failures. This is illustrated by an incident in Belgium in 1934. A 12 m long I-beam of high-strength steel fractured suddenly while lying flat on the shop floor, with an explosive noise (Ref 10). Figure 2.16 shows the beam, which had split along the entire length of the web. Both halves had curved with an outside concavity of the flanges, with deflections up to 8 cm. On the day before, skew cuts had been made at its two ends with a torch. The spontaneous fracture was attributed to the state of stresses introduced during the hot rolling of the beam. The web

Fig. 2.18 Fracture surface of the primary failure, showing beach marks

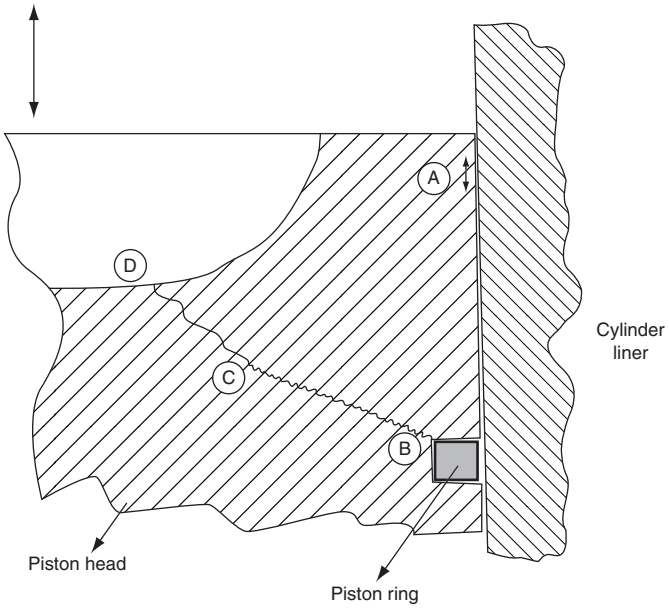

Fig. 2.20 Sketch illustrating piston head misalignment, fatigue crack initiation, and propagation. A, region of misalignment; B, sharp corner of piston ring groove; B-C, fatigue crack; and C-D, sudden overload failure

cooled faster than the flanges. The contraction of the flanges by cooling was prevented by the web, which induced high stresses in the beam. This state of precarious internal equilibrium was disturbed by the flame cutting. It is believed that under the heavy state of residual stresses, flame cutting followed by cooling produces a kind of artificial strain aging and hardening locally and generates cracks. These cracks must have grown slowly, until reaching the critical length.

A somewhat similar beam failure was reported at the Indira Gandhi Centre for Atomic Research, Kalpakkam, the crack in this case following a path along which there was excessive sulfur segregation (Ref 11).

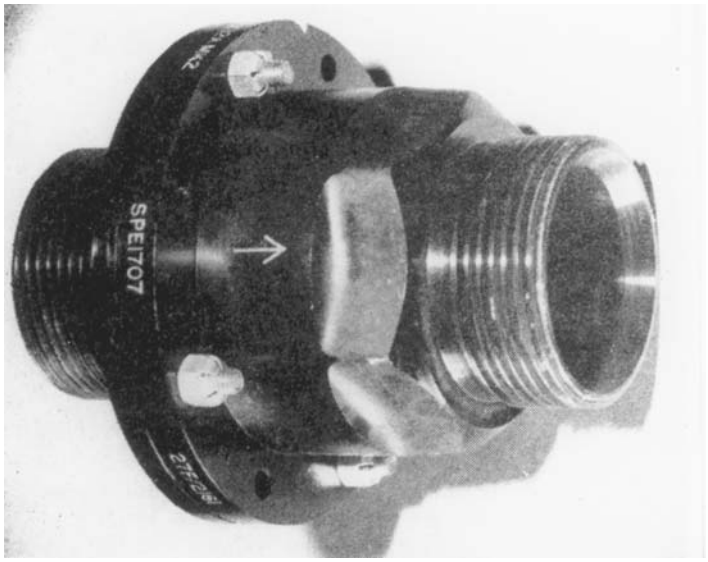

Fig. 2.21 A non-return valve that can be fitted incorrectly because of its design. Source: Ref 12. With kind permission of Royal Aeronautical Society

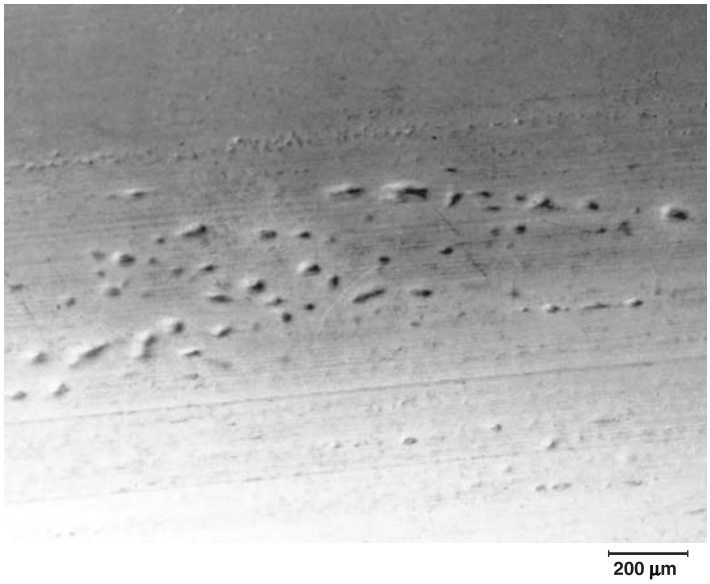

Fig. 2.22 Blisters in aluminum alloy extrusions

2.3.3 Failures due to Assembly

Example: Misalignment: Failure of a Piston in a Marine Engine. With the best component design and choice of the best ma-

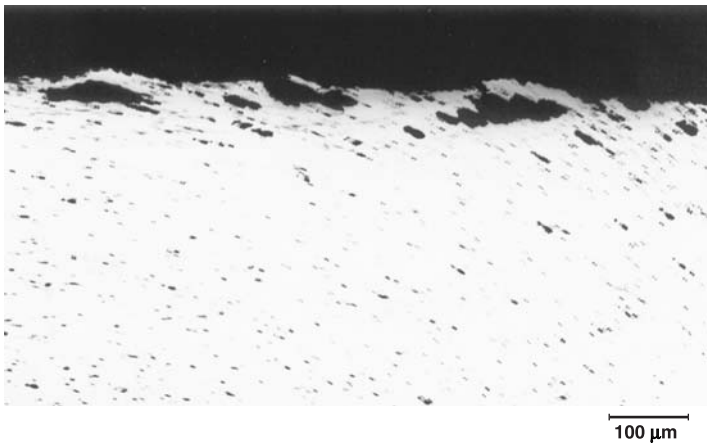

Fig. 2.23 Transverse section of the blistered extrusions, showing cavities near the surface, about to open up

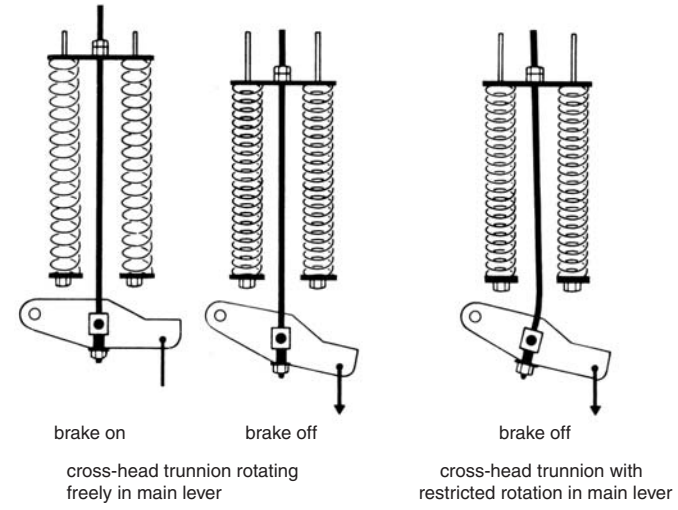

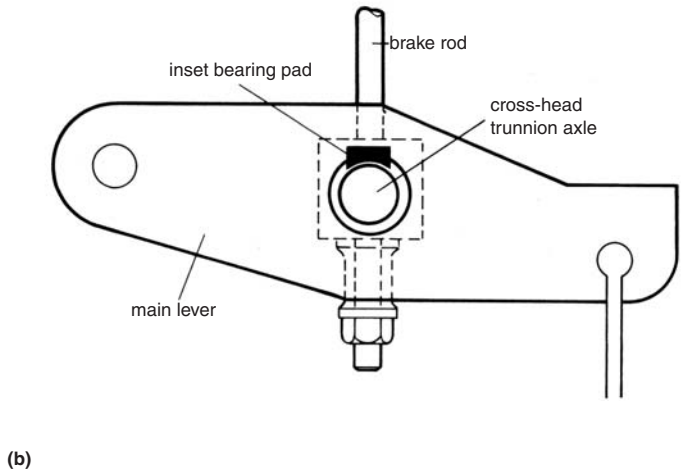

Fig. 2.24 Spring nest center rod and trunnion. Source: Ref 13. With kind permission of Her Majesty's Stationery Office

terial, sometimes mistakes can happen during the assembly of a structure. This is illustrated by the failure of an Al-Si alloy piston during the test run of an 8-cylinder 1100 kVA marine engine because of a slight departure from alignment. After about 100 hours of test running at less than full power, one of the pistons broke into a multitude of pieces, some of which got pulverized. The connecting rod had worked its way outward, breaking the cylinder liner and the engine block.

Figure 2.17 shows the broken piston head. Presence of beach marks on the fracture surface (Fig. 2.18) and striations revealed by electron fractography confirmed that the piston had failed by fatigue, the crack starting from a corner of the piston ring groove. A secondary crack had formed along the plane through two bolt holes located diametrically opposite. The continued pounding action of the piston had broken the rest of the piston beyond recognition.

The cause of the failure can be understood from Fig. 2.19, which shows abnormal wear on the side of the piston head. The scoring on the cylindrical surface of the piston head and not on the piston ring indicates that the ring had been sunk well inside the groove. Due to improper alignment and clearance, there has been friction between the piston head and the cylinder liner, which, during the reciprocatory motion of the piston could lead to cyclic stresses, which in turn could be magnified at notches and sharp corners. The mechanism of failure is illustrated in Fig. 2.20. The major secondary crack had occurred along the two bolt holes that were located at the thinnest section of the piston head.

Example: Assembly Error in Aircraft Accidents (Murphy's Law). The significance of assembly errors leading to serious failures has been well appreciated in aviation accidents. In some of the earlier designs of aircraft, it was possible to assemble certain parts incorrectly with the same parts required in a correct assembly. For example, a non-return valve in the fuel line of an aircraft (Fig. 2.21) had the two ends of the same size and same thread. Fitting it in reverse resulted in a fatal accident (Ref 12). The mechanical ability to do so, coupled with human errors, was the cause for the havoc. In another accident, the fault was traced to the end fittings of the landing gear hydraulic jack assembled the wrong way. In a micronic oil filter, the design permitted its fitting in reverse. Its end cap was blown off by pressure in the incorrect assembly, al-

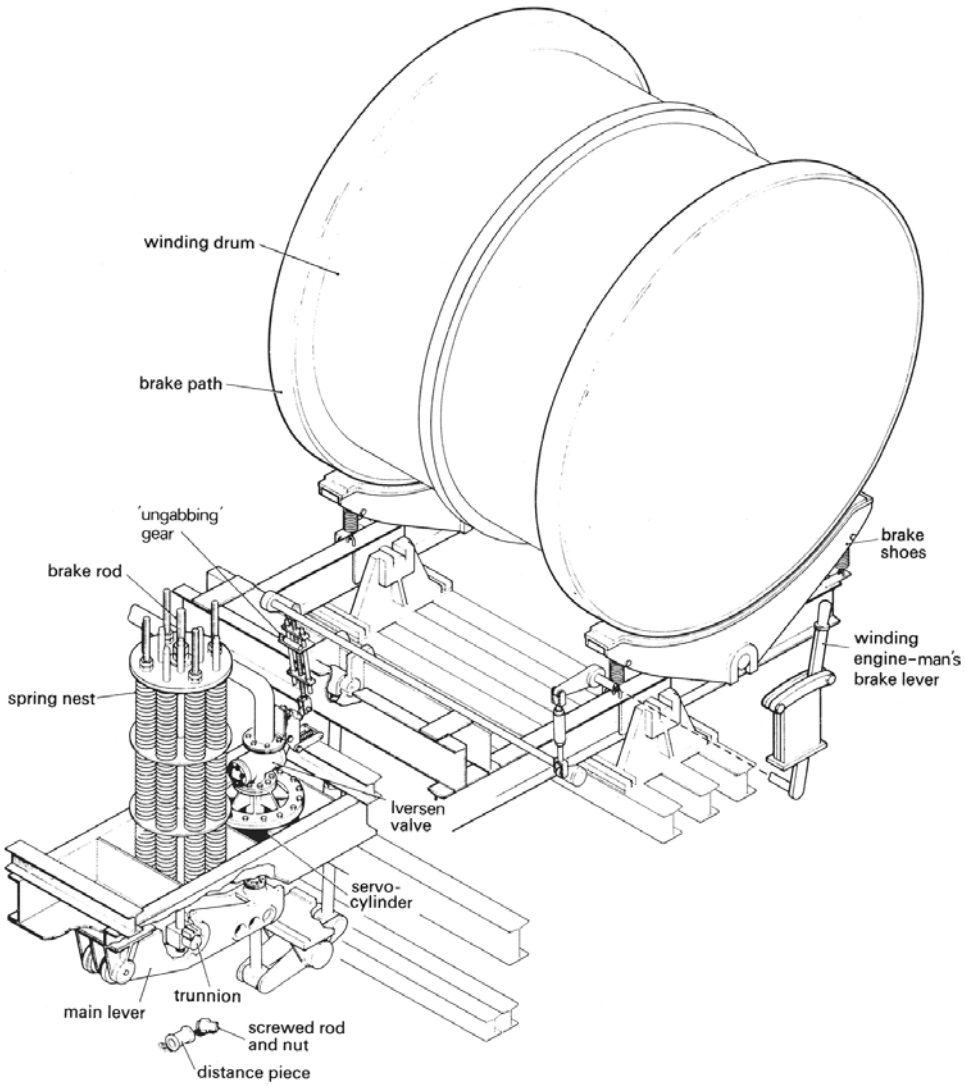

Fig. 2.25 Shaft winding engine and brake system. Source: Ref 13. With kind permission of Her Majesty's Stationery Office

lowing unfiltered oil to pass into the vital flight control mechanism. Because such mistakes cannot be tolerated, the best way to avoid mishaps is to eliminate such possibilities by careful consideration of design and anticipation of human errors.

2.4 Inspection and Maintenance

Inspection is an important stage in the manufacture of a component before it is released for the end use, and periodical inspection is necessary for monitoring the health of a component and the structure of which it forms a part. By proper inspection procedures, it was possible to reject defective structural members in an aircraft industry and obtain free replacement from the suppliers.

Example: Blisters in Aluminum Alloy Extrusions. In one batch of aluminum alloy extrusions to be used for aircraft wing roots, blisters (Fig. 2.22) were noticed during inspection. They were found to increase in number and size after a solution heat treatment. A section through the extrusion, after metallographic polishing, indicated holes near the surface, about to open up as cavities (Fig. 2.23). Such blisters are formed due to the presence of hydrogen picked up during melting. Proper degassing would eliminate this problem. Good inspection procedures helped in detecting these in time and obtaining free replacements. Use of blistered extrusions could have led to initiation of cracks in the structure.

Example: Infrequent Inspection: A Mine Accident. In the Markham coal mine in North Derbyshire, England, there was a fatal accident in which 18 miners died and 11 sustained serious injuries on July 30, 1973. The cage in which they were traveling in a shaft crashed into the pit bottom with tremendous force, the speed of impact estimated to be 43 km per hour (Ref 13). When these miners were being lowered into the shaft, the brake system failed to work. The brake system consisted of a pair of brake shoes applied by the action of a compressed nest of springs operating through a system of levers. The force from the spring nest was transmitted to the main lever of the brake system by a steel rod, 50 mm in diameter and 2.7 m long, located in the center of the

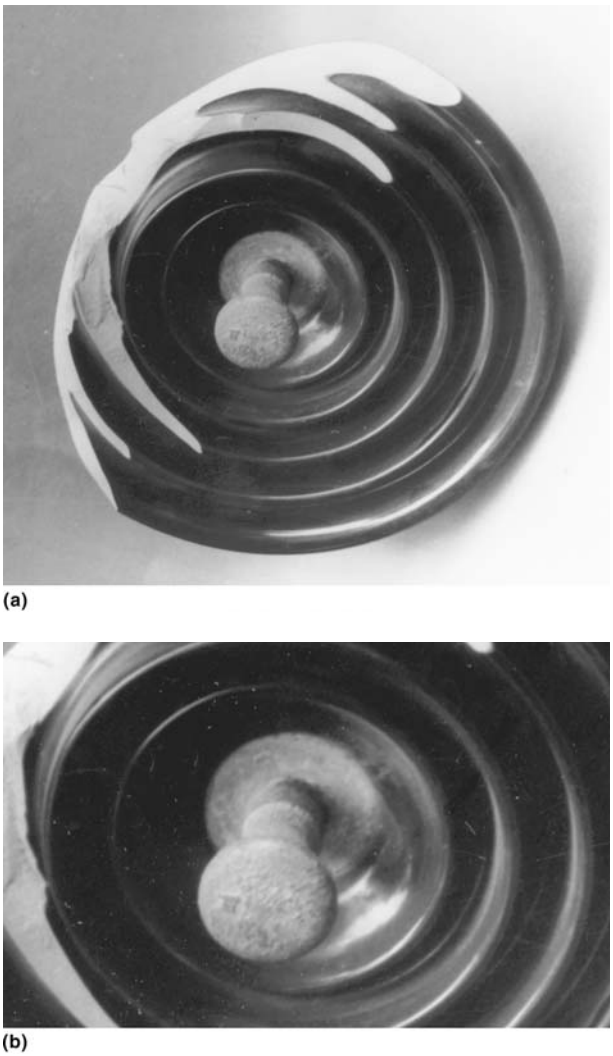

Fig. 2.26 (a) Porcelain insulator showing the step in its shank and (b) magnified view of the shank

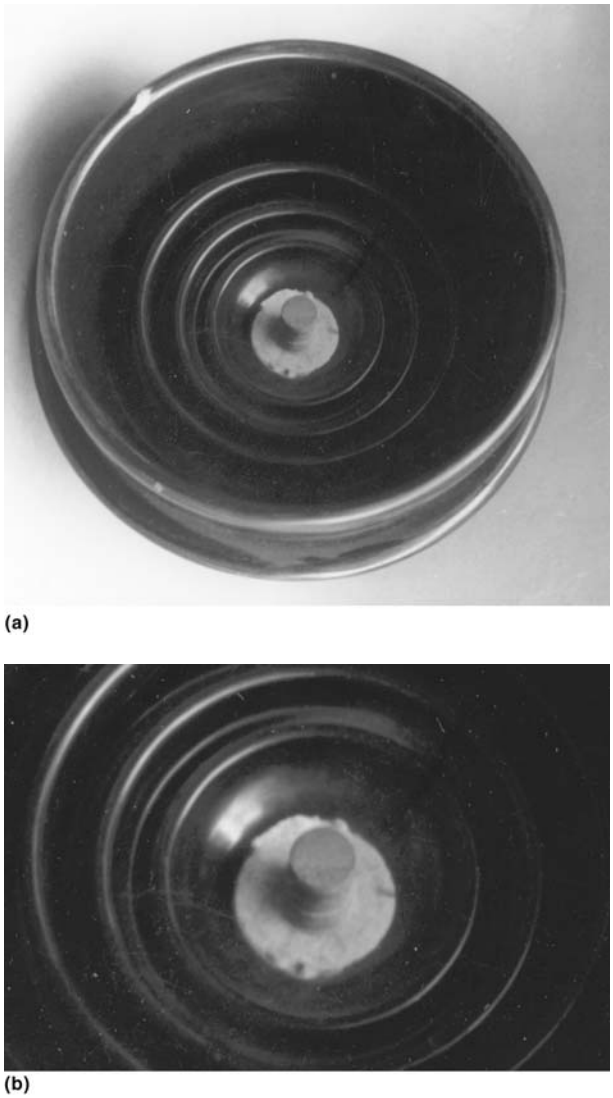

Fig. 2.27 (a) Fracture at the step in the shank and (b) magnified view of the fracture

nest, constrained by a plate at the top and connected by a cross head trunnion to the main lever at the bottom (Fig. 2.24, 2.25). The failure of the brake system was attributed to the fact that this central rod had failed by fatigue with a crack that had propagated to a depth of 27 mm before failure.

The central rod in the spring nest of this braking system is an example of a "single line" component on which the safety of the miners was entirely dependent. The recommendation after this investigation was that such components should either be eliminated or designed to prevent danger; for example, failure of any single-line component in a braking system should cause the winding system to be brought safely to rest. Overspeed and overwind protection should not rely on single-line components, but where this is not possible, they should be reliable and monitored to give warning of failure, or alternatively, should be fail-safe.

The accident at the Markham colliery could have been averted if the central rod inside the spring nest had been inspected more frequently.

2.5 Service Abnormalities and Abuses

Components can occasionally experience service abnormalities that were not anticipated but are capable of producing failures. These abnormalities could be unexpected overloads, temperature changes, environment changes, undesirable vibrations, and so forth. The following are some examples.

Example: In-Service Aeolian Vibrations: Failure of Transmission Line Insulators. Porcelain insulators with ball-ended pins are joined together as a tension chain and used in power transmission lines. In one such chain, running parallel to a mountain, on a windy day, one of the insulators broke at the step in the shank of the pin (Fig. 2.26, 2.27). The failure occurred due to the excitation of aeolian vibrations on the transmission line because of the wind velocity in the mountainous area. The step on the shank was sharp and the machined finish on the pin surface was coarse. This combination of factors promoted fatigue failure. Installation of vibration dampers, provision of a generous fillet radius at the step of the shank, and better surface finish would have prevented the failure.

Other Service Abnormalities. Ballooning or localized bulging of boiler tubes in thermal stations is not an uncommon phenomenon. Any obstruction to the normal flow of fluids inside the boiler tube can lead to a local rise in temperature, resulting in the weakening of the tube wall at the hot spot. Rise in temperature can also increase the alkali concentration of the water, which in turn can cause caustic cracking of the tube wall, thereby weakening the structure. Such failures may result in the shutdown of the entire plant. Good housekeeping is thus mandatory in such plants to avoid service abnormalities.

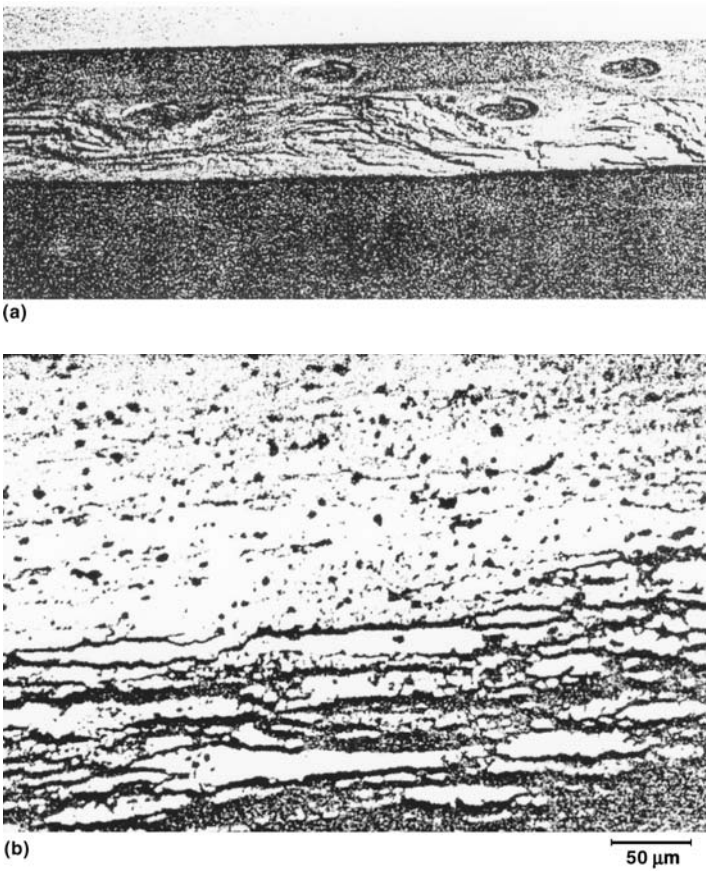

Fig. 2.28 Exfoliation corrosion on a structural member of an aircraft. (a) Cracking in the direction parallel to the rolled surface. (b) Cracks along the boundaries of elongated grains

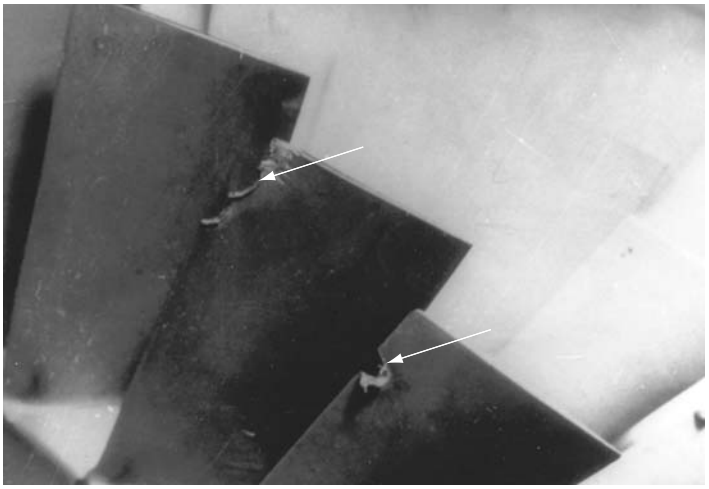

Fig. 2.29 Damage to fan blades of an aircraft engine by a foreign object

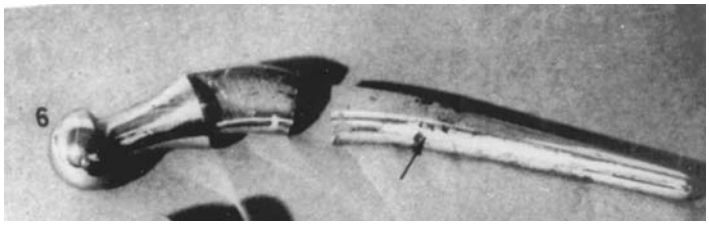

Fig. 2.30 Hip prosthesis failed by fatigue following fretting. Source: Ref 8. With kind permission of Chapman and Hall Limited

Abnormal temperature excursions in gas turbines result in creep deformation, cracking, and failure of nickel-base superalloy turbine blades.

A peculiar failure of electric traction rails was reported in the early 1950s (Ref 14). The rails failed in fatigue, originating from deep craters on the bottom surface. The craters had formed due to short circuiting.

Failures are also caused by abuses in service. It is an aphorism that if a product can be abused, it will be. Many a failure has been witnessed in various walks of life when products were abused without recognizing their load-bearing limitations.

2.6 Environmental Effects

Environmental effects include various types of corrosion, erosion, stress corrosion, fretting, and so forth. A number of case histories dealing with failures caused by environmental effects have been investigated and some of them are presented in subsequent chapters under different categories of components. Some categories are illustrated subsequently.

Exfoliation Corrosion: Deterioration of Aircraft Stringers. An aircraft parked in a seacoast area for a prolonged period had suffered extensive corrosive attack, and exfoliation corrosion on its aluminum alloy components had rendered them unsuitable for any further use (Fig. 2.28).

Foreign Object Damage of Turbine Blades. Damage to fan blades and compressor blades of aircraft engines by foreign object impact is a common phenomenon at airports. Figure 2.29 shows the damage to the leading edge of blades in an aircraft engine. Such situations call for immediate replacement of the damaged blades.

Fretting Damage: Failure of an Implant. Fretting is a phenomenon by which material removal from components takes place as a result of parts moving in close contact with each other. It is one of the sources of fatigue failure. Fretting is particularly dangerous in corrosion-resistant materials because the fretting action can abrade and remove the protective film responsible for corrosion protection and thereby expose the underlying metal to the aggressive environment. This is illustrated by the failure of a hip prosthesis that failed by fatigue following fretting (Ref 8). Figure 2.30 shows the hip replacement device that had to be removed from a patient after six years of use. During the first operation, for surgical reasons, a stainless steel wire loop had been placed in contact with the stem of the prosthesis. Continued movement of the wire loop had fretted the metal surface and initiated a crack in the stem that was exposed to the hostile environment of the interior of the human body.

2.7 Sabotage

Deliberate damages are caused by sabotage by antisocial elements. In almost every major accident, the first suspect is sabotage until disproved. Sabotage by deliberate detonation of powerful explosives has been practiced by such elements to cause destruction of structures, plants, and machinery. Such damages are characterized by certain fracture features and surface features that enable the investigators to identify explosive sabotage. Two major aircraft accidents were caused to Indian carriers by explosive sabotage (Ref 15, 16). Details of these investigations are described elsewhere in this volume.

REFERENCES

1. "Standard Terminology for Nondestructive Examinations, Metals Test Methods and Analytical Procedures," E 1316–00a, *Annual Book of ASTM Standards,* Vol 3.03, ASTM International
2. C.O. Smith, Products Liability and Design, *Failure Analysis and Prevention,* Vol 11, *ASM Handbook,* ASM International, 2004, p 71
3. A.C. Raghuram, S. Radhakrishnan, R.V. Krishnan, and V. Ramachandran, *Handbook of Case Histories in Failure Analysis,* ASM International, Vol 1, 1992, p 239
4. R.J. Parker et al., *The Flixborough Disaster—Report of the Court of Inquiry,* Her Majesty's Stationery Office, London, 1975
5. J.C. Mecklenburgh, *Inst. Chem. E. Symposium Series No. 45,* 1977, A-2-1
6. A. Joshi, L.E. Davis, and P.W. Palmberg, Auger Electron Spectroscopy, *Methods of Surface Analysis,* A.W. Czanderna, Ed., Elsevier, Amsterdam, 1975, p 159
7. S. Radhakrishnan, National Aeronautical Laboratory, Bangalore, India, private communication
8. E. Smethurst and R.B. Waterhouse, *J. Mater. Sci.,* Vol 12, 1977, p 1761
9. S. Radhakrishnan, A.C. Raghuram, R.V. Krishnan, and V. Ramachandran, *Handbook of Case Histories in Failure Analysis,* ASM International, Vol 2, 1993, p 299
10. W.R. Osgood, *Residual Stresses in Metals and Metal Construction,* Reinhold Publishing Corp., New York, 1954
11. R.K. Dayal, J.B. Gnanamoorthy, and P. Rodriguez, *Trans. Indian Inst. Met.,* Vol 5, 1979, p 421
12. E. Newton, *J. Royal Aero. Soc.,* Vol 68, 1964, p 156
13. J.W. Calder, *Accident at Markham Colliery,* Her Majesty's Stationery Office, London, 1974
14. S.C. De and T.V.N. Kidao, *Proceedings of the Symposium on Industrial Failure of Engineering Metals and Alloys,* National Metallurgical Laboratory, Jamshedpur, India, 1953, p 82
15. R.V. Krishnan, S. Radhakrishnan, A.C. Raghuram, and V. Ramachandran, Investigation of an Aircraft Accident by Fractographic Analysis, *Advances in Fracture Research,* Vol 5, S.R. Valluri et al., Ed., Pergamon Press, 1984, p 3677
16. B.N. Kirpal, V. Ramachandran, J.S. Gharia, J.S. Dhillon, J.K. Mehra, B.K. Bhasin, and S.N. Sharma, "Report of the Court of Inquiry Investigating Accident to Air India Boeing 747 Aircraft VT-EFO, Kanishka on 23 June 1985," New Delhi, 1986

Failure Analysis of Engineering Structures: Methodology and Case Histories
V. Ramachandran, A.C. Raghuram, R.V. Krishnan, S.K. Bhaumik, p19-23
DOI:10.1361/faes2005p019

CHAPTER 3

Failure Analysis Methodology

FAILURE ANALYSIS is a multidisciplinary activity. The approach to failure analysis and the methodology adopted are often governed by the expertise of the analyst. Because a single analyst may not be equipped with knowledge in various disciplines such as metallurgy, materials science, structural mechanics, corrosion engineering, propulsion engineering, aerodynamics, and so on, which may be necessary for analyzing a particular failure or accident, a team effort is always desirable to arrive at the correct solution to the problem.

3.1 Background Information

Whenever a failure analysis is to be carried out, at the outset, it is essential to collect the relevant background information. This facilitates the developing of a complete case history about the failure. The information to be collected falls into two groups:

- Information about the failed component
- Information about the failure itself

Information about the failed component includes:

- Name of the component, identification number, manufacturer, and user
- Location
- Intended function
- Service life since new
- Service life since last overhaul
- Design loads, actual service loads, and load orientation
- Frequency of loading
- Service parameters such as temperature, pressure, rotation, etc.
- Environment
- Materials of construction
- Specifications and codes
- Concessions given in the components
- Strength parameters
- Fabrication processes
- Thermomechanical treatments
- Surface treatments
- Inspection techniques and records
- Maintenance records
- Ad hoc modifications

Information about the failure itself includes:

- Date and time of failure/malfunction
- Extent of damage to the surrounding structure, personnel, etc.
- Operating conditions just prior to failure
- Service abnormalities
- Sketches and photographs of the failed component and surrounding areas
- Wreckage distribution map
- Eyewitness and earwitness accounts

The investigator should visit the failure site and make a firsthand examination and estimation of the damages. These should be documented immediately. Photography, preferably in color, is the best method of recording the damages for further detailed investigation. Any delay can alter the condition of the failed component because of handling by unauthorized people, environmental influences, and attempts to put the pieces together.

3.2 Location of the Failed Component

Determining and documenting the location of the failed component in a larger structure is an important task in the preliminary examination of a failure. The part may sometimes get thrown a considerable distance as in the case of a rotating component or in the case of a moving or flying vehicle. It is important to photograph the entire wreckage. Also, a wreckage distribution map in Cartesian or polar coordinates must be prepared. Secondary failures are not uncommon and may obliterate the primary failure. Hence, before selecting pieces for further laboratory examination, photographic documentation of the wreckage in the "as-is, where-is" condition should be completed.

The investigation itself should be properly planned. The various tests to be carried out must be judiciously selected and the sequence of tests should be carefully planned. Decisions on any test that would involve destruction of part of the component should be made very carefully. A wrong sequence of tests could destroy some of the important evidence or introduce features that could be confusing.

3.3 Specimen Collection

Collection of specimens for further laboratory examination is a crucial step in any failure analysis or accident investigation. This has to be done very judiciously. Wrong choice can, apart from wasteful work, lead to confusion and wrong direction of the investigation. Primary failure must be distinguished from numerous

secondary failures. Samples from the suspected primary failure region must be collected carefully, and their location in the wreckage and in the original structure must be recorded. Any other samples that can provide secondary or additional evidence must also be collected.

The fracture surfaces must be handled very carefully because they can provide a fund of useful information about the mode and mechanism of fracture during detailed laboratory examination. In the field, it is better to keep the samples in plastic covers with suitable desiccants and seal them and secure the bags with suitable identifying tags. The fracture surfaces may be sprayed with a transparent lacquer before sealing. Touching the fracture surfaces must be avoided because human sweat is a corrodant. The mating surfaces of a fracture should never be made to touch each other (though this is a normal, tempting tendency) because this would cause abrasion and thereby lead to loss of vital microfractographic evidences.

3.4 Preliminary Examination

Visual examination of the component and the fracture surface immediately reveals the presence of adhering debris and corrosion products; change in surface color, abrasion, and rub marks; metal slivers and burrs sticking out, and so forth. This examination also indicates the quality of workmanship in the manufacture of the component and any abuses the component might have experienced during service. The preliminary examination of the fracture surface is best carried out by naked eye or with a low-power microscope of the stereobinocular type. Documentation at this stage must be completed with the help of sketches and macrophotographs. Details of macrophotography are covered in another chapter.

3.5 Microscopic Examination

Detailed examination of the fracture surfaces should be carried out at various levels of magnification and resolution using optical and electron microscopes. These should be supplemented by metallographic examination of selectively chosen sections of the component. The fund of information that can be generated from these tests is phenomenal and is extremely useful to pinpoint the cause, mechanism, and sequence of the failure event. A separate chapter is devoted to cover these details.

3.6 Chemical Analysis

Chemical analysis of samples from the component provides information regarding any deviation from the standard specifications, compositional inhomogeneities, impurities, inclusions, segregations, and so forth. It also helps in identifying the nature of corrosion products, coatings, external debris, and so on. Analysis at microscopic levels provides information about the nature of inclusions, phases, and surface layers. Several cases of service failures are known to have been caused by the presence of deleterious inclusions from which cracks start in the component and propagate, leading to fracture. Certain impurities are known to cause embrittlement in metals. Segregation of constituent elements sometimes provides an easy path for crack propagation. Hence, identification of these harmful constituents is very important in failure analysis. A variety of instruments are available for bulk chemical analysis and microchemical analysis. The principles, capabilities, and limitations of these tools are described in detail in Ref 1 to 3. A few features are listed subsequently.

Techniques for average bulk chemical analysis

- *Spectrophotometry:* Applicable to nearly all elements and organic functional groups; accessible range, 0.001 to 50%; accuracy, 2 to 5%
- *Atomic absorption spectrometry:* Applicable to practically all elements; accessible range, 0.001 to 10%; accuracy, 2 to 5%
- *Emission spectroscopy:* Applicable to all elements; accessible range, 0.005 to 10%; accuracy, 2 to 5%
- *X-ray fluorescence analysis:* Normally applicable to elements heavier than sodium; accessible range, 0.005 to 10%; accuracy, 2 to 5%

Techniques for local composition variations

- *Laser probe microanalysis:* Applicable to nearly all elements; accessible range, 0.01 to 100%; accuracy, semiquantitative; lateral resolution, 20 to 200 μm
- *Electron probe microanalysis:* Applicable to elements heavier than boron; accessible range, 0.001 to 10%; accuracy, 5 to 10%; lateral resolution, 0.2 to 1 μm

Techniques for surface chemical analysis

- *Auger electron spectroscopy:* Applicable to all elements except hydrogen and helium; accessible range, >0.1%; accuracy, 5 to 10%; analysis depth, 10 to 20 Å
- *X-ray photoelectron spectroscopy:* Applicable to all elements except hydrogen and helium; accessible range, >0.01%; accuracy, qualitative and semiquantitative; analysis depth, 5 to 25 Å

3.7 Mechanical Properties

Evaluation of the mechanical properties of the component is an important step in any failure analysis. This process enables the investigator to judge whether the material with which the component is made meets the strength specifications and whether the component was capable of withstanding the service stresses. If the size of the failed component permits, samples can be taken from the component, and the conventional mechanical testing can be done by standard test procedures (Ref 4). A test for tensile properties is generally the most useful one in many cases. Other properties such as impact strength, toughness, and creep rupture provide clues for the mechanism of failure. Sometimes, even tests on miniature specimens would provide vital information. If the condition of the component does not permit tensile or other mechanical tests, even a hardness measurement would help in estimating the tensile strength. This method has been adopted in quite a few failure cases. Defects due to improper processing or inadequate heat treatment would result in poor mechanical properties.

In some situations, evaluation of the mechanical properties of components that have not yet failed but are still in service may be necessary. For this, a device for extracting miniature samples from components without destroying their integrity has been developed by Exponent Failure Analysis Associates (Ref 5). Using the miniature sample, the fracture toughness properties can be evaluated by the small punch test developed by them under the sponsorship of the Electric Power Research Institute (Ref 6).

3.8 Nondestructive Evaluation

Most of the failures are the end result of cracks originating in the component from flaws that already existed or that formed during service. Nondestructive evaluation (NDE) is employed to detect at an early stage subsurface flaws and internal flaws in the component, their type, size, orientation, and location. In a failed component, there may still be flaws similar to the one that was primarily responsible for the failure. These flaws can be detected by NDE methods. Also, flaws in similar components from the same batch as the failed one can be detected so that their use can be avoided or restricted. Various techniques are available for examining a component for flaws without actually destroying it. Their principles and typical applications are described in Ref 7. For detecting any one type of flaw, more than one technique can be adopted. These methods are summarized subsequently. Most of the conventional techniques are applicable to a variety of components, including castings, forgings, tubular products, weldments, billets and bars, boilers, and pressure vessels.

3.8.1 Conventional Nondestructive Evaluation Techniques

Visual examination is an easy and widely used method for detecting surface flaws in a variety of components. Visual examination is carried out with the naked eye and with instruments such as borescopes and interference microscopes. Borescopes are very handy for examining surface flaws in inaccessible areas of structures.

Liquid Penetrant Testing. In this method, a liquid of low surface tension is allowed to penetrate into surface flaws and a visible indication is developed. It detects only discontinuities open to the surface, in metals and ceramics. This can be based either on a color dye or a fluorescent dye.

Magnetic Particle Testing. A magnetic field is created in the component by suitable magnetization. Any surface or subsurface discontinuity can be revealed by magnetic powder particles that collect wherever the magnetic field is broken. This technique is applicable only to components made of ferromagnetic materials.

Eddy Current Inspection. Eddy currents are induced in the component by an electrical coil. Discontinuities in the component are detected as they alter the path of the induced current. The method is useful for detecting surface and subsurface flaws, for sorting dissimilar metals, for detecting variations in composition and microstructure, and for measuring the thickness of nonconductive coatings. The method is limited to conducting materials.

Radiography using x-rays, γ-rays, and neutrons uses penetrating electromagnetic radiation or particle radiation. Internal flaws are detected by the difference in absorption of the radiation by the various regions of the component. Flaws in the component are recorded permanently on a film or examined on a fluorescent screen. In x-radiography, the size of the flaw can be estimated by using penetrameters. Gamma rays have greater penetrating power than do x-rays and hence can be used for thicker sections. They are obtained by the radioactive decay of isotopes such as cobalt 60, cesium 137, thulium 170, or iridium 192. Gamma ray equipment is very useful for fieldwork. In neutron radiography, thermal neutrons from a reactor are made to impinge on the component and the emitted β-rays are made to expose a film. Depth of penetration is much more than in conventional radiography. Radiographic techniques are extensively used for the NDE of castings, weldments, boilers, and pressure vessels.

Ultrasonic inspection is used for detecting surface and subsurface flaws in metals, ceramics, and polymers. Ultrasonic waves are sent through the component. From the reflected waves, flaws such as cavities, cracks, bursts, debonds, and inclusions are detected and their locations and size are determined.

3.8.2 Special Techniques

In addition to these conventional NDE techniques, there are certain other techniques that are employed under special circumstances.

Acoustic Emission. Acoustic emissions are stress waves produced in components and structures when some form of internal movement of defects takes place under stress. The movement can be that of dislocations or propagation of cracks. The conventional NDE techniques detect existing flaws in components whereas acoustic emissions are associated with defect movement. The technique is complementary to other techniques. It has been extensively used in the testing of aircraft, ground vehicles, buildings, pipelines, rotating machinery, tanks, pressure vessels, and so on, as well as in monitoring wear, corrosion, machining, welding, fluid flow, and so forth. It is a condition-monitoring technique and is very useful in predicting failures.

Computed Tomography (CT). In this technique, a thin beam of radiation, generally x-rays, is made to pass through the component and the image of a thin cross-sectional slice is detected. The beam, and the detector, which is usually a linear array of radiation sensors, are in the same plane as the surface imaged. The attenuation of the radiation is related to the thickness, density, and composition of the material. By scanning and collecting the attenuation data from different angles, the image of the component is reconstructed by a computer. The technique can be used for detecting voids, inclusions, porosity, density variations, cracks, and machining defects in metals and delaminations in composites.

The electric current perturbation method (ECP) is suitable for nondestructive examination of surface and subsurface defects in electrically conducting nonferromagnetic materials. When an electric current, either ac or dc, passes through a component, a magnetic flux is generated. Where there is a flaw, the current flow is disturbed and the magnetic flux density is changed. With a magnetic field sensor, this change in flux density is detected. By scanning the entire surface, the position of the flaws such as notches

and cracks is determined. The technique has been adopted to detect surface flaws in aircraft engine components.

Acoustic Microscopy. High-frequency ultrasound in the GHz range is passed through the component of interest. The transmitted wave is detected by a rapidly scanning laser beam on the opposite surface. Transmission of these waves is interrupted by flaws present in the material. The attenuation of the ultrasound differs between homogeneous regions and regions with flaws. The resulting image has characteristic light and dark features. Variations of this technique include reflection type imaging by scanning a transducer in a raster pattern over the sample surface. The method has been successfully applied to detect flaws in metals, ceramics, composites, and microelectronic components.

X-ray diffraction is a common method for identifying phases in metallic materials, corrosion products, and surface deposits. Several cases of component failures due to locked-in residual stresses have been encountered in service. Residual stresses can readily be determined by x-ray diffraction method. Textures in metals that have a bearing on their mechanical behavior can be determined through pole figure computation through x-ray diffraction.

3.9 Simulation Studies

Quite often, it is helpful to test the component under simulated service conditions. Such studies throw light on the suitability or otherwise of the material of construction, the adopted design, and the processing history of the component in question. If components from the same batch as that of the failed component did not fail during simulation tests, then the cause of the failure is singular to the particular failed component. Also, examination of a similar component in service that has not failed would provide additional useful information. The simulation test paves the way for further investigation into other possible causes.

3.10 Analysis of Data

The most important task in any failure analysis is the consolidation and systematic connection of all the data obtained in the tests just described. For every failure, all of these tests may not be necessary. The results of tests must be compared against the specifications and deviations, if any, and should be carefully considered as possible contributing factors. At this stage, expertise from other related disciplines would be quite useful in interpreting the data.

A fund of information on various aspects of the failure would become available through a proper analysis. These include the failure initiation site or sites, crack length, its propagation path and speed, and the nature and direction of load acting on the component. The role of other factors such as temperature, corrosion, wear, component manufacturing history, assembly and alignment, repair and maintenance history, service abnormalities, and abuses, if any, would also become clear during the analysis. Ultimately, the sequence of the failure would get established, differentiating between the primary cause of the failure event and the consequential secondary failures and damages.

In complex systems, a number of causes may be seen to lead to the failure. Detailed investigation into each of these causes may be time consuming and prohibitively expensive. A systematic logical deduction technique called the "fault tree technique" is available, and it helps in identifying the basic events whose combinations could lead to the failure. Details of this technique and its applications are described elsewhere.

Finally, it must be borne in mind that in some cases, it may not be possible to specify with certainty the cause or causes of the failure. At the most, one may be able to indicate the most probable cause among various possibilities. In such cases, it must be stated clearly which conclusions are based on determined facts and which are based on conjecture and circumstantial evidence.

3.11 Preparation of the Report

For effective communication of the results of failure analysis, documentation is extremely important. The report should be clear and contain the logic behind the conclusions. The following components form the essential sections of the report:

- Description of the failed component
- Circumstances leading to the failure
- Operational parameters and conditions at the time of failure
- Background history
- Visual examination of general physical features
- Laboratory investigations including metallurgical, mechanical, chemical, and other tests and their results
- Anomalies, if any
- Discussion of mechanism or possible mechanism of failure and sequence of events
- Conclusions and recommendations for the prevention of recurrence of such failures
- References to relevant literature
- Summary

In addition to these elements, the report should contain an executive summary to enable the management to take appropriate action at various levels for avoiding future failures.

It is extremely important for the investigator to keep track of the follow-up action based on his or her recommendations. Continued interaction with the designer, manufacturer, and operator is highly desirable.

Failure analysis is a challenging task. It is exciting, and the analyst learns something new in every failure. If the analysis is carried out with utmost care and caution, the effort will be amply rewarding.

REFERENCES

1. A.W. Czanderna, Ed., *Methods of Surface Analysis,* Elsevier, Amsterdam, 1975
2. S.R. Rajagopalan, Chemical Analysis: A Tool for Failure Investigation, *Proceedings of the Workshop on Fracture, Fatigue and Failure Analysis,* National Aeronautical Laboratory, Bangalore, India, 1979

3. *Materials Characterization,* Vol 10, *Metals Handbook,* 9th ed., American Society for Metals, 1986
4. *Mechanical Testing,* Vol 8, *Metals Handbook,* 9th ed., American Society for Metals, 1985
5. J.D. Parker, A. McMinn, and J. Foulds, Material Sampling for the Assessment of Component Integrity, *Life Assessment and Life Extension of Power Plant Components,* T.V. Narayanan et al., Ed., PVP, Vol 171, American Society of Mechanical Engineers, 1989
6. J.R. Foulds, P.J. Woytowitz, T.K. Parnell, and C.W. Jewett, Fracture Toughness by Small Punch Testing, *J. Test. Eval.* (JTEVA), Vol 23 (No. 1), Jan 1995, p 3
7. *Nondestructive Evaluation and Quality Control,* Vol 17, *Metals Handbook,* 9th ed., ASM International, 1989

Failure Analysis of Engineering Structures: Methodology and Case Histories
V. Ramachandran, A.C. Raghuram, R.V. Krishnan, S.K. Bhaumik, p25-30
DOI:10.1361/faes2005p025

CHAPTER 4

Examination Methods

IN FAILURE ANALYSIS, examination is done at various levels of magnification and resolution to provide a wealth of useful information about the failed component (Ref 1, 2). The origin of a crack, the crack propagation mode, the direction of crack propagation, the extent of deformation prior to failure, deterioration due to corrosion and wear, and type of loading responsible for the failure are some of the important features revealed by microscopy. These details are extremely useful in determining the mechanism of failure of components. In the investigation of major failures where a machine or structure has broken into a multitude of pieces, the microscopic processes can help in isolating the region of primary failure from those of subsequent or secondary failures.

Examination in failure investigations is generally carried out by three techniques: macroscopy, optical microscopy, and electron microscopy. In this chapter, the usefulness of examination at these three levels in failure analysis is described with examples.

4.1 Macroscopic Examination

Macroscopic examination is carried out with unaided eye or a simple handheld magnifier, or a stereobinocular microscope with a magnification generally below 100 diameters. In the stereobinocular microscope, reasonably large specimens can be handled, and the microscope can easily be adopted for examination of components in the field or accident site. The amount of information one can obtain by macroscopic examination is remarkable. The features revealed during macroscopic examination are:

- Type of fracture
- Origin of fracture
- Presence of secondary cracks
- Presence of external debris or corrosion products
- Discoloration
- Presence of wear marks in the vicinity of fracture
- Plastic deformation preceding fracture
- Dimensional changes in the component
- Evidence of any overheating
- Post-fracture damage such as rub marks

The aim of macroscopic examination is to have a general appreciation of the features of the failed component and, in particular, the fracture surface. When a component fractures, certain distinct features can be observed on the fracture surface. These features may be termed the signatures of fracture. These signatures are characteristic of the type of loading and the relative ductility or brittleness of the component. The science of studying the fracture surface is termed *fractography.* Thus, depending on the level of examination, one can have macrofractography and microfractography.

4.1.1 Macrofractography

The signatures of fractures on the fracture surfaces can easily be lost or obliterated by subsequent damages caused by oxidation (as in the case of fire or thermal exposures), corrosion, abrasion due to improper handling, and so forth, and hence, the fracture surfaces should be carefully handled and preserved. Oil and grease on the fracture surface can be removed with organic solvents. The corrosion and oxidation products often hide the true fracture surface beneath. Fine fissures on the surface of these corrosion products may sometimes mislead because they do not represent the real features of the original fracture surface. Mild chemicals such as acetic acid, phosphoric acid, sulfamic acid, ammonium oxalate, ammonium citrate, and NaOH, in dilute solutions, and 6N solution of HCl inhibited with 2g/l hexamethylene tetramine, are available for the removal of these layers. However, the best method of cleaning the fracture surface is by a blast of air followed by repeated cleaning with replicating tape until the tape comes out clean and free from adhering debris, as described later.

One of the features often revealed by macrofractography is the origin of fracture. In many instances, the origin is apparent even to the naked eye. Once a crack is initiated, then during the propagation of the crack, other features such as radial lines, chevron marks, and beach marks develop and are left behind.

A ductile tensile fracture in a component of circular cross section consists of three distinct zones (Fig. 4.1) (Ref 3). The inner flat zone with a fibrous appearance is where the fracture starts and grows slowly. The fracture propagates fast along the intermediate radial zone. The radial lines extended backward point to the fracture origin. Sometimes the radial lines start from the origin itself. The fracture finally terminates at the shear lip zone that is the annular region near the periphery of the fracture surface. The shear lip zone is at an angle of 45° to the tensile stress direction.

Fast, unstable crack propagation may sometimes be manifested as a series of chevron marks or herringbone pattern on the fracture surface (Fig. 4.2). The apexes of these chevrons point to the origin of fracture.

In fatigue failures, the origin is indicated by the presence of beach marks or clam shell marks, which also signify the direction of advancement of the crack (Fig. 4.3). Fatigue failure is also char-

acterized by the presence of a smooth region on the fracture surface denoting the crack propagation zone and a rough region indicating the final rapid overload failure. Because of longer exposure to the environment, the smooth fatigue crack propagation region appears slightly tarnished, whereas the final fracture appears relatively bright. When there are multiple fatigue crack origins, for example, in a shaft, the approaching cracks meet and form a step. This results in a series of small steps or ratchet marks around the periphery of the fracture surface (Fig. 4.4).

Ductile fractures are characterized by significant plastic deformation prior to fracture. Unlike in fatigue failures, the origin is not so well defined in ductile fractures. Dimensional changes in the failed component also denote effects such as wear, erosion, and corrosion. In some materials, thermal excursions experienced by the component can be discerned by the oxidation colors on the surface. Blueing of steels is an example.

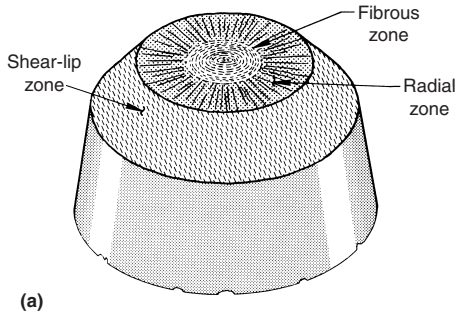

(a)

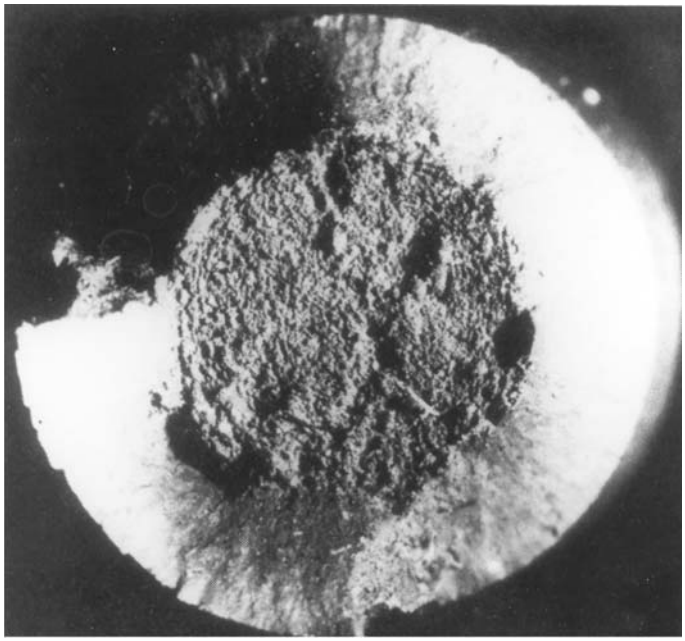

(b)

Fig. 4.1 The three distinct zones on the fracture surface of a ductile material failed under tensile load. Source: Ref 3

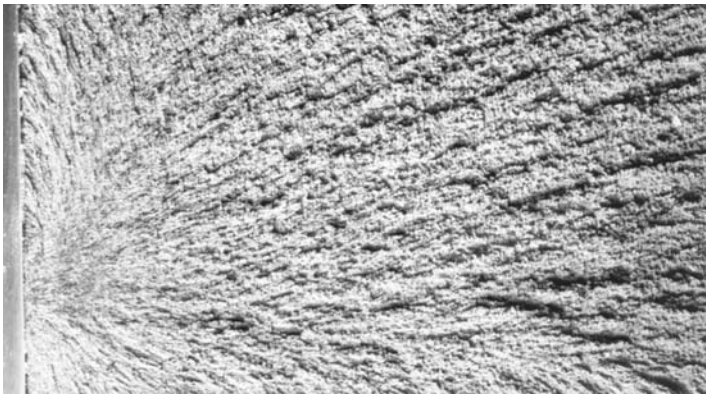

Fig. 4.2 Chevron marks indicating fast fracture

4.1.2 Other Macro Features

Macroscopic examination after some sectioning and surface preparation can provide additional information about the malfunctioning or failure of certain components. Two such cases are illus-

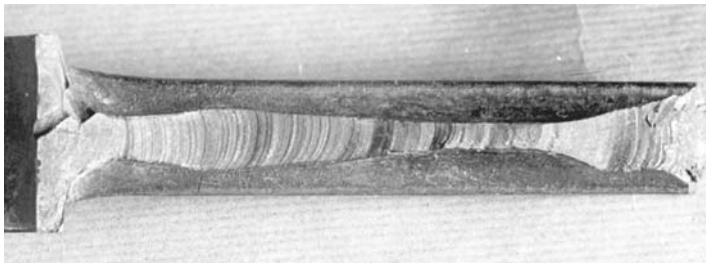

Fig. 4.3 Beach marks characteristic of fatigue fracture. Source: Ref 3

Fig. 4.4 Ratchet marks around the perimeter of a shaft that failed in fatigue indicate multiple origins of fracture.

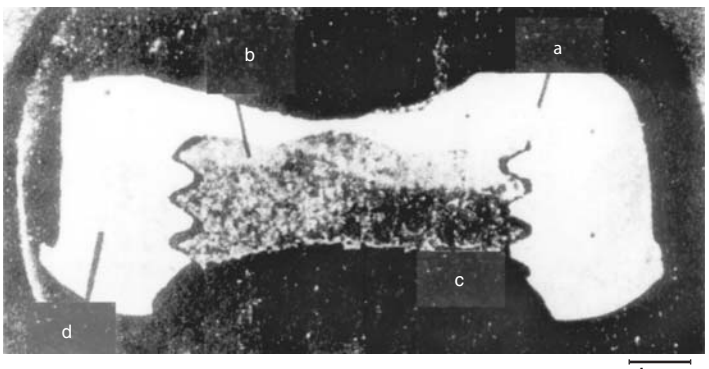

Fig. 4.5 Polished and etched longitudinal section of a bolt-nut assembly. The bolt and nut are held together by very few threads.

trated here. It must be noted that sectioning is a destructive operation and should be conducted only if necessary and after completing the microfractography described later in this chapter.

In a turbogenerator, the turbine was coupled to the gear box by a set of bolts and nuts. In addition, the nuts were also welded to the bolts. One of the nuts failed and the turbine was separated from the gear box, resulting in a catastrophe. Macroscopic examination after sectioning the bolt-nut assembly in the longitudinal direction and polishing clearly indicated that only a few threads were holding the nut to the bolt (Fig. 4.5). Further, the welding operation had altered the microstructure of the bolt in the heat affected zone, rendering it brittle.

In metal forming operations, the metal flows in specified directions, depending on the tooling and the forces employed. The direction of metal flow can be delineated by revealing the flow-line pattern. This is done by sectioning the component, grinding, polishing, and deep etching. The flow-line pattern can be discerned by macroscopic examination. Discontinuities in the flow-line pattern are sources of material weakness and can eventually lead to service failures. These are common in forged components having disrupted flow-line patterns (Fig. 4.6). This technique has been useful in the analysis of failures of such components as crane hooks, crankshafts, and so forth.

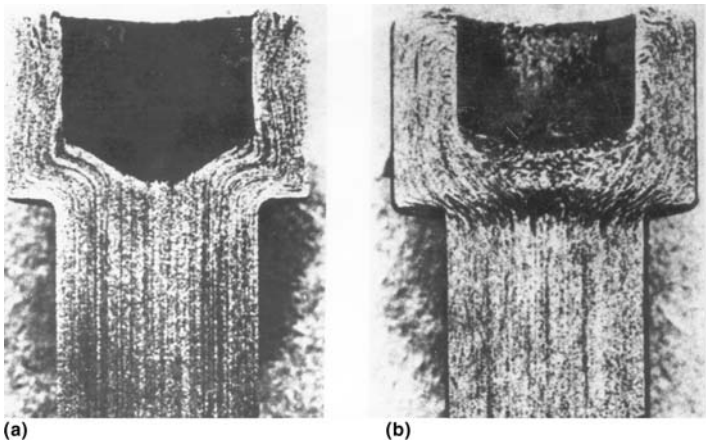

Fig. 4.6 Comparison of (a) desirable and (b) undesirable flow lines in forged components. Source: Ref 4. With kind permission of Elsevier Publishing Company

4.2 Microscopic Examination

The information thus gathered at the macroscopic level has to be integrated with the observations on detailed examination at the microscopic level so that meaningful conclusions can be drawn regarding the cause of failure. Microscopic examination is carried out using optical microscopes and electron microscopes, the choice dictated by the magnification and resolution desired. Microscopic examination is carried out on the fracture surface to study the fracture features and also on a section transverse to the fracture surface to study the internal structure of the material. The latter is a destructive test and should be carried out only at the end after recording all the microfractographic features. The additional information one can obtain through microscopy includes:

- Microstructure of the material through metallography
- Path of fracture
- Mode of fracture
- Length of the crack that preexisted and propagated by fatigue
- Length of the fatigue crack before it became critical
- Presence of inclusions, pits, or other flaws at the origin
- Striation spacing of the fatigue crack
- Presence of corrosion products

The length of the fatigue crack and the striation spacing are of importance in fracture mechanics calculations.

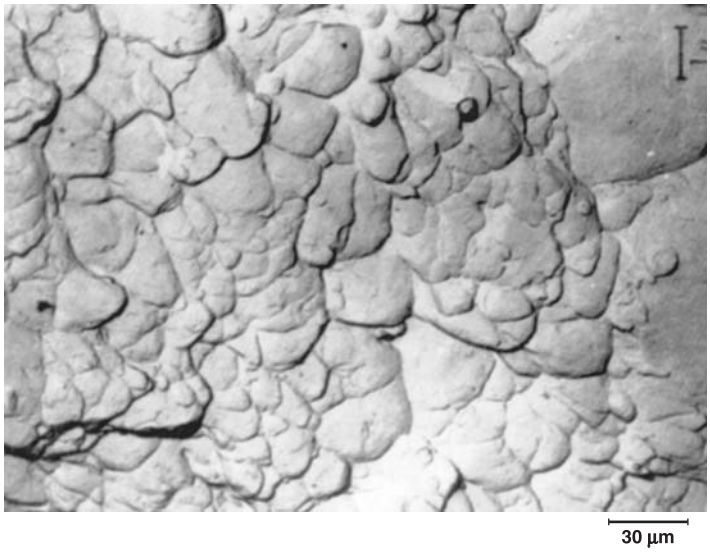

Fig. 4.7 TEM fractograph showing equiaxed dimples caused by tensile overload. Source: Ref 5. With kind permission of Metals and Ceramics Information Center

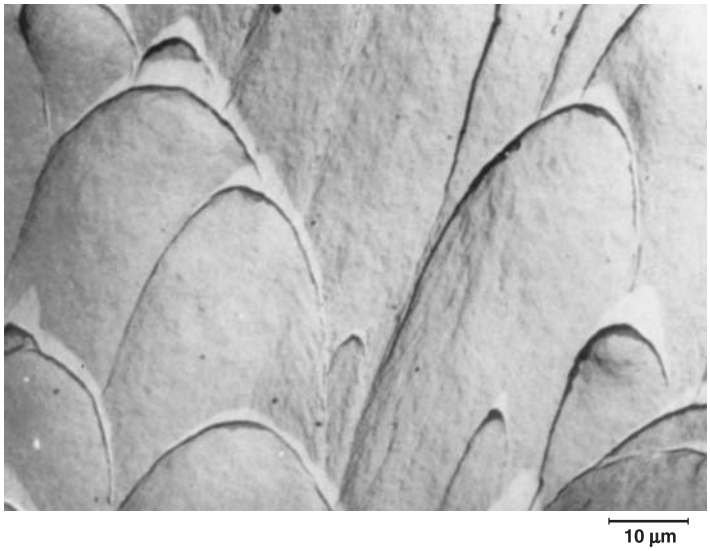

Fig. 4.8 TEM fractograph of a shear fracture, characterized by open-ended dimples. Source: Ref 5. With kind permission of Metals and Ceramics Information Center

4.2.1 Microfractography

The fracture surfaces are generally rough and cannot be easily studied entirely by an optical microscope because of its limited depth of focus and resolution. However, the optical microscope can be used in failure analysis for certain other tasks described in a later section. For microfractography, instruments with better depth of focus and resolution are necessary. These requirements are met by the electron microscope of which there are two types: the transmission electron microscope (TEM) (Ref 5) and the scanning electron microscope (SEM) (Ref 6, 7). The latter is more convenient for rapid examination of fracture surfaces.

Transmission Electron Microscopy. For many years, TEM has been a powerful tool for the study of fracture surfaces at high magnifications. However, its use in microfractography has become less frequent since the advent of SEM. A failed specimen cannot be directly placed for study in a TEM because bulk metals are not transparent to electrons. A plastic replica of the fracture surface is prepared. Replication is usually done in two stages. A replicating tape made of cellulose acetate, softened in acetone, is pressed on the fracture surface with a piece of soft rubber and allowed to dry. The tape is slowly peeled off. In this process, the debris adhering to the fracture surface gets removed. The process is repeated a few times until a clear replica is obtained. This replica carries a negative impression of all the features on the fracture surface. The plastic replica is then placed in a vacuum chamber and shadowed at an angle with a thin layer (about 200 Å) of a heavy metal such as gold, chromium, or platinum. The replica is then uniformly coated with a carbon film of about 300 Å thickness. The shadowing helps in obtaining better contrast of the image produced in the TEM. The coated replica is then sliced into small pieces, and the plastic backing is dissolved in acetone, leaving behind a positive replica of heavy-metal-shadowed carbon. This is then lifted onto a copper grid. This specimen is examined in the TEM, the features observed on a fluorescent screen and recorded in a pho-

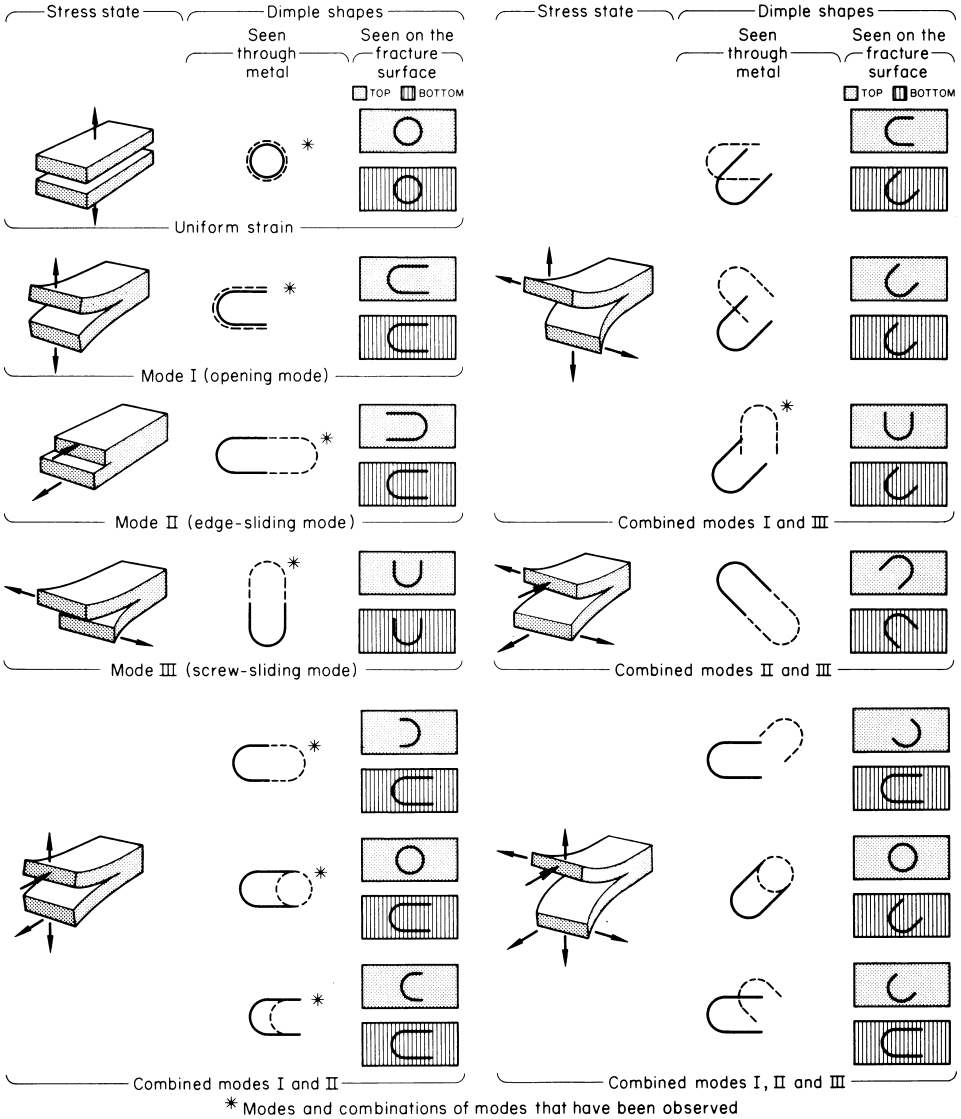

Fig. 4.9 Possible combinations of mating dimple shapes resulting from different stress states, which cause the crack tip to deform by various modes. Source: Ref 3

tographic film. The image is then interpreted to throw light on the mechanism of fracture.

Figure 4.7 is a typical TEM fractograph of a ductile material failed by overload in tension. Tensile overload fracture is caused by the coalescence of microvoids in the material and is manifested as equiaxed dimples in the magnified electron fractograph. If the ductile failure is due to shear forces, for example, as in torsion fractures, the dimples will be elongated, with an open end (Fig. 4.8).

The shape and orientation of the open-ended dimples depend on the loading conditions leading to fracture and thus on the state of stress and plastic flow at the crack tip. These are described by Beachem (Ref 3) and illustrated in Fig. 4.9.

One difficulty in the use of TEM for fractography is that for a given point on the fracture surface, the corresponding point on the image is difficult to locate unless laborious procedure is adopted by imaging the replicas placed on numbered grids. Presently, TEM observation is carried out only when observation at high resolution is called for, for example, in the observation of high-cycle fatigue striations.

Scanning Electron Microscopy. The difficulties in the use of TEM for fractography are significantly mitigated in the SEM. In this, the failed specimen can be directly placed in the microscope for viewing. Modern SEMs can accommodate specimens as large as 50 mm in diameter. A primary beam of electrons is moved to

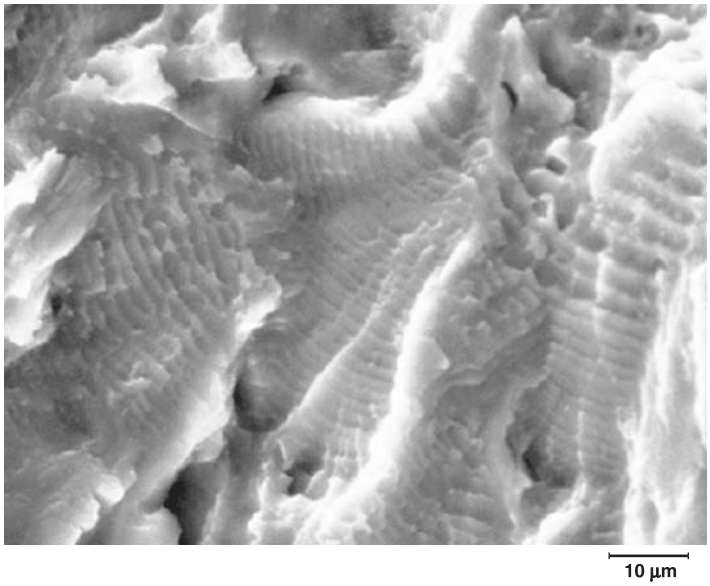

Fig. 4.10 SEM fractograph showing fatigue striations

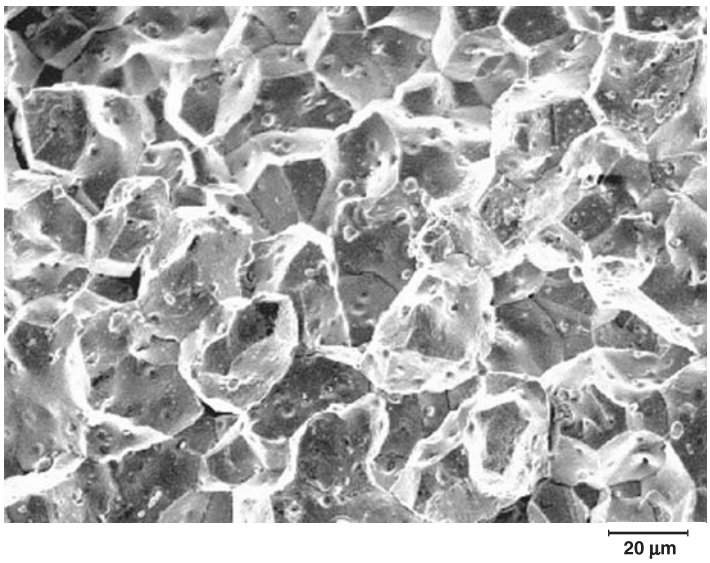

Fig. 4.11 SEM fractograph of an intergranular fracture caused by hydrogen embrittlement in a high-strength steel component

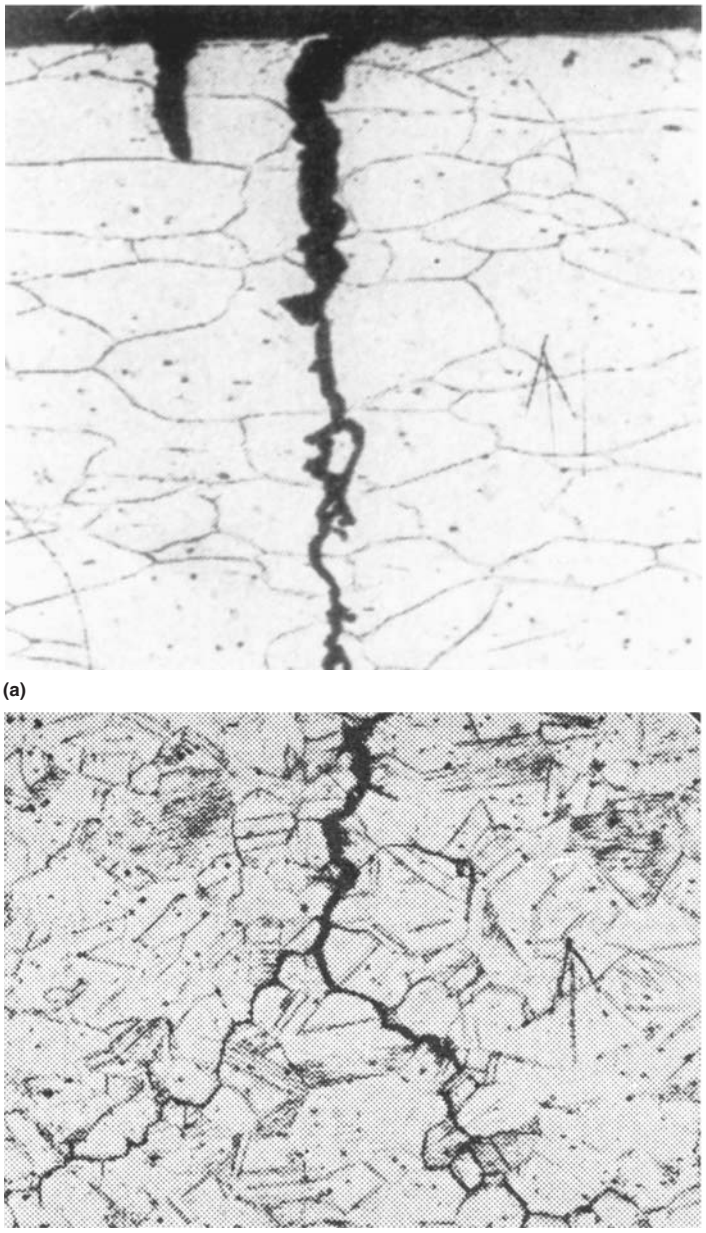

Fig. 4.12 Optical microstructure showing (a) transgranular and (b) intergranular crack propagation. Source: Ref 4. With kind permission of Elsevier Publishing Company

scan the specimen surface, line by line. The signals emanating from the surface of interest, especially the secondary electrons and the backscattered electrons, produce points of varying intensity to form the image. Because of the high depth of focus, all the undulations on the fracture surface will be simultaneously in focus in the final image. For any point on the specimen surface, the corresponding point on the image can be easily located. Any local point can be examined further in the SEM at higher magnifications to obtain more details. Figure 4.10 is a SEM fractograph showing the striations in a component failed due to fatigue. The striations have a curvature with center at the origin of fracture. A SEM fractograph of an intergranular fracture in a high-strength steel component due to hydrogen embrittlement is shown in Fig. 4.11.

When the electron beam strikes a point on the specimen surface in the SEM, x-rays are emitted, and these are characteristic of the chemical elements present in the specimen. Thus, with an x-ray spectrometer used in conjunction with a SEM, in situ chemical analysis can be carried out. This facility is very useful in failure analysis. For example, nonmetallic inclusions are deleterious in metal components. Cracks can originate from these inclusions and propagate during service, leading to failures. These inclusions can be seen in the SEM and in situ chemical analysis carried out to determine their identity. With this information, the source of the inclusions such as the melting practice can be traced and steps taken to eliminate them.

Metallography. The metallurgical microscope is yet another instrument very useful to the failure analyst (Ref 8–10). After collecting all the information through fractography of the failed component, a section of the component can be cut transverse to the fracture surface. This section is then polished and examined in the metallurgical microscope, both before and after etching. Inclusions present in the material are observed on the as-polished surface. The inclusion rating can be determined by standard quantitative microscopy techniques. By differences in color, reflectivity, and refractive index, they can also be identified with some prior experience.

The polished specimen is then etched with suitable etchants to reveal the microstructure of the material. Abnormalities in the microstructure that may have been responsible for the failure can be identified at this stage. The path of a crack, whether it is intergranular or transgranular, and branched or not branched, will be clear in the microstructure. Cracks due to stress corrosion, hydrogen embrittlement, and liquid metal embrittlement are generally intergranular with some exceptional situations. Fatigue cracks are transgranular. If a stress-corrosion crack propagates by fatigue, the transition from intergranular to transgranular mode can be seen in the microstructure. Stress-corrosion cracks in certain stainless steels are transgranular with extensive branching. Plastic deformation of the component prior to fracture can be recognized in the microstructure by the elongated grains. Abnormal grain growth, segregation of brittle or weak phases at the grain boundaries, and recrystallization are some of the other features that can be identified by metallography. Figure 4.12 shows the intergranular and transgranular modes of crack propagation, revealed by metallography.

REFERENCES

1. J.L. McCall and P.M. French, *Metallography in Failure Analysis,* Plenum Press, New York, 1978
2. I. LeMay, Use of Microscopy in Failure Analysis, *Applied Metallography,* G.F. Vander Voort, Ed., Van Nostrand Reinhold Co., New York, 1986
3. *Fractography and Atlas of Fractographs,* Vol 9, *Metals Handbook,* 8th ed., American Society for Metals, 1974
4. V.J. Colangelo and F.A. Heiser, *Analysis of Metallurgical Failures,* Wiley-Interscience, New York, 1974
5. G.F. Pittinato, V. Kerlins, A. Phillips, and M.A. Russo, *SEM/TEM Fractography Handbook,* Metals and Ceramics Information Center, Battelle Columbus Laboratories, Columbus, 1975
6. A. Phillips, V. Kerlins, R.A. Rawe, and B.V. Whiteson, *Electron Fractography Handbook,* Metals and Ceramics Information Center, Battelle Columbus Laboratories, Columbus, 1976
7. L. Engel and H. Klingele, *An Atlas of Metal Damage,* by S. Murray, Trans., Wolf Publishing Ltd., London, in association with Carl Hanser, Verlag, Munich, 1981
8. G.L. Kehl, *The Principles of Laboratory Metallographic Practice,* 3rd ed., McGraw Hill Book Co., New York, 1949
9. G.F. Vander Voort, *Metallography Principles and Practice,* McGraw Hill Book Co., New York, 1984
10. *Failure Analysis and Prevention,* Vol 11, *Metals Handbook,* 9th ed., American Society for Metals, 1986

Failure Analysis of Engineering Structures: Methodology and Case Histories
V. Ramachandran, A.C. Raghuram, R.V. Krishnan, S.K. Bhaumik, p31-44
DOI:10.1361/faes2005p031

CHAPTER 5

Advanced Techniques of Failure Analysis

WITH THE EVOLUTION of the methodology of failure analysis, and keeping pace with the complexities of failures in modern intricate machines and structures, newer techniques have been established for carrying out the various stages of failure analysis. Some of these techniques are described in this chapter.

5.1 Material Sampling (In-Service and Post-Fracture)

It is often necessary to remove a sample of material from a failed component to assess its quality and conformation to specifications. Also, in aging power plants and process plants, condition monitoring becomes necessary for evaluating the fitness of the plant for continued service and life prediction. In these cases, the effects of in-service degradation such as graphitization, temper embrittlement, radiation embrittlement, cracking, and so forth have to be assessed by a variety of tests.

Various techniques are used to evaluate in-service degradation or post-fracture properties of components. For example, portable instruments for grinding, polishing, etching, and microscopic examination are often used to evaluate the microstructure of in situ components without compromising the integrity of the components (e.g., Ref 1). This includes preparation of replicas from the polished surfaces of a component when circumstances do not allow examination with a portable microscope.

Extraction of miniature samples is another technique. Replicas cannot yield some information, such as chemical makeup or mechanical properties of the workpiece. Therefore, it is sometimes necessary to cut a small sample from the component to conduct additional testing. In this case, a small "boat" sample or "plug" sample can be taken from a noncritical location on the workpiece. As noted in Ref 1, a handheld hacksaw or a portable band saw can be used to remove the sample. A handheld grinder fitted with an abrasive cut-off wheel also can be used. For very hard materials, a boron nitride-coated blade may be sufficient to cut a sample. In some cases, a diamond-impregnated hole-drilling saw blade can be used to extract a small cylinder of material. For hard materials, an electrodischarge machining device can be used to provide a pin sample (Ref 1).

Specially designed devices for sample extraction are also available. For example, surface-sampling devices (e.g., SSam, developed by Failure Analysis Associates) can recover undeformed specimens from a component without compromising structural integrity. A thin, waferlike sample is removed with negligible effect on the integrity of the component, due to the geometry and smooth depression. This device removes samples up to 2.5 mm thickness and 2.5 cm diameter. It can be operated by remote control and can be used externally or internally on any surface for which there is at least a working clearance of 7.5 cm. The device uses a hardened steel hemispherical shell cutter, 5.0 cm diameter, 0.25 mm thickness, with cubic boron nitride grit applied to the edge. Figure 5.1 shows schematically the cutter head.

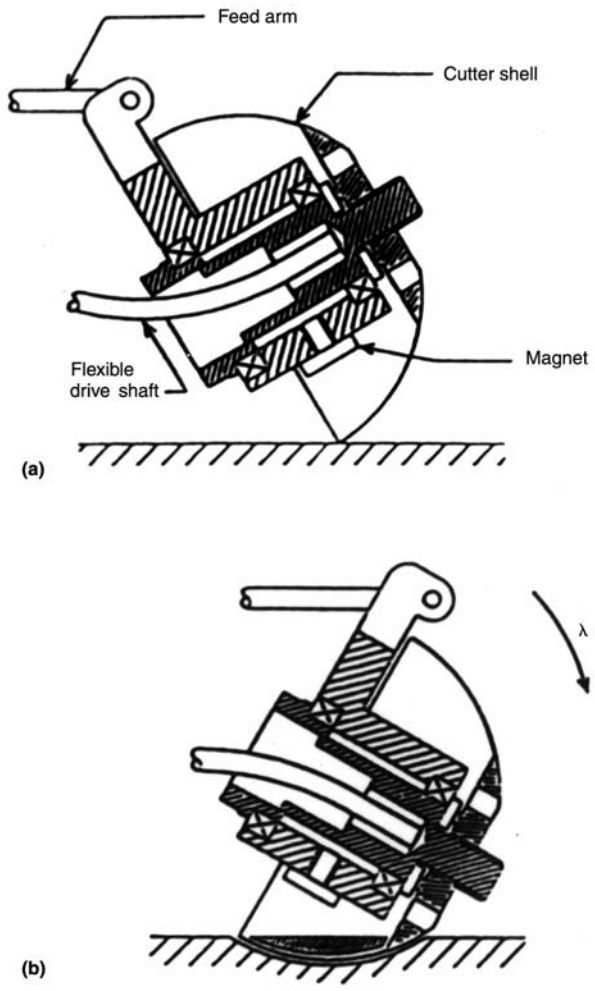

Fig. 5.1 SSam surface sampling system: schematic of cutting process. Source: Ref 2. With kind permission of Exponent Failure Analysis Associates

As described in the following section, bulk mechanical properties can be obtained from miniature samples by punch testing. Creep properties can be obtained by indentation testing of miniature samples. In addition, the chemical composition, microstructure, fabrication history, and extent of microdamage can also be assessed (Ref 2). The technique has been successfully used to monitor the condition of power plant components such as main steam pipe weldments; turbine-generator rotors; steam turbine disks; steam control valves; headers; piping; heat exchangers; and chemical, petrochemical, and nuclear reactor vessels.

5.2 Fracture Parameters by Small Punch Testing

A test method has been developed by Exponent Failure Analysis Associates under the sponsorship of Electric Power Research Institute (EPRI) for evaluating the fracture toughness properties of samples from aging plants through a punch test (Ref 3–5). The volume of sample material required for conventional fracture toughness testing is so large that direct testing is not practical in the case of many in-service components because material removal would seriously affect the integrity of the component. Also, it is very desirable to know the fracture toughness at the location of interest in the component. The method developed uses miniature specimens, 6.4 mm diameter and 0.5 mm thick. The method is material-independent, requires no prior knowledge of the mechanical properties, and is based on analytical interpretation.

The test consists of punching a flat specimen with a ball or hemispherical head punch. The punch is advanced at a constant displacement rate, deforming the specimen against a die. The load is recorded as a function of the punch displacement. A borescope with a video camera is used to examine continuously the bulged specimen surface for detecting crack initiation. The video image is synchronized with the load-displacement record and, thus, the point of crack initiation on the load-displacement curve is defined. The spatial location of the crack on the specimen surface with respect to the punch axis is also obtained from the video image.

Figure 5.2 shows typical small-punch load-displacement curves for brittle and ductile materials. The points of apparent crack initiation are indicated on the curves. In the case of ductile materials, initiation takes place well before reaching the peak load. The small punch test energy, J, is defined as the energy absorbed up to the maximum load in the load-deflection curve and measured as the area under the curve up to the peak load.

Tensile Stress-Strain Behavior. The observed load-displacement curve can be matched to a curve from a database of curves corresponding to a range of stress-strain constitutive behavior. Such a database can be generated by small-punch tests on materials with known stress-strain behavior or through a series of iterative finite-element analyses (FEAs) of small-punch tests. Researchers have demonstrated excellent matching between the observed small-punch load-displacement curve and the matched database curve for A533B pressure vessel steel (Ref 4). The tensile stress-strain behavior predicted from the small-punch test is also found to match well with the conventionally measured behavior, within 5% (Ref 4).

Fracture Appearance Transition Temperature (FATT). It has been established that steels exhibiting ductile-to-brittle fracture transition behavior with decrease of temperature in a standard Charpy impact test also show a ductile-to-brittle energy transition behavior with decrease of temperature in the small-punch test. In a plot of the small-punch energy versus test temperature, the average of the upper shelf energy and the lower shelf energy is defined as the small-punch transition temperature, T_{SP}. For a given steel, typically T_{SP} is shifted downward from the Charpy FATT by an amount empirically established. Several correlations between T_{SP} and FATT have been developed for CrMo, CrMoV, and NiCrMoV steels and applied to a range of in-service power plant components such as HP/IP turbine rotors and LP steam turbine disks (Ref 3).

Fracture Toughness (K_{IC} and J_{IC}). The local strain energy density accumulated at the location and time of crack initiation in the small-punch test specimen is computed using large-strain FEA and a computer code. Using the constitutive behavior, the absorbed strain energy density at the observed crack initiation location is then computed up to the load level experimentally identified by the point of visible cracking. This critical strain energy density, w_{SP}, defines the fracture initiation criterion and is applied to the crack tip of a standard compact tension fracture test specimen. The strain energy density, w_{CT}, averaged over some expectedly material-dependent distance x ahead of the crack tip, and denoted by $\bar{w}_{CT}$, is computed. J_{IC} is obtained from the load level at which this averaged $\bar{w}_{CT}$ is equal to the critical strain energy density, w_{SP} measured previously. K_{IC} is then derived from J_{IC} from a knowledge of the elastic modulus E and the Poisson's ratio ν of the material because $K_{IC} = [EJ_{IC}/(1 - \nu^2)]^{1/2}$ (Ref 4).

The small-punch test has also been applied to assess the integrity of thermal barrier coated surfaces of hot section components in engines by determining the ceramic tensile spalling strain and fracture toughness (Ref 6).

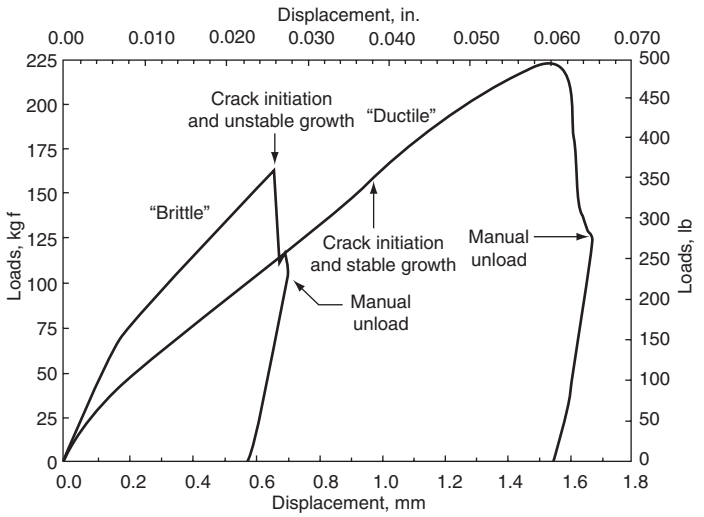

Fig. 5.2 Typical load-displacement curves in small punch tests for ductile and brittle behavior. Small punch energy is measured as the area under the curve up to the peak load. Source: Ref 3. With kind permission of Springer Science and Business Media

5.3 Quantitative Fractography

Generally, fracture surfaces that are invariably nonplanar are studied using the projected images formed in a scanning electron microscope (SEM), stereometry, and profile generation via serial sectioning. Individual projected features and systems of projected features that could be obtained through these techniques are described in Ref 7 and 8.

Roughness Parameters. The roughness of a fracture surface is characterized by a profile roughness parameter, R_L, and a surface roughness parameter, R_S. R_L is the ratio of the true length of a profile to its projected length; R_S is the ratio of true surface area to its projected area. R_L is measured directly from a vertical section of the fracture surface. Experimental R_L reported for various materials vary between 1.06 and 2.39. For a fracture surface with randomly oriented surface elements and no overlap, $R_S = 2$. The best fit to all known experimental data is given by the linear parametric equation, $R_S = (4/\Pi)(R_L - 1) + 1$. From these two roughness parameters, the various features on the fracture surface such as the length of a linear or curvi-linear feature, perimeter length of a closed figure, area of a curved two-dimensional feature, or mean area of curved two-dimensional features can be derived (Ref 7). The true length of a feature is the measured length multiplied by R_L, and the true area is the measured projected area multiplied by R_S.

A typical application is quantitative measurement of dimple size from SEM photomicrographs. Measurements made directly on the SEM picture can be erroneous, unless corrections are applied using the roughness parameters described previously. In a typical case of fracture in 4340 steel, the true corrected area of the dimples was found to be nearly twice that of the uncorrected area measured on the SEM fractograph (Ref 7).

Fractal Character of Fracture Surfaces. Fractal geometry has found application in the study and characterization of fracture surfaces (Ref 9, 10). Consider a lineal feature such as a curved profile length, L, being measured in steps of size, η. The smaller the measuring step, the longer will be the measured length. The profile length, L, when measured in steps of η, can be described by the equation:

$$L = L_0 \eta^{(1-D)}$$

where L_0 is a constant and D is a non-integer exponent, independent of η and dependent on the particular profile under measurement; D is the fractal dimension of the curve.

Fractal information from irregular fracture surfaces can be derived by obtaining fracture surface profiles from metallographic vertical sections cut perpendicular to the fracture surface. Profiles can also be obtained from serial sections cut parallel to the fracture plane. If the projected length of the profile is L', then the lineal roughness parameter R_L is given by:

$$R_L = L/L' = R_0 \eta^{(1-D)}$$

where R_0 is a constant. Plots of $\log(R_L)$ versus $\log(\eta)$ generally have the characteristic shape of a reverse sigmoidal curve (RSC) with segments of different slopes. The extent of linearity of such plots with the slope $(1 - D)$ indicate the dimensions over which fractal character is exhibited by the fracture profile.

Thus, the entire fracture surface cannot be characterized by a single fractal dimension. The range of validity of such fractals can be associated with prominent microstructural and fractographic features. For example, in a 3.1% Mn steel fractured at room temperature in a ductile mode with microvoid coalescence, the fractograph had two distinct features, namely, the dimples and the slip steps on the dimple walls. The dimples had the size range of ~6 to 50 μm and the slip steps ~0.8 to 4 μm. The fractal dimensions derived from the log R_L versus log η plot were 1.18 for the dimples and 1.06 for the slip steps.

For the same steel, fractured at 77 K to produce an intergranular fracture, there were three distinct fractographic features: the grain boundary slip steps with the spacing of ~0.8 to 4 μm, grain boundary particles with the spacing of ~6 to 15 μm, and the grain boundary facets with the size of ~20 to 150 μm. The corresponding fractal dimensions were 1.06, 1.09, and 1.28, respectively.

Fractal dimension is not singular for each fracture mode. However, the extent of fractal behavior could be correlated to the microstructural and fractographic features over a wide range of dimensions.

5.4 Fracture Surface Topography Analysis (FRASTA)

In conventional fractography using optical and SEMs, fracture surfaces of broken components are examined to determine the crack initiation site, crack propagation direction, and fracture mode. When distinct features such as fatigue striations are present on the fracture surface and when there is a one-to-one correspondence between such features and the load cycle, the crack growth rate can be readily determined from striation spacing. In stress-corrosion cracking (SCC), repeated formation and fracture of the corrosion product layer at the crack tip may produce distinct features that can be measured and related to crack growth rate. There are many situations where well-defined features are not readily discernible on the fracture surfaces and the load/environment histories of the failed component are not known. For such cases, an advanced technique is now available for reconstructing the fracture event in microscopic detail. In this technique, the three-dimensional topographies of the conjugate fracture surfaces are simultaneously analyzed to obtain quantitative information on fracture toughness, crack nucleation times, and crack growth rates without the need for a fracture mechanics test or instrumented impact test. This technique, called fracture surface topography analysis (FRASTA), was developed by SRI International, Menlo Park, Calif. (Ref 11, 12). The technique enables reconstruction of the fracture process and allows identification of the changes in load and environment with the position of the crack front.

The Concept. When a component is loaded, events occur in the following sequence: elastic deformation, localized inelastic deformation at sites of defects or stress concentration, and development of a microcrack in or near the inelastic deformation zone.

The stresses drop to zero on the newly formed microfracture surfaces. The applied load is redistributed to sound material ahead of the crack tip, which continues to deform inelastically to microfracture, and the process repeats to other areas. The deformation that existed at the moment of microcracking is thus "frozen" in the material immediately below the fracture surface. This material undergoes no further inelastic deformation.

The previously mentioned sequence of nucleation, growth, and coalescence of microfractures produces different amounts of inelastic deformation in the component as a function of distance from the microfracture nucleation site. The varied amount of local inelastic deformation results in an irregular fracture surface (Fig. 5.3). The topography of the fracture surface is a permanent record of the evolution of all the microfracture events that resulted in the macrofracture.

Surface irregularity is also produced as the crack tip interacts with the microstructure of the component. When there is no inelastic deformation, crack tip interaction with the local microstructure would produce conjugate fracture surfaces with their profiles matching precisely. Any mismatch between the profiles of the conjugate fracture surfaces indicates inelastic deformation, the extent of which can be determined with a computer. This information is used to reconstruct the fracture sequence at the microscopic level.

The Methodology. Using a scanning laser microscope (SLM), the fracture surface photograph and the topographic map of each of the two conjugate fracture surfaces are first recorded. The topograph data are digitized and stored in a computer. The sequence of the fracture event is reconstructed using the computer. One topograph is inverted and positioned with respect to the other so that the pair of topographs represent the fracture surfaces. The two conjugate topographs are first brought together until they overlap everywhere. Then they are gradually separated. As the displacement between them increases, small nonoverlapping areas appear. These nonoverlapping areas represent areas on the fracture surfaces that formed first; i.e., they are the sites where microcracks nucleated. As the relative displacement between the topographs is increased, new nonoverlapping areas appear, representing nucleation of new microcracks; existing nonoverlapping areas become larger, representing growth of microcracks; and adjacent nonoverlapped areas merge, signifying microfracture coalescence. Thus, the fracture process is reconstructed. When the two conjugate topographs are aligned and juxtaposed so that the most protruding features just touch, the configuration of the space between the two topographs is a representation of the crack configuration at the stage of final separation. From a knowledge of total fractured area as a function of topograph displacement, crack growth rate can be computed.

The information is used to create a series of fractured-area-projection plots (FAPP) and a series of cross-sectional plots (XSP). A FAPP is equivalent to a radiograph taken perpendicular to the fracture plane. It provides information on microcrack initiation sites and projected areas of microcracks and macrocracks (Fig. 5.4). A XSP is a section perpendicular to the fracture surface. It shows the profile of the microcracks, the macrocrack tip opening

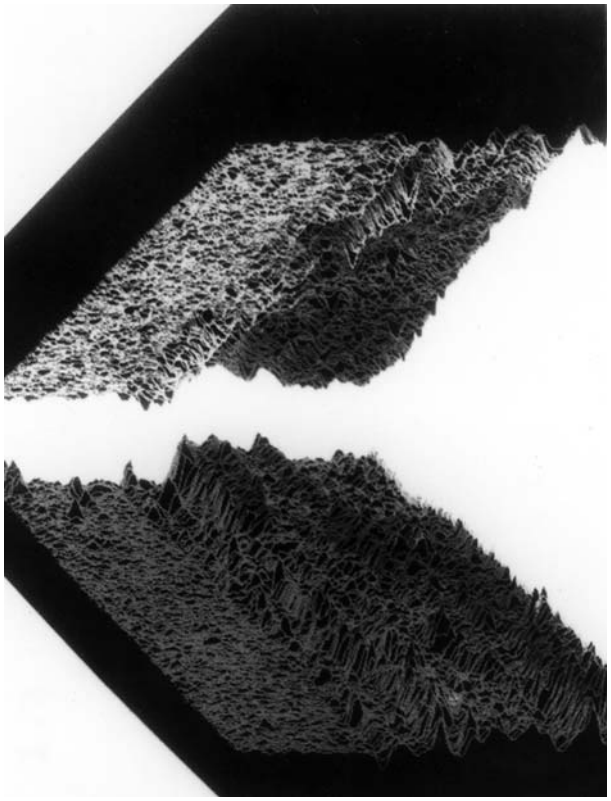

Fig. 5.3 Perspective view of conjugate fracture surfaces. Source: Ref 11

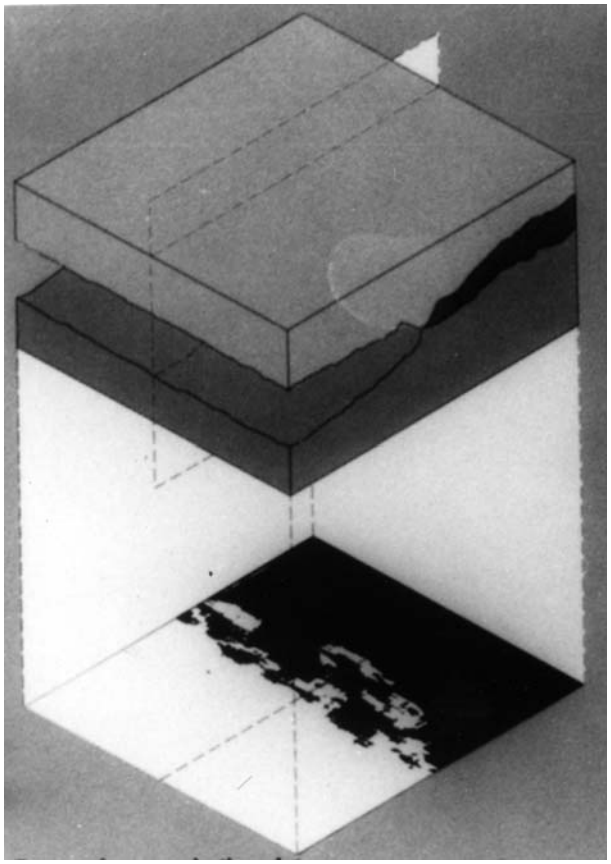

Fig. 5.4 Fractured-area-projection plot. Source: Ref 11

angle and displacement, and the amount of inelastic deformation necessary before fracture (Fig. 5.5).

Fracture surface topography analysis is a powerful tool and its applications include identification of fracture mechanisms, deduction of crack history in components in service, and determination of fracture parameters. The following examples illustrate the use of the FRASTA technique.

Stress-Corrosion Cracking (SCC) in a Stainless Steel. Stress-corrosion cracking is difficult to detect prior to component failure, and unexpected SCC can lead to disasters. The crack initiation and propagation may respond in different ways in different environments. Crack initiation in a given material generally depends on the bulk environment, whereas crack propagation depends on the crack-tip environment, which could be different from the bulk environment. Figure 5.6 shows the SEM fractographs and the corresponding topographs of the two conjugate fracture surfaces of a notched tensile test specimen of sensitized 304 type stainless steel tested for SCC in clean water for one week at a strain rate of $7 \times 10^{-8}\ s^{-1}$ and then pulled to fracture at room temperature (Ref 13). Intergranular SCC can be seen at the ten o'clock and two o'clock positions in the fractographs. Cracks have initiated on the surface and propagated inward.

A series of FAPPs were taken at various displacements of the topographs (Fig. 5.7). Cracked regions are seen as white patches, corresponding to nonoverlapping areas of the topographs.

The unfractured area (dark area in the FAPP) is plotted against the topographic map displacement and the result is shown in Fig. 5.8. The displacement is correlated to specimen elongation and hence, time. Thus, knowing the time for the duration of the test (total elongation) and the time for crack growth (elongation associated with the crack growth period), the time for crack initiation (first appearance of microcrack) could be computed. In the present case of SCC in clean water, it is done as follows. Test duration (171.8 hours) multiplied by the specimen gage length (25 mm) and the strain rate ($7 \times 10^{-8}\ s^{-1}$) gives the total elongation as 1082 μm. From the ratio of the elongation associated with the crack propagation period to the total elongation, the time of crack propagation can be found (577 μm − 64 μm) × 171.8 hours/1082 μm = 81.4 hours. Thus, the time taken to initiate the first microcrack is 171.8 − 81.4 = 90.4 hours. It was also found that this time corresponded to a discontinuity in the load/time record in the testing machine. Knowing the crack penetration length and the time for crack propagation, the crack-growth rate is readily computed. In the present case, it is about 2×10^{-6} mm/s.

In a test for SCC of the same material in water deliberately contaminated with 1 ppm sulfuric acid, FRASTA technique revealed that the crack initiation and growth started in the interior and only after considerable growth, the internal cracks merged with the surface. The crack initiation time in this case was 46 hours and the crack propagation rate about 4×10^{-6} mm/s.

Fracture Parameters. The cross-sectional plot XSP of a fracture surface can be used to compute the fracture toughness of the material. A compact specimen of a thermally embrittled stainless steel was fatigue-precracked, then loaded monotonically to extend the crack. The cracked area was heat-tinted for easy identification and then the fracture surfaces opened (Ref 14, 15). Figure 5.9 shows the XSP obtained by displacing the topographs along a center plane normal to the fracture surface. The crack tip opening displacement, δ, is measured at the tip of the fatigue precrack, i.e., at the onset of crack extension.

The fracture toughness *J*-integral or stress intensity factor *K* of the material for crack initiation can be computed from the crack tip opening displacement, using the relations:

$$J = \sigma_0 \delta$$

and

$$K = [JE/(1 - \nu^2)]^{1/2} = [E\sigma_0\delta/(1 - \nu^2)]^{1/2}$$

where *E* is the elastic modulus; δ is the crack opening displacement; σ_0 is the flow stress, i.e., the average of yield strength and ultimate tensile strength; and ν is the Poisson's ratio. The values computed through FRASTA agreed well with the values obtained by conventional fracture toughness testing (Ref 14, 15).

Other Practical Applications. The FRASTA technique has been successfully applied to determine when a crack initiated in a boiler tube during its 22 years of service and at what rate the crack grew. The technique revealed that the tube had periods of accelerated and decelerated crack growth (Ref 16).

In a nuclear reactor vessel of stainless steel subjected to repeated thermal shock, the crack initiation time was computed through the application of FRASTA technique (Ref 15).

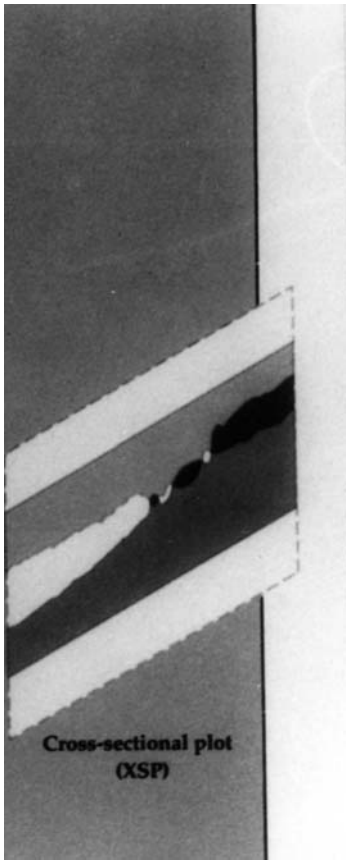

Fig. 5.5 Cross-sectional plot. Source: Ref 11

There are many instances where corrosion pits in structures have led to fatigue cracks, ultimately resulting in failure. This is particularly true in structures such as aircraft flying in marine environment. The accident of the Boeing 737 aircraft of Aloha Airlines near Maui, Hawaii on April 28, 1988 is one such incident in which a section of the fuselage tore away in flight. Tiny cracks at the rivet holes had joined to form a larger crack of critical length. An insight into the evolution of corrosion pit to fatigue crack and the time for such a transition was obtained by the application of FRASTA technique to specimens of aircraft skin material, i.e., 2024-T3 aluminum alloy tested in fatigue after exposure to salt solution (Ref 17).

Other applications of FRASTA include understanding the fracture process in ceramic fiber (silicon carbide) reinforced metal matrix (titanium aluminide) composite, and in polyethylene gas pipeline material (Ref 12).

5.5 Oxide Dating for Failure Analysis

In the failure analysis of high-temperature power plant components, the major difficulty encountered is the masking of all fractographic features by the thick layer of the metal oxide formed during service. Moreover, formation of the thick oxide layer also involves consumption of the metal from the underlying fracture surface. Thus, oxidation modifies the fracture surface significantly. Revealing the original fracture surface is not guaranteed by the removal of the oxide layer by any means. This is a handicap from the fractography point of view. However, from measurements of the thickness of the oxide scale formed, and a study of its morphology and the lattice parameter of its constituents, an estimate of the time and temperature of exposure of the component to the oxidizing service environment can be obtained, knowing the kinetics of oxide growth on the material. Thus, oxide layer characterization provides yet another technique for failure analysis, especially for steel components. This technique is known as "oxide dating."

Kinetics of Oxide Growth. The kinetics of oxide growth on steels can be described by the general expression:

$$x = Kt^m$$

where x is the oxide scale thickness, K is a rate constant, and t is the time of exposure at a given temperature. The value of K de-

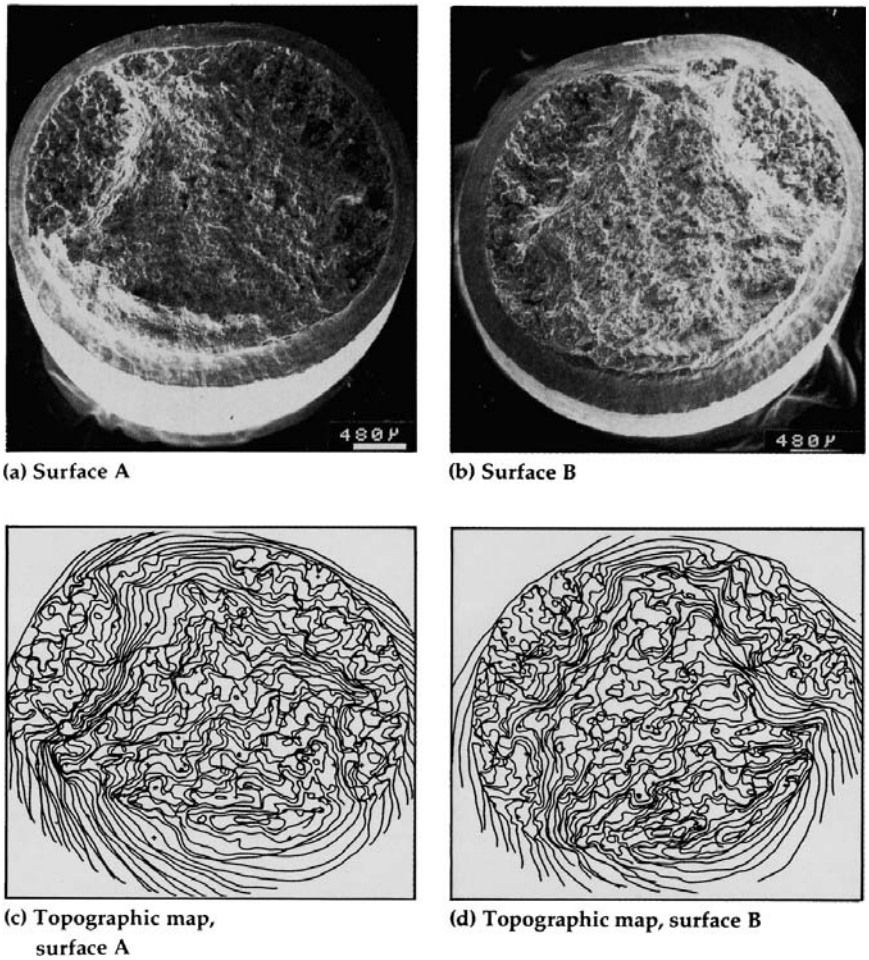

Fig. 5.6 Scanning electron fractographs and corresponding topographs of conjugate fracture surfaces of sensitized 304 stainless steel tested in clean water. Source: Ref 11, 13

pends on the temperature and alloy chemistry. The value of m can vary from 0.3 to 0.7, depending on the material and exposure conditions. The phases present in the oxide scales of steels are hematite (Fe_2O_3); magnetite (Fe_3O_4); wustite (FeO); and spinel, which can be of the type $(FeCrMo)_3O_4$. For mild steel and low-chromium alloy steel, at a given temperature, the thickness of the total scale or individual phases increases with time typically following the parabolic law, $x^2 = K_p t$. The parabolic rate constant, K_p, changes with temperature according to an Arrhenius relation, so that $\log K_p \propto 1/T$.

With data on the oxidation kinetics of the material, and the measured thickness of the oxide scale, the time required for forming the scale at a given temperature can be readily estimated. Alternatively, knowing the service life of the component, and the thickness of the oxide, generally measured by the ultrasonic technique, the temperature of exposure can be calculated. Any measured oxide thickness can be formed by any combination of time and temperature that satisfies the kinetic data. Therefore, for components that have been operating for unknown times at unknown temperatures, the method is not so straightforward. For mild steel and low-chromium alloy steels, two methods have been described (Ref 18). One method is based on the oxide morphology and the other on the oxide lattice parameter. Up to 650 °C (1200 °F), the relative thicknesses of the different oxide phases are temperature sensitive, and their temperature dependence is documented. From the measured thicknesses of the phases, the temperature of exposure can be estimated. The variation of the lattice parameter of the phases with the temperature of formation is also known for low-chromium alloy steels. Hence, lattice parameter measurements provide another method for estimating the temperature of exposure. From this estimated temperature, using the oxidation kinetic data, the age of a defect or crack, i.e., crack initiation time, can be computed. For example, for a crack originating from the surface of a component and growing freely inward, the oxide scale thickness would decrease from the crack mouth to the crack tip. Knowing the service life and temperature of the component and the measured thickness of the oxide along the crack length, the age of the crack can be estimated.

The possible sources of error in such computations for practical applications have been described (Ref 19). The largest change in the calculated component life is caused by errors in the value of m, the exponent in the kinetic equation, and T, the temperature of exposure.

Other Correlations. A number of other correlations between oxide thickness, time, and temperature have been proposed for low-alloy Cr-Mo steels (Ref 20):

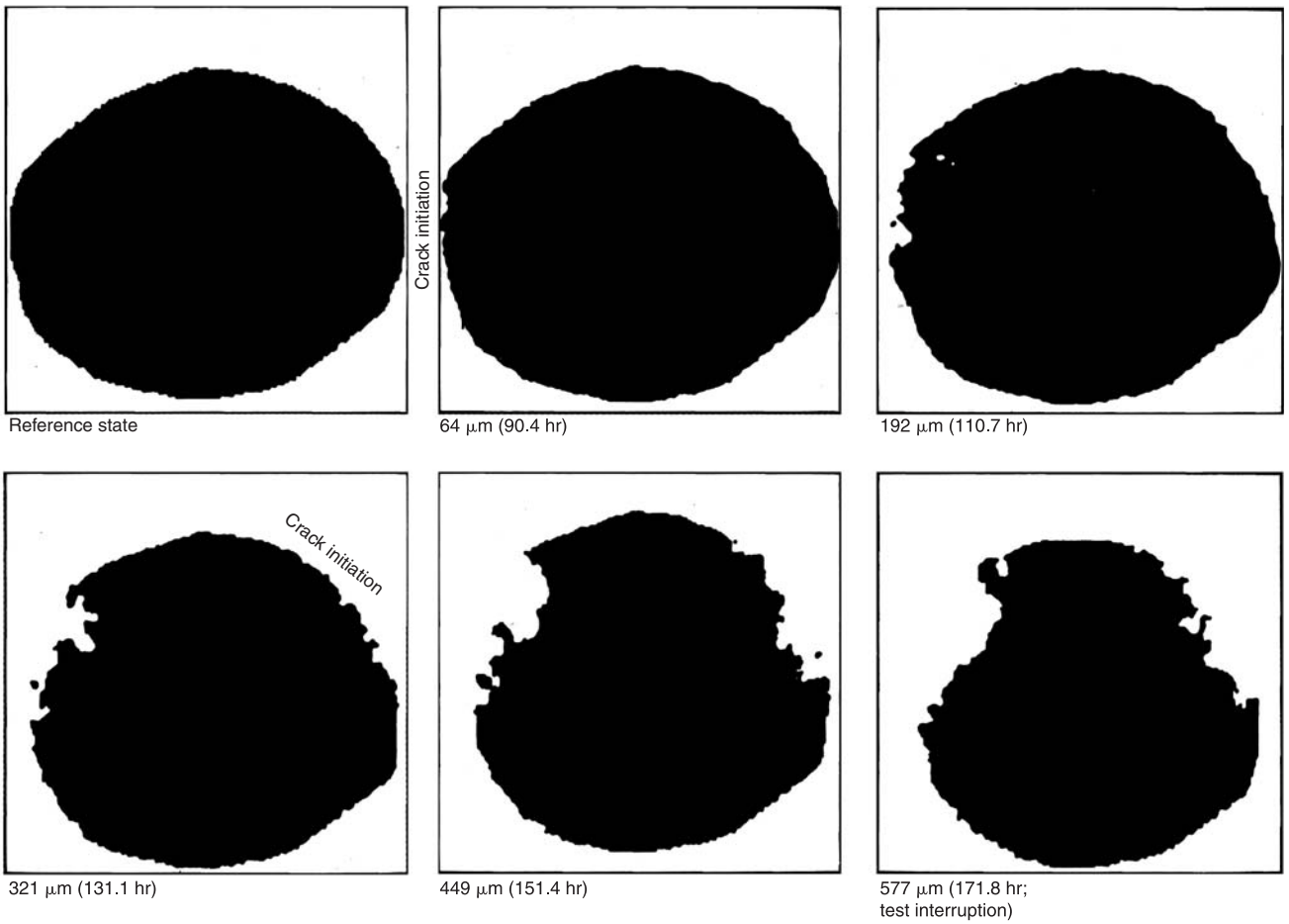

Fig. 5.7 FAPPs for the stainless steel specimen referred to in Fig. 5.6. White areas indicate cracks. Source: Ref 11, 13

$$x^3 = Kt$$

$$x^{2.1 \text{ to } 2.6} = Kt$$

$$x = Kt$$

$$x^{2.6 \text{ to } 3.0} = Kt$$

These are specific to the steels and the oxide phases and for specific temperature ranges.

5.6 Fault Tree Analysis (FTA)

Failure analysis involves the collection of a large body of information in terms of background data, observation of features, laboratory testing, metallography, fractography, and analysis of data. The information gathered in these stages must be systematically linked to arrive at the cause or the most probable cause of the failure.

The use of fault trees is one important diagnostic tool that helps sort out data and identify probable causes. The fault tree method is a procedure used in failure modes and effects analysis (FMEA), where failure modes for each item in a system are identified, and then the effects of each failure mode are itemized. It is a structured, logical, and systematic analysis. The fault-tree method in FMEA is a top-down technique that graphically structures events with Boolean operators (i.e., "AND" and "OR" gates), as briefly described in this chapter. Initially, FMEA procedures were used primarily as a safety analysis on the system hardware (Ref 21, 22), often after the design was nearly complete and thus when changes would be difficult or expensive. More recently, refinements in the methodology have expanded the types of failures that can be analyzed, and FMEA procedures have become a "traditional" reliability analysis technique that is also used to analyze the cause of the failure (Ref 23, 24).

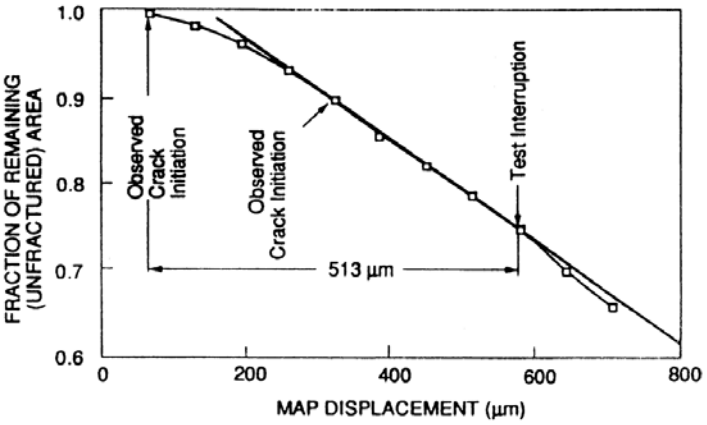

Fig. 5.8 Relationship between unfractured area (black areas in the FAPPs) and topographical map displacement for the specimen referred to in Fig. 5.6. Source: Ref 11, 13

The Concept. Failure of a machine or structure is considered a fault or undesirable event. The fault tree is a graphical description of the combinations of possible basic events that can lead to the undesired fault. The basic events are linked through Boolean logic gates, mainly the AND and OR gates. The input events passing through the AND gate are necessary but not sufficient and should occur simultaneously to produce the output event. Any one of the input events passing through an OR gate is sufficient to produce the output event of that gate. An AND gate increases the size of a branch of the fault tree whereas the OR gate increases the number of branches. The other logic symbols used for the construction of the fault tree are described in detail in Ref 25 and 26.

Figure 5.10 is a simple fault tree with one AND gate. The failure of a component is the top event that can happen only if both events G1 and G2 occur. The event G1 can happen if either of the two

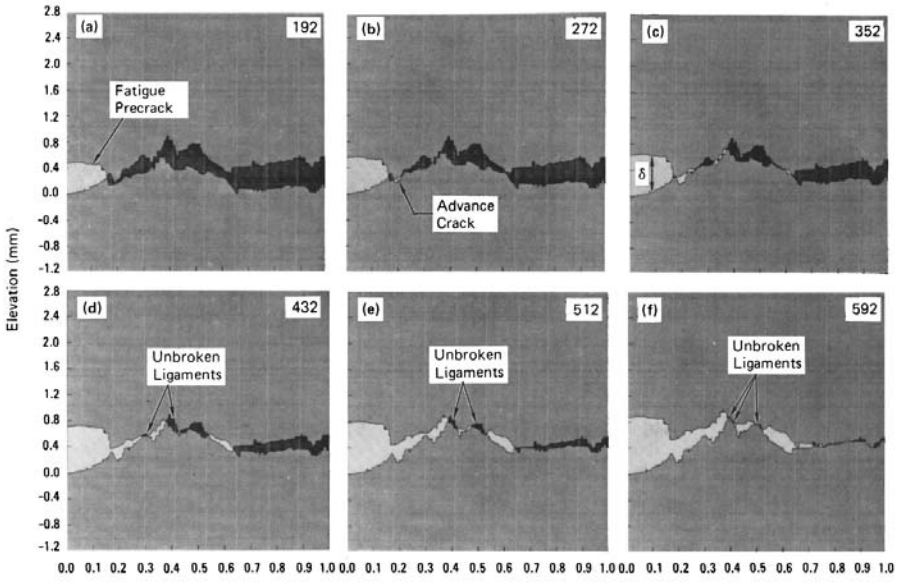

Fig. 5.9 XSP of crack tip showing successive stages of crack propagation in a thermally embrittled stainless steel. Source: Ref 14, 15

basic events E1 OR E2 takes place. E1 and E2 are the basic component faults. The event G2 can result if any one of the three basic events E1, OR E3, OR E4 takes place. An OR gate connects E1 and E2 to event G1. Another OR gate connects E1, E3, and E4 to event G2. In this manner, the entire fault tree can be constructed using all the information gathered during failure investigation.

For example, component failure by SCC can take place only when there is critical stress intensity AND critical concentration of the species causing cracking. Component failure by hydrogen embrittlement can happen only when there is a critical hydrogen content AND critical stress intensity. The critical hydrogen content can be present either in the bulk of the component OR in local regions within the component.

Evaluation of the Fault Tree. To evaluate the fault tree and determine the failure path, it is necessary to find the various minimal cut sets of the tree. A cut set is a set of basic events that have to take place for the top event to occur. A cut set is said to be minimal when each of the basic events in the set is necessary and whose combination is sufficient to cause the top event. For evaluating the fault tree, it is necessary to find the number of minimal cut sets. Each minimal cut set is an independent path for the failure to occur.

In the preceding example, the cut sets are E1-E1, E1-E3, E1-E4, E2-E1, E2-E3, and E2-E4. E1 can cause G1 and also G2, which together can cause the top failure event. The minimal cut sets of this fault tree are E1, E2-E3, and E2-E4. These are the three independent paths to cause the failure.

After constructing the fault tree with all the available information, the minimal cut sets for the main failure event must be identified. This can be done by inspection in simple cases or through computer programs for complex failure problems. Using this information judiciously along with other observations and evidences such as metallography and fractography, the most probable failure path can be identified.

Applications. Application of FTA to a few cases of failure analysis has been described in Ref 25 and 27 and also to the failure process of hydrogen embrittlement in Ref 25 and 28. Sometimes, it is difficult to distinguish between SCC and hydrogen embrittlement based on fractography alone. Often, both mechanisms produce intergranular fracture with well-defined crystalline facets. Fault tree analysis, in combination with metallographic and fractographic observations, can resolve the issue. This has been described in Ref 25. Fault tree analysis has been successfully applied to determine the cause of failure of two boiler tubes in a power plant, which failed by two different modes (Ref 27).

A fault tree has been developed for adequately describing the process of hydrogen embrittlement (Ref 28). Figure 5.11 shows the details of the tree.

Fault tree analysis is not only a versatile tool for failure investigation but can also help in safety analysis of complex systems. By assigning numbers to the probability of occurrence of each basic event, the overall probability of occurrence of the top event can be evaluated.

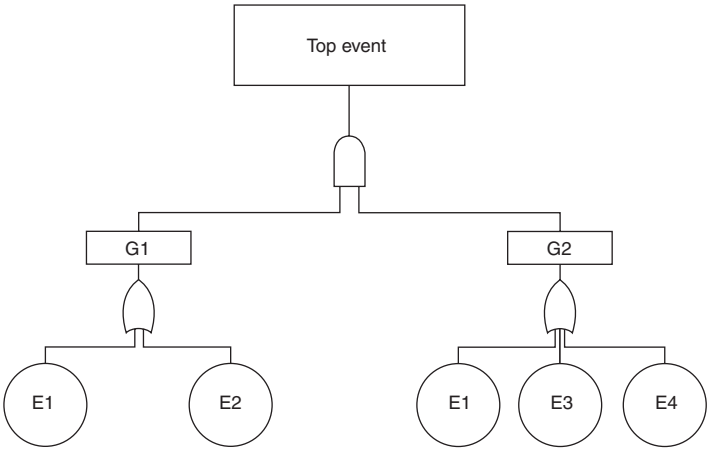

Fig. 5.10 Schematic of a simple fault tree. Source: Ref 26

5.7 Failure Modes and Effects Analysis (FMEA)

As previously noted, FMEA (Ref 29, 30) is a procedure in analyzing reliability and safety of complex machines and structures. Fault tree analysis described in the previous section is often a tool in the application of FMEA procedures.

The Concept. Any complex structure is made up of numerous hardware parts, assemblies, and subsystems, each serving a defined function. Failure of each one of these could lead to the malfunction or failure of the total structure under certain conditions. The purpose of FMEA is to study the possible failure modes and to identify the effects of the failure of individual hardware items on the performance of the total system. This is known as the hardware approach. The other approach considers the designed functions of each item that can be classified as outputs, and their failure modes are analyzed. For complex systems, both approaches may be desirable. The analysis can be started with the total system and carried down to the individual hardware component (top-down approach) or vice versa (bottom-up approach).

The Methodology. For conducting FMEA by the hardware approach, all information about each part or subsystem is collected from various sources such as design data, drawings, operation records, and earlier failure or malfunction histories. The information so collected is listed by item and presented in a detailed format, resembling an accounting spreadsheet or store inventory. The possible role of each component or subsystem toward failure of the entire structure is then evaluated. Each potential failure is identified and ranked by the severity of its effect on the immediate function and on the integrity and safety of the total system or the mission. The severity ranking is used during design to establish priorities for corrective actions.

Following is a typical FMEA spreadsheet. The procedure for the construction of a FMEA spreadsheet is described in detail in Ref 30. Each heading in the spreadsheet is self-explanatory. For each hardware item entered, its intended function is listed. It is followed by various aspects of its assumed failure. The parameters related to the failure can be many. A few of them are listed for illustration. The list can be as exhaustive as one wants.

Identification No.	Part	Intended function	Failure						Method of Detection	Remedial Measures
			Mode	Cause	Result	Consequences	Probability	Severity		

A failure mode such as fracture of a component can be due to several causes. For each failure mode, all possible independent causes should be listed. Some of these causes are overload, fatigue, corrosion, stress corrosion, embrittlement, and service abnormalities. For each item listed in the spreadsheet, the result of the assumed failure mode on the function of that item is listed next. This helps in deciding corrective measures such as redesign of that particular item. The next column describes the consequences of the assumed failure on the performance of the total system. These can be fatalities, total loss of the system, injuries to personnel, damage to property, and so forth. More columns can be added in between, such as the effect of the assumed failure of one item on the performance of other neighboring or related items in the assembly.

The probability of the failure is indicated using the following codes:

- *Level A:* Frequent, i.e., a single failure mode probability greater than 0.2 of the overall probability of failure of the system
- *Level B:* Reasonably probable. 0.10 $<$ probability $<$ 0.20
- *Level C:* Occasional. 0.01 $<$ probability $<$ 0.10
- *Level D:* Remote. 0.001 $<$ probability $<$ 0.01
- *Level E:* Extremely unlikely. Probability $<$ 0.001
- *Level F:* Impossible

The severity of the consequences of the failure is classified into four categories:

- *Category I:* Catastrophic
- *Category II:* Critical
- *Category III:* Marginal
- *Category IV:* Minor

The method of detection of the failure by the operator is listed next. One can also include, if available, information on service history, life expectation, and so forth. Finally, what remedial measures or precautions could be taken to prevent the malfunction or failure of the item under consideration are listed.

Having recorded all the details, an evaluation is made regarding how each component or subassembly could eventually lead to a system failure. Collection of data from various sources for filling the FMEA spreadsheet is time-consuming and expensive. However, surprisingly, FMEA along with FTA can pinpoint how a seemingly insignificant item can lead to a major failure and how quality assurance is important for such items. Such an analysis enables the establishment of corrective action to control or eliminate high-risk hardware items. The analysis and the conclusions are totally transparent for any one to review.

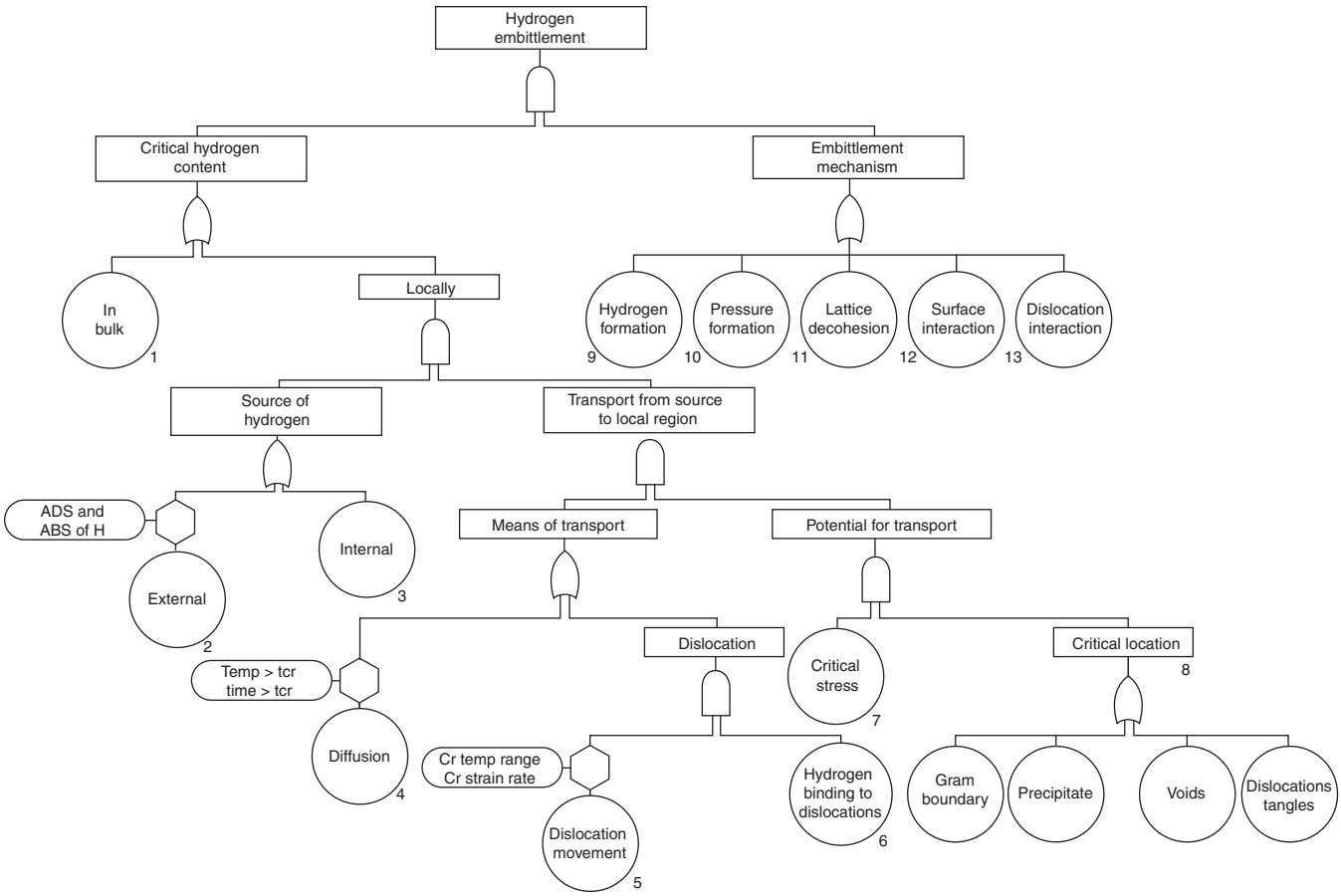

Fig. 5.11 Fault tree for hydrogen embrittlement. Source: Ref 28

5.8 Failure Experience: Information Storage and Retrieval

Failure prevention is a matter of great concern for all designers, fabricators, and users of engineering hardware. When an engineering structure fails in service, the normal practice is to carry out investigations, establish the cause or causes for the failure, take immediate remedial action, record the effectiveness of the remedial action over a period of time, and document the entire experience for future reference. This documentation is extremely important and very valuable because it serves as a guide for investigating similar failures that might take place later. A reference to the records of previous failures and, in particular, the remedial action taken and its effectiveness provides an economical means for failure prevention through appropriate modifications in design and manufacturing parameters. However, the information so generated in-house in one industry rarely gets disseminated to other industries and organizations and not even to other departments in the same organization. Computerized information technology offers obvious advantages in the storage and retrieval of failure analysis information. However, the general availability of such databases may be limited due to the proprietary nature of information on failures. The relative ease of creating a database also offers the flexibility to create databases for particular needs, type of components, or industry. Thus, companies may keep statistics on failures with various types of database fields (e.g., type of failure, material, root cause, etc.) depending on their needs. The following is just one example.

Example: Failure Database of Helicopter Components. Reference 31 describes a three-dimensional database matrix for storage of vital information and data on failures. The matrix is referred to as a "failure-experience" matrix. The three axes of the matrix represent the following variables:

- Failure modes (e.g., contact fatigue, ductile rupture, stress corrosion, etc.)
- Element (part) function (e.g., supporting, force transmitting, sealing, etc.)
- Corrective action (e.g., direct replacement, change of material, design improvement, etc).

Cells in this three-dimensional field are defined by the intersection of categories along the axes (Fig. 5.12). Of course, a database with additional fields could be considered. For example, other fields could be product form (bar, plate, gear) material (brass, bronze, Cr-Mo low-alloy steel, etc.), and perhaps most importantly, the likely primary root cause (forging seam, grinding burn, inadequate radius). The potential complexity becomes obvious, especially with regard to the field of root cause, which could involve multiple factors with complex combinations of root causes. For purposes of description, only a three-field system is considered.

To start with, failures of U.S. Army helicopter components were chosen and failure experience data for over 500 individual failed components of helicopters were collected and stored in the matrix (Ref 32). Each failed part was classified with respect to failure mode, elemental mechanical function, and corrective action and, using a computer, the data were inserted in one cell of the matrix, along with an identification number for the part. A typical data entry was as follows (Ref 32):

- Identification: 8A: Main rotor hub radius ring 204-012-116
- Failure mode: Wear, scoring
- Function: Sealing, sliding, shielding
- Corrective actions: Applied surface coating (tungsten carbide), UI

The matrix contained about 147,000 cells. Although only 5% of the cells were populated with the data on existing failure experience, the population could be expanded with the storage of additional failure experience for all types of component failures from various industries.

Failure Modes. After examining the individual failed parts of helicopters, there were 40 failure modes that were included in the matrix. Some of the common and frequent modes were wear, ductile rupture, fatigue, impact, corrosion, erosion, delamination, and so forth, and their variations.

Elemental Mechanical Functions. The basic function of a component, without reference to its specific application in service, is termed the elemental mechanical function. Sometimes, it may not be possible to describe the elemental mechanical function of a component by a single term. In such cases, an antecedent adjective is used along with the term to describe the complete function of the component. Collins and others (Ref 32) have provided a list of 46 key words to describe the elemental mechanical function, along with a list of 40 antecedent adjectives. Typical key words are balancing, conducting, deflecting, fastening, linking, reinforcing, sealing, and so forth. Typical antecedent adjectives are aerodynamic, force, heat, liquid, motion, position, power, torque, and so on. The functions of the helicopter components studied could

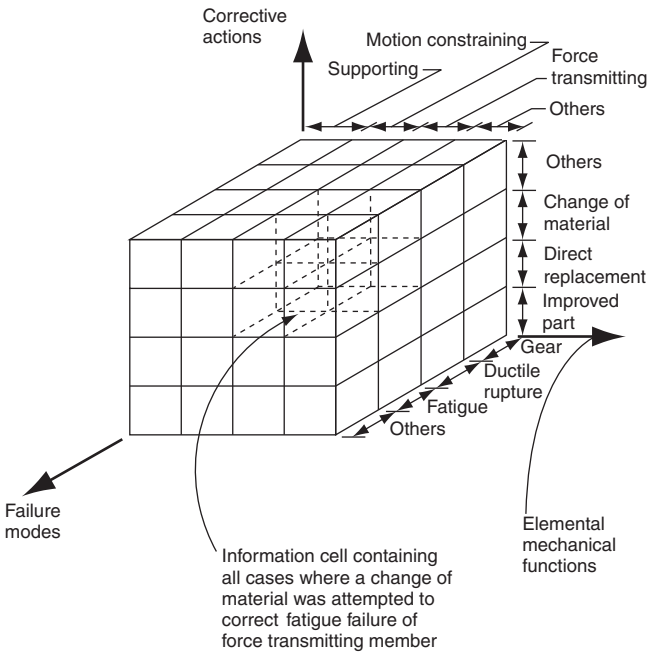

Fig. 5.12 A portion of the failure-experience matrix for documenting failures of helicopter components. Source: Ref 32. With kind permission of American Society of Mechanical Engineers

be described by 105 unique combinations of key words and antecedent adjectives, such as force transmitting, oscillatory sliding, continuous rolling, and so forth.

Corrective action is a measure or combination of measures to return the failed component to the status of performing its intended function satisfactorily. In the study of helicopter component failures, the corrective actions taken could be classified into 35 broad categories. Some examples are direct replacement, changed dimensions, repaired, strengthened part, changed vendor, applied surface coating, and so on. For entries regarding corrective action, descriptors such as UI for "used with improvement" and UNI for "used with no noted improvement" were considered.

Usefulness of the Matrix. This example of a failure information database is illustrated here as a potential aid not only for failure analysis but also for design and development. For failure analysis, the failure mode of the component is first identified. Knowing its elemental mechanical function, one can enter the matrix and read out the corrective action. For designing a component, if its intended mechanical function is known, one can enter the matrix and find out the failure modes most likely to occur and the corrective action most likely to prevent the failure. In the case of the failure-experience matrix for helicopter components, it was possible to determine:

- Frequency of usage of all corrective actions for a particular failure mode
- Frequency of occurrence of mechanical functions to which a particular corrective action was applied
- Frequency of occurrence of failure modes associated with a particular corrective action
- All mechanical functions impaired by a particular failure mode that were corrected by the same corrective action

5.9 Expert Systems for Failure Analysis

Expert systems represent a type of computer software program in the field of artificial intelligence (AI). Rudimentary expert systems were developed in the 1960s, and research on more robust applications has grown as computer systems have become more powerful and affordable. In terms of developing expert systems on failure analysis, work was done in the early 1990s on development of knowledge-based systems for the failure analysis of integrated circuit (IC) components and led to an IC failure analysis expert system known as FastAdvice (Electronics Quality and Reliability Center, Sandia National Laboratory). Another AI concept in failure analysis experts is that of case-based reasoning (Ref 33).

Potential benefits of expert systems for failure analysis may include:

- Capture failure analysis expertise: Failure analysis is a discipline that has a long learning curve, and any expert systems may help capture expertise and facilitate training.
- Centralize failure analysis information in a system for more effective retrieval and interpretation

On the latter point, the failure analyst may face a situation where the customer wants an immediate answer as to how and why a component failed. While trying to provide a quick answer, it is possible that some important detail that could have provided the clue might be overlooked or ignored. A failure might have resulted by the synergistic action of a number of factors and not necessarily a single cause. In such situations, for an unbiased diagnosis, an expert system might be very helpful. Sometimes, sales and service people, with limited experience in understanding failures and their causes, also may have to handle customer problems in the field. As noted, expert systems have been developed for various investigations. One such expert system has been designed for field investigation of bearing failures (Ref 34) and is described in the following section. Expert systems work on a number of "if-then" rules. A good expert system should transform the experience and knowledge of the failure analyst into a structured system for effective retrieval and interpretation of supporting data.

Expert Systems in Bearing Failures. The expert system proposed in Ref 34 has several modules. In the module for a preliminary diagnosis, all the symptoms that first indicated a bearing failure or malfunction are keyed in. Some of the common symptoms are seizure, vibration, temperature, noise, and so forth. Each of the symptoms is indicative of one or more causes responsible for the failure. From these lists, a two-dimensional matrix is constructed, with columns as the symptoms and rows as the possible causes. The cell of each symptom/cause pair is then filled with a number from 0 to 100, indicating the level of confidence the human expert has in the symptom/cause combination.

In another module, detailed diagnosis after the failed bearing was removed from the machine and dismantled is described. The user is presented with a screen to select one or more general observations such as "significant discoloration," "spalls," "smears on race surfaces," and so forth. The user is then presented with symptoms either singly or in groups where there is a common attribute. At this stage, based on previous user answers, an interim list of possible causes is presented to the user by the computer, with the probability of each cause indicated by the length of the bar. At this stage, the user can delete those causes that are inappropriate to the observations and consider additional possible causes. With successive iterations, the user finds the current top 10 most probable causes. Still, ultimately the satisfactory conclusion is reached with human intuition.

Logic Programming. Using logic programming languages such as PROLOG and LOGLISP for automated reasoning, expert systems have been developed for failure analysis. Application of one such system for the investigation of the failure of a pressure vessel is described in Ref 35. A pressure vessel made of annealed type 301 stainless steel had fractured explosively along the circumference near a circumferential weld. The orientation of the fracture surface was normal to the principal stress axis. Scanning electron fractography revealed clear intergranular fracture. The visual observation that the fracture surface was normal to the direction of principal stress and the attribute that the fracture was intergranular together suggest 20 different possibilities as described in Ref 35. Some of the possibilies are, for example: tension-overload—high-temperature, tension-overload—corrosion, tension-overload—weld-sensitized, tension-overload—SCC, bend-overload—high-temperature, torsion-overload—high-temperature, fatigue—high-temperature, and so on.

With the additional visual observation that the fracture was at the center of a necked down region, all modes other than tension overload were eliminated. That reduced the choice of failure mode-attribute combination to four: tension-overload—high-temperature, tension-overload—corrosion, tension-overload—weld-sensitized, and tension-overload—SCC. Further, grooves were observed on either side of the circumferential weld. With this new attribute added to the other modes and attributes, it could easily be concluded that the failure of the pressure vessel was due to tension overload of a corroded region, the intergranular corrosion being due to weld sensitization.

Weiss (Ref 35) also suggested the possibility of designing hybrid expert systems by including other useful programs such as fatigue data analysis, finite-element stress analysis, quantitative metallography, or spectroscopy systems to the logic programming expert system to make it more versatile for failure analysis.

REFERENCES

1. B.L Bramfitt and S.J. Lawrence, Field Metallography Techniques, *Metallography and Microstructures,* Vol 9, *ASM Handbook,* ASM International, 2004, p 478–492
2. J.D. Parker, A. McMinn, and J. Foulds, Material Sampling for the Assessment of Component Integrity, *Life Assessment and Life Extension of Power Plant Components,* T.V. Narayanan et al., Ed., PVP, Vol 171, The American Society of Mechanical Engineers, 1989, p 223
3. J. Foulds and R. Viswanathan, Small Punch Testing for Determining the Material Toughness of Low Alloy Steel Components in Service, *J. Eng. Mater. Technol.,* Vol 116, 1994, p 457
4. J.R. Foulds, P.J. Woytowitz, T.K. Parnell, and C.W. Jewett, Fracture Toughness by Small Punch Testing, *J. Test. Eval.* (JTEVA), Vol 23 (No. 1), Jan 1995, p 3
5. J.R. Foulds and R. Viswanathan, Nondisruptive Material Sampling and Mechanical Testing, *J. Nondestr. Eval.,* Vol 15 (No. 3/4), 1996, p 151
6. W.H. Müller, M. Kümmel, O. Hansen, and J.R. Foulds, An Analytic Feasibility Study for Use of the Small Punch Test to Assess Integrity of Coated Structures, *Materials Ageing and Component Life Extension,* Vol I, V. Bicego, A. Nitta, and R. Viswanathan, Ed., Engineering Materials Advisory Services Ltd., Warley, U.K., 1995
7. E.E. Underwood and K. Banerji, Quantitative Fractography, *Fractography,* Vol 12, *Metals Handbook,* 9th ed., ASM International, 1987, p 193
8. A. Gokhale, Quantitative Fractography, *Failure Analysis and Prevention,* Vol 11, *ASM Handbook,* ASM International, 2002, p 538–556
9. E.E. Underwood and K. Banerji, Fractal Analysis of Fracture Surfaces, *Fractography,* Vol 12, *Metals Handbook,* 9th ed., ASM International, 1987, p 211
10. R.H. Dauskardt, F. Haubensak, and R.O. Ritchie, On the Interpretation of the Fractal Character of Fracture Surfaces, *Acta Metall. Mater.,* Vol 38 (No. 2), 1990, p 143
11. T. Kobayashi and D.A. Shockey, FRASTA: A New Way to Analyse Fracture Surfaces, Part 1: Reconstructing Crack Histories, *Adv. Mater. Process.,* Vol 140 (No. 5), Nov 1991, p 28
12. T. Kobayashi and D.A. Shockey, FRASTA: A New Way to Analyse Fracture Surfaces, Part 2: Determining Fracture Mechanisms and Parameters, *Adv. Mater. Process.,* Vol 140 (No. 6), Dec 1991, p 24
13. T. Kobayashi, D.A. Shockey, and R.L. Jones, Deriving SCC Initiation Times and Growth Rates from Post-Test Fractographic Analysis, *Corrosion,* Vol 47 (No. 7), July 1991, p 528
14. T. Kobayashi and D.A. Shockey, A Fractographic Investigation of Thermal Embrittlement in Cast Duplex Stainless Steel, *Metall. Trans.,* Vol 18A, Nov 1987, p 1941
15. T. Kobayashi, Reconstruction of Crack History from Conjugate Fracture Surfaces, *Fatigue Crack Measurement: Techniques and Applications,* K.J. Marsh et al., Ed., Engineering Materials Advisory Services Ltd., U.K. 1991, p 389
16. T. Kobayashi, D.A. Shockey, G. Ogundele, D.D. McNabb, and D. Sidey, Deducing Crack History in an Aged Boiler Tube from Fracture Surface Topography, *J. Test. Eval.* (JTEVA), Vol 22 (No. 4), July 1994, p 309
17. T. Kobayashi, C.G. Schmidt, and D.A. Shockey, A Detailed Look at the Transition from Corrosion Pit to Fatigue Crack in Aircraft Skin, Materials and Process Challenges: Aging Systems, Affordability, Alternative Applications, *SAMPE Proceedings,* March 1996, Vol 41 (No. 1), p 86
18. L.W. Pinder, Oxide Characterisation for Service Failure Investigations, *Corros. Sci.,* Vol 21 (No. 11), 1981, p 749
19. E. Metcalfe, M.R. Taylor, and J.P. Broomfield, Oxide Dating for Service Failure Investigations: An Error Assessment of the Technique, *Corros. Sci.,* Vol 24 (No. 10), 1984, p 871
20. R. Viswanathan, *Damage Mechanisms and Life Assessment of High Temperature Components,* ASM International, 1989
21. F.A. Scerbo and J.J. Pritchard, Fault Tree Analysis: A Technique for Product Safety Evaluation, ASME Publication 75-SAF-3, 1975
22. J.B. Fussell and D.P. Wagner, Fault Tree Analysis as a Part of Mechanical Systems Design, *Engineering Design,* Proceedings of the Mechanical Failures Prevention Group, 25th Meeting, NBS 487, National Bureau of Standards, 1976, p 289–308
23. M. Krasich, Use of Fault Tree Analysis for Evaluation of System-Reliability Improvements in Design Phase, *Proc. Annual Reliability and Maintainability Symposium,* 2000, p 1–7
24. John B. Bowles, Failure Modes and Effects Analysis, *Failure Analysis and Prevention,* Vol 11, *ASM Handbook,* ASM International, 2002, p 50
25. M.R. Louthan, Jr., Fault Tree Technique and Failure Analysis, *Metallography,* Vol 11, 1978, p 33
26. A.R. Shamala and A.C. Raghuram, Fault Tree Technique for Failure Analysis, Part 1: Fundamentals of Fault Tree Analysis and Its Uses, *Trans. Indian Inst. Met.,* Vol 35 (No. Special), April 1982, p 1
27. A.R. Shamala and A.C. Raghuram, Fault Tree Technique for Failure Analysis, Part II: Application of Fault Tree Technique for Failure Analysis, *Trans. Indian Inst. Met.,* Vol 35 (No. Special), April 1982, p 7
28. A.R. Shamala and A.C. Raghuram, Application of Fault Tree

Technique to Hydrogen Embrittlement, *Trans. Indian Inst. Met.,* Vol 35 (No. Special), April 1982, p 53
29. C.E. Witherell, Mechanical Failure Avoidance Strategies and Techniques, McGraw-Hill, New York, 1994
30. U.S. MIL-STD-1629A, 24 Nov 1980, "Procedures for Performing a Failure Mode, Effects and Criticality Analysis," Department of Defense, Washington, D.C.
31. J.A. Collins, B.T. Hagan, and H.M. Bratt, The Failure-Experience Matrix—A Useful Design Tool, *J. Eng. Ind. (Trans. ASME),* Vol 98, 1976, p 1074
32. J.A. Collins, B.T. Hagan, Jr., and H.M. Brett, Helicopter Failure Modes and Corrective Actions, *Proceedings 1975 Annual Reliability and Maintainability Symposium,* Jan 28–30, 1975 (Washington, D.C.), p 504
33. P.R. Roberge, M.A.A. Tullmin, K.R. Trethewey, Failure Analysis by Case-Based Reasoning, *http://www.corrosionsource.com/events/intercorr/techsess/papers/session7/*; Web site accessed April 2005
34. H.W. Walton, Failure Diagnostics—Application of Expert Systems in Proceedings of the First International Conference on Failure Analysis, July 8–11, 1991 (Montreal, Quebec, Canada), J.I. Dickson et al., Ed., ASM International, p 207
35. V. Weiss, *Towards Failure Analysis Expert Systems,* ASTM Standardization News, April 1986, p 30

Failure Analysis of Engineering Structures: Methodology and Case Histories
V. Ramachandran, A.C. Raghuram, R.V. Krishnan, S.K. Bhaumik, p45-51
DOI:10.1361/faes2005p045

CHAPTER 6

Explosive Sabotage

DAMAGE BY EXPLOSIVE SABOTAGE continues to be a serious and increasing threat to structures all over the world. This is particularly true for international targets such as passenger aircraft. As the speed and seating capacity of modern aircraft increase, so do the number of fatalities and extent of damage caused.

In such accidents, positive identification of damages caused by the explosive forces is extremely important. This task becomes difficult because of the extensive subsequent damage to the structure by the crash impact forces. Delineation of the damages due to the two types of forces is important for the investigation of such accidents. Extensive experimental work (Ref 1) has established that certain unique and permanent features are found in the fragments of aircraft materials that disintegrated as a result of the explosion. These have been useful in the detection of explosive sabotage of aircraft (Ref 2–6).

Three major accidents have taken place in the history of Indian civil aviation due to mid-air explosion: the Super Constellation aircraft, Kashmir Princess of Air India over the South China Sea, in 1955; the Boeing 737 aircraft, VT-ECR, of Indian Airlines on a scheduled flight from Trivandrum to Madras, in 1979; and the Boeing 747 aircraft, VT-EFO, Kanishka, of Air India over the Atlantic Ocean, in 1985, during a scheduled flight from Montreal to London. The details of the latter two are described in later sections.

Explosive chemicals under suitable impulse undergo decomposition at a very fast rate. This liberates a large amount of energy with the evolution of a large volume of gas at very high pressure and temperature. Particle velocities during explosion can be as high as 8000 m per second. Pressures generated can be of the order of 200,000 to 400,000 atm and temperatures of the order of 3000 K.

In the primary zone of explosion, that is, close to the detonating charge, the energy is sufficient to shatter the aircraft material. The primary fragments are either those of the container of the explosive or the metal in contact with the explosive device. Away from this primary zone, the forces may not be sufficient to shatter the material but can produce large tears. The pieces from these two zones have certain characteristic features, such as surface markings, edge characteristics, specific shapes, and microstructural changes that could have been caused only by explosive forces. These are the "signatures" that help in confirming damage due to explosion.

6.1 Signatures of Explosion

In aircraft accidents, fractures of metals caused by explosive forces are distinct from those caused by normal crash impact forces. The signatures of explosive deformation and fracture are found only in a small fraction of shatter fragments. The vast majority of fragments have no specific description. Disintegration of such ductile metals as aluminum into a very large number of tiny fragments is a feature not normally found in wreckages due to other causes. Hence, presence of many small fragments of such nonbrittle materials as aluminum in the wreckage is a strong indication of explosion. The guiding rule is that the presence of fragments of maximum dimension less than 25 times the thickness is a strong indication that they were produced by explosive forces rather than impact forces.

6.1.1 Petaling and Curling

The metal nearest to the explosive charge fractures first as a result of the high-intensity shock. The adjacent areas are restrained. Hence, the part that fractured first tends to curl over onto the restrained area, away from the blast center. Figure 6.1 shows the typical petaling and curling on the reverse side of a sheet subjected to explosion.

6.1.2 Chemical Residues

When an explosive detonates near a structure, the decomposition is never complete, and hence, residues of the explosive chemical or its decomposition products get deposited on nearby surfaces. Modern high explosives such as trinitrotoluene (TNT),

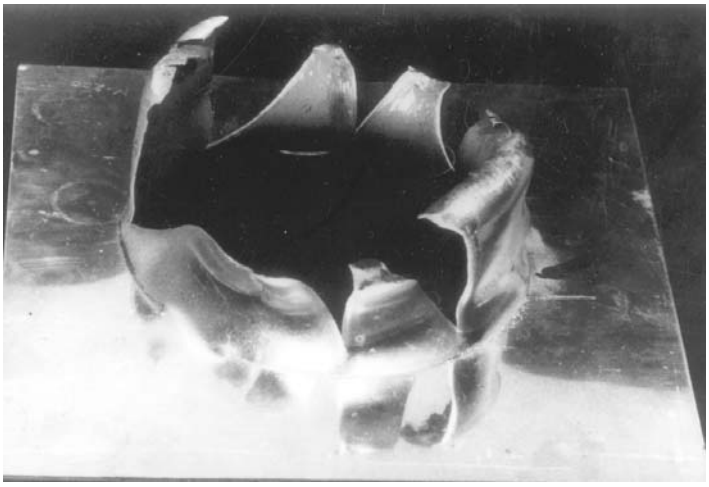

Fig. 6.1 Petaling and curling on the reverse side of a sheet subjected to explosive fracture

cyclotrimethylene trinitramine (RDX), cyclotetramethylene tetranitramine (HMX), tetryl (trinitrophenyl methylnitramine), and pentaerythritol tetranitrate (PETN) contain nitro and nitramine groups. Various microanalytical techniques and spot tests are available for detecting and identifying these residues even in traces. Microchemical analysis is complementary to metallurgical examination. The chemical tests should also include tests for other materials such as Wood's, metal used as an absorbent in dynamite, manganese dioxide, magnesium chloride, mercury from batteries, and sulfur and potassium nitrate from gun powder.

6.1.3 Shapes of Fragments

Wire and Rod Fragments. The fragments shattered from the primary zone of explosion have certain characteristic shapes. Some of them are in the form of thin rods, their cross section being a parallelogram or triangular. These are formed when two 45° shears run across the thickness of a metal sheet, parallel to each other or intersecting at an angle. The length-to-thickness ratio of such fragments is generally in the range 20:1 to 50:1.

Fig. 6.2 A curled fragment

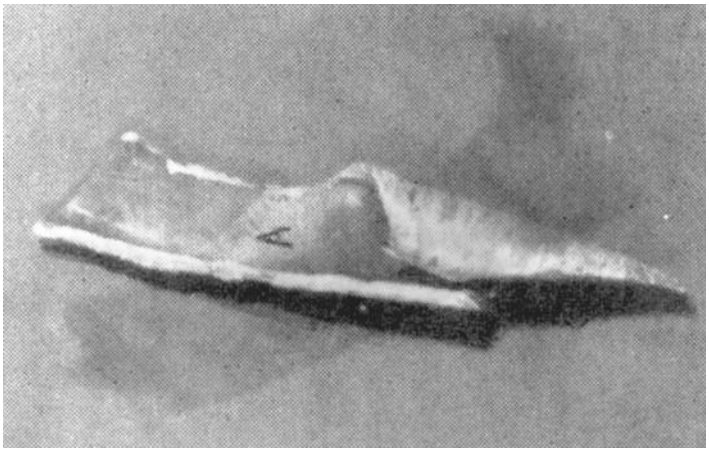

Fig. 6.3 A curved fragment

Curled Fragments. When fracture occurs in sheet metal due to explosion and results in a tear, the free end of the strip of metal is subjected to high acceleration forces while the other end is still attached to the main sheet. This results in the formation of tight rolls of one or two turns in thin sheet and spirals in thicker sheets. It is reported that this feature can be produced also by other means, and hence, immediate conclusions cannot be drawn from the presence of these curls alone. Figure 6.2 shows a typical curled fragment.

Curved Fragments. Some of the fragments assume shallow shapes with small radii of curvature, as shown in Fig. 6.3. These are not formed by impact forces and their presence in the wreckage may be taken as an indication of explosive damage.

Spalling. Explosions produce shock waves both longitudinal and transverse, which traverse through the thickness of metal. As the waves meet the edges of the sheet, additional waves are created. The encounters between the various waves create highly localized stress inhomogeneities, which lead to peculiar fractures. A compression wave through the sheet metal is reflected as a tension wave from the rear surface of the sheet. Their interference results in a fracture on a plane parallel to the sheet surface. This phenomenon is called *spalling.* Figure 6.4 shows a typical spalled fragment where part of the thickness is lost. Spalled fragments are found in the primary zone of explosion.

6.1.4 Edge Features

Reverse slant fracture is a characteristic feature that can be observed on the edges of fragments produced by explosion (Fig. 6.5). The metal has failed in a 45° slant fracture over a short distance. The fracture continues in the same general direction but with the slope of the slant reversed. The frequency of the reversal of this slant fracture is greatest close to the explosion center.

Spikes. By a combination of tear and shear forces, a series of spikes are formed along the fracture edges in small fragments of size ranging from 6 to 50 mm. The number of spikes ranges from

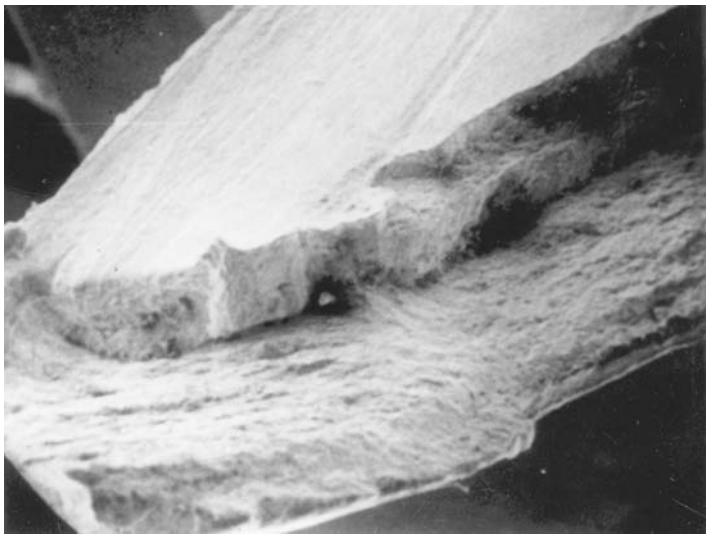

Fig. 6.4 A spalled fragment. Note the fracture on a plane parallel to the sheet surface.

a few to several dozen. The spikes need not be sharp; they can also be wavy. Figures 6.6 and 6.7 show a typical set of spikes on the fracture edge of a fragment. These are produced only by explosive forces and not by any other means.

Fig. 6.5 Reverse slant fracture

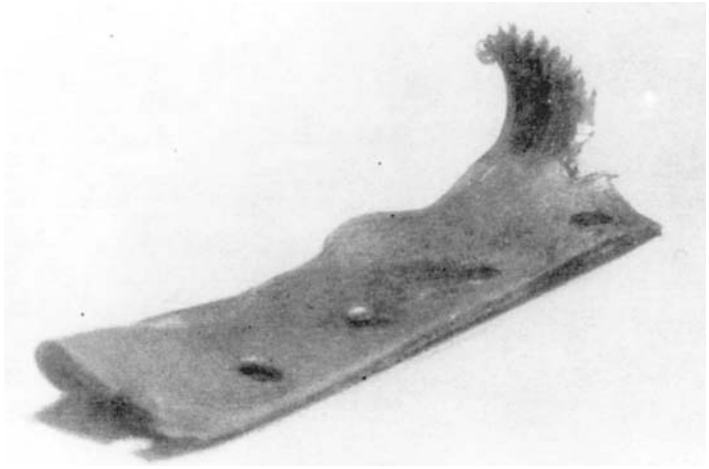

Fig. 6.6 Spikes on the fracture edge of a fragment

Fig. 6.7 SEM photograph of the spikes

6.1.5 Sheet Surface Features

Craters. Explosive charges contain minute porosity. On detonation, these pores collapse to form tiny gas jets of high velocity. These jets impinge on the sheet metal surface and produce numerous craters, ranging in size from pinpoint to pinhead, usually with raised rims. Particles of incompletely detonated explosives and filler materials can also strike the sheet metal surface and produce these craters. These craters cannot form by any other means. Presence of these craters is a conclusive proof of damage by chemical detonation. Figure 6.8 shows typical craters.

Metal Deposits. High-velocity shock waves moving over a metal surface can erode and transport the metal, which can get deposited in regions away from the center of explosion. Such deposits are generally loose and can be easily peeled off and analyzed. Residues of explosives may be found on such deposits.

Surface Erosion. Whenever metal has been removed by the previously mentioned mechanism, the remaining parent surface can be seen as severely eroded. This is generally observable in thick sheets. In thin sheets, fragmentation follows erosion, and finding eroded fragments in a wreckage is generally difficult.

Rippling. Deformation of the surface layers sometimes produces a rippled surface similar to the one shown in Fig. 6.9. This can happen when the surface of the sheet is disturbed by a high-velocity shock wave moving obliquely. This rippling effect can also be produced when a fragment hits a hard surface at a high velocity.

Fissures. By fracture on very closely spaced planes, the surface of a shatter fragment assumes a fissured appearance. The numerous open cracks run through the sheet thickness. This feature is seen in tiny fragments from the primary zone of explosive fracture.

6.1.6 Microstructural Changes

Deformation under explosive conditions takes place at very high strain rates, of the order of $10^6\ s^{-1}$. Two important microstructural changes, namely, adiabatic shear and twinning, can take place under such conditions.

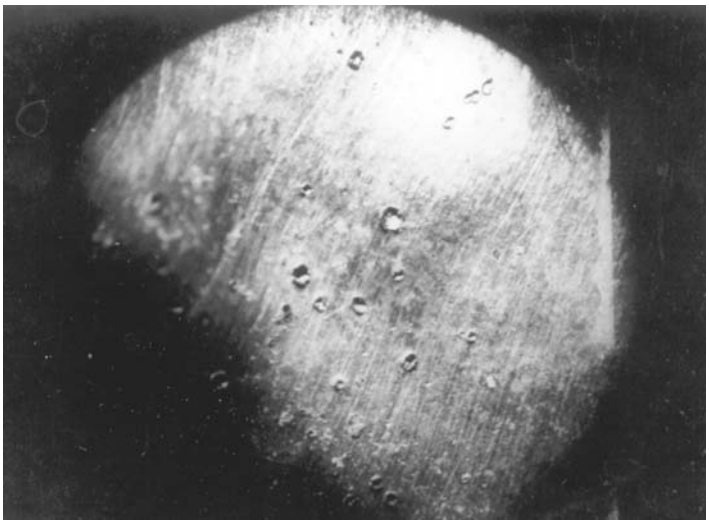

Fig. 6.8 Typical explosion craters in a fragment

Adiabatic shear. When the deformation is highly localized, and the heat of plastic deformation cannot be dissipated fast, adiabatic shear bands are produced in metals and can be readily recognized in their microstructure. Such shear bands have been seen in steels, copper, titanium, and aluminum alloys subjected to projectile impact and explosive fragmentation. However, formation of shear bands alone cannot be taken as conclusive proof for explosive damage because they can be formed even under relatively less severe conditions.

Twinning. Deformation in many metals under normal strain rates takes place by dislocation motion on definite slip planes. This is a thermally activated process. At high strain rates, dislocation motion cannot cope with the strain rates imposed. There is insufficient time for thermally activated dislocation motion to occur. Under these conditions, other mechanisms of deformation operate. Twinning is such a mechanism. In iron and mild steel, metallographic studies on fragments recovered from some of the air crashes caused by chemical explosion clearly indicated the presence of deformation twins (Ref 7). Twins were also detected in explosively fragmented mild steel in laboratory experiments (Ref 8).

Aluminum alloys have many slip systems and their stacking fault energy is high. Slip is the normal deformation mode in these alloys. They are not prone to twinning under normal deformation conditions. However, in fragments produced in the laboratory by detonation, deformation twins have been found in the 2024 aluminum alloy. Figure 6.10 shows twins in the microstructure of some of these fragments. Formation of twins in aluminum-4% copper alloy under explosive deformation conditions has also been reported (Ref 9). Twins in the microstructure of aluminum alloy fragments from an aircraft wreckage is conclusive proof for explosive damage.

With a knowledge of the previously mentioned signatures of explosive damage, the cause of two major aircraft accidents, namely, the accident to a Boeing 737 aircraft of Indian Airlines at Madras and the accident to a Boeing 747 aircraft of Air India, off the west coast of Ireland, has been established to be explosive sabotage (Ref 5, 10, 11). The details of these major investigations are given in the following sections.

6.2 Aircraft Accidents due to In-Flight Detonation

Accident to a Boeing 737 Aircraft. In 1979, a Boeing 737 aircraft on a scheduled flight from Trivandrum to Madras suffered a mid-air explosion about 20 minutes before landing, causing injuries to the crew and damage to the cockpit instruments and the front toilet area. In spite of multiple emergencies, the pilot continued to fly and made an emergency landing at Madras. The aircraft overshot the runway, the engines got severed, and the undercarriage and underside were damaged. Although it was known that a mid-air explosion had occurred, it was necessary to provide material evidence to the Court of Inquiry to establish the cause.

Detailed examination of the wreckage including the nature and extent of damage to the aircraft clearly pointed to the front toilet area as the possible center of explosion. References 5, 6, and 10 provide details of this investigation. A large number of tiny metal fragments were recovered from the front toilet compartment, the cockpit, and the ground below and were studied in detail by optical and scanning electron fractography.

The waste towel receptacle, which is usually kept below the wash basin in the toilet, had disintegrated into fragments that were found to have certain distinct features. They were found twisted and curled. Some of them had holes pierced through them. Some had both sharp and glancing dents. Their orientation indicated explosive damage from the inside to the outside. Curling was pronounced along the fracture edges and at the free ends of the tongues of metal around the holes. The signatures of explosive deformation and fracture described earlier could be readily recognized in these fragments (Fig. 6.11).

Further evidence for explosive damage was provided by the nature of damage to the structure and fittings in and around the

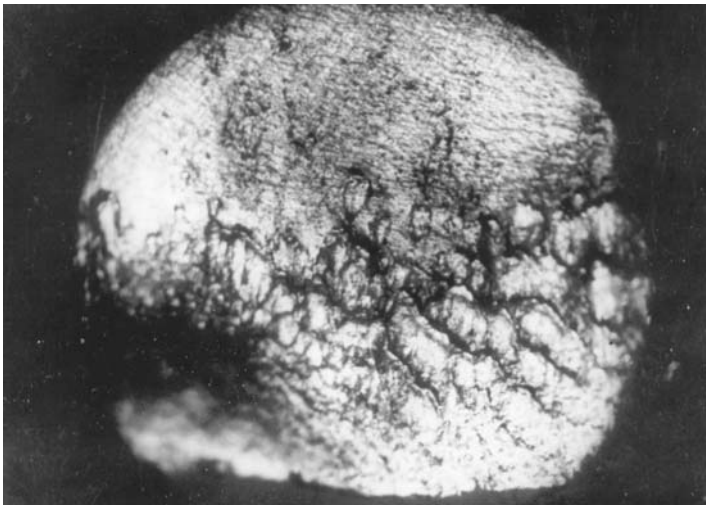

Fig. 6.9 A fragment showing a rippled surface

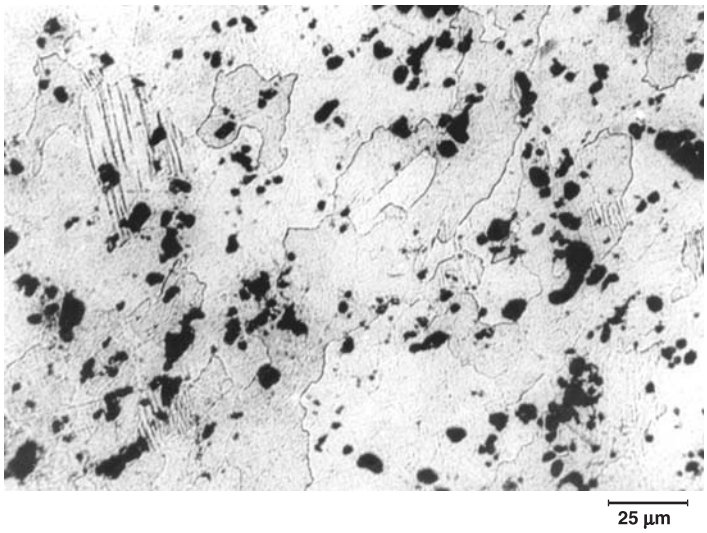

Fig. 6.10 Microstructure of a 2024 aluminum alloy fragment showing twins

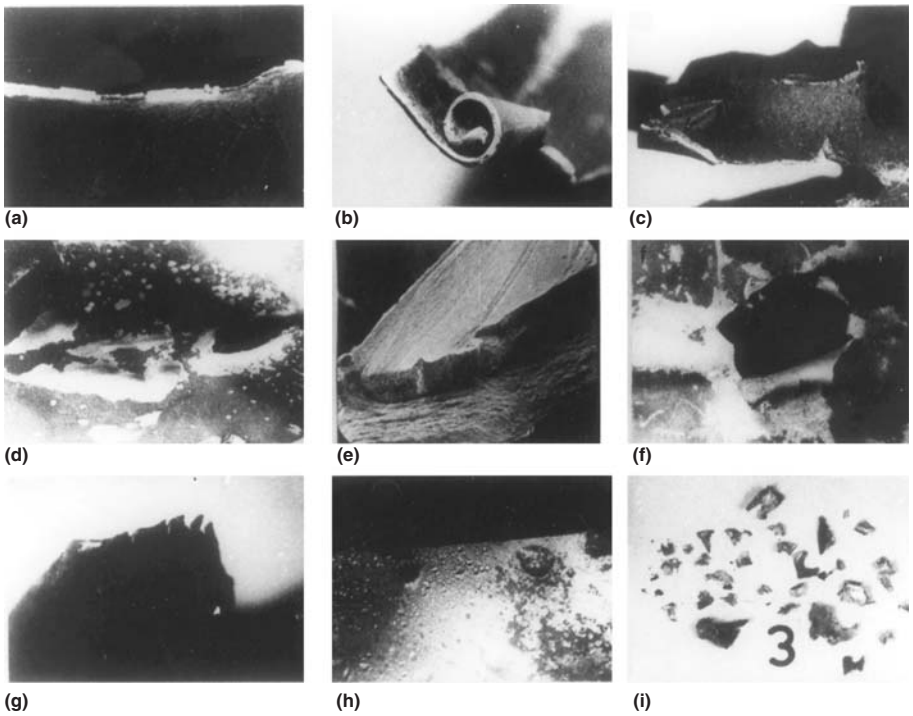

Fig. 6.11 Signatures of explosive deformation and fracture on fragments retrieved from the wreckage. (a) Reverse slant. (b) Curled fragment. (c) Curved fragment. (d) Dent. (e) Spalled fragment. (f) Petaling and curling. (g) Spikes along fracture edge. (h) Craters on sheet metal surface. (i) Nondescript fragments

front toilet. Guided by these and by tracing the trajectories of projectiles in the damaged front portion of the aircraft, investigators established the inside of the waste towel receptacle below the wash basin in the front toilet compartment as the center of explosion. Thus, by fractography, the primary cause of the accident was proved to be the detonation of an explosive. Damage to the underside and undercarriage of the aircraft was secondary and had taken place as a result of emergency landing at high ground speed.

Accident to a Boeing 747 Aircraft. In 1985, a Boeing 747 aircraft on a scheduled flight from Montreal to London en route to India suddenly plunged into the Atlantic Ocean, about 110 miles off the west coast of Ireland. Using state-of-the-art technology, with the help of a remotely operated unmanned submersible vehicle known as a search craft aiding repair and burial (SCARAB) vehicle, originally intended for laying telephone cables beneath the ocean floor, the wreckage was located and its distribution documented by extensive underwater photography and videography. The wreckage was distributed over an area of 15 square miles on the floor of the ocean, 6700 feet deep. After studying a few thousand underwater photographs and viewing a few dozen video tapes, about 20 pieces of wreckage considered essential for further laboratory examination were retrieved from the ocean floor, with the help of SCARAB and two ships working round the clock for a few weeks. A large number of small fragments could also be retrieved along with the larger pieces. Study of the disintegrated aircraft indicated maximum damage in the front portion of the aircraft, especially in and around the front cargo hold.

The most mangled piece of wreckage was the bottom skin of the front cargo compartment (Fig. 6.12). Severe damages such as holes and tears were seen at 25 different locations on this piece. This accident was yet another instance where the features on explosively damaged pieces did survive further crash impact forces as well as immersion in seawater for several weeks.

Many of the important signatures of explosive damage were seen in this piece and on several fragments from this region (Fig. 6.13–6.15). Another important evidence was the mode of fracture

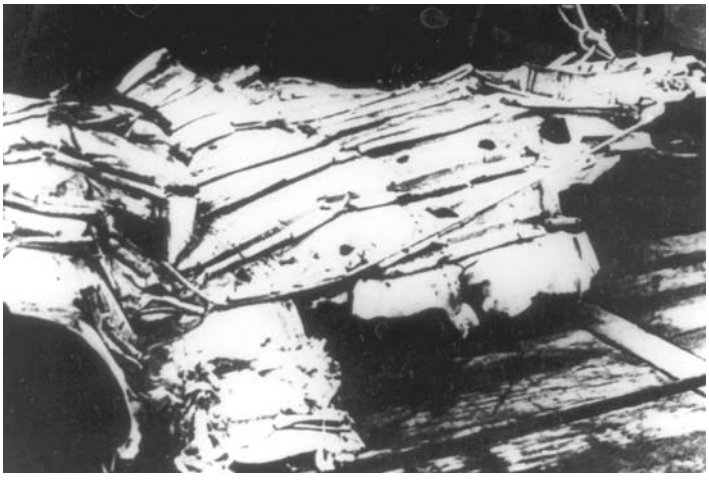

Fig. 6.12 Bottom skin of the front cargo hold of the Boeing 747 aircraft, retrieved from the ocean. Source: Ref 11

of a structural member in the front cargo compartment. This member, referred to as a stantion, is a square tube in which the fracture was followed by the distinct curling of the metal tongue inward, toward the interior of the tube (Fig. 6.16a). This type of inward curling by more than one turn, shown in the radiograph, Fig. 6.16(b), is certainly a shock wave phenomenon.

The most conclusive evidence was provided by metallography. Metallographic examination was carried out on several fragments retrieved from the front cargo area, on petals around holes, on regions adjacent to the spikes, and on regions close to the curl in the stantion. Twins were seen in the microstructure on all of them. Figure 6.17 shows a typical microstructure revealing twins.

To obtain a further confirmation of the earlier conclusions, fragments were also produced in the laboratory by deliberately exploding 2024 aluminum alloy sheets and boxes made out of such sheets. All the features described previously could be recognized in the fragments thus generated. This produced further evidence for confirming the cause of the two accidents described previously as in-flight explosion (Ref 10, 11).

In this chapter, methods of identifying damages caused by explosive forces have been described. These have helped in the investigation of accidents to aircraft, caused by deliberate detonation of explosives in flight. The principles can be extended to damages on other structures as well.

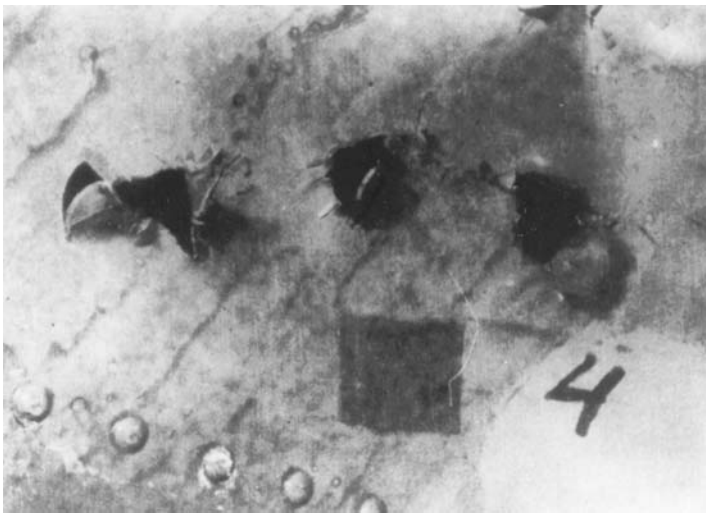

Fig. 6.13 Petaling around holes in the bottom skin of the front cargo hold. Source: Ref 11

Fig. 6.15 Spikes along fracture edge. Source: Ref 11

Fig. 6.14 Curling of metal tongues. Source: Ref 11

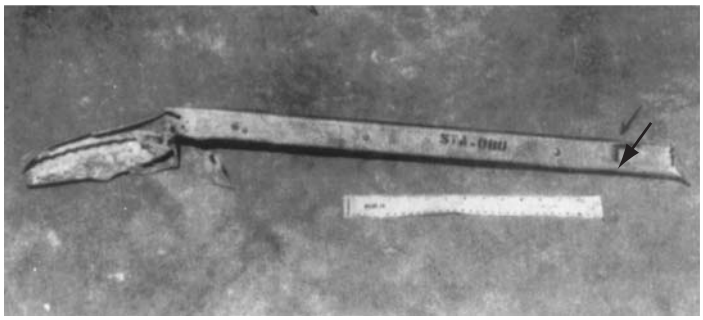

(a)

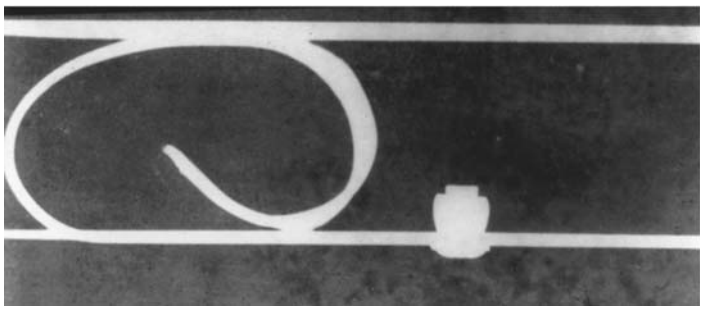

(b)

Fig. 6.16 (a) Fracture in a stantion. (b) Radiograph showing metal curling inward. Source: Ref 11

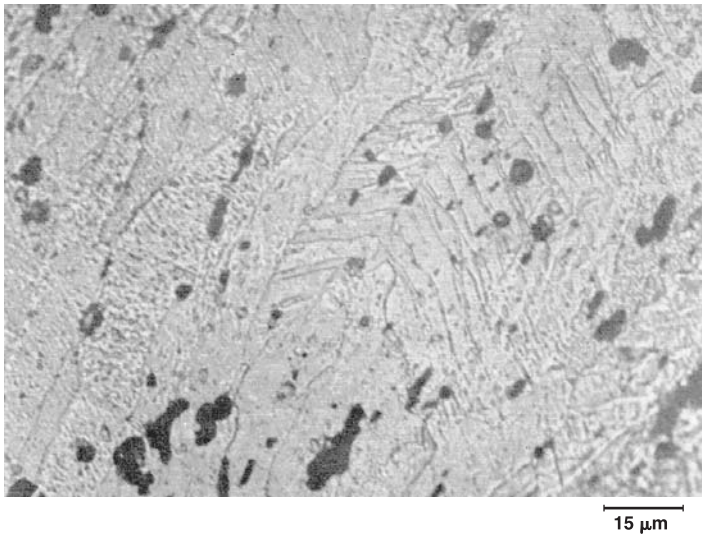

Fig. 6.17 Microstructure of a fragment from the front cargo compartment showing twins. Source: Ref 11

REFERENCES

1. H.P. Tardif and T.S. Sterling, *J. Forensic Sci.,* Vol 12 (No. 3), 1967, p 247
2. E. Newton, *Can. Aeronaut. Space J.,* Vol 14, 1968, p 385
3. H.P. Tardif and T.S. Sterling, *Can. Aeronaut. Space J.,* Vol 15, 1969, p 19
4. R.D. Barer and T.S. Sterling, *Met. Prog.,* Vol 98 (No. 5), 1970, p 84
5. R.V. Krishnan, S. Radhakrishnan, A.C. Raghuram, and V. Ramachandran, Investigation of an Aircraft Accident by Fractographic Analysis, *Advances in Fracture Research,* S.R. Valluri et al., Ed., Pergamon Press, Vol 5, 1984, p 3677
6. A.C. Raghuram, S. Radhakrishnan, R.V. Krishnan, and V. Ramachandran, *Sci. Age,* Vol 3 (No. 8), 1985, p 32
7. V.T. Clancey, *Can. Aeronaut. Space J.,* Vol 14, 1968, p 337
8. J.S. Rinehart and J. Pearson, *Behaviour of Metals under Impulsive Loads,* Dover Publications Inc., New York, 1954, p 171
9. M. Stelly, J. Legrand, and R. Dormeval, Some Metallurgical Aspects of the Dynamic Expansion of Shells, *Shock Waves and High-Strain-Rate Phenomena in Metals—Concepts and Applications,* M.A. Meyers and L.E. Murr, Ed., Plenum Press, New York and London, 1980, p 113
10. R.V. Krishnan, S. Radhakrishnan, A.C. Raghuram, and V. Ramachandran, Aircraft Accident Caused by Explosive Sabotage, *Handbook of Case Histories in Failure Analysis,* Vol 2, ASM International, 1993, p 3
11. B.N. Kirpal, V. Ramachandran, J.S. Gharia, J.S. Dhillon, J.K. Mehra, B.K. Bhasin, and S.N. Sharma, "Report of the Court of Inquiry Investigating Accident to Air India Boeing 747 Aircraft VT-EFO, Kanishka on 23 June 1985," New Delhi, 1986

Failure Analysis of Engineering Structures: Methodology and Case Histories
V. Ramachandran, A.C. Raghuram, R.V. Krishnan, S.K. Bhaumik, p53-57
DOI:10.1361/faes2005p053

CHAPTER 7

Forensic Failure Analysis

FORENSIC SCIENCE refers to that part of science that is used in courts of law for administration of justice. Service failures of machines and accidents to engineering structures result in serious, expensive, and prolonged litigations, affecting the credibility of the manufacturer and the reliability of its products. When defective consumer products fail to perform their intended functions and thereby cause injuries to personnel or damage to property, the user resorts to product liability litigations. Litigations also follow when damages to structures, life, and property are caused by deliberate acts of sabotage by antisocial elements.

Investigations of such mishaps are of two kinds, preventive and punitive, i.e., inquisitorial and accusatorial. In the former, attempts are made to find out the cause of the malfunction or failure of a component with a view to making technical and procedural improvements to prevent its recurrence. Various techniques available for such inquisitorial investigations are described in earlier chapters. In the accusatorial type, the investigation is legal in character and requires generation of data of sufficiently high standard to provide proof for the judiciary to justify penal and censure action for the violation of established laws and codes. Such high standards are necessary even in departmental inquiries, without the involvement of the judiciary, for fixing responsibilities. Most of the failures of machinery and accidents to engineering structures involve a combination of component malfunction and mismanagement. In many such situations, both types of inquiry are necessary.

Industrial machinery and structures are made of materials, mostly metallic. As seen in earlier chapters, when these structures fail, they leave certain distinct tell-tale marks. These marks, when properly documented, can provide the exacting evidence the judiciary is looking for in litigations following such failures. The courts are now depending more and more on the metallurgical profession for making correct decisions in such litigations. A few case histories, including product liability litigations, are presented in this chapter to illustrate the importance of metallurgical jurisprudence or how the judiciary can take advantage of the metallurgical profession and expertise in administering justice.

7.1 Product Liability Litigations

Product liability litigations pose many challenges to manufacturers. If a consumer product is defective and during its usage causes injuries to the user, the manufacturer of that product becomes *liable* and is sued in courts. When a product is sold, there is a written warranty or contract about its performance. The second aspect of the contract that is implied is that the product should be reasonably safe. Failure to perform its intended function satisfactorily and safely constitutes a breach of warranty and, hence, liability. In courts of law, product liability is extended not only to the manufacturer of the whole product but also to the designer, the maker of component parts, the assembler, the person who installs it, the repairer, and also the distributor and the retail seller. The absence of privity of contract, i.e., direct connection between the plaintiff and the defendant, does not preclude liability in tort. Thus, in a product liability litigation, liability is imposed also on people behind the scenes.

In order to provide for an orderly and logical flow of evidence, some product liability advocates prefer what is called a seriated trial. According to this proposal, the trial is conducted in three stages:

1. The first segment of the trial involves evidence pertinent only to the product and ultimately whether it was defective and unreasonably dangerous, considered apart from the actual injury-producing event.
2. If a positive decision is reached, the trial continues. Evidence relative to the injury-producing event is presented on the basis of which the jury/court must determine whether the defective product caused the accident.
3. If a positive decision is reached, the trial then turns to the final question of the extent of liability of the manufacturer. This methodology ensures that the jury/court will be properly informed of the design and use of the product and, consequently, will be able to make knowledgeable decisions.

Product liability litigations, each requiring technical skills of varying degrees of complexity, have become more common in many cases, and product liability insurance premiums have become a major cost in some industries. One or two product liability litigations can potentially wipe out a small company by way of legal expenses and compensation paid to the victims. It is not uncommon that product liability cases are settled between the parties out of court. A few product liability cases are described next.

Collapse of Domestic Ladders. Several litigations following the collapse of aluminum ladders have been reported. In one case, when a woman, standing on a ladder, was trying to remove dry leaves from the roof of her house with a rake, the ladder collapsed. She sustained hip injuries and sued the company that manufactured the ladder. In another case, when a man was trying to paint his

house, his ladder collapsed, causing him injuries. He sued the ladder manufacturer and also the retail store that sold him the ladder.

Collapse of ladders has been attributed to improper riveting of the cross supports to the side rails of the ladder; excessive projection of the legs below the first rung of the ladder; and improper heat treatment of the ladder material resulting in the precipitation of brittle intermetallics along the grain boundaries, reducing the toughness of the alloy. In several cases, even though the correct grade of alloy had been used for making the ladder, stress analysis, taking into account the lateral forces generated during operations such as painting, proved that the ladder had mechanical instability.

Manufacturer's Liability. If a product is proved to be defective, replacement of the defective part is the liability of the manufacturer. Anticipating malfunctions, failures, accidents, and litigations to follow, some of the manufacturers have wisely taken corrective actions to avoid mishaps and litigations. The following are some of the examples.

A company had developed a compost thresher machine and introduced it in the market. Soon, the company realized that the speed of the intake mechanism was very great and might exceed the human reaction time. The operator's hands could be sucked into the machine. Realizing this design flaw, the company stopped production to avoid liability litigations (Ref 1).

In the 1100 kVA marine engine, described in Chapter 2, "Common Causes of Failures," the piston head failure was due to misalignment. Following the failure investigation, a campaign was ordered by the manufacturer to check the alignment and balancing of the pistons in all the engines sold by them.

A batch of aluminum alloy extrusions was procured for use in the fabrication of aircraft wings. During inspection for acceptance, blisters were noticed on their surface. When the extrusions were solution treated, the blisters were found to increase in size and number. Sectional metallography revealed the presence of cavities below the blisters, and these could open up easily during service. These blisters are formed due to hydrogen pickup during melting and remain in the metal due to inadequate degassing. Use of blistered extrusions would endanger the aircraft because these blistered areas are vulnerable for crack initiation. The manufacturer, realizing the liability, replaced the entire batch of extrusions with acceptable grades.

In the automobile industry, cases have been reported regarding withdrawal of entire lots of cars from the market for repair and replacement, after realizing that the cars had serious defects that made them unsafe.

7.2 Litigations Following Accidents

A Traffic Accident. It is amazing that complex legal issues have been solved by the thorough visual examination of the failed component and its surroundings by an experienced metallurgist. One such case has been reported (Ref 2). The case followed a traffic accident involving an automobile and a motorcycle, in which the motorcyclist received serious injuries and sued the automobile driver. The lawyer for the defendant hired the services of a consulting firm, which presented a report stating that it was its opinion that at the time of the accident, the headlight of the motorcycle was not switched on and hence the motorcyclist was at fault. The report of the consulting firm in this case contained only photographs of the motorcycle and the scene of the accident and no technical evidence to support its opinion. It was further observed (Ref 2) that many consulting firms depended on established relationships with insurance companies for their financial survival and, hence, rendering unbiased opinions in such circumstances would be difficult.

The lamp had two sets of metal posts with attached tungsten filaments. Macroscopic examination of the damaged headlamp gave very clear evidence (Fig. 7.1) that particles of melted and solidified glass were sticking to one of the filaments. This filament must have been on at the time of the accident. The other filament was off as shown by the shiny appearance of its two ends, but its central portion was oxidized. The impact of the accident had caused this filament to contact the other filament that was on. This had resulted in heating of the central portion and oxidation when the lamp shattered and exposed the hot filament to atmosphere. Having established the exacting evidence that the lamp was on, the case was settled in favor of the plaintiff, the motorcyclist.

A Machine Shop Accident. When seeking exacting evidence in litigations following accidents, one should go to the correct expert. In a machine shop, during a grinding operation, a fragment of metal entered the operator's eye and he lost his eye. The metal fragment was recovered and given to a scientist who dissolved it

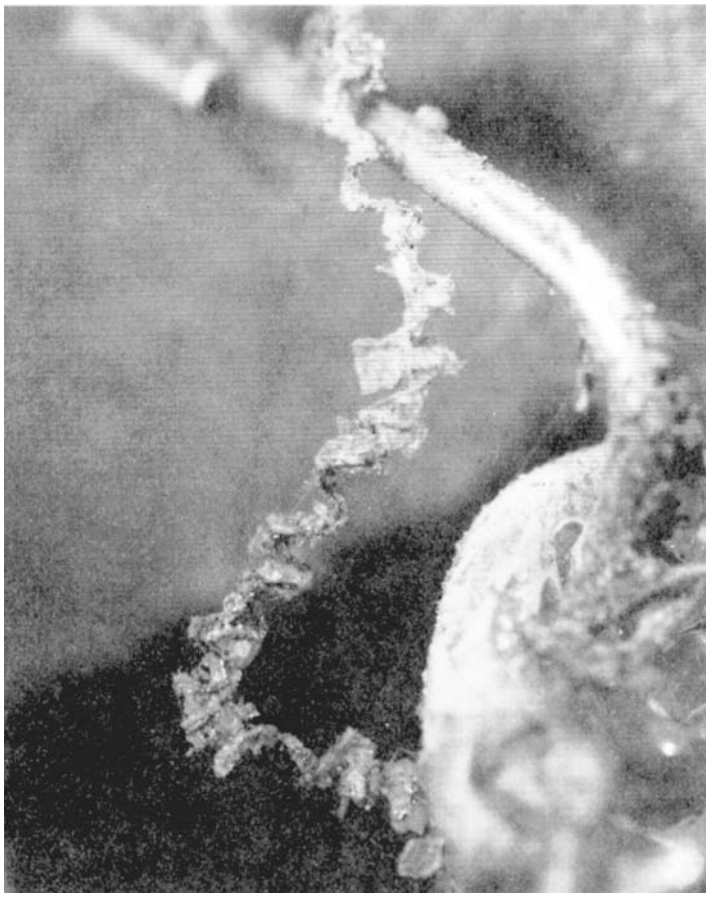

Fig. 7.1 Glass particles fused to a filament. Source: Ref 2. With kind permission of Elsevier Publishing Company

in acid for chemical analysis. In so doing, important evidence was lost. If the piece had been given to a metallurgist, he would have studied it in the scanning electron microscope (SEM), identified the fracture mode and fracture origin, and also analyzed it in a nondestructive way by energy-dispersive x-ray spectroscopy (EDS). Going to the right expert is thus imperative in accident investigations (Ref 1).

A Tool Accident. A man was trying to split logs of wood using steel wedges and striking them with a sledgehammer (Ref 2). While striking for the second time, suddenly a chip from the wedge flew into his eye, and he eventually lost his eye. Litigation followed against the supplier of the hammer and the wedges. The case hinged on metallurgical investigations of the hammer and the wedges. It was impossible to cut the head of the chipped wedge with a cut-off wheel, indicating very high hardness. The hardness of the wedge was found to be 52 HRC, against the manufacturer's specification of 38 to 42 HRC. Hammerheads are usually heat treated to a hardness level of 52 to 55 HRC. The lower hardness of 38 to 42 HRC is specified for the head of the wedges so that when struck with the hammer, the wedge head can absorb the energy and plastically deform to take a mushroom shape, thereby warning of imminent chipping.

Metallography of the wedge head showed the presence of adiabatic shear bands with untempered martensitic structure. Impact of the hammer as a result of high strain rate produces localized shear, the local temperature rising high enough to produce austenite, which rapidly cools to martensite. On striking again, cracks form in and around the sheared area leading to chipping. Proof of very high hardness of the wedge head above the specifications and microstructure vulnerable for cracking supported the plaintiff's case (Ref 2).

7.3 Cases of Sabotage

Mechanical Sabotage. Two cases involving deliberate damage of multi-strand steel cables are described next. A crane cable broke while lifting a load of concrete into a multi-storeyed hotel under construction, causing considerable damage to the lower portions of the building. In the litigation that followed, the crane company claimed that the cable was defective because the load of the concrete was well below the maximum load limit of the cable. The cable manufacturer claimed that the crane operation allowed the cable to flex at the area of failure and, in effect, created a cyclic stress that was responsible for the underrated load failure. To look for the evidence of fatigue failure, investigators examined the broken cable in an SEM. While there was no evidence of fatigue, surprisingly, it was found that the strands exhibited two distinct fracture features. Many of the strands had uniformly necked down as in a classical tensile failure, but others showed evidence of cut by a shearing tool. A criminal act was suspected. Further investigations revealed that a disgruntled worker had sabotaged the operation by hacking about half the cable with an axe, thereby reducing the load bearing capacity of the remaining strands and leading to failure (Ref 1).

A more serious sabotage was caused by deliberate damage of the control cables in a passenger aircraft. While this aircraft was being prepared for flight, it was noticed that some of the vital control cables were partly cut. These cables were of the multi-strand type. About half the strands in each cable had been cut by a shearing tool, as evidence of shear was noticed at the tips of the fractured strands. If the aircraft were flown under those conditions, the cables might have snapped at any moment during takeoff or cruise, leading to a catastrophe. Evidence of shear led to suspicion of deliberate damage. For further investigations, all the cutting tools, a few hundred in number, in the possession of the technicians working in the area, were seized for identification of the tool that had caused the damage to the control cables.

In one of the cables, the cutting tool had left a tool mark, which was studied in detail by microscopic examination. The shape of the tool mark indicated clearly that it had been made by a tool with a serrated edge. The serrations on the cutting edge and their pitch are class characteristics that distinguish such tools from straight-edge tools. All serrated tools were then segregated from the rest. Experimental cuts were made on a similar cable with all the serrated tools, and the tool marks thus made were individually compared, in a comparison microscope, with the one that was observed on the damaged control cable in the aircraft. By this process, one tool out of a few hundred, which alone could have caused the cut, was identified.

While comparing the tool marks in a comparison microscope as described previously, identification of the specific tool of interest was facilitated by paying careful attention to the individual characteristics of the tools and the tool marks individually produced by them.

The cutting edges of these tools are chromium plated for wear resistance. Over a period of time, the chromium plating on the cutting edges wears out. The pattern of wear varies from tool to tool and imparts an individual characteristic to the tool. This feature is like the fingerprint of an individual, which is unique to the person. Thus, when a cut is made with a tool having a particular wear pattern on its cutting edge, a faithful reproduction of the pattern is left on the tool mark. The matching between the tool marks of the experimental cut and the observed cut was perfect only in the case of one tool out of the lot of a few hundred tools. It was this feature that is an individual characteristic that established the identity of the tool that had been used for the damaging cut on the aircraft cable. This enabled the authorities to identify the owner of the tool for further investigation.

Explosive Sabotage. Deliberate damage and demolition of structures, especially international targets such as passenger aircraft, has been on the increase with the coordination of terrorists throughout the world. In aircraft accidents due to explosive sabotage, extensive damage is caused not only primarily by the explosion, but also by crash impact forces that cause secondary damages. In courts inquiring into such accidents, it is imperative to establish positive proof for damages caused by detonation of explosives. Detection of residues of undecomposed explosive chemicals by microanalytical techniques and identification of metallurgical evidence of high strain rate deformation and fracture through microscopy provide the exacting evidence to the courts. Details regarding detection of explosive sabotage, with special reference to accidents to a Boeing 737 aircraft and a Boeing 747 aircraft, are described in an earlier chapter (Ref 3). Though the discussion

is with respect to aircraft structure, the principles indicated therein are applicable to other structures as well.

7.4 A Patent Litigation

Litigations about patents may involve serious laboratory research to provide the exacting evidence. In one such case, the problem involved the ternary phase diagram W-Ti-C. The litigation was between a steel manufacturer and a carbide manufacturer. The steel company had a patent that implied that the two compounds WC and TiC formed a solid-solution series. The carbide company claimed a single compound WTiC. Ultimately, the case hinged upon an expert testimony that WC and TiC do indeed form a solid-solution series (Ref 4).

7.5 Smuggling

The popular yellow metal gold readily attracts smugglers. Various methods are adopted by the smugglers to conceal the gold from the eyes of the customs authorities. In one case, the metal was concealed in an ingenious way. In the baggage of an air traveler, three similar-looking electric pressing irons were found. On suspicion, when the irons were opened, the usual gray-colored steel/cast iron pieces as shown in Fig. 7.2 were found inside. These are generally fitted as part of the iron to make it heavy enough for effective pressing of clothes. As no yellow metal was found inside the iron, the next suspicion was that it might have been somehow hidden inside the steel gray pieces. The gray pieces were taken to a professional jeweler to test them for presence of gold. The conventional commercial method of testing by rubbing the pieces against an abrasive surface failed to reveal any streak of gold.

Next, the pieces were taken to a metallurgical laboratory with sophisticated facilities. The gray pieces were examined in an SEM and in situ EDS chemical analysis was carried out. Surprisingly, the pieces were found to have nearly 87% gold, and the rest was copper and aluminum. When these three metals are melted together, the yellow color is lost in the alloy. This was a revelation, and the results of the analysis helped the authorities to proceed further with the case. From this case, one learns that "all that does not glitter can still be gold."

Adulteration of Antiques. Ancient silver pieces contained significant amounts of copper. This fact was often disguised in an ingenious way. The silver-copper alloy antique is heated under oxidizing conditions until it forms a thick scale of cuprous and cupric oxides. The surface layers of the alloy thus become enriched in silver. When the copper oxide layer is dissolved in acid or polished off, the metal exhibits the color of pure silver. The disguised alloy is sold as pure silver. Thus, a higher price is claimed for the adulterated silver. The camouflaging can be easily brought to light by various metallurgical techniques such as sectional metallography, microhardness, EDAX, and so forth.

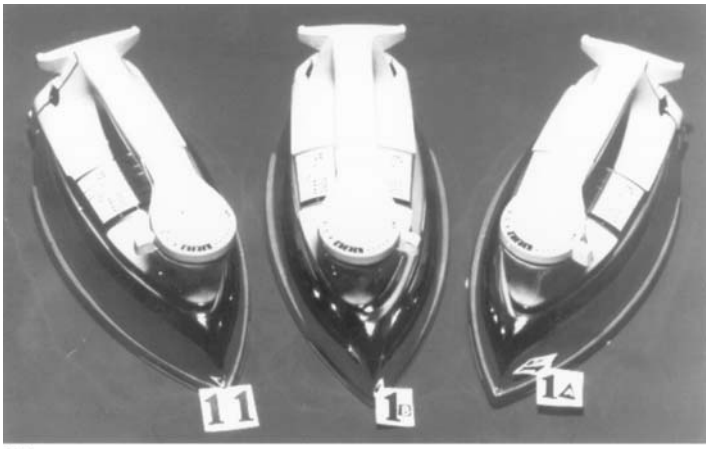

(a)

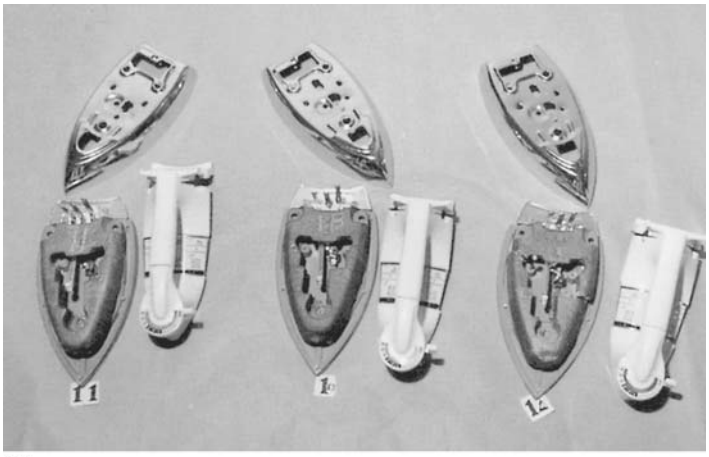

(b)

Fig. 7.2 (a) Innocent-looking electric irons. (b) Gray pieces inside the irons containing 87% gold

7.6 Theft and Counterfeiting

Icons and Art Treasures. One often hears about litigations following theft and counterfeiting of idols and art treasures. Attempts are made to sell counterfeit icons as genuine original ones. While the sculptors are adept in casting good idols, with minimum casting defects, no two similar-looking idols cast by the same sculptor have the micro defects such as porosity and inclusions at the same locations inside the two idols. Thus, if a radiograph of the idol is taken, it is unique to the particular idol. When an idol is suspected to be counterfeit, it is enough to compare its radiograph with that of the original idol, if available. Archeological departments and museums preserve the radiographs of their art treasures. Holograms are also used for similar identification.

Telegraphic Wires. Another common crime is theft of telegraphic wires for their expensive copper content. Such cases are resolved in courts by a combination of tests. When a piece of stolen telegraphic wire is recovered from a suspect, it is compared with the original wire through metallography; tool mark comparison at the cut edge surfaces; measurement of conductivity and hardness; and analysis for trace elements, which are sometimes deliberately added in the original wire.

7.7 Primary Cause and Immediate Cause

In accident investigations, while the forensic experts try to determine the primary cause of the accident, the court of inquiry is sometimes concerned about and concentrates on the immediate cause or the event immediately preceding the accident. Knowledge of the immediate cause helps in determining how the accident could have been averted. In a passenger aircraft powered by two engines, immediately after takeoff, one of the engines was on fire. A compressor disc had an uncontained fracture. Its rim got separated and flew outward, damaging the fuel line, causing the engine fire. The pilot turned the aircraft around and before he could manage to land on the runway, the fire engulfed the rest of the aircraft, damaging the vital control surfaces. The aircraft made a nose dive and all the occupants died.

In this investigation, the fracture of the compressor disc was due to a fatigue crack that rapidly propagated, separating the rim. The origin of the fatigue crack was a defect in the disc. Investigations were going on to identify the nature of the defect that originated the crack. The court, however, concerned about the immediate cause for the accident, concluded that the accident could have been avoided if only the pilot had turned off the fuel supply to the burning engine and attempted landing on one engine, for which the aircraft was designed and the pilot had been trained. Thus, in such court inquiries, the primary cause for a mishap is lost sight of.

7.8 Exacting the Evidence at Any Cost

When a court of inquiry is investigating a major disaster such as an aircraft accident, in which there are many casualties and the aircraft is a total loss, a number of organizations and agencies are concerned about the outcome of the investigation as it has several legal implications. In the case of an aircraft accident, many may face liability and risk of losing credibility, reputation, and business. These are the manufacturer, their suppliers of components and subsystems, the authorities certifying airworthiness, the carrier airline, their agents, and so on. Hence, thoroughness of the investigation is warranted. Concern arises regarding the effort for and the cost of the investigation. Need arises for exacting the evidence at any cost. A typical example is the accident to the Boeing 747 aircraft of Air India, which during a normal flight, suddenly disintegrated and plunged into the Atlantic Ocean, killing all of the 329 occupants. The accident attracted international attention. Even though mid-air explosion was suspected as the cause of the accident in the initial stages of the inquiry by the court, it was absolutely necessary to produce the exact evidence, which was a formidable and, of course, a very expensive task, as detailed subsequently.

The aircraft was lost in the Atlantic Ocean off the west coast of Ireland where the ocean depth was about 2040 m (6700 feet). To locate the wreckage, a sophisticated remotely operated state-of-the-art submersible vehicle was deployed from a ship and the ocean floor was surveyed. A wreckage distribution map was prepared. The wreckage was distributed over an area of about 15 square miles, 5 miles in the direction of flight and 3 miles in the north-south direction. About 400 pieces or groups of wreckage were located. With transponders dropped into the ocean from a ship, and with the help of a computer in the control system of the submersible, the latitude-longitude coordinates of each piece of wreckage were established. By extensive underwater photography and videography, and by referring to numerous aircraft parts catalogues, the pieces were identified. This operation took nearly two months.

At the court of inquiry, a decision was taken to retrieve the wreckage from the ocean. To retrieve one piece of wreckage from the ocean floor, two ships had to work for 25 to 30 hours. The cost of operation of a ship was about $25,000 per day. Hence, out of the hundreds of pieces located, after studying the extent of damage to the pieces with the help of thousands of underwater photographs and dozens of videotapes, a priority list of items to be recovered was prepared by a team of engineers. In the next month or so, about 20 major items of wreckage were retrieved, with two ships involved in the salvage operations. The conditions of those pieces were immediately documented. Part of the investigating studies were made onboard the recovery ship itself.

The retrieved pieces of the wreckage were brought to the shore and later shipped to India. Scientists from the National Aerospace Laboratories (NAL), Bangalore, and Bhabha Atomic Research Centre (BARC), Bombay, carried out the investigations, also using the expertise and facilities of the Defence Research and Development Organisation (DRDO) laboratories, and proved that the accident to the aircraft was due to mid-air explosion, caused by detonation of a device during flight (Ref 3).

As the accident had many legal and international implications, finding its cause with adequate evidence was extremely important whatever be the cost and extent of effort. This is an example of a very expensive investigation in the history of aviation, which produced the necessary evidence (Ref 3).

The preceding examples illustrate how the engineering and metallurgical profession can assist the judiciary. All the evidence produced by the expert would certainly be subject to serious cross examination in the courts. Yet one can arrive at the truth by strictly following the professional ethics and maintaining one's integrity and credibility.

REFERENCES

1. L.E. Murr, *What Every Engineer Should Know about Material and Component Failure, Failure Analysis, and Litigation,* Marcel Dekker, Inc., New York, 1987, p 85
2. G.F. Powell, Forensic Metallurgy, *Microstructural Science,* Vol 5, J.D. Braun et al., Ed., Elsevier, New York, 1977, p 11
3. B.N. Kirpal, V. Ramachandran, J.S. Gharia, J.S. Dhillon, J.K. Mehra, and B.K. Bhasin, "Report of the Court of Inquiry Investigating Accident to Air India Boeing 747 Aircraft VT-EFO, Kanishka on June 23, 1985," New Delhi, 1986
4. Prof. F.N. Rhines, University of Florida, Gainesville, private communication.

Failure Analysis of Engineering Structures: Methodology and Case Histories
V. Ramachandran, A.C. Raghuram, R.V. Krishnan, S.K. Bhaumik, p59-61
DOI:10.1361/faes2005p059

CHAPTER 8

Failure Analysis and After

THE LESSONS LEARNED from failure analysis have resulted in improvements in the overall housekeeping and discipline in many industries. Disaster investigations have led to improved designs and use of better materials, with enhanced reliability and safety of operations. In some cases, the entire plant has been redesigned or the entire manufacturing process altered to ensure better safety standards. The design codes, standards, specifications, and regulations for various engineering applications have been suitably modified, after identifying the deficiencies. These modifications are very significant from the safety point of view. A few examples are presented to illustrate these aspects.

8.1 Process Modification

The Flixborough Disaster. A plant at Flixborough, U.K., manufacturing caprolactam was completely destroyed and reduced to ashes, and the surrounding community was demolished with many fatalities, following a powerful explosion of warlike dimensions inside the plant (Ref 1). The details of this disaster have been described in Chapter 2, "Common Causes of Failures." The process used for making caprolactam before the disaster occurred was oxidation of cyclohexane, which is a highly inflammable and very hazardous material to handle. When copious amounts of hot cyclohexane escaped to the atmosphere due to the bursting of a pipe, spontaneous explosion was but natural, and the damages to the plant and the community were inevitable.

It may be recalled that the court of inquiry concluded that when the leaking reactor No. 5 was replaced by a dog-leg pipe with bellows at the two ends, to bridge reactors 4 and 6, there was no proper design study, no proper consideration for the need for a support, no safety testing, no reference to the relevant standards, and no reference to the bellow manufacturer's "Designer's Guides." The important outcome of the investigation was the realization that any modification in a plant should not be ad hoc, but be designed, constructed, tested, and maintained to the same standards as the original plant.

Following the disaster investigation, at Flixborough, the process itself for making caprolactam was changed, based on hydrogenation of less-hazardous phenol instead of oxidation of the highly inflammable cyclohexane.

8.2 Design Philosophy for Better Safety

In the accident at the Markham colliery, as described in Chapter 2, several miners died as a result of the cage carrying them crashing into the bottom of the pit with great force (Ref 2). The shoes of the brake system were actuated by a nest of compressed springs. The main member transmitting the force from the nest of springs through levers to the brake system was a single steel rod at the center of the nest of springs. This steel rod fractured due to a fatigue crack that was not detected earlier. It resulted in the failure of the brake system, and the miners' cage could not be stopped from rapid descent and crash.

It was obvious that the steel rod at the center of the nest of springs was an important structural member of the brake system for winding and unwinding the cable of the shaft. Thus, the safety of the miners was vitally dependent on the integrity of this single steel rod, which is an example of a "single line component."

After this accident, the design philosophy for safety was changed so as to eliminate such single line components in vital systems where overspeed and overwind protection is extremely important. Or, the system should be so designed that in the event of such a failure, the winding drum will be slowly brought to rest. Condition monitoring should be incorporated to provide warning of failure.

8.3 Use of Cleaner Materials of Construction

In a passenger aircraft, there was an uncontained fracture of a compressor disc whose fragments hit the fuel line, causing an in-flight fire and resulting in a serious accident. All the occupants of the aircraft died and the aircraft was a total loss. Investigations revealed that the subject steel disc had been made by conventional air melting followed by casting, forging, and machining to shape. Air-melted steel is not a clean steel and is known to contain deleterious nonmetallic slag inclusions. If these inclusions are of significant size and are located in certain critical locations in the rotating disc, cracks can initiate from these inclusions and propagate to dangerous dimensions. Following this accident, the manufacturers replaced the air-melted compressor discs with vacuum-melted discs, which are known to be cleaner.

8.4 Modification of Codes and Standards

Collapse of Ashland Oil Storage Tank. On Jan. 2, 1988, a 4 million gallon oil storage tank collapsed during the first filling after a reconstruction, producing a major environmental impact. The

tank was first built in 1940, dismantled in 1986 leaving the old welds in place, and reconstructed in 1987, radiographed and leak tested. It was a case of brittle fracture in the base metal of the tank, alongside a weld. The investigation revealed that the fracture initiated from a defect in the base metal. The defect existed prior to reconstruction. The metal did not have adequate toughness to arrest the propagation of the crack. The region around the defect had been embrittled by heating due to cutting and welding. The steel did not meet the API 650 Standard of the American Petroleum Institute.

A task force of API studied a number of tank failures built in the period 1897 to 1979 and found that most of the failures were after some modification or repair. The Standard 650 did not cover repair, reconstruction, or modification of oil storage tanks. Later, requirements to minimize fracture were added. Further investigations and follow-up work resulted in the modification of their standard for "Welded Steel Tanks for Oil Storage." API 653 (1990) for "Tank Inspection and Repair" was introduced to include maintenance, inspection, repair, alteration, and relocation and also to provide procedures to assess risk of brittle fracture (Ref 3).

8.5 Safety Regulations for Transmission Pipelines

Failures of Oil Transmission Pipelines. A pipeline for gasoline, in Minnesota, constructed in 1957 with electric resistance welded (ERW) pipes, burst on July 8, 1986, without warning, causing fatal injuries and damage to environment and property. The failure was due to a defect in the ERW seam weld and corrosion. On Dec. 24, 1988, in Missouri, a pipeline carrying oil burst without warning and 800,000 gallons of crude oil spilled into the Missouri River, causing a major ecological problem. The pipeline was constructed in 1949, using ERW pipes. Here again, the failure was at the ERW weld seam.

A number of agencies studied the problem of liquid pipeline failures. The findings were very interesting; ERW pipelines constructed before 1970 had weld defects and low toughness in the seam where there was preferential corrosion. Hydrostatic testing of pipes and nondestructive testing of seam weld were not required.

Subsequently, safety regulations by the Department of Transportation stipulated hydrostatic testing of all interstate pipelines constructed before 1971 and all intrastate pipelines constructed before 1985 to 125% of maximum operating pressure or reducing the maximum operating pressure to 80% of the original level (Ref 3).

Failures of Gas Transmission Pipelines. In another incident, in Kentucky, a seamless steel tube ruptured completely during filling of compressed natural gas from a gas well after six months of service. The steel was A-372 class 5, quenched and tempered to a tensile strength of 1100 to 1170 MPa (160 to 170 ksi). The cause of the rupture was environmentally assisted cracking due to water and hydrogen sulfide in the gas (500 ppm).

Following this mishap, the regulations were modified to limit the maximum tensile strength to 870 MPa (126 ksi). Gas purity requirements were also enforced to limit the water and hydrogen sulfide content of the gas, to a level of 0.5 lb per million cubic feet and 0.1 gm per 100 cubic feet, respectively (Ref 3).

8.6 Aviation Security and Explosives Sensors

Aircraft Accidents by Explosive Sabotage. Explosive sabotage of aircraft continues to be a serious threat to aviation throughout the world. After investigating the various aircraft accidents caused by deliberate in-flight detonation of explosive devices, an increased awareness to air safety, aircraft security, and airport security has been felt by every airline. The types of explosive devices deployed, the explosive species employed, the methods of concealment, and the timing devices used by the saboteurs are now better understood. The catastrophies to the Boeing 747 aircraft of Air India off the west coast of Ireland and that of Pan American Airways at Lockerbie have proved that it has been possible for someone to place the explosive device inside the aircraft without being detected. These two accidents have led to a significant increase in the security measures adopted at the airports for baggage and cargo check-in.

Airlines stretched technology to its limits in the search for explosive devices in passengers' baggage (Ref 4). Large-scale efforts and funding continued for developing fool-proof instruments for detecting the presence of explosives in the baggage. One such machine that was developed and tested in a few major international airports was the thermal neutron analysis (TNA) machine in which the baggage is made to pass through a beam of thermal neutrons generated from radioactive californium-252. Plastic explosives are denser than other organic materials and contain two to six times more nitrogen than other plastics. Nitrogen atoms absorb the thermal neutrons and emit gamma rays. Detection of more gamma rays is an indication of higher nitrogen density and hence the possible presence of plastic explosives. Thermal neutron analysis machines had certain drawbacks because of their weight and the possibility of false alarms.

In another type of instrument, x-rays of two different energies are made to pass through the material. Each material attenuates the two sets of x-rays differently. By comparing the attenuated beams, the effective atomic number of the material can be estimated. Using such a system, dense organic material such as explosives can be distinguished from dense inorganic materials such as metals. Explosives can be distinguished from less-dense organic materials such as ordinary plastics.

In yet another machine, which is a computerized tomography scanner, x-ray scans are taken around an object and the different views combined on a computer to produce a slice image in a second. Screening a bag takes 9 to 12 slices. For bags arousing suspicion, the machine projects two images taken from different directions for the operator to make a decision. If necessary, further scanning can be done focusing on particular areas in the baggage.

Techniques and instruments are also being developed for detecting the vapors given out by the explosives. However, there are limitations because plastic explosives are not very volatile. These are some of the significant developments toward aircraft security against bomb threats.

The examples cited indicate the importance of continuous improvement in safety and reliability standards of engineering struc-

tures, which has been possible through the lessons learned from systematic failure analysis and accident investigations.

REFERENCES

1. R.J. Parker et al., "The Flixborough Disaster—Report of the Court of Inquiry," Her Majesty's Stationery Office, London, U.K., 1975
2. J.W. Calder, "Accident at Markham Colliery," Her Majesty's Stationery Office, London, U.K., 1974
3. J.L. Gross, J.H. Smith, and R.N. Wright, Ashland Tank Collapse Investigation, *J. Performance of Constructed Facilities,* Vol 3 (No. 3), 1989, p 144
4. D. Clery, Can We Stop Another Lockerbie?, *New Sci.,* 27 Feb 1993, p 21

Failure Analysis of Engineering Structures: Methodology and Case Histories
V. Ramachandran, A.C. Raghuram, R.V. Krishnan, S.K. Bhaumik, p65-66
DOI:10.1361/faes2005p065

CASE 1

Failure of a Throttle End Fitting in an Aircraft

Summary

An aircraft was forced to land after the engine did not respond to throttle movement. The throttle end fitting did not function because a stud in that fitting had failed by fatigue, initiated by cracks formed at the time of riveting.

Background

An aircraft force-landed after the engine did not respond to the throttle movement. From the wreckage, the tube assembly of the throttle front end fitting to the engine was recovered in a broken condition.

Pertinent Assembly Details

The assembly consisted of a steel tube with two steel end fittings, the tube and end fittings having the same hardness. These end fittings were fixed to the tube by two steel rivets at right angles to each other, separated by a short distance.

Visual Examination of General Physical Features

At the front end of the tube assembly, the end fitting stud inserted into the tube was found fractured and had come out of the tube. The mating part of this stud was still stuck in the tube. Visual examination of the fractured end indicated clearly that the rivet holes through the stud were unsymmetrical with respect to the diameter of the stud (Fig. CH1.1). One of the rivet holes and the rivet driven through it had a taper. The other rivet hole was too close to the edge of the stud, leaving a very small net cross section. Also, the two rivet holes were found too close to and overlapping each other (Fig. CH1.2). The fracture regions marked A, B, C, and D in Fig. CH1.1 vary in cross sectional areas, C and D being much smaller than A and B.

Testing Procedure and Results

Scanning Electron Fractography

Examination of the fracture regions in a scanning electron microscope (SEM) revealed that at the time of riveting, areas C and D, and a thin region of areas A and B adjacent to the rivet hole, suffered tearing mode of fracture. Figure CH1.3 shows the characteristic dimple structure from one of these regions. Immediately adjacent to this region, fatigue striations were observed (Fig. CH1.4).

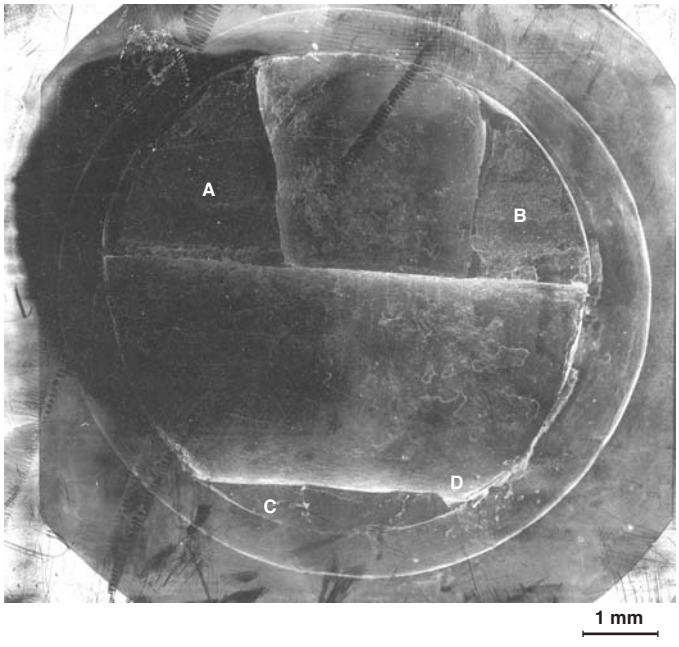

Fig. CH1.1 Fracture surface on one-half of the stud showing the rivet holes. Note the taper of one of the holes and noncentering of the other.

Discussion

Presence of striations in regions A and B clearly indicates crack propagation by fatigue. At the time of riveting, because the cross section of the component in regions C and D was too small, these regions fractured along with some portion of regions A and B close to the rivet. These cracks had propagated further by fatigue, breaking the stud.

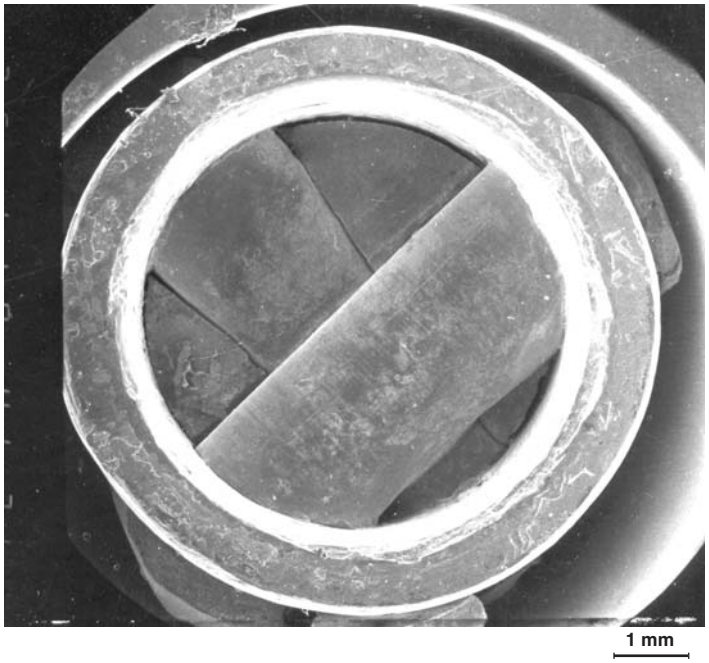

Fig. CH1.2 Fracture surface of the mating half of the stud, from inside the tube with rivets still in position

Conclusion and Recommendations

The malfunction of the throttle end fitting was due to the failure of the stud by fatigue, initiated by cracks formed at the time of riveting.

How Failure Could Have Been Prevented

If the four regions A through D were of uniform cross section, fracture in areas C and D would not have occurred and led to the fracture of the stud.

Remedial Action

In addition to the noncentering of the rivet holes, one of the rivets was tapered and the two rivets were overlapping. From the design considerations, this is not a correct procedure. The rivet holes should be centered, and when cross riveting is done, sufficient distance should separate the two rivet holes.

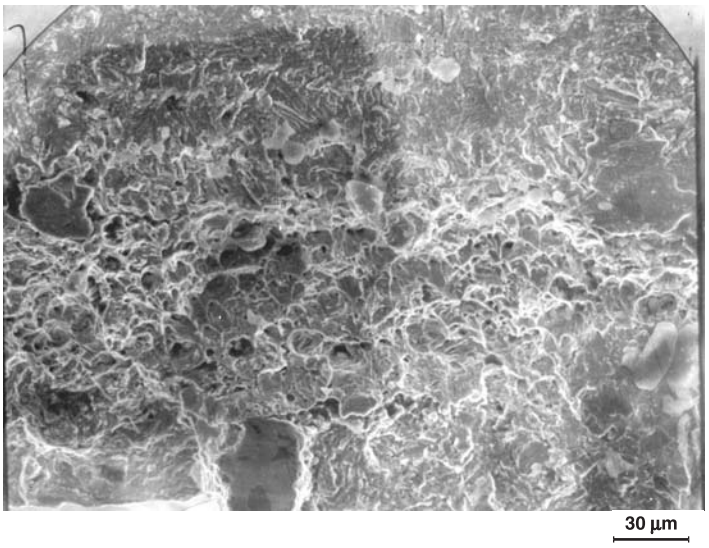

Fig. CH1.3 SEM fractograph of region A of Fig. CH1.1, close to the rivet hole, showing tearing mode of fracture

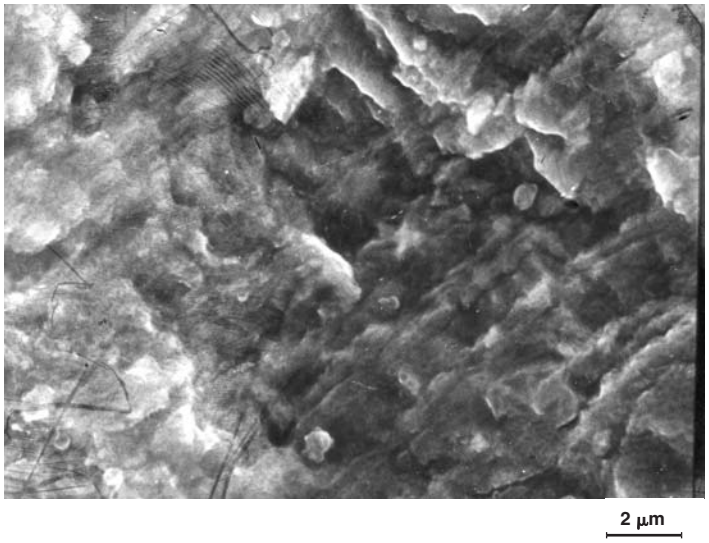

Fig. CH1.4 SEM fractograph of region A of Fig. CH1.1, showing fatigue striations

Failure Analysis of Engineering Structures: Methodology and Case Histories
V. Ramachandran, A.C. Raghuram, R.V. Krishnan, S.K. Bhaumik, p67-69
DOI:10.1361/faes2005p067

CASE 2

Failure of a Low-Pressure Turbine Rotor (LPTR) Blade

Summary

A low-pressure turbine rotor blade failed in service, causing extensive damage to the engine. The blade failed by stress rupture followed by fatigue due to high operating temperature.

Background

In an incidence of engine failure, a low-pressure turbine blade was found fractured, causing extensive damage to the engine. The blade was examined to establish the cause of failure.

Pertinent Specifications

The blades were made of nickel-base superalloys.

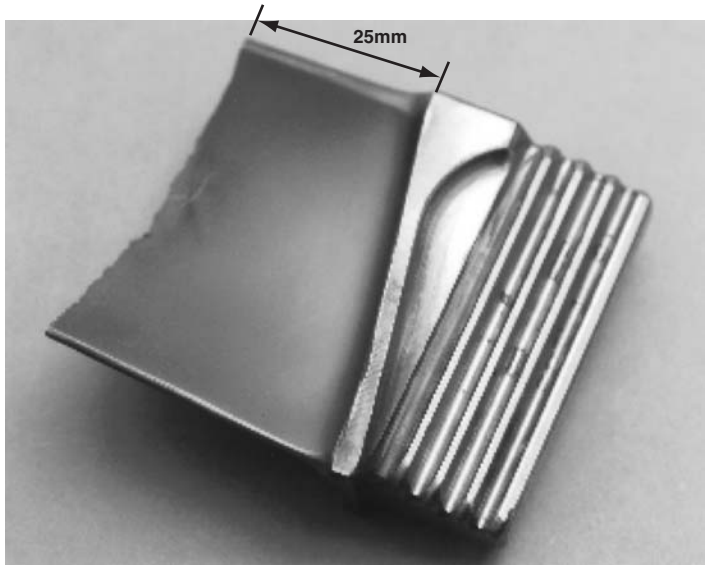

Fig. CH2.1 Photograph of the failed LPTR blade

Visual Examination of General Physical Features

The blade was found to have fractured in the airfoil section at a distance of about 25 mm from the blade root platform (Fig. CH2.1). The fracture surface was flat and perpendicular to the blade axis. On examination under low magnification, the fracture surface revealed a well-defined crescent-shaped area with smooth fracture features (Fig. CH2.2a), indicative of fatigue fracture. The fatigue crack was found to have initiated at the leading edge of the

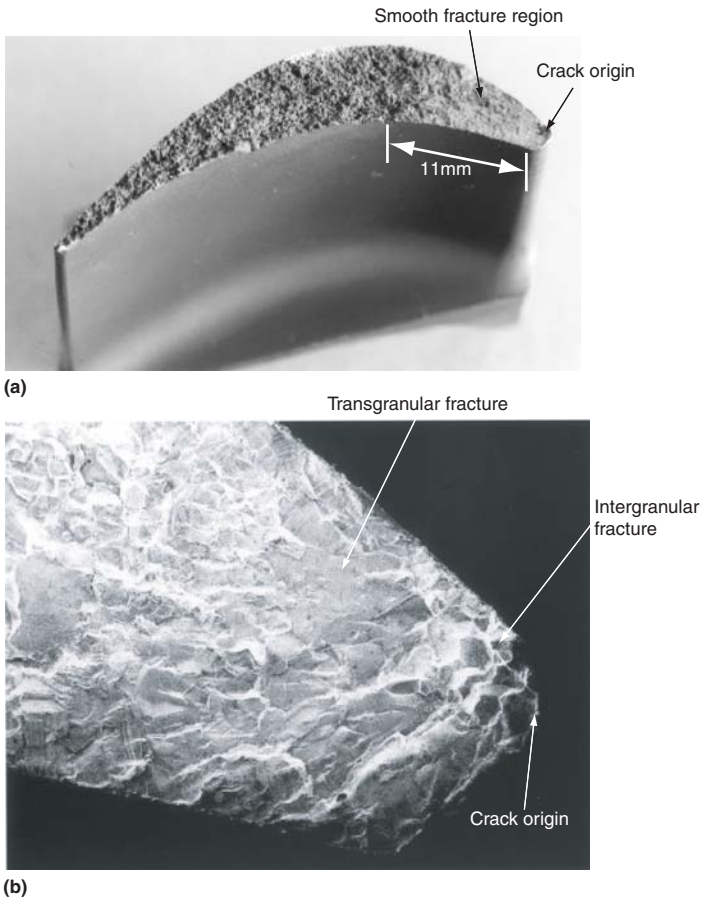

Fig. CH2.2 Photograph of the LPTR blade showing (a) entire fracture surface and (b) intergranular fracture features at the crack origin

blade. The remaining fracture surface had a crystalline appearance, typical of high-temperature overload failure in superalloys. The fracture surface near the leading edge was discolored due to oxidation and exposure to high temperatures.

Testing Procedure and Results

Scanning Electron Microscopy and Fractography

A faceted/intergranular fracture zone was observed over a distance of about 1 mm from the leading edge followed by a transgranular fracture zone of about 11 mm (Fig. CH2.2a, b). The intergranular fracture at the leading edge of the blade is shown in Fig. CH2.3. In the transgranular fracture zone, well-defined beach marks, typical of fatigue, could be seen (Fig. CH2.4a). At higher magnifications, striations were seen confirming the fatigue crack propagation (Fig. CH2.4b).

Metallography

A piece from the blade close to the fracture surface was prepared for metallography and examined after etching. The microstructures of the blade at the leading edge and away from the leading edge are shown in Fig. CH2.5. The γ-prime precipitates in the blade material at the leading edge were found completely dissolved (Fig. CH2.5a). The microstructure elsewhere in the blade was found satisfactory (Fig. CH2.5b).

Hardness

A hardness survey conducted on the airfoil cross section indicated lower hardness at the leading edge (350 HV) compared with 400 HV at the mid-chord section and the trailing edge.

Discussion

Fractographic study revealed that the fracture surface of the LPTR blade consisted of three distinctive fracture zones. The blade at the leading edge fractured in intergranular mode. Such fracture features were confined to about 1 mm from the leading edge. Intergranular initiation and propagation of cracks are the principal mode of fracture in high-temperature creep/stress rupture. Void formation and cracking occur principally along the grain boundaries normal to the major stress axis of the blade. The progress of

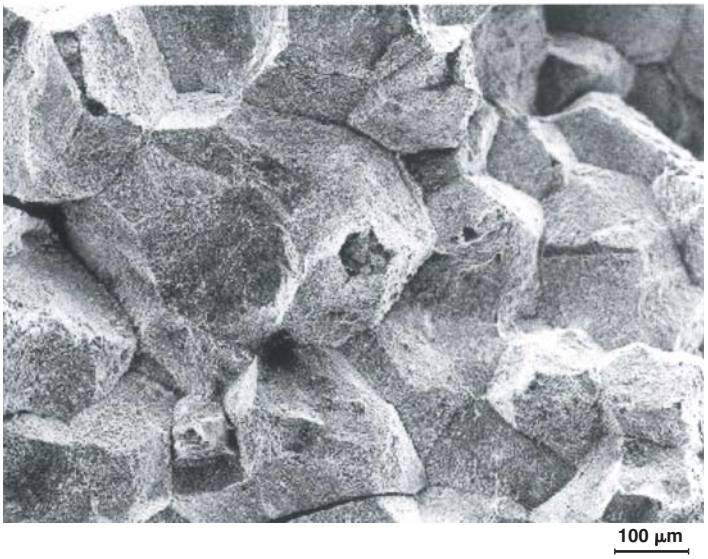

Fig. CH2.3 SEM fractograph showing intergranular fracture at the leading edge of the LPTR blade

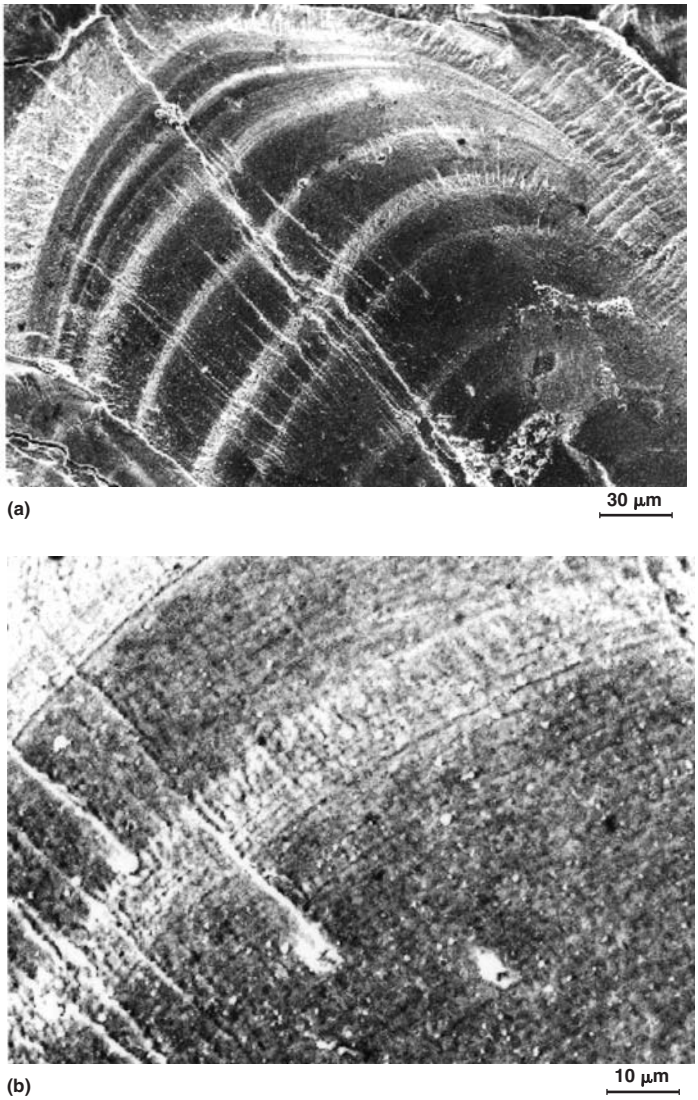

Fig. CH2.4 SEM fractographs showing (a) beach marks and (b) striations in the fatigue failed region

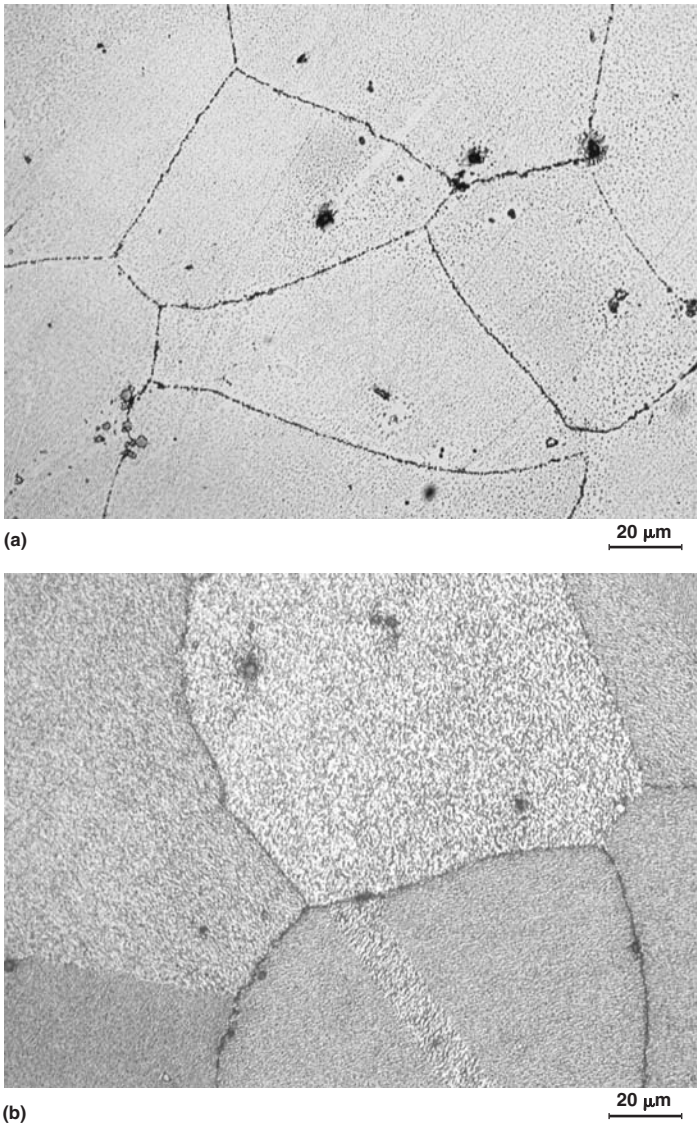

Fig. CH2.5 Optical micrographs at the (a) leading edge and (b) midchord section of the LPTR blade. Note the γ-prime precipitates dissolution at the leading edge.

the crack in the second zone is purely by transgranular mode. The incremental crack growth is evidenced by the presence of closely spaced striations. Therefore, it appears that the crack initiated at the leading edge of the blade by stress rupture and propagated fast to a distance of about 1 mm. In the second stage, this crack acted as a notch for stress concentration and led to the propagation of the crack by fatigue. The fatigue crack then propagated progressively up to about 11 mm from the leading edge before giving way to overload fracture.

Microstructural analysis of the blade at the region of fracture revealed considerable variations. The dissolution of γ-prime precipitates at the leading edge clearly indicates that the blade was exposed to high temperatures. It also indicates that the blade experienced temperatures as high as γ-prime solvus temperature (approximately 1175 °C, or 2150 °F). The high-temperature strength of nickel-base superalloys is derived from the presence of high volume fraction of γ-prime precipitates. Dissolution of γ-prime precipitates reduces the creep resistance of the blade drastically. The decrease in hardness observed at the leading edge of the LPTR blades is due to dissolution of γ-prime precipitates.

Conclusion

The cracking of the LPTR blade primarily took place by stress rupture. The factors responsible for such cracking are high operating temperatures and stresses. Once the initial crack had formed due to stress rupture, the crack further propagated under the cyclic loading experienced by the blade during service.

Failure Analysis of Engineering Structures: Methodology and Case Histories
V. Ramachandran, A.C. Raghuram, R.V. Krishnan, S.K. Bhaumik, p70-71
DOI:10.1361/faes2005p070

CASE 3

Failure of Bolts in a Radar Antenna System Reflector Joint

Summary

Cadmium-plated high-strength steel bolts used in a radar antenna system reflector joint fractured at the fillet of the head. The fracture was intergranular. The bolts had improper seating, making contact only at the periphery. This resulted in high stress concentration at the fillet and subsequent cracking, aggravated by the presence of hydrogen in the material due to cadmium plating.

Background

High-tensile steel bolts used in a radar antenna system reflector joint were found to have cracked at the fillet of the head and inside the allen key socket.

Pertinent Specifications

The bolts were made to clause 12.9 of DIN 267 specification and cadmium plated.

Visual Examination of General Physical Features

One of the broken bolts is shown in Fig. CH3.1. A circumferential crack was found all around the fillet. There was also an elliptical crack inside the allen key socket.

Testing Procedure and Results

Scanning Electron Fractography/Metallography

Sections were cut from the bolt head to study the fractography features. Figure CH3.2 shows the sectioned bolt head. Figure CH3.3 shows the intergranular nature of the fracture with dimples in some of the facets. Figure CH3.4 is a metallograph showing the fracture path. There is clear evidence of intergranular cracking. The microstructure showed tempered martensite, which is normal for this class of steel. A hardness survey along the length of the

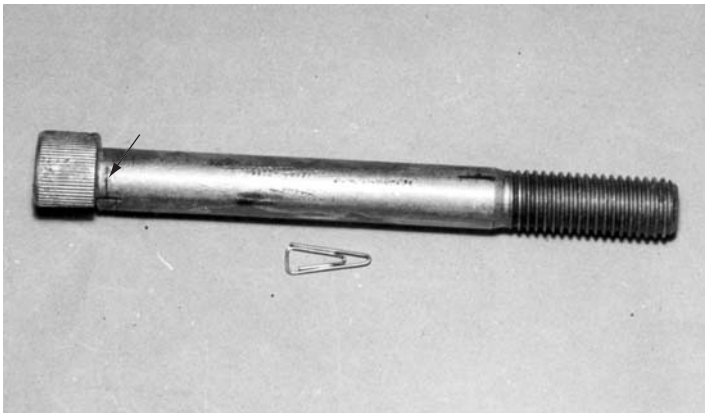

Fig. CH3.1 A bolt in the as-received condition

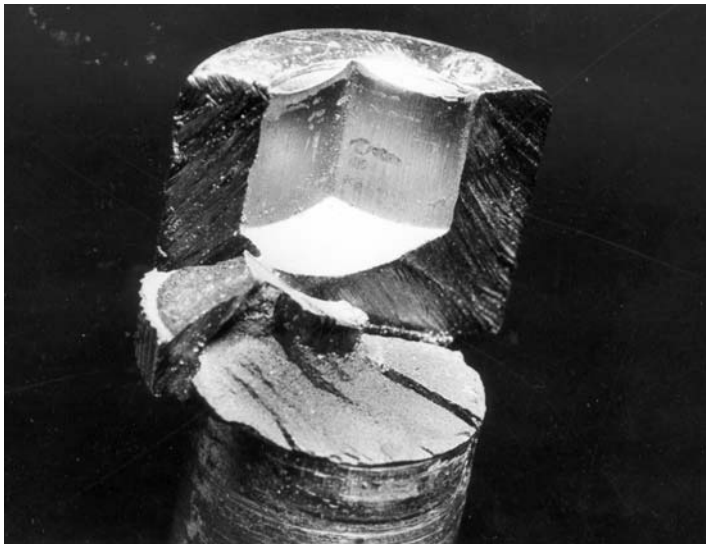

Fig. CH3.2 Bolt head after sectioning

bolt indicated uniform hardness of 45 HRC. Similar features were noted in a few other cracked bolts.

A grain flow study was made to check the quality of forging, especially near the fillet and the socket. The flow lines were uniform as shown in Fig. CH3.5, confirming proper forging.

It was also seen that the bolt heads were not seated properly and the entire load bearing area of the bolt head was not utilized. The contact was only at the periphery to a width of about 1 mm (Fig. CH3.6).

Discussion

The improper seating resulted in very high stress concentration at the fillet and subsequent cracking. The intergranular nature of fracture suggests failure due to hydrogen embrittlement, starting from the fillet. Cadmium plating makes the bolts vulnerable to hydrogen embrittlement. The situation is aggravated by the presence of residual hydrogen left after cadmium plating. Once the cracking had progressed sufficiently, the core pulled out by tensile loading.

Conclusion and Recommendations

The socket head bolts had improper seating making contact only at the periphery. This resulted in cracking at the fillet, aggravated by the presence of hydrogen in the material due to cadmium plating.

Use of spring washers in the assembly may be considered.

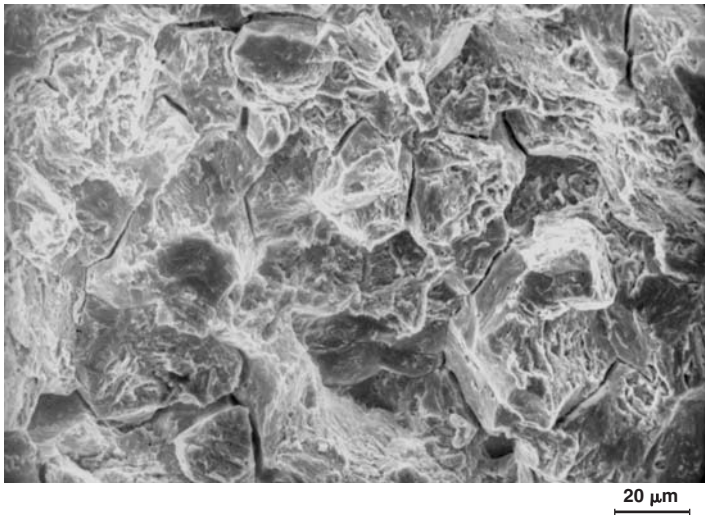

Fig. CH3.3 SEM fractograph showing intergranular fracture

Fig. CH3.4 Intergranular path of the crack

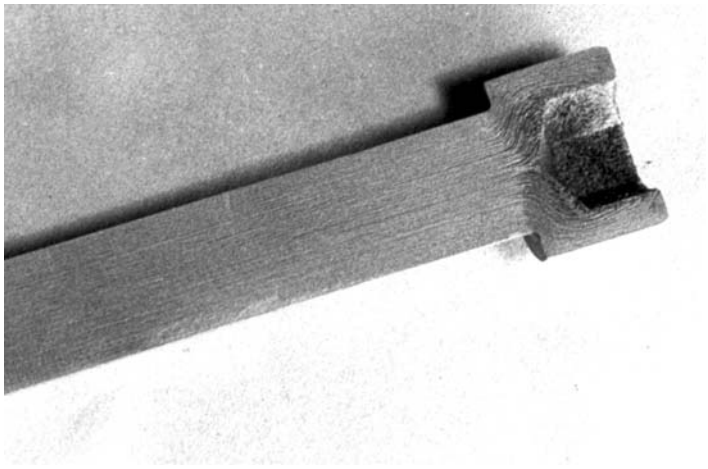

Fig. CH3.5 Flow lines on a longitudinal section of the bolt

Fig. CH3.6 Bolt head seating showing that only a fraction of the total load-bearing area near the periphery had been in contact with the mating component

Failure Analysis of Engineering Structures: Methodology and Case Histories
V. Ramachandran, A.C. Raghuram, R.V. Krishnan, S.K. Bhaumik, p72-73
DOI:10.1361/faes2005p072

CASE 4

Failure of a Main Wheel Bearing Housing Flange in an Aircraft

Summary

The main wheel bearing housing of an aircraft failed, with the fracture occurring in the hub. It was a fatigue failure. At the time of the last servicing, when ceramic disc and friction plates were changed, there was no indication of cracking. There was heavy rubbing on the inside of the hub, possibly due to improper alignment of the assembly. It was suggested that the state of damage to the roller bearings be examined to confirm this.

Background

The starboard main wheel bearing housing of an aircraft failed after 298.10 hours of flight in which the aircraft had made 403 landings. The hub of the wheel had broken. A portion of the failed hub is shown in Fig. CH4.1. The aircraft was serviced after 100 hours when the ceramic disc and friction plates were changed and taxiing checks were carried out. After the last servicing at 290 hours, the aircraft had made 12 landings. The number of tires changed on the starboard wheel was 15.

Fig. CH4.1 Portion of the broken hub in the as-received condition

Visual Examination of General Physical Features

The fracture surface after cleaning showed beach marks as clear evidence of fatigue failure. The fatigue crack had progressed to about one-third of the segment (Fig. CH4.2). The region diametrically opposite the fatigue origin is shown in Fig. CH4.3. Heavy rubbing and metal flow could be seen in this region on the inside.

Testing Procedure and Results

Scanning Electron Fractography and Metallography

Figure CH4.4 is a SEM fractograph showing striations in the region shown in Fig. CH4.2, as further proof of fatigue crack propagation. The microstructure and hardness did not reveal any abnormalities in the material.

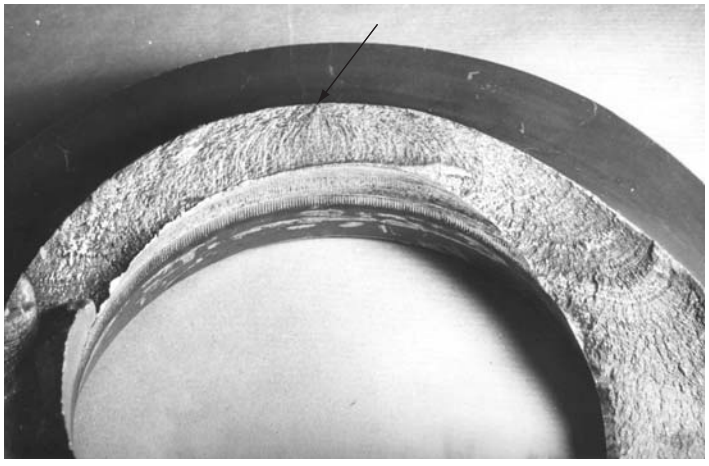

Fig. CH4.2 Close-up view of the fracture showing the beach marks typical of fatigue. Arrow indicates the origin.

Discussion

At the time of the last overhaul, the component had served 290 hours. It was reported that there was no indication of cracking at the time of fixing ceramic discs and friction plates. This clearly indicates that the part must have been subjected to bending stresses in the last 8 to 10 hours of use during which 12 landings had taken place.

The heavy rubbing on the inside of the hub is possible only if the assembly is not perfectly aligned. From a study of the section drawing supplied, it could be inferred that an improper assembly of electric motor and the roller bearing can cause this type of failure. This can be confirmed by examining the state of damage to the roller bearings and the corresponding damage on the inside of the hub.

Conclusion and Recommendations

The component failed due to fatigue. A thorough nondestructive examination should be carried out at the time of every 100 hours of service.

Fig. CH4.3 The arrow indicates the area having rubbing and metal flow.

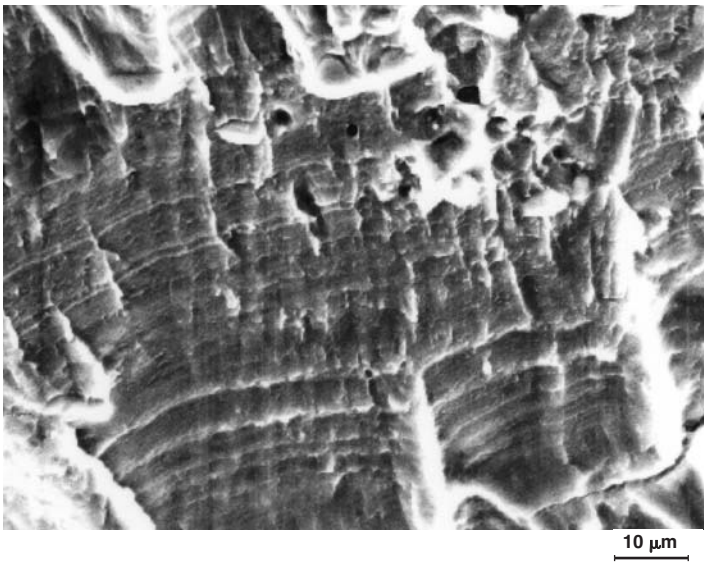

Fig. CH4.4 SEM photograph showing fatigue striations

Failure Analysis of Engineering Structures: Methodology and Case Histories
V. Ramachandran, A.C. Raghuram, R.V. Krishnan, S.K. Bhaumik, p74-75
DOI:10.1361/faes2005p074

CASE 5

Failure of an Aircraft Engine Fuel Pump

Summary

A fuel pump in an aircraft engine failed to operate because the camshaft had fractured. Wear of a spring inside the piston resulted in the formation of small metal slivers that could have blocked the orifice in the spring seat, resulting in starvation of lubricant between the slipper pads and the cam plate. The friction between the slipper pads and the cam plate resulted in torsional overload of the camshaft and its fracture.

(a)

(b)

Fig. CH5.1 (a) Rotor assembly of the fuel pump showing the damaged slipper pads. (b) Severe damage on two of the slipper pads

Background

The damaged fuel pump of an aircraft engine was retrieved from the wreckage of a crashed aircraft. It was reported that the accident was caused due to the failure of the fuel pump.

Visual Examination of General Physical Features

Parts of the damaged fuel pump are shown in Fig. CH5.1 and CH5.2. All seven slipper pads in the rotor assembly of the pump had been damaged, some of them severely. These pads were made of copper-beryllium alloy. The orifice of some of the pads got completely covered by smeared copper. The pads had rubbed heavily against the surface of the cam plate. The original silver plating on the pads was completely missing. The copper layer from

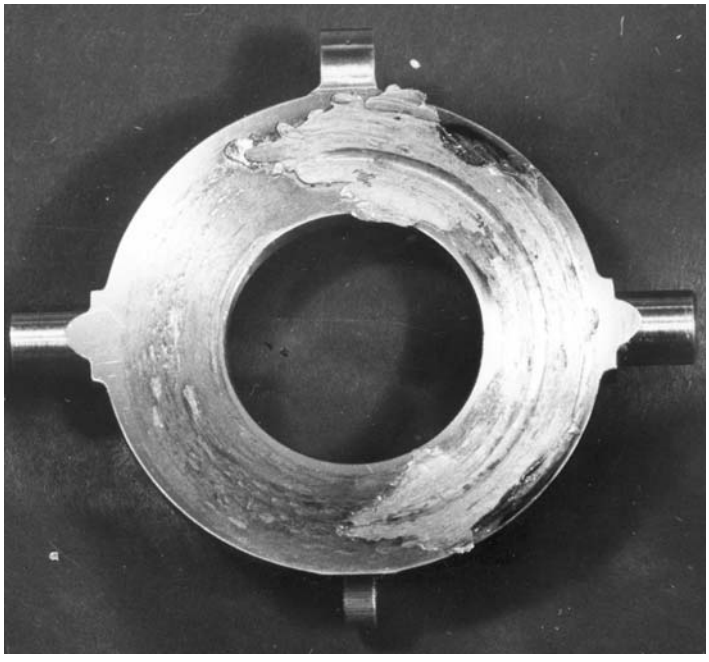

Fig. CH5.2 Cam plate showing adhesion of copper from the slipper pads

the cam plate could not be removed because it had been welded (Fig. CH5.2). The camshaft of the pump had fractured.

Each slipper pad was attached to the end of a hollow piston inside which a steel spring, a spring seat, and a spring guide were located. Four of the seven springs had suffered abnormal wear at the spring seat end.

Six spring seats were available for examination. Three of them contained the impression of the springs on one side only, and the other three had the impression on both sides.

Testing Procedure and Results

Scanning Electron Microscopy

Figure CH5.3 shows a typical wear pattern, with metal slivers separating from the surface. Five of the seven springs had decreased in length, the decrease ranging from 1 to 3 mm.

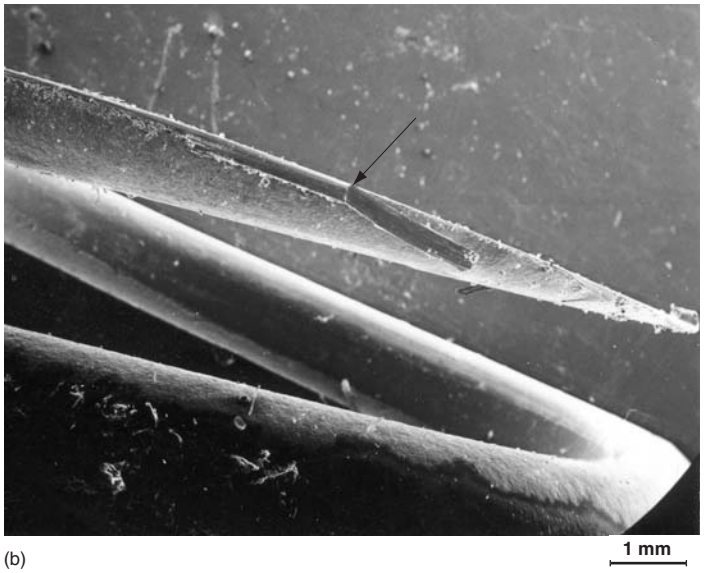

Fig. CH5.3 (a) and (b) Wear on spring No. 2. Arrow indicates a sliver.

Chemical Composition

One of the severely worn springs was compared with a life-expired spring from another fuel pump. Qualitative x-ray chemical analysis indicated similar chemical composition.

Small slivers were found inside some of the hollow pistons. In situ x-ray microanalysis indicated the slivers contained iron. The interior of the ball-and-socket joint of the piston was cleaned and the residue was collected. The residue contained small copper alloy flakes. Figure CH5.4 shows a SEM of a copper alloy flake removed from one of the pistons.

Discussion

The wear of the spring resulted in the formation of small slivers inside the piston. These slivers might have blocked the orifice in the spring seat inside the piston, resulting in starvation of lubricant between the slipper pads and the cam plate. This must have initiated adhesive wear of the slipper pad, resulting in the welding of the slipper pad material onto the surface of the cam plate. The top surface of the slipper pads normally has a layer of plated silver. The silver plating might have been removed by the rubbing action of the metal particles, causing an increased friction between the top surface of the slipper pad and the cam plate. This again could result in enhanced adhesive wear and welding of the copper with the cam plate.

It is possible that in some of the pistons the swiveling action was impaired by the presence of metal particles in the ball-and-socket assembly. This could explain the wear of the slipper pad at the bottom surface.

The steel slivers carried into the ball-and-socket joint by the fluid pressure could lead to rubbing action and formation of small copper alloy flakes.

Conclusion

Excessive friction between the slipper pads and the cam plate resulted in torsional overload of the camshaft and its fracture.

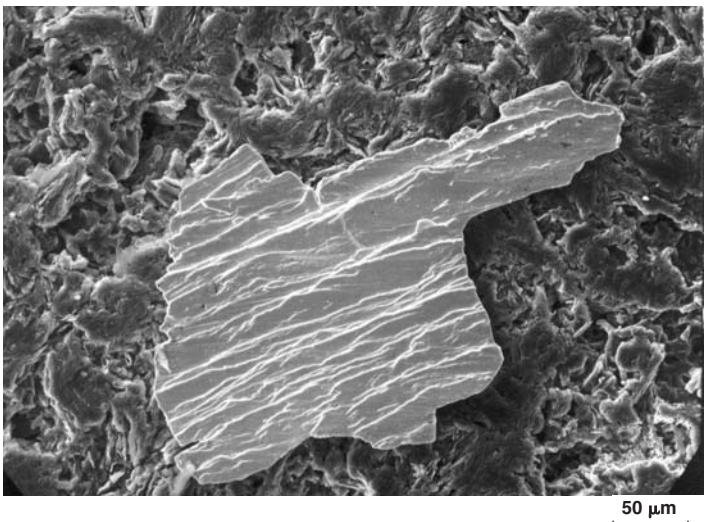

Fig. CH5.4 SEM photograph of a copper flake

Failure Analysis of Engineering Structures: Methodology and Case Histories
V. Ramachandran, A.C. Raghuram, R.V. Krishnan, S.K. Bhaumik, p76-77
DOI:10.1361/faes2005p076

CASE 6

Failure of an Adaptor Assembly in an Electronic Pod in an Aircraft

Summary

In an aircraft carrying electronic pods, while attempting to overcome certain control problems during a flight, the adaptor of one of the control pods got sheared off. A bolt connecting the adaptor to the pylon also had fractured. The bolt and the adaptor failed by overload. Use of twin suspension hooks is recommended for better flight stability.

Background

An aircraft experienced serious control problems during a flight. The aircraft was carrying two electronic pods. During attempts to overcome the control problems, the adaptor of one of the electronic pods was sheared off. The aircraft regained control after four of the stores got separated in flight. A bolt connecting the adaptor to the pylon was also found broken.

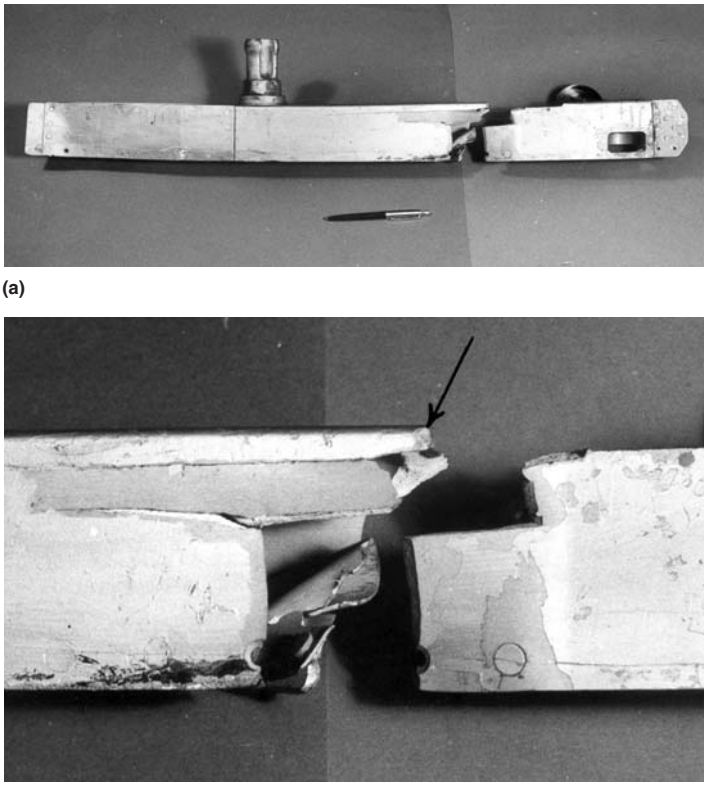

(a)

(b)

Fig. CH6.1 (a) The failed adapter for pod. (b) Close-up view of the sheared portion of the adaptor

Visual Examination of General Physical Features

The failed adaptor is shown in Fig. CH6.1, and the close-up view of the sheared portion is shown in Fig. CH6.2. The fractured bolt that connected the pylon with the adaptor is shown in Fig. CH6.3.

Testing Procedure and Results

Scanning Electron Fractography

The fracture surfaces indicated by arrows in Fig. CH6.2 and CH6.3 were examined in a SEM. Figures CH6.4 and CH6.5 are

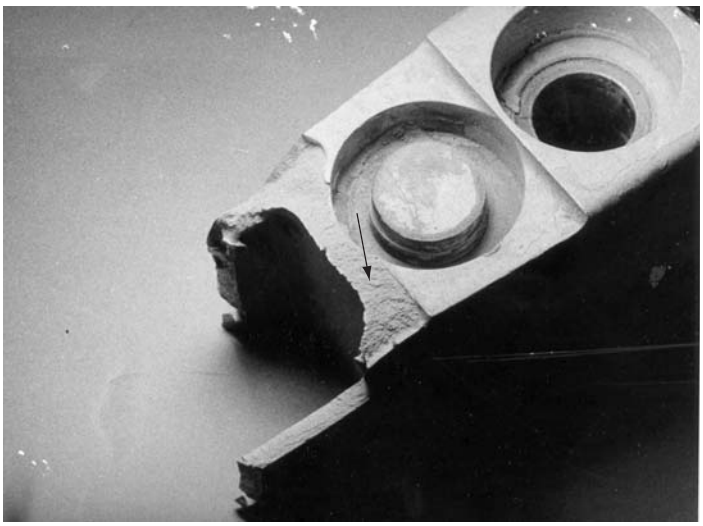

Fig. CH6.2 Close-up view of the fracture surface in the adaptor

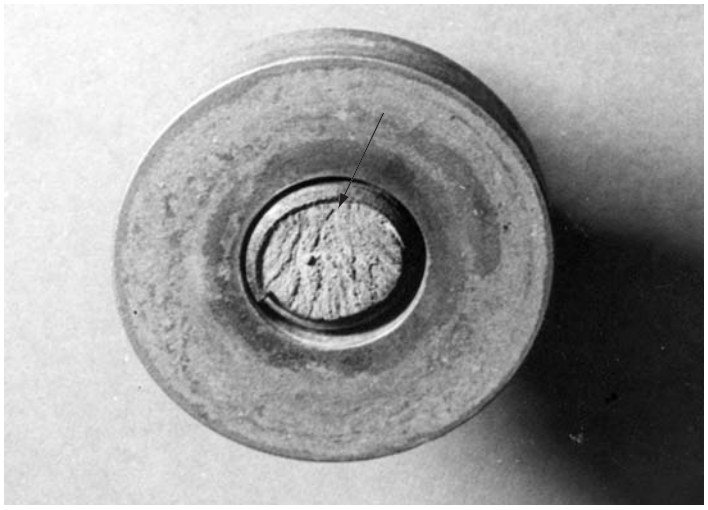

Fig. CH6.3 The fractured bolt that connects the pylon with the adaptor

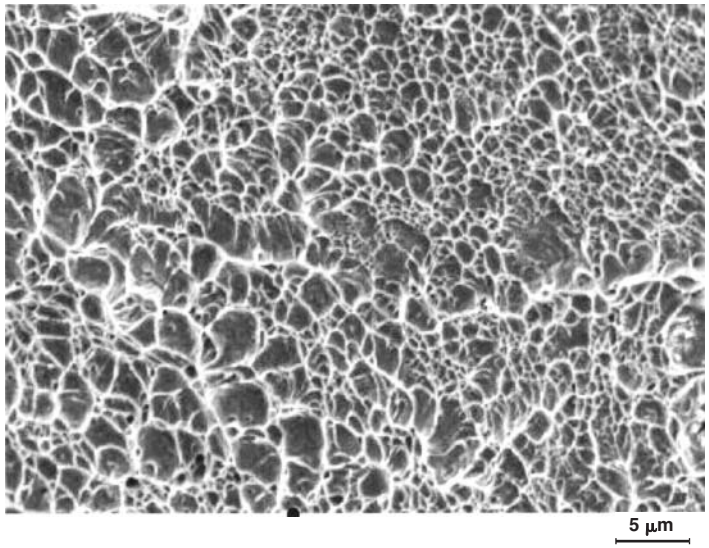

Fig. CH6.4 SEM fractograph of the bolt shown in Fig. CH6.3, showing dimples typical of overload fracture

the SEM fractographs of the two regions. The fractographs indicate dimples characteristic of failure by overload. There are no indications of progressive failure.

Conclusion and Recommendations

The bolt connecting the electronic pod to the adaptor and the adaptor itself failed by overload.

Use of twin suspension hooks is recommended for better stability during flight.

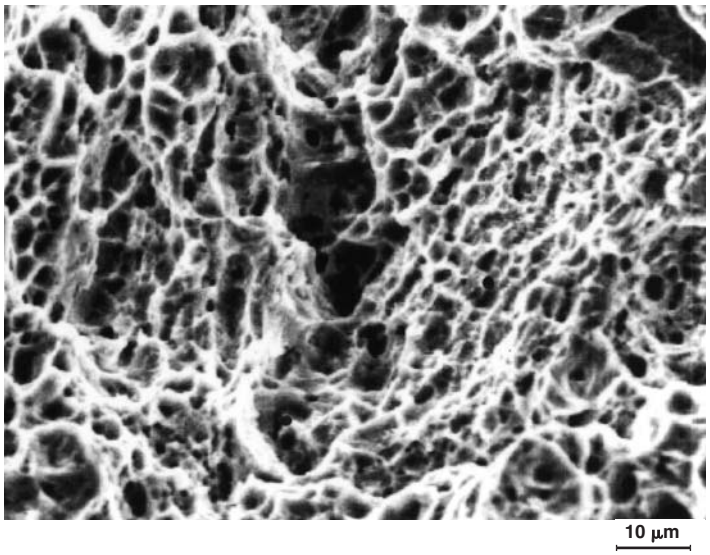

Fig. CH6.5 SEM fractograph of the region indicated in Fig. CH6.2, showing characteristics of overload fracture

Failure Analysis of Engineering Structures: Methodology and Case Histories
V. Ramachandran, A.C. Raghuram, R.V. Krishnan, S.K. Bhaumik, p78-79
DOI:10.1361/faes2005p078

CASE 7

Failure of a Stabilizer Link Rod in an Aircraft

Summary

In an aircraft that had an accident, the port side stabilizer link rod had fractured in the thread region. Considerable bending was also noticed near the fracture. Fractography revealed that the link rod failed by overload, possibly by a combination of tension and bending forces.

Background

In an aircraft accident, it was found that the port side stabilizer link rod had broken. The starboard stabilizer link rod was intact.

Visual Examination of General Physical Features

The starboard stabilizer rod in good condition and the broken port side stabilizer rod are shown in Fig. CH7.1. The fracture in the port side rod had taken place in the thread region. Considerable bending was noticeable as revealed by the uneven pitch of the thread along the circumference near the fracture (Fig. CH7.2).

Fig. CH7.1 Starboard stabilizer link rod and broken port stabilizer link rod

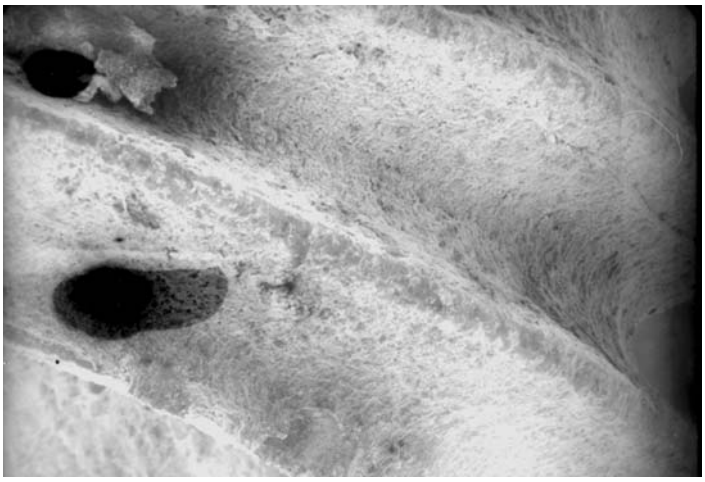

Fig. CH7.2 Damage to the threads of the link rod, near the fracture surface, as a result of bending

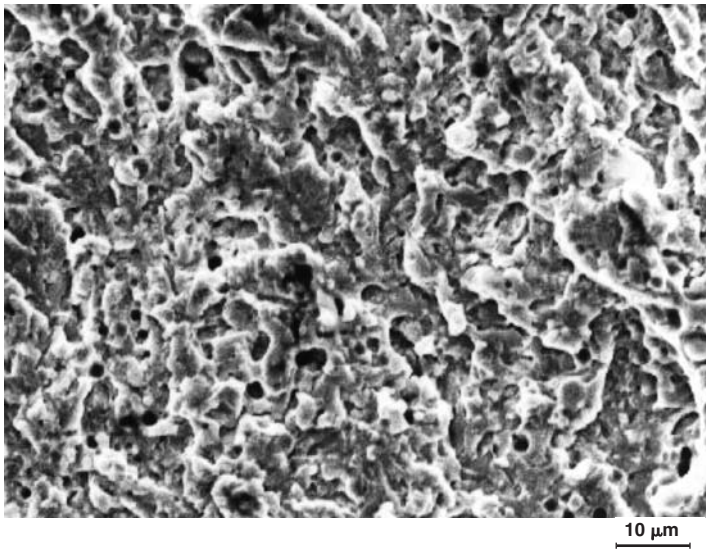

Fig. CH7.3 SEM fractograph showing dimples characteristic of overload fracture

Testing Procedure and Results

Scanning Electron Fractography

The fracture surface shows dimples characteristic of overload failure (Fig. CH7.3). There is no evidence of any delayed failure.

Conclusion

The rod failed by overload, possibly by a combination of tension and bending forces.

Failure Analysis of Engineering Structures: Methodology and Case Histories
V. Ramachandran, A.C. Raghuram, R.V. Krishnan, S.K. Bhaumik, p80-81
DOI:10.1361/faes2005p080

CASE 8

Failure of a Tie-Rod in an Aircraft Towing Tractor

Summary

The tie-rod of an aircraft towing tractor failed during tow. A bracket had been welded to the tie-rod to connect a hydraulic jack. The fracture occurred near one of the circumferential welds on the bracket. The fracture was by brittle mode initiated from a zone of poor-quality weld.

Background

The tie-rod of a 75 ton aircraft towing tractor failed during trials.

Pertinent Specifications

The tie-rod is said to be made of 0.5% carbon steel.

Visual Examination of General Physical Features

Figure CH8.1 shows the broken tie-rod. A bracket was welded to the tie-rod to connect a hydraulic jack. The rod had fractured near one of the circumferential welds on one side of the bracket, away from the hydraulic jack. The circumferential welds had also given way on the other side of the bracket. The close-up view of the fracture surface is shown in Fig. CH8.2. The surface appears to have characteristics of brittle fracture. The welds appear to be of very poor quality.

Fig. CH8.1 The broken tie-rod of the developmental aircraft towing tractor

Testing Procedure and Results

Scanning Electron Fractography and Metallography

Scanning electron microscopic examination of the fracture surface shown in Fig. CH8.2 revealed characteristics of brittle fracture (Fig. CH8.3). In order to study the effect of circumferential welding, a section was cut near the fracture surface to include a weld. Optical metallography of this section revealed a heat-affected zone (HAZ) and a crack at the interface between the parent metal and the weld (Fig. CH8.4).

Fig. CH8.2 Close-up view of the fracture surface

Discussion

Welding of 0.5% carbon steel has to be carried out with adequate precautions; otherwise, the quality of the weld will be poor and result in brittle material at the interface. In this case, the fracture initiated from the zone of poor weld quality, in the highly stressed region.

Conclusion and Recommendations

The tie-rod failed in a brittle manner from a poor-quality weld interface.

It is preferable to use a cold-drawn low-carbon steel for the tie-rod to facilitate better welding. If, however, 0.5% carbon steel has to be used, adequate preheating and post-heat-treatment procedures must be followed to get a sound weld. Also, suitable welding electrode (low-hydrogen variety) should be used to get a better weld. Nondestructive inspection of the weld should be carried out before the tie-rod is put into service.

A modified weld design was suggested for the fork end of the tie-rod (Fig. CH8.5). After this modification, the tie-rod was proof loaded as per requirements, and a dye-penetrant test was carried out. The tie-rod withstood the proof loading and there was no cracking after proof loading.

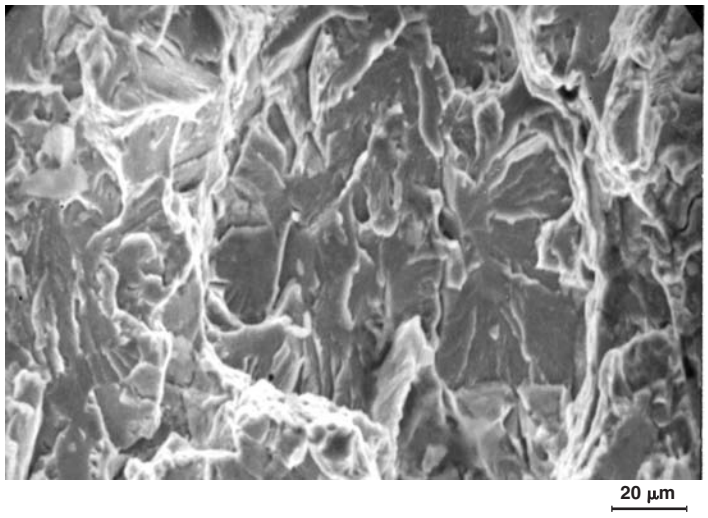

Fig. CH8.3 SEM fractograph showing the brittle nature of fracture

Fig. CH8.4 Optical micrograph of the weld zone showing a crack and the heat-affected zone

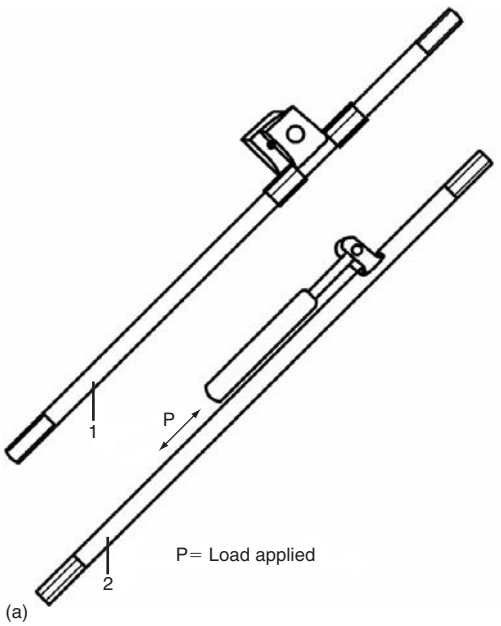

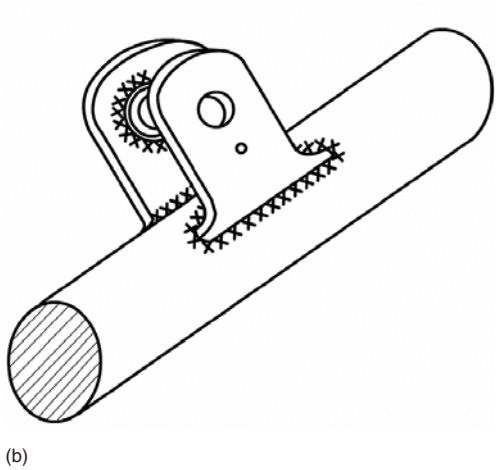

Fig. CH8.5 (a) 1. Original tie-rod that failed in the trial run. 2. Modified tie-rod. (b) Modified design of fork end

Failure Analysis of Engineering Structures: Methodology and Case Histories
V. Ramachandran, A.C. Raghuram, R.V. Krishnan, S.K. Bhaumik, p82-83
DOI:10.1361/faes2005p082

CASE 9

Failure of a Tail Rotor Blade in a Helicopter

Summary

In a helicopter, during flight, one of the three tail rotor blades sheared off at the outboard rib trailing edge. The tip had been pulled out from the rivets by tearing. The failure is attributable to a hit by a foreign object near the outboard tip at the leading edge.

Background

Severe vibration was experienced during a test flight of a helicopter and the flight was abandoned. On landing, it was found that one of the three tail rotor blades had sheared off at the outboard rib trailing edge. The other two tail rotor blades were intact. It was reported that the blades were subjected to extreme weather conditions in Antarctica.

Visual Examination of General Physical Features

The damaged blade is shown in Fig. CH9.1. No inherent defects were detected. However, there was sufficient evidence for external damage. On both sides, the blade showed severe inward caving at the midsection, very near the outboard rib. Cracking of the paint on the outer skin was noticed in this region and also in the region of the caving, a little inboard (Fig. CH9.2).

Part of the blade near the outboard tip had been torn and sheared off. The extent of this tear can be seen in Fig. CH9.1. Figures CH9.3 and CH9.4 show the tear of the tip at the rivet hole. The direction of the tear at the rivet hole is away from the leading edge. Cracking of the paint can also be seen near the rivet hole.

Discussion

The blade did not have any inherent defect. From the preceding visual observations, it is clear that the tip had been pulled out from the rivets by tearing when the tip of the blade hit a foreign object.

Conclusion

The observed damages are attributable to a hit by a foreign object near the outboard tip at the leading edge. Exposure to Antarctic climate has no bearing on this failure.

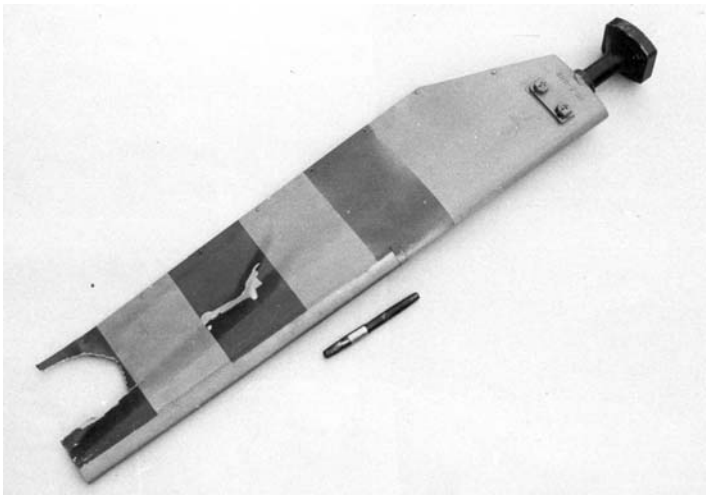

Fig. CH9.1 Damaged tail rotor blade

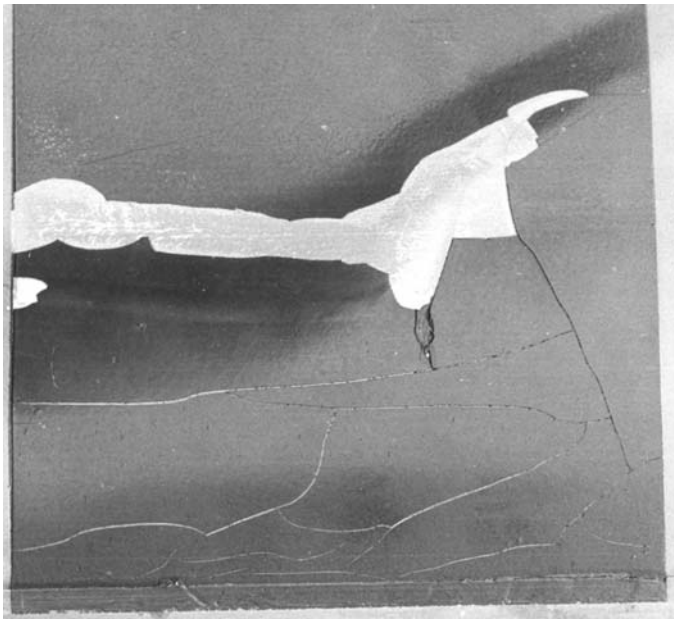

Fig. CH9.2 Cracking of paint on the airfoil surface

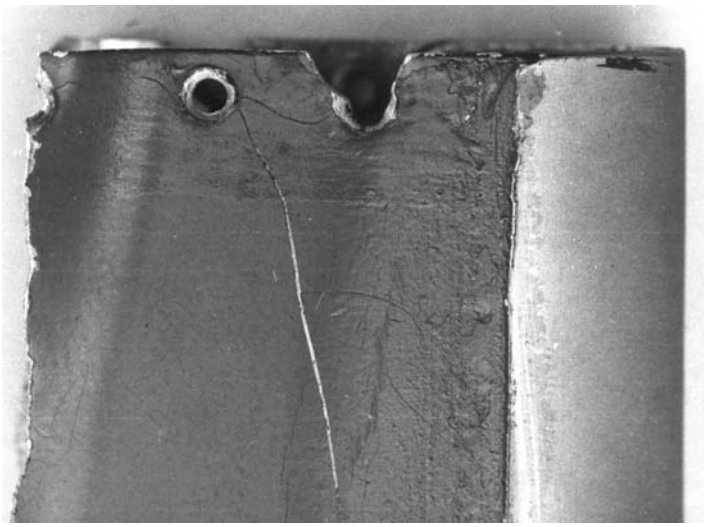

Fig. CH9.3 Tear damage at the blade tip

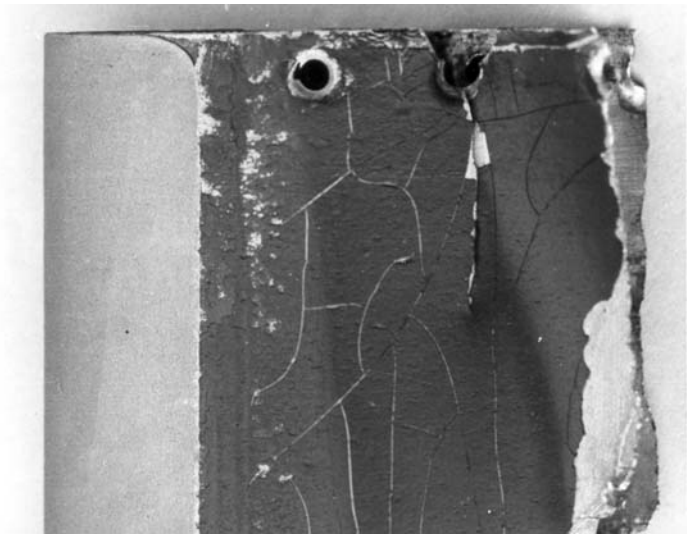

Fig. CH9.4 Tear damage at the blade tip, side opposite that in Fig. CH9.3. Cracking of the paint can also be seen.

Failure Analysis of Engineering Structures: Methodology and Case Histories
V. Ramachandran, A.C. Raghuram, R.V. Krishnan, S.K. Bhaumik, p84-86
DOI:10.1361/faes2005p084

CASE 10

Failure of a Wheel Hub in an Aircraft

Summary

A tire in an aircraft burst while inflating. The hub of the wheel had sheared off. Parallel to the fracture surface, there was circumferential cracking near the fillet of the flange. The crack had proceeded from the outer surface at the fillet to the inner. Fractography revealed cleavage mode. The rim had failed due to excessive pressure of air charged.

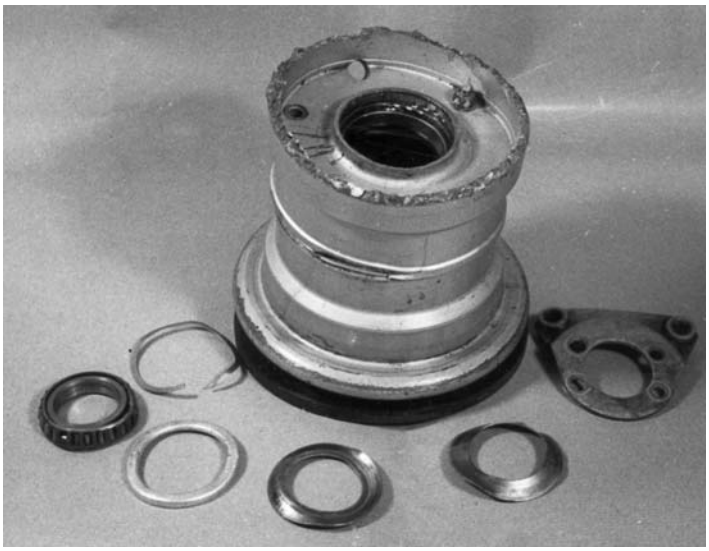

Fig. CH10.1 Damaged hub in the as-received condition

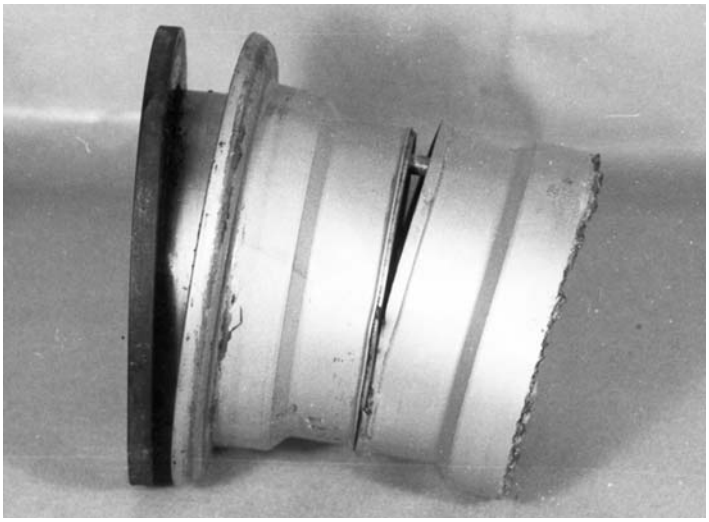

Fig. CH10.2 Separation of the hub

Background

In an aircraft, a tire burst occurred while charging the wheel. The hub of the wheel sheared off in the process.

Visual Examination of General Physical Features

The damaged parts are shown in Fig. CH10.1. The hub is made of two halves held together by three tie-rods, 120° apart. These hubs are made of magnesium-aluminum alloy. Figure CH10.2 shows clearly the separation of one-half of the hub toward outboard and the complete absence of the flange. The tire is held in position by the two flanges.

A close-up view of the fracture surface of the hub is shown in Fig. CH10.3. Two of the three tie-rods can be seen with the nuts intact. The bolt hole closer to the air valve where the tie-rod is

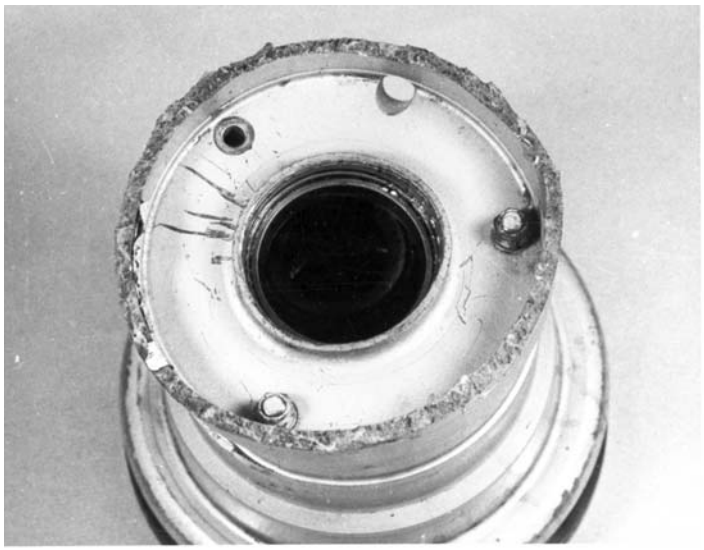

Fig. CH10.3 Fracture surface of the hub

missing is elongated inward, toward the axle. This indicates that the rim had exerted a very heavy force on this tie-rod before the nut had been sheared off.

Testing Procedure and Results

Metallography and Scanning Electron Fractography

To check the quality of the hub material, metallographic examination was carried out on a small portion cut from near the fracture surface. The microstructure is shown in Fig. CH10.4. The material is homogeneous and free from porosity and voids.

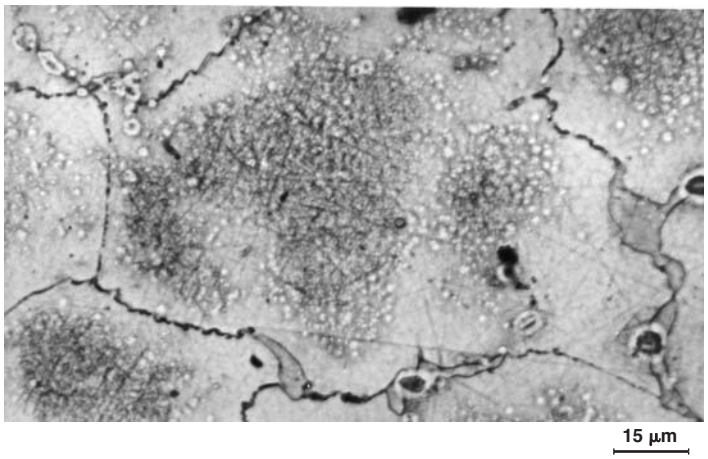

Fig. CH10.4 Microstructure of the hub material

Close examination all around the fracture surface indicated severe circumferential cracking near the fillet of the flange, parallel to the fracture surface, as shown in the SEM (Fig. CH10.5).

A small portion of the fracture surface was cut and scanned through the thickness. Figure CH10.6 shows the limited ductile nature of the material, near the cracked area shown in Fig. CH10.5. On the interior of the fracture surface, cleavage fracture is seen (Fig. CH10.7), indicating fast fracture. There was no evidence of delayed fracture on this surface.

Discussion

Metallographic examination indicated the quality of the hub material was good. The fracture surface of the hub is jagged because of the limited ductility of the material. Circumferential cracking all around the fillet of the flange indicates uniform forces had been exerted by the tire.

The nature of fracture near the periphery indicates deformation before the final rapid fracture. The crack proceeded from the outer surface at the fillet to the interior.

Upon inquiry concerning the pressure in the tire at the time of bursting, it was reported that no pressure gage was used during charging to measure the tire pressure.

Conclusion and Recommendations

The rim failed due to excessive pressure of air charged to the tire at the time of inflating. There is no evidence of delayed failure or substandard material.

Fig. CH10.5 Circumferential cracks near the fracture surface

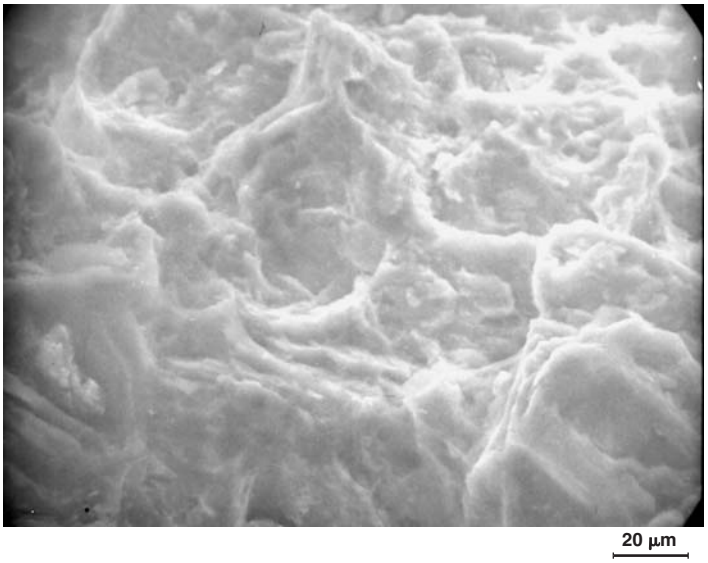

Fig. CH10.6 SEM fractograph near the periphery, showing dimples

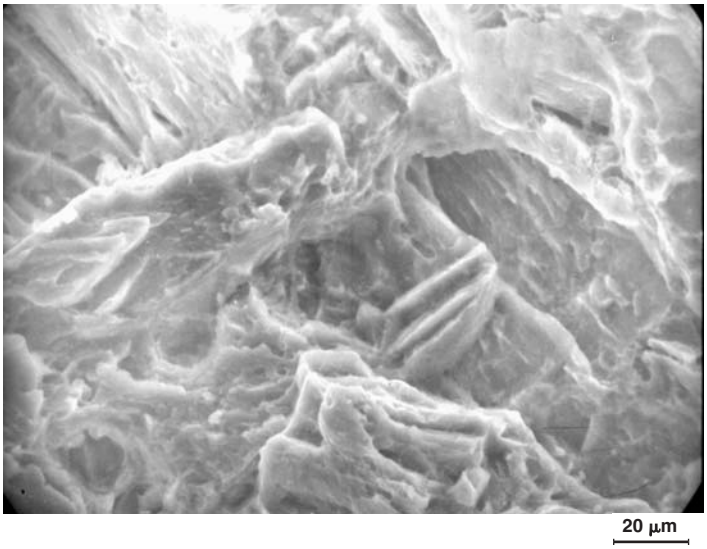

Fig. CH10.7 SEM fractograph on the interior, showing cleavage

It is mandatory to charge the tires, monitoring the pressure with a pressure gage. This pressure also varies, depending on the temperature of the tire. This should be taken into account while charging. It is less harmful if the tire pressure is slightly below the recommended pressure than to exceed the pressure.

Failure Analysis of Engineering Structures: Methodology and Case Histories
V. Ramachandran, A.C. Raghuram, R.V. Krishnan, S.K. Bhaumik, p87-89
DOI:10.1361/faes2005p087

CASE 11

Failure of a Turbine Blade in an Aircraft Engine

Summary

A blade from the last turbine stage of an aircraft engine failed in service. The fracture occurred at the root, above the fir tree region. A similar failure of the last-stage turbine blade had occurred in another engine of the same aircraft. These were the only two instances of last-stage turbine blade failure in 20 years of service of the aircraft. The blade had failed in fatigue. The exact cause of fatigue crack initiation could not be established. However, material defects, improper root loading, and temperature excursion were ruled out.

Background

One of the blades from the last-stage turbine of an aircraft engine failed during service. The adjoining blade and the locking device were found to be intact.

It was also reported that a similar failure of the last-stage turbine blade had occurred in another engine of the same aircraft. Only these two occurrences of turbine blade failures of this kind had been reported during the last 20 years this aircraft had been in service.

The following components were available for investigation:

- A leftover portion of the failed blade
- A blade adjoining the one that failed (in the assembly, these two blades are placed together in one slot)
- Blades positioned in the turbine rotor, diametrically opposite the failed blade
- A new, unused blade from the store
- A used blade from one of the engines that had been operating normally

Visual Examination of General Physical Features

The fracture occurred at the root portion of the blade, just above the fir tree region, shown schematically in Fig. CH11.1. The fracture initiated from the trailing edge side.

The fracture surface showed clear beach marks, with varying degrees of oxidation, indicating delayed type of failure. The beach marks covered an area of about 40% of the total fracture.

The load-bearing surfaces of the fir tree root of the failed blade did not show any abnormal features.

Examination of the other blades did not indicate the presence of cracks in this zone. The leading and trailing edges of the other blades were also found to be normal.

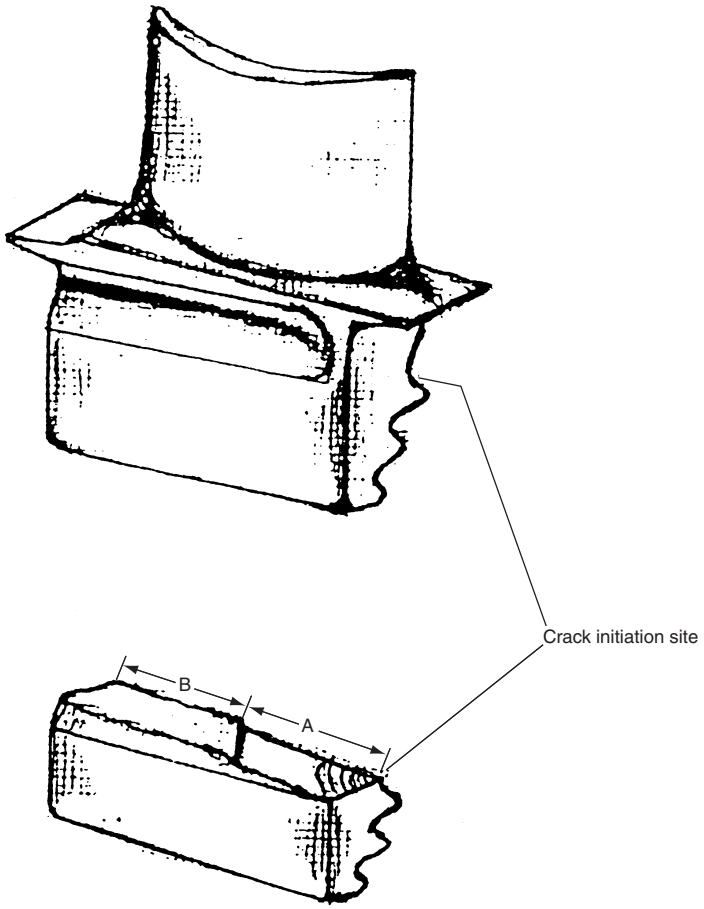

Fig. CH11.1 Schematic diagram showing location of fracture

Testing Procedure and Results

Scanning Electron Fractography and Metallography

The fracture surface of the failed blade was examined in a SEM. The gross features of the flat area containing beach marks are shown in Fig. CH11.2. Fatigue striations were observed in this region at higher magnifications (Fig. CH11.3). The features of the fast-fracture region are shown in Fig. CH11.4.

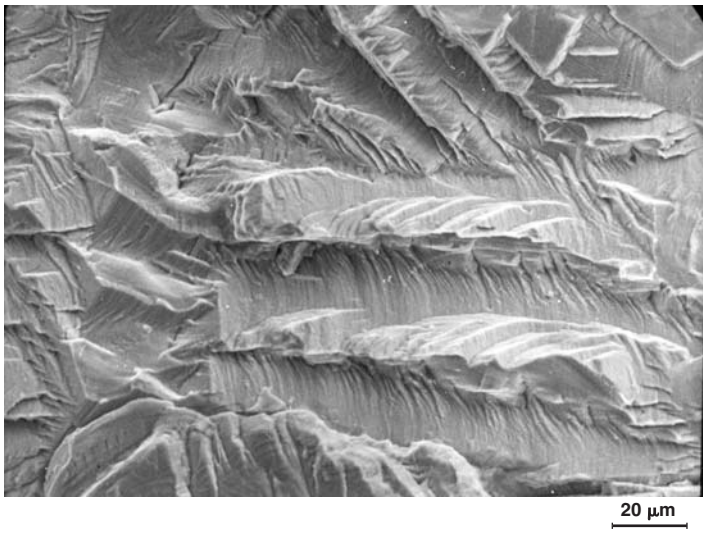

Fig. CH11.2 SEM fractograph of the failed blade

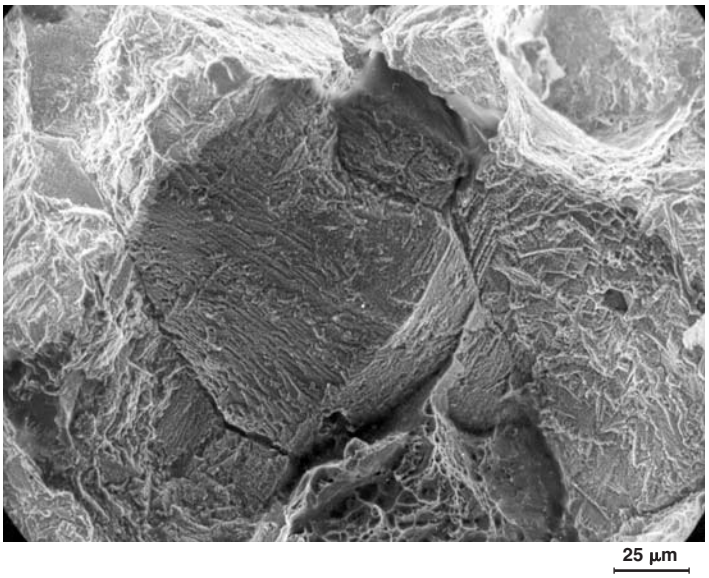

Fig. CH11.4 SEM fractograph of the fast-fracture region

Metallographically prepared specimens taken from the root region and from the center section of the failed blade were examined in optical and scanning electron microscopes. The microstructure was found to be satisfactory without any abnormalities (Fig. CH11.5). Qualitative elemental analysis indicated that the alloy contained nickel, chromium, titanium, aluminum, iron, and molybdenum (Fig. CH11.6). Metallographic examination of the adjacent blade and a good blade indicated that the microstructures in all of them were similar.

Discussion

Fractography indicated that the blade had failed due to a fatigue crack initiated at the trailing edge of the blade and the final fracture occurred when the crack reached critical length.

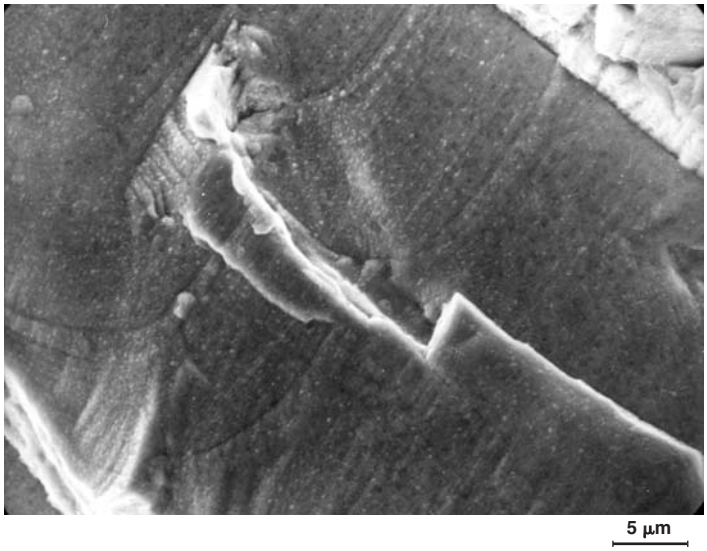

Fig. CH11.3 SEM fractograph of the failed blade, showing fatigue striations

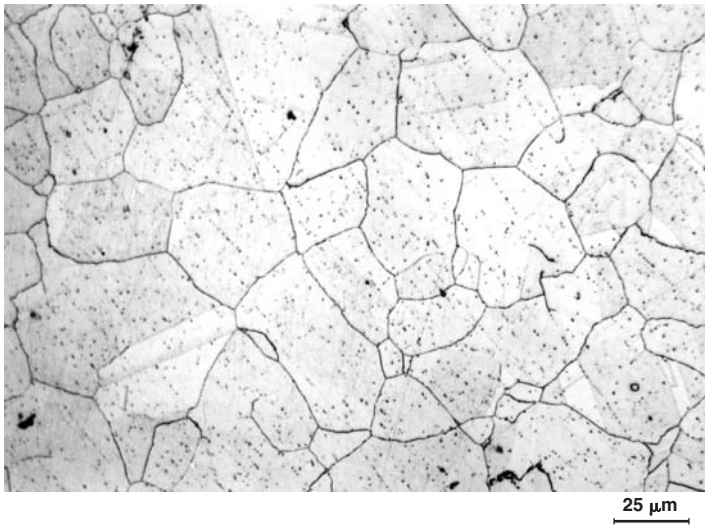

Fig. CH11.5 Microstructure of the failed blade

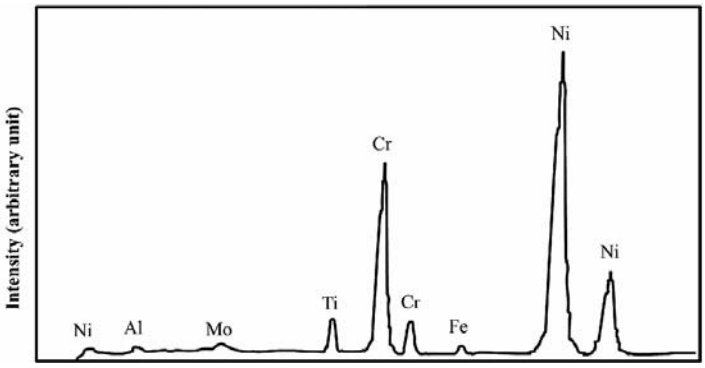

Fig. CH11.6 Energy-dispersive spectrum of the blade material

Examination of the γ-prime precipitates in the microstructure of the airfoil center section did not indicate any exposure to abnormally high temperatures. If any temperature excursion had occurred, it should have manifested in this region first. Hence, it is very unlikely that a temperature excursion was the primary reason for this failure.

Conclusion

The blade failed due to a fatigue crack. The exact cause of fatigue crack initiation could not be identified. However, temperature excursion, improper root loading, and material defects can be ruled out as primary causes for this failure.

Failure Analysis of Engineering Structures: Methodology and Case Histories
V. Ramachandran, A.C. Raghuram, R.V. Krishnan, S.K. Bhaumik, p90-91
DOI:10.1361/faes2005p090

CASE 12

Failure of an Aileron Control Cable in an Aircraft

Summary

A cable controlling the aileron movement in an aircraft had broken. This cable, made up of seven strands of seven wires each, connects a vertical pulley to a horizontal pulley through a set of two guiding pulleys. Evidence of thinning of the strands due to contact wear at the pulleys was found in the majority of the wires. The snapping of the cable was due to excessive thinning of the wires.

Background

The port side aileron control cable of an aircraft was found snapped. This cable is vital in transmitting the pilot's input to the control surface. It connects a vertical pulley to a horizontal elliptical pulley through a set of two guiding pulleys. It was reported that the cable is subjected to a spring load of 25 to 30 lb. The failed port side cable is shown in Fig. CH12.1, along with the other side cable.

Visual Examination of General Physical Features

The cable failed at approximately 35 cm from the eye end. About 3 cm on either side of the failure, the cable wore out along a line. This region of the cable runs over the pulley.

Testing Procedure and Results

Microscopy and Scanning Electron Fractography

The failed cable was examined in a stereobinocular microscope and in a SEM. The cable was made up of seven strands of seven wires each. Out of these, 40 wires contained evidence of thinning due to wear and subsequent failure. Figures CH12.2 and CH12.3 show the thinned portion of the wire.

The remaining nine wires had failed in tension. Figures CH12.4 and CH12.5 show the fracture surfaces of these wires, the latter showing dimples characteristic of tensile failure.

Evidence of similar wear was also noticed in the other cable in the same region. Therefore, the wear was attributable to the contact with the pulleys.

Conclusion

The snapping of the cable was due to excessive thinning of its strands due to contact wear.

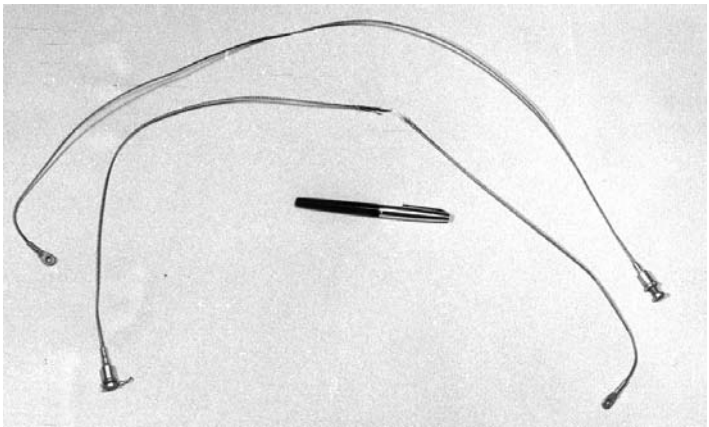

Fig. CH12.1 Snapped aileron control cable and another cable in service

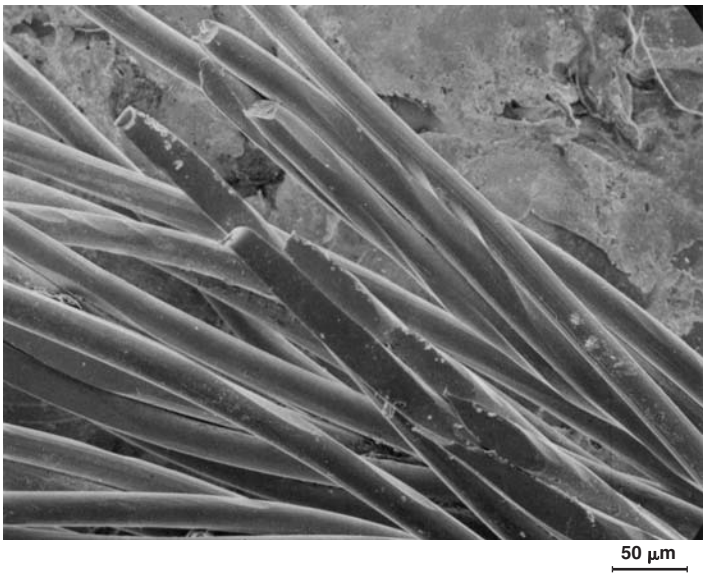

Fig. CH12.2 SEM fractograph showing strands thinned and broken

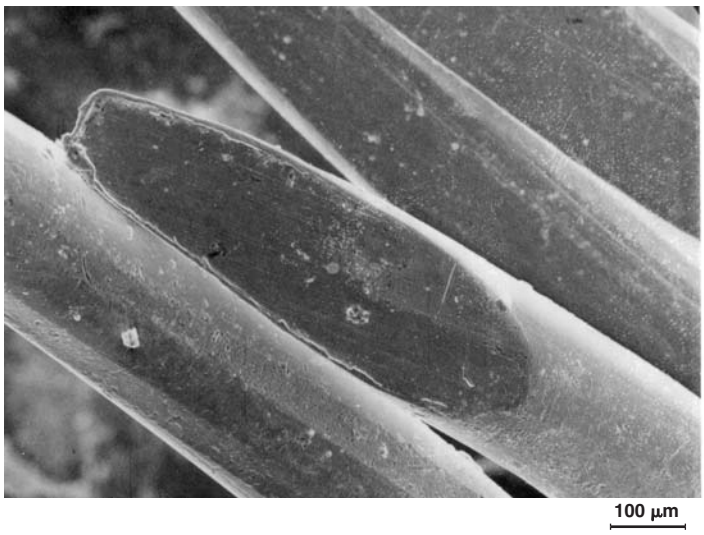

Fig. CH12.3 SEM photograph showing the extent of wear in a few wires

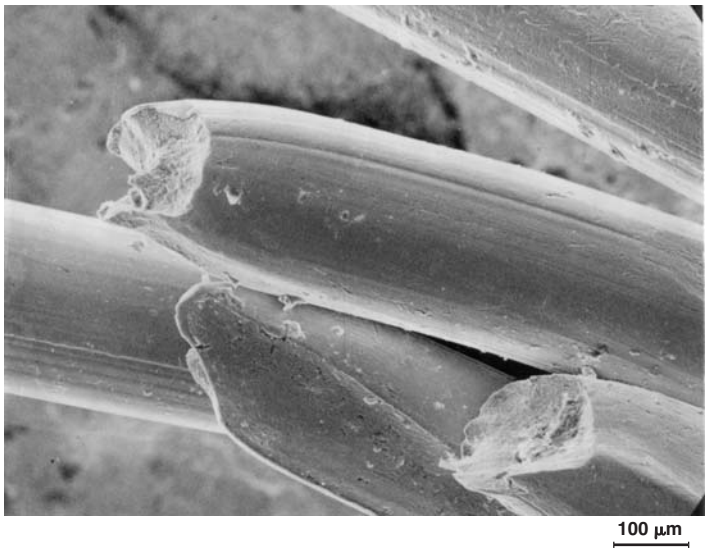

Fig. CH12.4 Some of the wires failed in tension, showing cup and cone fracture

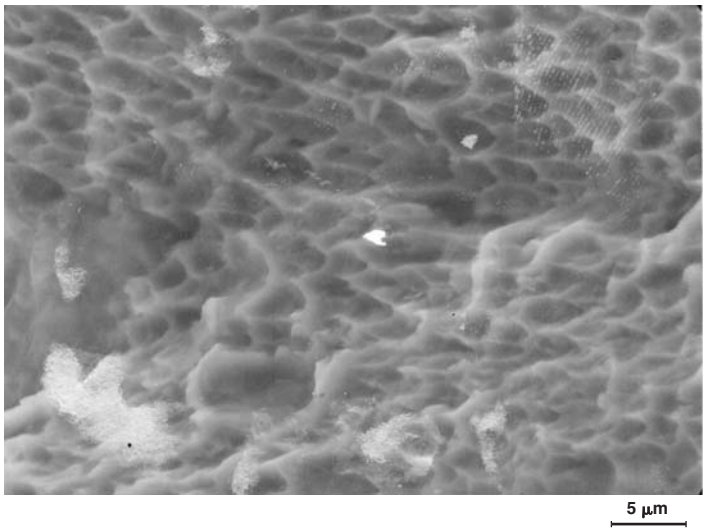

Fig. CH12.5 Fracture surface of one of the wires showing dimples characteristic of tensile failure

Failure Analysis of Engineering Structures: Methodology and Case Histories
V. Ramachandran, A.C. Raghuram, R.V. Krishnan, S.K. Bhaumik, p92-94
DOI:10.1361/faes2005p092

CASE 13

Failure of a Fuel Pump in an Aircraft

Summary

The fuel pump in an aircraft failed, resulting in engine flame-out. One of the seven pistons had broken into several pieces. This failure resulted in the fracture of the quill shaft of the pump. The fracture surface of the quill shaft had suffered severe rubbing. The available fracture surface of the piston indicated beach-mark-like features. Diametrically opposite the apparent origin of the beach marks was a nick on the barrel surface. These facts suggest that there was a preexisting crack that propagated by fatigue.

Background

In an aircraft that met with an accident, the fuel pump had failed. It was reported that the failure of the fuel pump resulted in engine flame-out just after takeoff.

Visual Examination of General Physical Features

The quill shaft of the pump had fractured and the fracture surface had rubbed due to the running of its mating part (Fig. CH13.1). The rotor is shown in Fig. CH13.2. Of the seven piston holes in the rotor, one of them had suffered severe damage. The metal around the hole had plastically deformed in the direction of rotation. Significant metal flow around this hole can be seen in Fig. CH13.3.

The corresponding piston also had suffered severe damage and had broken into several pieces. It was reported that some brass inside this piston hole had to be scooped out before recovering the broken pieces of this piston. The slipper pad of this piston was not available for investigation. Some pieces of the broken piston were

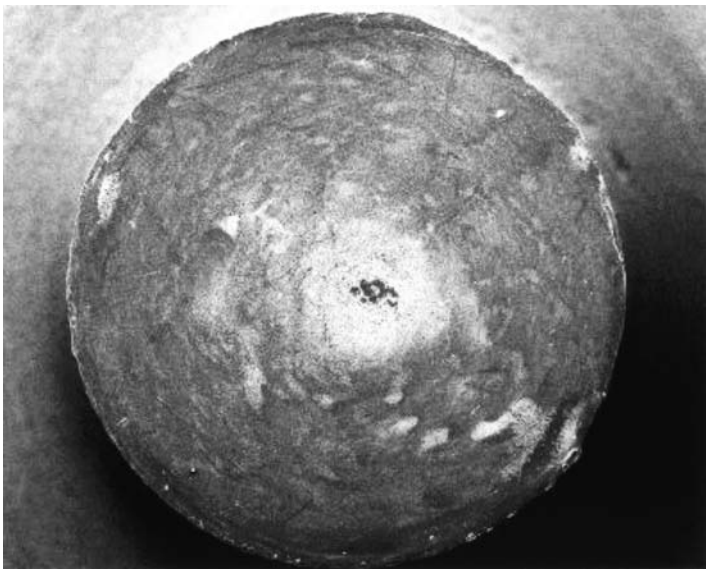

Fig. CH13.1 Fracture surface of the quill shaft

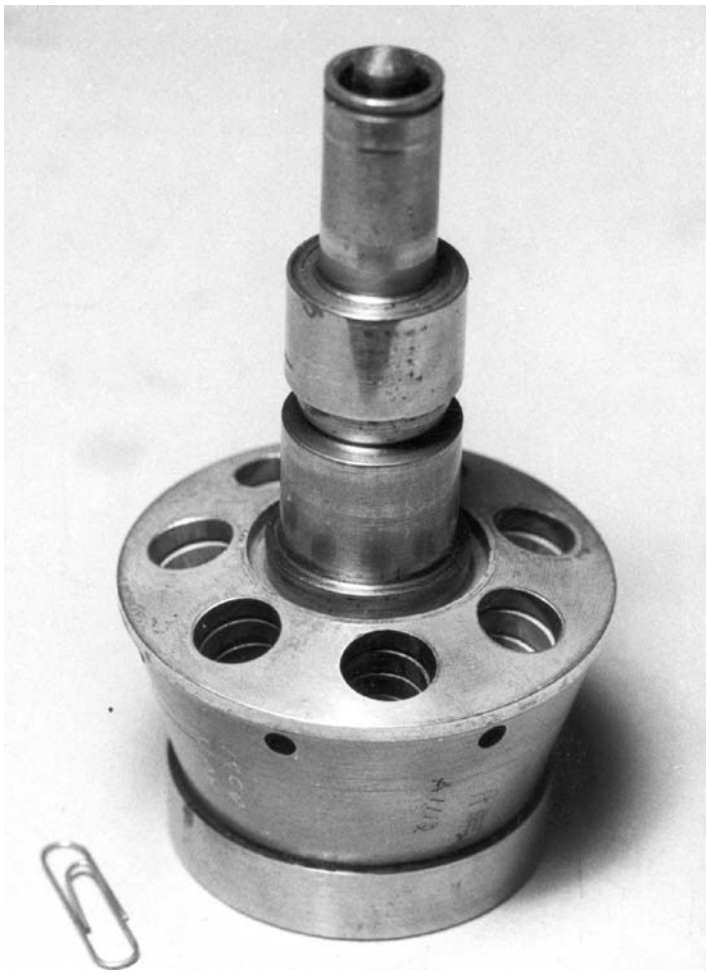

Fig. CH13.2 Rotor of the fuel pump

missing. Part of the fracture surface had been cut for earlier investigations elsewhere. Figure CH13.4 shows a sketch of the broken piston.

Fig. CH13.3 Deformation and metal flow around the piston hole

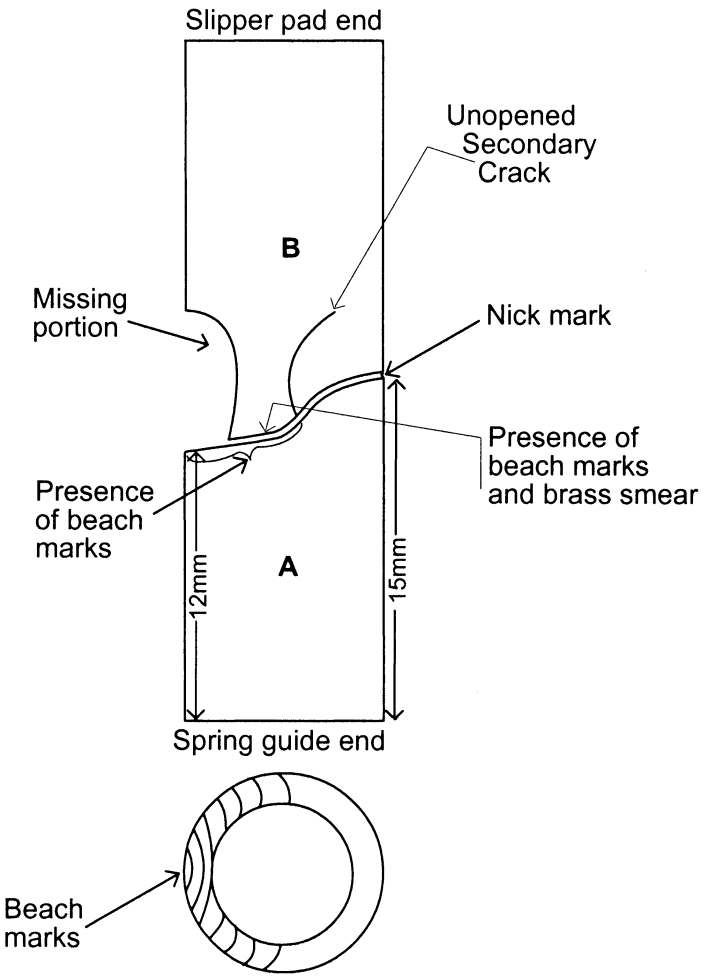

Fig. CH13.4 Sketch showing the fracture pattern of the failed piston

The other six pistons and their respective slipper pads did not show any abnormalities.

All of the seven springs were in good condition with no sign of excessive wear. The seven spring guides showed some wear at the spring seating. Two of these are shown in Fig. CH13.5. The spring seats did not show any abnormality.

Testing Procedure and Results

Microscopy

The available fracture surface on the broken piston, "A" in Fig. CH13.4, was examined under a stereobinocular microscope. About 50% of the cross-sectional area was flat, and the rest showed a jagged surface. The features on the flat region had the appearance of beach marks, although the surface had been rubbed (Fig. CH13.6). Scanning electron microscopy did not clearly reveal fatigue striations.

The mating fracture surface, "B" in Fig. CH13.4, showed a small crack. A small region near this crack corresponded to the flat region of the mating fracture surface A. When the mating surface B was examined in the SEM, a beach-mark-like appearance was seen only on a heavily rubbed fracture area, with brass from the rotor smeared on it. There was no brass deposit on the mating surface A.

Diametrically opposite the area where the beach marks appeared to have originated, a small nick, which could have been the result of final failure of the piston against the top edge of the rotor hole, was found on the barrel surface. Fretting damage to the barrel surface could be seen (Fig. CH13.7).

The microstructure of the piston material was satisfactory. The hardness on the barrel surface was 830 HV, and that on the core was 620 HV.

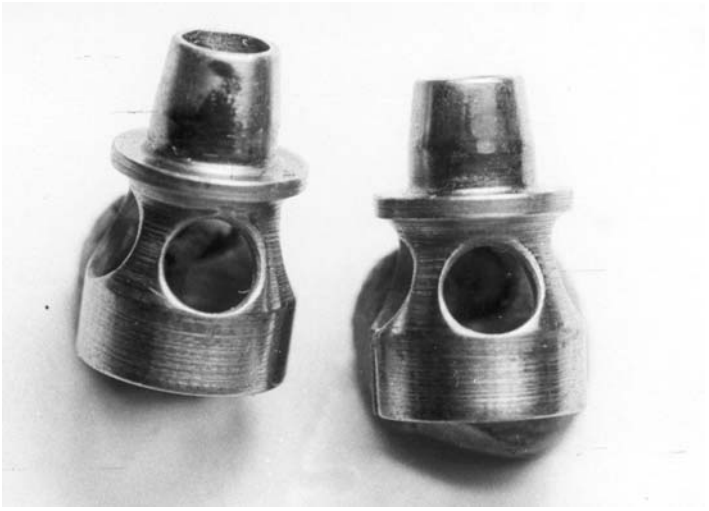

Fig. CH13.5 Wear on the spring guides

Discussion

The primary cause of the failure of the fuel pump was due to the fracture of one of the seven pistons in the rotor. The failure of the quill shaft was the result of the failure of this piston.

The piston made of case-hardened steel failed by fretting fatigue, the crack initiating at the surface. The beach-mark-like appearance on the fracture surface could not be due to rubbing because the two mating surfaces showed similar marking, and one of the surfaces had brass smeared on it. If the beach-mark appearance were due to rubbing after fracture, then the brass smear should be on both the fracture surfaces. Because the patterns were similar and only one had the brass smear, it could be concluded that the beach marks were there before final fracture. The other corroborative evidence is the secondary cracking observed on one of the fracture pieces.

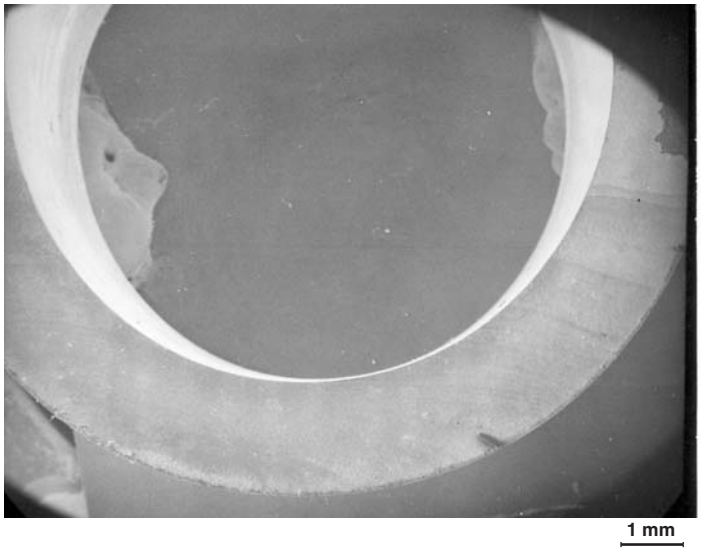

Fig. CH13.6 Features resembling beach marks on the fracture surface of the failed piston. SEM fractograph

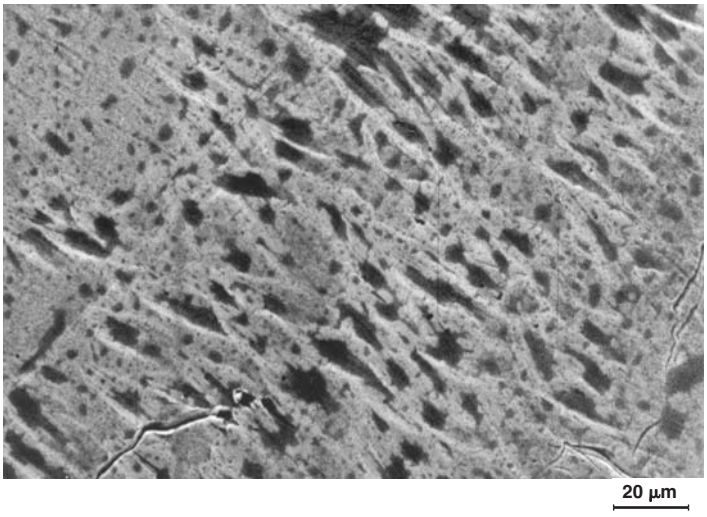

Fig. CH13.7 Fretting damage on the barrel surface of the failed piston. SEM photograph

All these facts and the nick opposite the fracture origin proved that there was a preexisting crack that propagated by fatigue, leaving beach marks. Fatigue striations could not be observed on this surface possibly because the piston was made of a hard material and, secondly, the fracture surfaces had suffered damage.

The cause and type of loading pattern for fatigue crack initiation and propagation could not be ascertained.

The probable cause could be fretting fatigue. The exact sequence could not be established because of the absence of all the fractured pieces.

The pump had failed due to the fracture of one of the pistons. This piston failed due to fretting fatigue arising from fretting fatigue crack on the barrel, and the exact cause of the fretting fatigue could not be identified.

Conclusion

Most Probable Cause

The most probable primary causes were:

- The spring guides not being properly positioned
- Spring seat not in proper position
- Spring stiffness not being uniform with respect to other springs
- Slipper pad jamming

Any one of these conditions singly or collectively can cause fretting fatigue or nonuniform loading on the piston, leading to failure.

Recommendations

- Change all the springs, spring seats, and spring guides every time the pump is overhauled.
- Check and use springs of correct length/stiffness.
- Check the clogging of slipper pad lubricating holes.
- The pistons should be of correct dimensions. In the pump itself, it was observed that the taper at the end of the piston varied from piston to piston. The taper is critical for avoiding spring wear.
- While dismantling the pump, it is always a good practice to identify the parts and their relative locations correctly.

Failure Analysis of Engineering Structures: Methodology and Case Histories
V. Ramachandran, A.C. Raghuram, R.V. Krishnan, S.K. Bhaumik, p95-96
DOI:10.1361/faes2005p095

CASE 14

Failure of Center Support Bearings in an Aircraft Engine

Summary

In an aircraft engine, two center support ball bearings failed. In one, the inner ring broke into pieces and in the other, it had deformed severely. All the balls had suffered rubbing and some had been flattened. Metallographic studies indicated that the balls had experienced temperatures above 825 °C (1520 °F), the A_{cm} temperature. This is also indicated by a drop in hardness from the normal level. The ball bearing race had suffered damage on only one side, indicating a directional thrust, possibly due to misalignment, which could lead to overstressing of the cage, overheating, and fracture.

Background

Two center support bearings of an aircraft engine failed in service.

Visual Examination of General Physical Features

The ball bearings were both of the single-row, deep-groove type with split inner rings and a cage. The cage was made of aluminum bronze. The rings and balls were made of steel, equivalent to 52100 bearing steel. These bearings were mounted side by side in the engine.

Both the bearings were severely damaged. In one of the bearings, the inner ring had broken into pieces (Fig. CH14.1), and in the other, it had suffered severe deformation (Fig. CH14.2). All the balls had suffered severe rubbing and some of them had flattened considerably. The cage also had suffered severe damage. Aluminum bronze from the cage was found embedded on the balls. Aluminum bronze was also found smeared on some portions of the outer ring. The ball bearing race was found damaged mainly on one side, indicating a thrust in that direction.

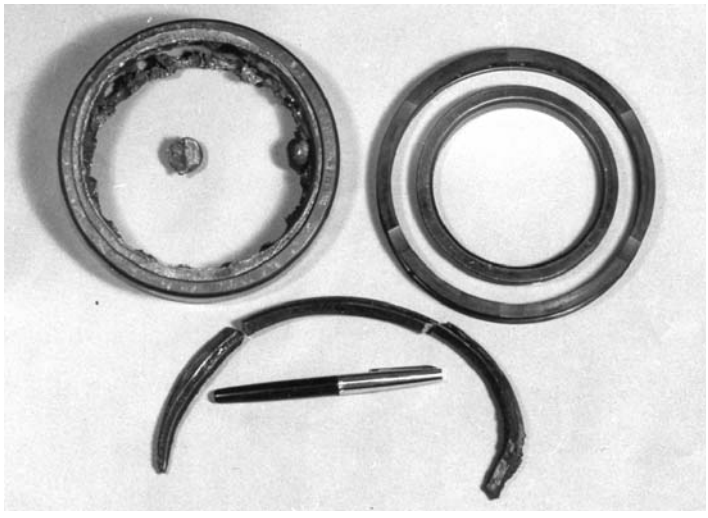

Fig. CH14.1 Severely damaged bearing parts. Note the broken inner ring and the severely rubbed ball bearing.

Testing Procedure and Results

Hardness

Hardness surveys were conducted on the inner and outer rings of the broken bearing and also on the balls. The hardness of the inner ring and the balls averaged 37 HRC and that of the outer ring was 42 HRC.

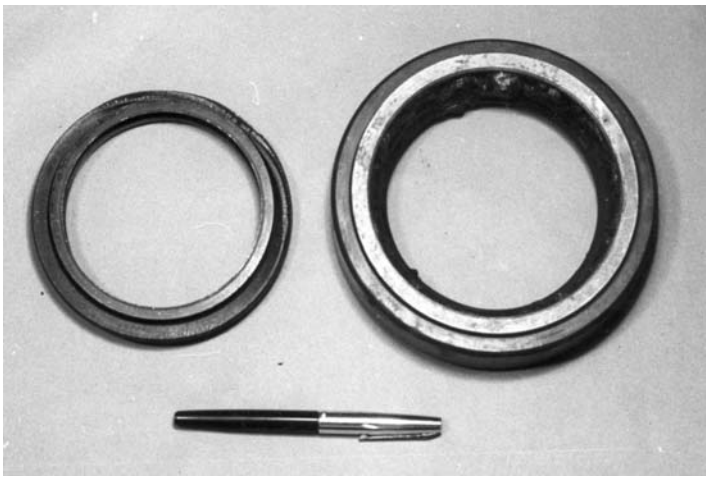

Fig. CH14.2 The second bearing with deformed inner ring

Metallography

Metallography of the outer ring showed tempered martensitic structure, tempered in the region around 600 °C (1110 °F), with spheroidal carbides (Fig. CH14.3), while that of the inner ring and the balls revealed fine and coarse pearlite, with carbide dispersion (Fig. CH14.4, CH14.5). No other material abnormality was found in any of the parts.

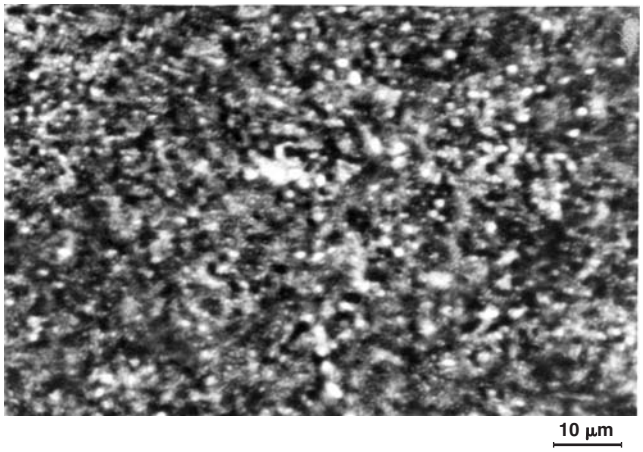

Fig. CH14.3 Microstructure of the damaged outer ring, showing tempered structure. Nital etch

Discussion

The microstructures and hardness indicated the balls and inner ring had experienced temperatures above 825 °C (1520 °F), the A_{cm} temperature. For a pearlitic microstructure with a cementite network to appear in this type steel, it is necessary to heat the metal to a temperature around 850 °C (1560 °F). This is also indicated by the drop in hardness to 37 HRC. Usually, the hardness specified for these parts is 60 HRC. The fall in hardness could be attributed to excessive overheating.

The fact that the ball bearing race had shown damage on only one side indicates a directional thrust. This may be due to possible misalignment of the bearing and shaft, although the exact cause of this cannot be pinpointed. The uneven wearing found in the ball pockets of the case also indicates misalignment. Such misalignment might have caused severe stressing of the cage material, leading to overheating and fracture.

Conclusion

The bearing failed due to overheating, possibly caused by misalignment. Insufficient lubrication coupled with high speeds might have aggravated the problem.

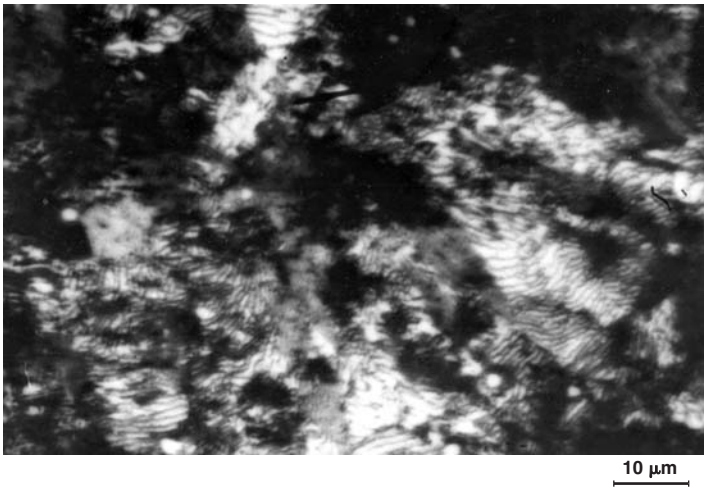

Fig. CH14.4 Microstructure of the broken inner ring showing resolved pearlite and spheroidal carbide. Nital etch

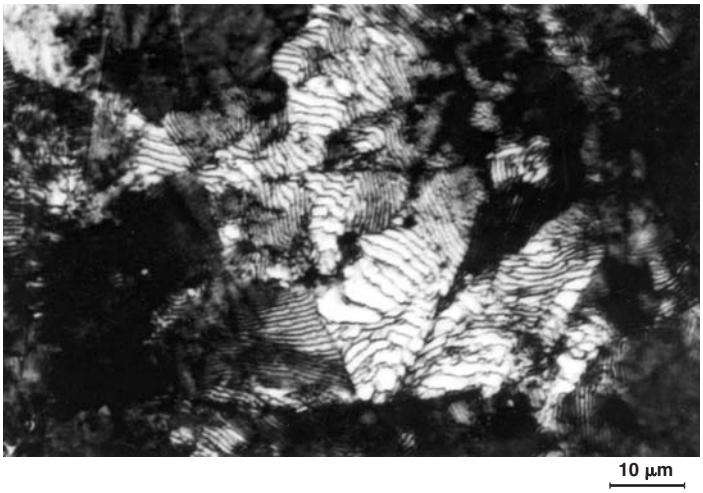

Fig. CH14.5 Microstructure of the damaged ball bearings showing resolved pearlite and spheroidal carbide. Nital etch

Failure Analysis of Engineering Structures: Methodology and Case Histories
V. Ramachandran, A.C. Raghuram, R.V. Krishnan, S.K. Bhaumik, p97-99
DOI:10.1361/faes2005p097

CASE 15

Failure of a Torque Sensor Bearing in an Aircraft Engine

Summary

An aircraft engine had cockpit warning of metal particles in the engine oil and in the oil filter. Analysis showed that the problem was due to excessive clearance between the outer race of the bearing and the steel housing, further assisted by insufficient lubrication. It was recommended that the designed clearance be reexamined and the bearing retaining plate be redesigned to allow more flow of oil to the bearings.

Background

An aircraft engine had a history of cockpit warning of metal particles in the engine oil and in the oil filter. After strip examination, the torque sensor assembly was removed for detailed examination.

Visual Examination of General Physical Features

Figure CH15.1 shows the torque sensor assembly. The assembly was disassembled. The disassembled components are also shown in this figure. It was found that the two matched bearings had been assembled properly. However, of the two bearings, the inner one (the bearing away from the retaining plate) showed evidence of excessive friction compared with the other bearing.

This inner bearing was disassembled for further examination. The inner race of this bearing showed excessive brinelling (Fig. CH15.2). Metal flow can also be seen in this figure. The corresponding ball bearings also showed excessive wear (Fig. CH15.3). Wear and deformation also were observed in the cage (Fig. CH15.4). Some of the holes were found flared, with metal flow resulting in formation of burrs at the hole edge. While disassembling, a sharp metal sliver of the same color as the cage was also found sticking to the inner surface of the outer race. Heat tinting was observed on the external surface of the outer race of the inner bearing.

A wavy washer positioned below the inner bearing showed excessive grooving along the periphery at the ridges (Fig. CH15.5). The shim washer also showed signs of chatter (Fig. CH15.6).

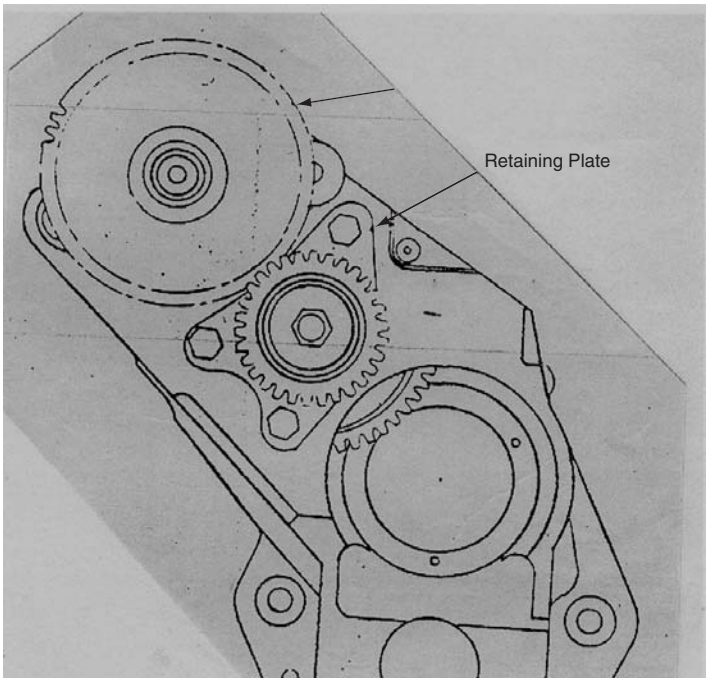

(a)

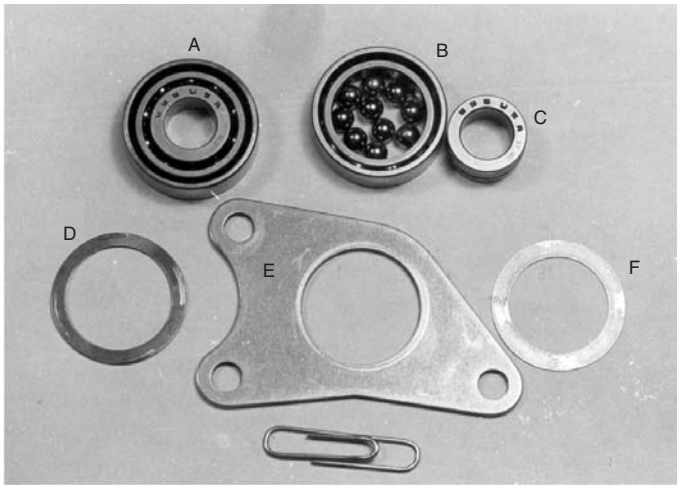

(b)

Fig. CH15.1 (a) Diagram showing the torque sensor assembly. (b) Disassembled components of torque sensor bearing. A, outer bearing; B and C, parts of inner bearing; D, wavy washer; E, retaining plate; and F, shim

The inner side of the bearing retaining plate showed extensive circular grooving (Fig. CH15.7). The diameters of grooving on the wavy washer and the bearing retaining plate correspond to the diameter of the outer race of the bearing.

Discussion

The bearing assembly was of the floating type, positioned inside a steel housing. The bearings rested on the wavy washer (Fig. CH15.8) and were restrained at the other end by the retaining plate. Shims were introduced so that the wavy washer would exert the required force on the retaining plate.

From the observations and assembly, it is clear that grooving on the wavy washer and the retaining plate had been caused by the rotation of the outer races of the bearings. Heat tinting observed on the external surface of the outer race of the inner bearing gives further evidence to rotation.

This rotation comes about by excessive clearance between the outer race and the steel housing abetted by insufficient lubrication in the bearings. Once grooving sets in, the tension on the wavy washer is altered from the set value. This would further assist in the rotation of the outer race inside the housing. The material removed by wear would show up during the analysis of the lubricating oil for metal particles.

(a)

(b)

Fig. CH15.2 (a) Inner race of the inner bearing showing brinelling. (b) Enlarged view of the inner race showing metal flow

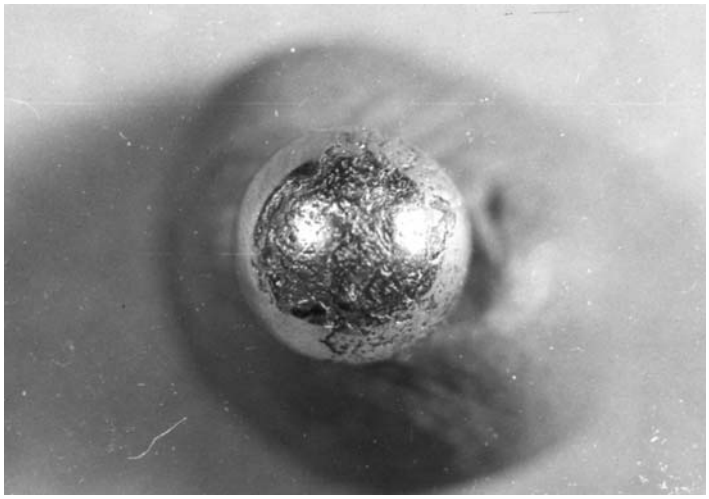

Fig. CH15.3 One of the balls of the inner bearing showing excessive wear

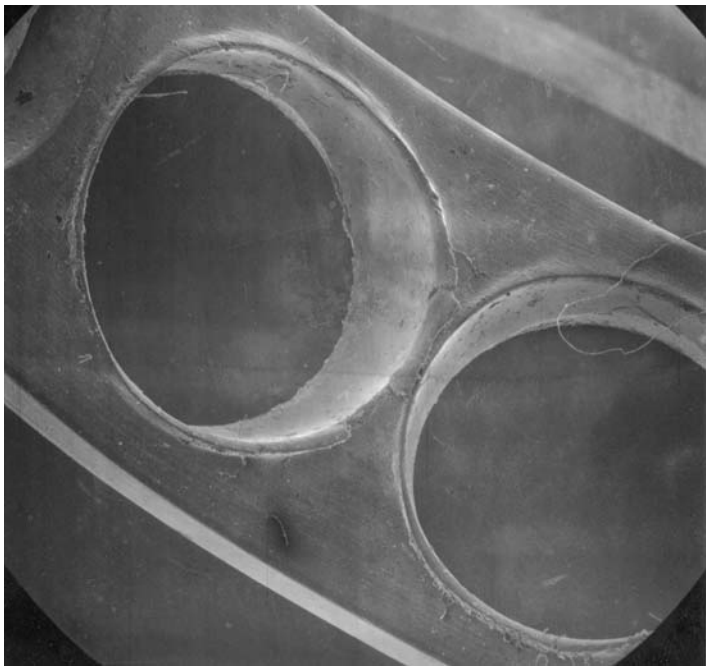

Fig. CH15.4 Wear and deformation of the cage of the inner bearing

Conclusion and Recommendations

The problem of metal particles in the engine oil arose from wear and excessive clearance between the outer race of the bearing and the steel housing and was further assisted by insufficient lubrication.

The recommended clearance between the housing and the outer race of the bearings should be reexamined.

The bearing retaining plate, which is in the path of the lubricating oil, could be redesigned to allow more flow of oil to the bearings, particularly to the inner bearing.

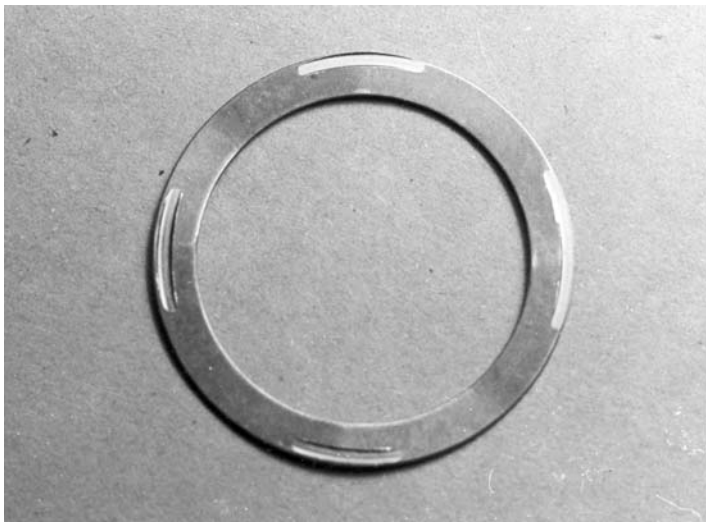

Fig. CH15.5 Wavy washer showing extensive grooving

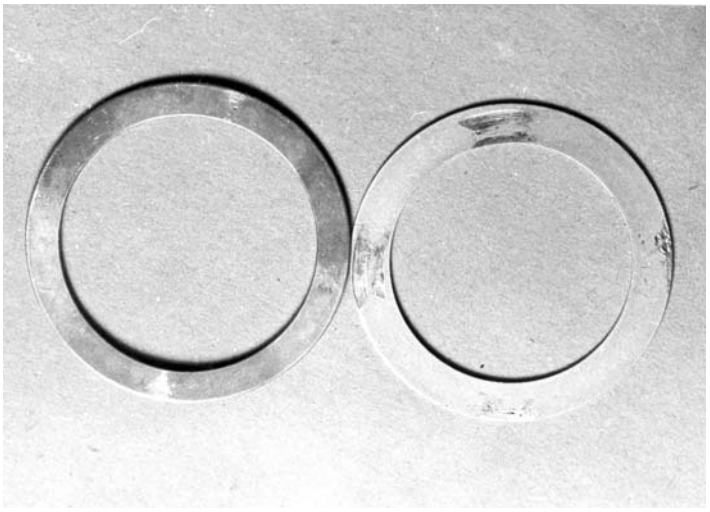

Fig. CH15.6 Mating surfaces of shim and wavy washer showing signs of chatter

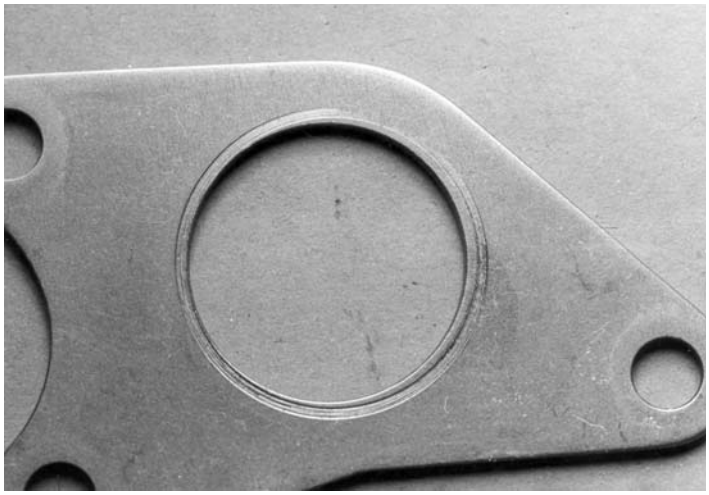

Fig. CH15.7 Inner side of the retaining plate showing extensive grooving

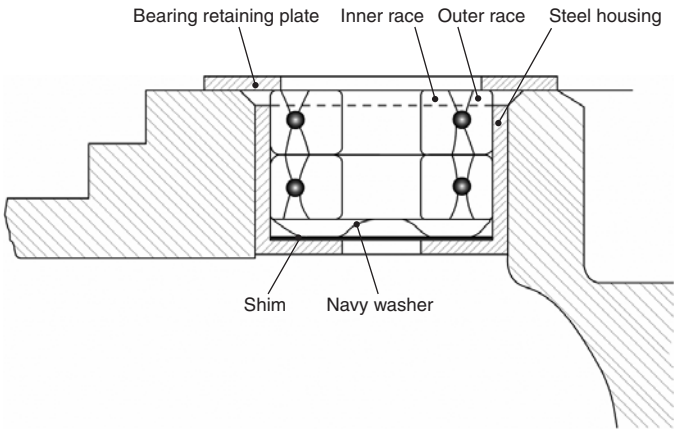

Fig. CH15.8 Schematic of the torque sensor bearing assembly

Failure Analysis of Engineering Structures: Methodology and Case Histories
V. Ramachandran, A.C. Raghuram, R.V. Krishnan, S.K. Bhaumik, p100-101
DOI:10.1361/faes2005p100

CASE 16

Failure of a Universal Joint in an Undercarriage in an Aircraft

Summary

During an attempt to land an aircraft, the starboard undercarriage was stuck midway and did not lock down in spite of normal as well as emergency lowering procedures. After various maneuvers and final landing, it was found that the universal joint on the actuating link rod of the inboard door of the starboard undercarriage was broken. Investigations revealed that the link rod had fractured due to the propagation of a preexisting fatigue crack.

Background

In a flying incident, there was a problem in lowering the starboard undercarriage while in flight. The nose and port legs came down, but the starboard leg was stuck midway and did not lock down in spite of normal and emergency lowering procedures. Eventually, the starboard leg was brought down by the use of positive and negative "g" maneuvers and a normal landing was made. On landing, it was reported that the universal joint on the actuating link rod of the inboard door of the starboard undercarriage had broken.

Visual Examination of General Physical Features

The undercarriage door control mechanism is shown in Fig. CH16.1. The universal joint made of an aluminum alloy with brass bushing had fractured (Fig. CH16.2a).

Testing Procedure and Results

Microscopy and Scanning Electron Fractography

The fracture surface was examined in a stereobinocular microscope. The fracture surface appeared jagged except at one corner where it was flat and slightly colored. There were indications from the bending that the fracture had initiated at this point and propagated in the direction shown in Fig. CH16.2(b).

The fracture surface was cleaned with replicating tape and observed in a SEM. Figure CH16.3 shows the general appearance of the flat region. Fatigue striations were observed in this region at higher magnifications (Fig. CH16.4), indicating propagation by low-cycle fatigue. The jagged fracture surface away from this region showed dimples characteristic of tensile mode of failure (Fig. CH16.5).

Discussion

From the fractographic features and direction of progress of fracture, it was concluded that the fatigue loading initiated a crack that progressed with time and the final fracture occurred due to bending tensile loading.

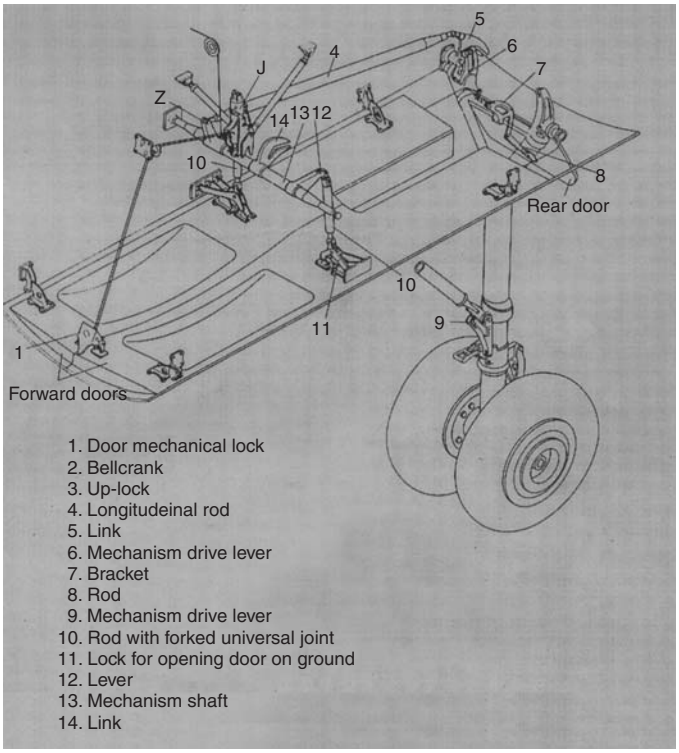

Fig. CH16.1 Starboard undercarriage door control mechanism, indicating the region of fracture of the link rod

Conclusion

The universal joint on the actuating link rod of the starboard undercarriage fractured due to a preexisting fatigue crack coupled with overload.

(a)

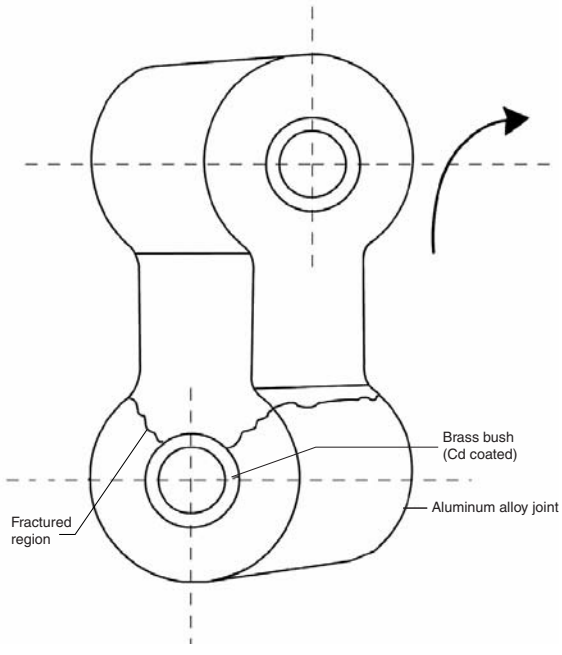

(b)

Fig. CH16.2 (a) Failed link rod and the universal joint. Arrow indicates the fracture. (b) Sketch showing the location of fracture in the universal joint

Fig. CH16.3 SEM fractograph showing the relatively smooth fatigue fracture region

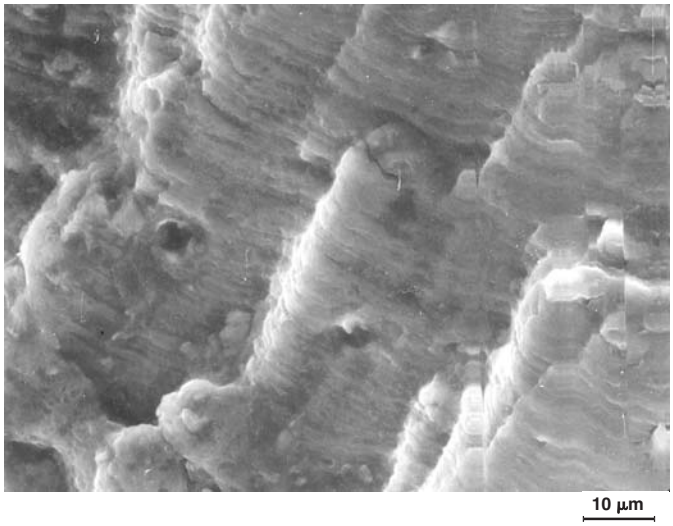

Fig. CH16.4 SEM fractograph showing fatigue striations in the region shown in Fig. CH16.3.

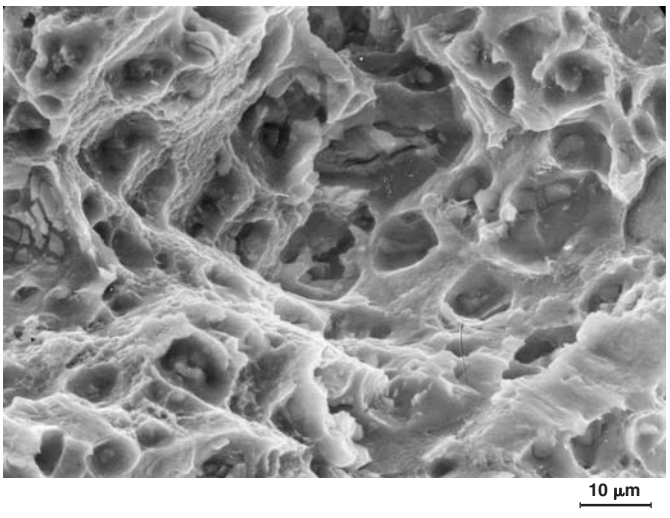

Fig. CH16.5 SEM fractograph of the rapid fracture region showing dimples characteristic of tensile overload failure

Failure Analysis of Engineering Structures: Methodology and Case Histories
V. Ramachandran, A.C. Raghuram, R.V. Krishnan, S.K. Bhaumik, p102-106
DOI:10.1361/faes2005p102

CASE 17

Failure of Dowel Bolts in an Aircraft Engine

Summary

The spur and bevel gears of an aircraft engine were fastened by a set of six dowel bolts. Following a few incidents of dowel bolt failure, the diameter of the bolts at the shank was increased. Still, there were a series of accidents caused by the failure of dowel bolts. Detailed investigations revealed that the bolts failed due to fatigue. Fatigue was initiated by fretting in some bolts.

Background

The spur and bevel gears of an aircraft engine were fastened together with a set of six dowel bolts of 8.5 mm diameter. Because there were a few incidents of dowel bolt failure, the bolt diameter at the shank was increased from 8.5 to 9.2 mm based on a seven-bolt configuration used in another engine. Since then, there were a series of accidents caused by the failure of the modified dowel bolts.

Pertinent Specifications and Manufacturing Details

The bolts were made from a low-carbon nickel-chromium-molybdenum steel. The specification permits partial substitution of molybdenum with tungsten. The bolts were heated to 860 °C (1580 °F) in a salt bath furnace, quenched in oil and tempered at 525–575 °C, or 980–1070 °F, followed by air cooling. The shank portion was finish ground to a surface finish of 8∇. The specified surface finish was 6∇. The bolts were given a final phosphate coating in an oxide phosphating bath. The interference between the bolt and the bolt hole was maintained near the higher limit of the specified 3 to 28 μm.

It was reported that in some engines, the torque setting of friction clutch was found to be 29 to 30 kg.m, compared with the specified range of 20 to 22 kg.m. In addition, the starting torques were reported to be much higher than the specified range.

Testing Procedure and Results

Macroexamination

The bevel and spur gears along with the failed dowel bolts in position are shown in Fig. CH17.1. All six bolts failed inside the bevel gear. The fracture surfaces of the halves held in the spur gear were damaged. Those in the bevel gear are shown in Fig. CH17.2. After removing the bolts, the distance from the bolt collar to the fracture origin was measured and found to range from 5.8 to 8.4 mm in one engine. The fracture surfaces of the six bolts are shown in Fig. CH17.3. All of them contained beach marks covering a major portion of the fracture surface. The fracture had originated at the outer periphery and progressed inward (Fig. CH17.4). In a few cases, two diametrically opposite origins were found (Fig. CH17.5).

The shanks of most of the bolts and bolt holes contained circumferential grooves (Fig. CH17.6, CH17.7). Severe fretting marks with associated debris were noticed in some bolts at the

Fig. CH17.1 Bevel and spur gears with the failed dowel bolts

fracture origin (Fig. CH17.8). The web portion of the spur gears showed lapping marks around the shaft over a large area, while wear marks were observed on either side of the bolt holes (Fig. CH17.9). Near the bolt hole, marks resembling erosion tracks with their origin at the hole and progressing radially outward were observed (Fig. CH17.10).

Scanning Electron Fractography

The failed bolts were examined in a SEM. In each assembly, there were a few bolts with two fracture origins. At the origin, fatigue striations were observed with an average spacing of 2.5 μm (Fig. CH17.11). At other places on the same fracture surface, striations were also observed with an average spacing of 0.4 μm. The bolts with double fracture origins showed dimple rupture at the central region (Fig. CH17.12). In each assembly, one or two bolts showed mixed intercrystalline and transcrystalline fracture features ahead of the beach marks (Fig. CH17.13).

Metallography

Metallographic examination was carried out on the barrel surface of a few failed bolts. A number of cracks were observed close to the fracture surface, propagating in inter and transgranular mode (Fig. CH17.14). The bolt heads, shanks, and longitudinal sections near the threaded region were also examined. Deep intergranular oxidation was observed on the bolts chosen at random, at all locations excluding the shank (Fig. CH17.15).

The steel was relatively clean and contained a few sulfide, oxide, and carbonitride inclusions. The steel was fine grained and the

Fig. CH17.2 Failed bolts in the bevel gear

Fig. CH17.3 Fracture surfaces of the six failed bolts in the bevel gear

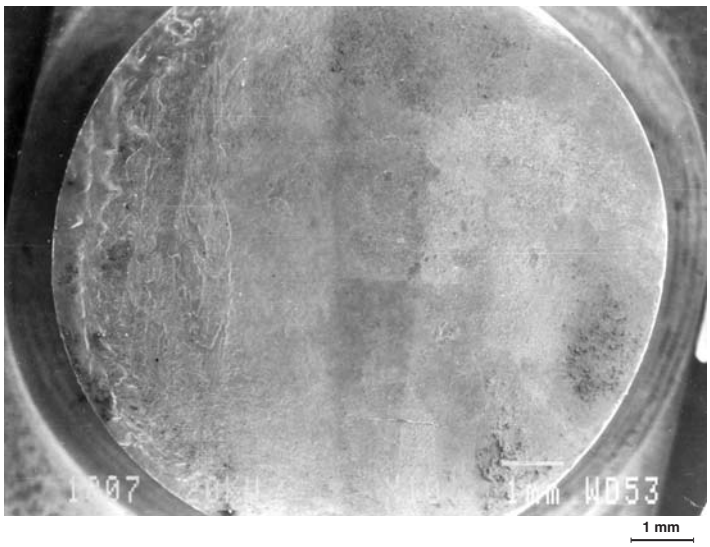

Fig. CH17.4 SEM fractograph showing crack initiation at the outer periphery and propagation inward

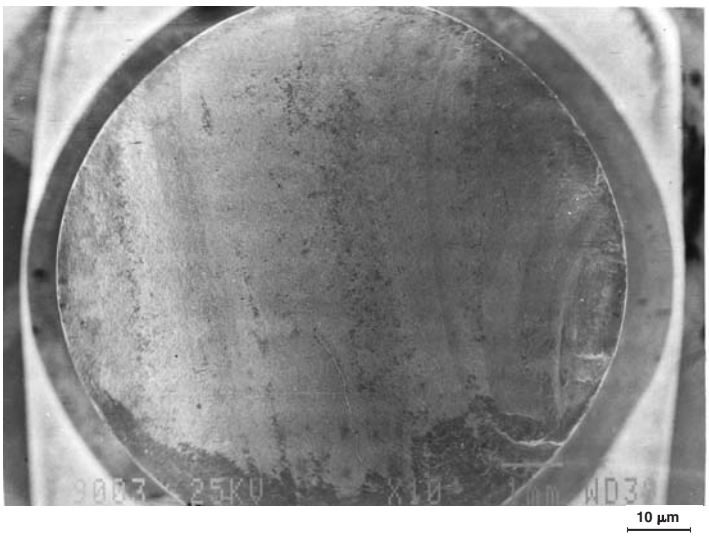

Fig. CH17.5 Two diametrically opposite fracture origins found in some bolts

microstructure was tempered martensite. The raw material also had a tempered martensitic structure.

Chemical Analysis

The chemical composition of the raw material and a failed bolt is given in wt%:

	Chemical composition	
Element	**Raw material**	**Failed bolt**
Carbon	0.19	0.16
Silicon	0.30	0.31
Manganese	0.39	0.31
Nickel	4.20	4.40
Chromium	1.5	1.4
Molybdenum	0.11	0.11
Tungsten	0.70	0.57
Sulfur	0.004	0.009
Phosphorus	0.007	. . .

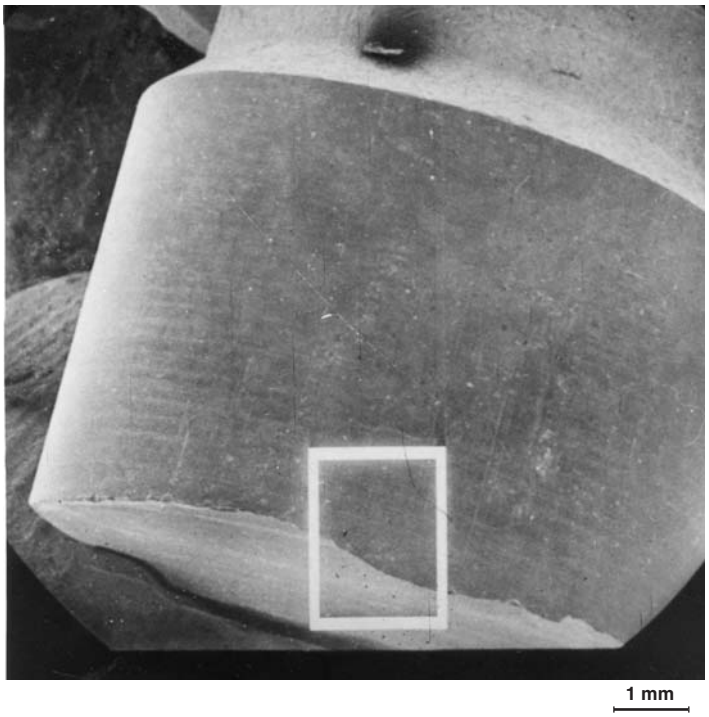

Fig. CH17.6 Circumferential grooves on the shanks of the bolts

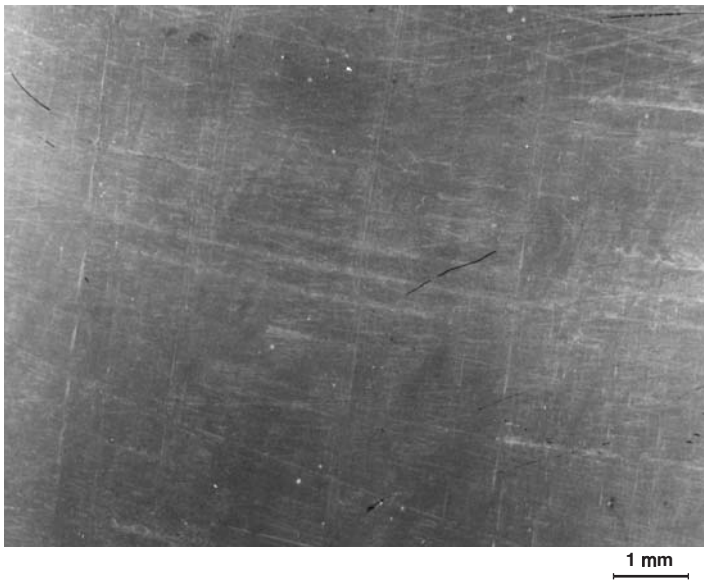

Fig. CH17.7 Circumferential grooves in the bolt holes

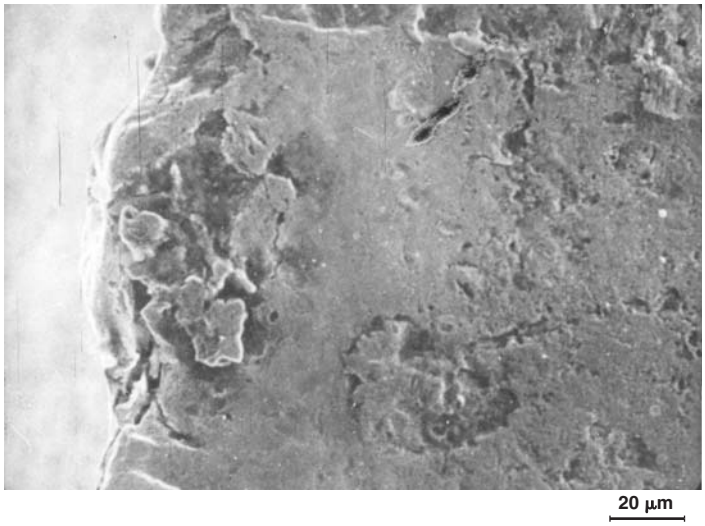

Fig. CH17.8 Fretting marks and debris at the fracture origin in some bolts

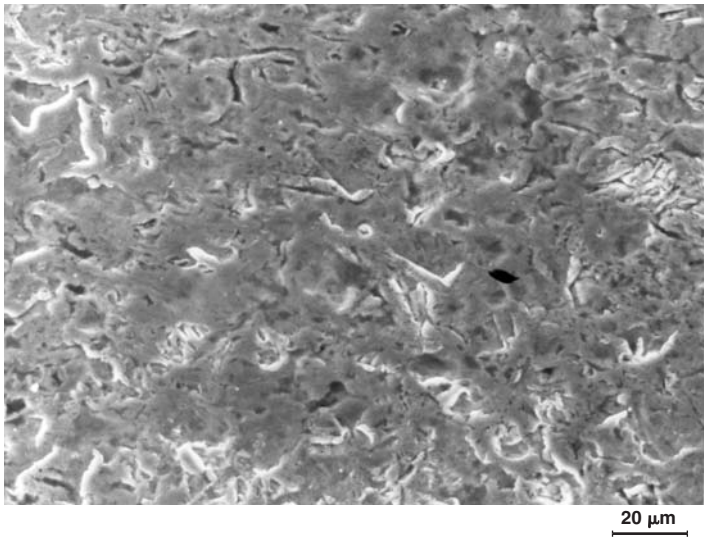

Fig. CH17.9 Wear marks in the bolt holes

Hardness

The average hardness at 10 kg load was 370 HV on the failed bolt and 430 HV on the raw material.

Low-Cycle Fatigue Tests

Low-cycle fatigue tests were carried out on heat treated and phosphated samples at stress amplitude of 904 MPa and plastic strain amplitude of 5.65×10^{-3}. The unphosphated samples withstood 680 cycles, while the phosphated samples, 590 cycles. Considering the usual scatter in fatigue tests, the difference is not marked. On the fracture surfaces, the ratio of fatigue crack area to the overload failure area was approximately 60:40.

Discussion

The chemical composition of the failed bolts conformed to the specifications. The cleanliness and microstructure of the steel were satisfactory. The hardness and microstructure suggested that correct heat treatment was given to the bolts. The intergranular oxidation in the bolts is an abnormality even though the failure is not directly related to this defect.

The presence of beach marks and striations on the fracture surface indicates clearly that the failure was due to fatigue. The dif-

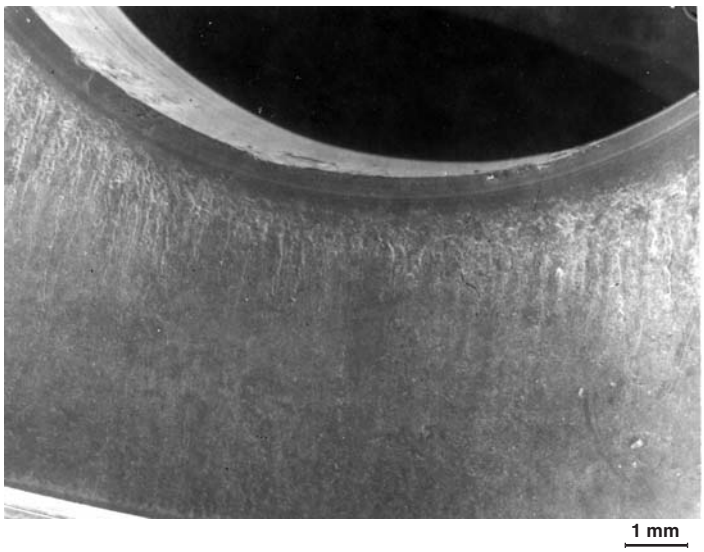

Fig. CH17.10 Marks resembling erosion tracks with the origin at the bolt hole

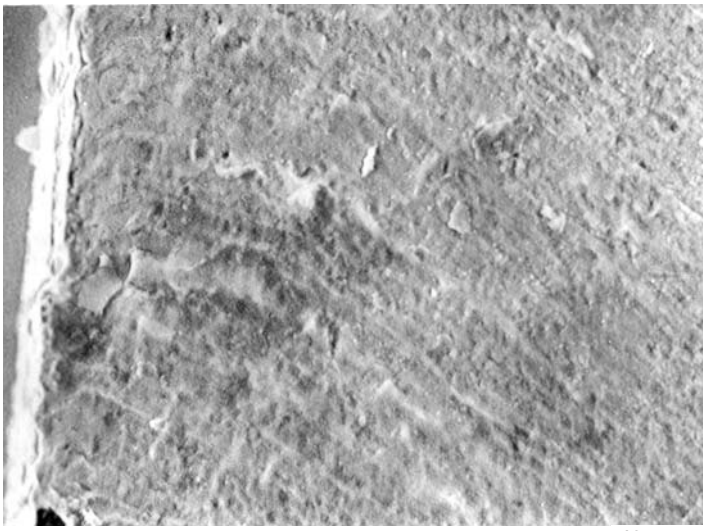

Fig. CH17.11 Fatigue striations in a failed bolt, at the fracture origin

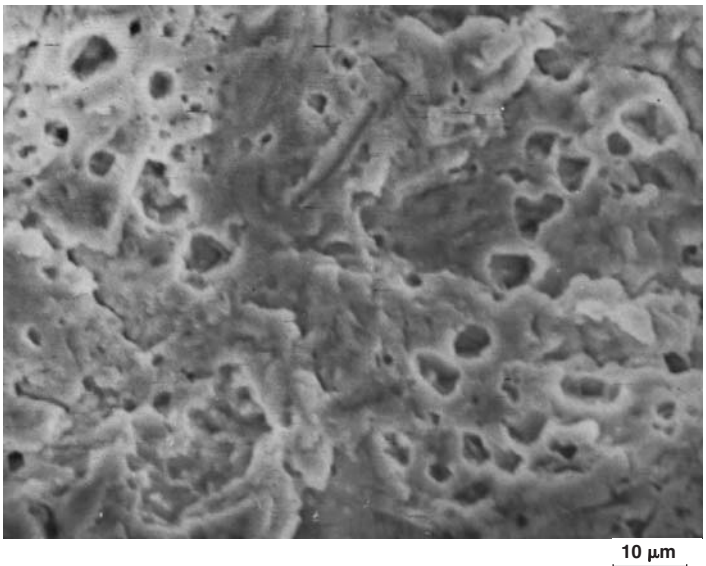

Fig. CH17.12 Dimple rupture at the central region of the fracture with double origins

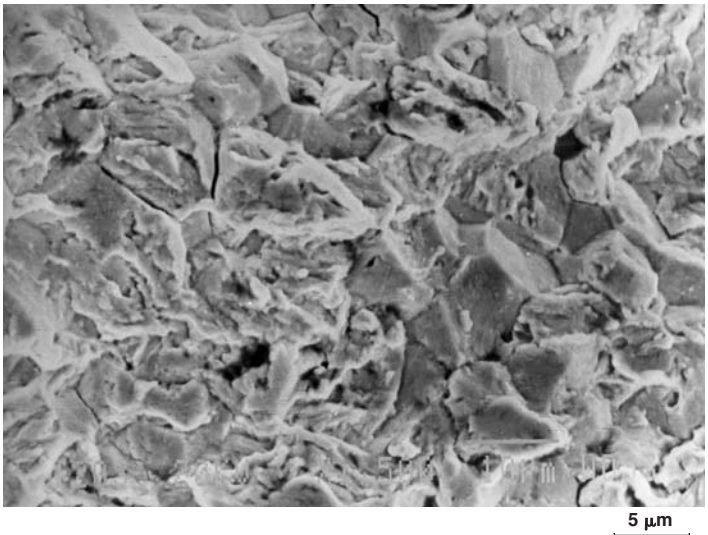

Fig. CH17.13 Mixed intercrystalline and transcrystalline fracture ahead of the beach marks in a bolt

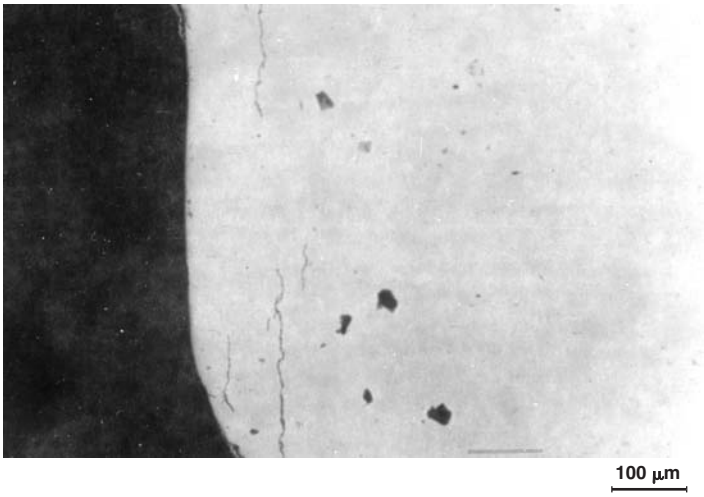

Fig. CH17.14 Cracks on the barrel surface of a failed bolt, close to the fracture surface, propagating in intercrystalline and transcrystalline modes

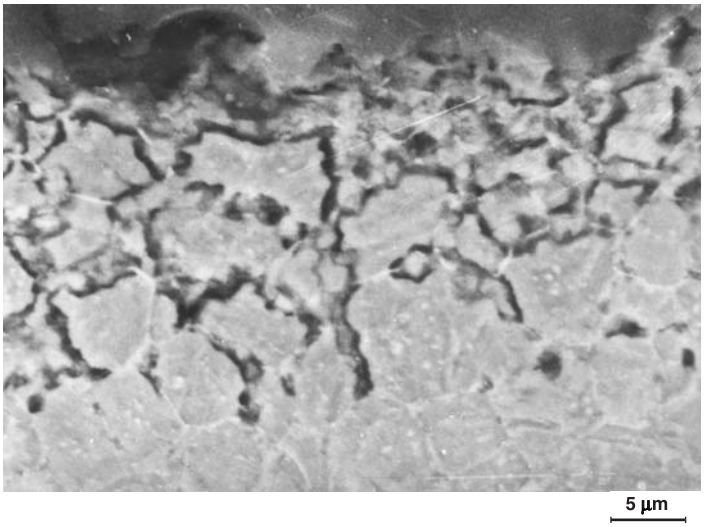

Fig. CH17.15 Intergranular oxidation on bolts chosen at random

ferent striation spacings coexisting on the same fracture surface suggest crack propagation initially in low-cycle mode and intermittently in high-cycle mode. This is in agreement with the fact that the torque generated at the time of engine start is high and it is stabilized to approximately one-third of the initial torque during continuous running of the engine.

The fretting marks on some bolts observed in conjunction with the area of contact between the two gears is indicative of flexing of the bevel gear over the spur gear. This is further corroborated by the presence of radial erosion marks on the spur gear near the bolt caused by the squeezed-out lubricating oil laden with solid particle debris. The oil squeezing is the result of flexing action of the bevel gear. The telltale marks on the gear assembly clearly indicate that there existed a cyclic relative motion between the bolt and the bevel gear, leading to fatigue failure. Poor surface finish inside the bolt hole, high interference tolerances and, probably, the existence of a burr at the chamfer at the interface could have accelerated the failure.

Conclusion

The dowel bolts failed due to fatigue. Fatigue was initiated by fretting in some bolts.

Recommendations

- Prevent the gap between the bevel and spur gears.
- To ensure specified contact area, blue ink check should be carried out even during overhauling.
- Chamfer edges should be smoothened after reboring during overhaul.
- Change of the bolt diameter from 8.5 to 9.2 mm is not desirable because the bolts have not failed because of overload or shear, and using the same diameter nut and the head section for the increased diameter of the shank without appropriate changes in the bolt hole configuration results in decreased load bearing areas.
- Decrease the interference tolerances. Higher interference will increase the fretting tendency if relative motion between the bolt hole and the shank is not prevented.
- Ensure the specified surface finish in the bolt holes.
- Ensure proper alignment of the bolt with respect to the hole as specified.
- Effective steps should be taken to prevent intergranular damage at the surface. The salt bath and phosphating baths need attention with respect to the bath composition and temperature.
- Quality control checks should be ensured to prevent occasional surface blemishes observed on the shank of unused bolts.

Failure Analysis of Engineering Structures: Methodology and Case Histories
V. Ramachandran, A.C. Raghuram, R.V. Krishnan, S.K. Bhaumik, p107-109
DOI:10.1361/faes2005p107

CASE 18

Failure of a Tail Rotor Blade in a Helicopter

Summary

The outboard rib of a tail rotor blade in a helicopter became separated in flight, causing severe vibrations. The rivets for fitting the rib to the blade were also missing. The skin of the blade was found torn off at a number of rivet holes. The separation of the rib is attributed to stress-corrosion cracking (SCC) in the regions adjacent to the rivets. Erosion of the skin and the rivets could also have contributed to the failure.

Background

A helicopter experienced severe vertical vibrations during flight. After landing, it was noticed that the outboard rib of a tail rotor blade was missing. The set of three tail rotor blades had completed cumulatively 1621 hours before the incident, compared with an expected life of 2500 hours.

Visual Examination of General Physical Features

The rib is fitted on the tail rotor blade by a set of six rivets, each passing through a pair of holes, indicated as A-A, and so forth, in the skin of the rotor blade (Fig. CH18.1). In the blade under investigation, in addition to the rib, all six rivets were missing. The skin of the blade was found torn off at seven of the 12 rivet holes. These tears are identified as A′, B, C, C′, D, D′, and F in Fig. CH18.1. Figure CH18.2 shows a typical tear in the rivet hole.

The inner surface of the skin near the tip where the rib was missing was found coated with soot. The red paint on the top skin near the leading edge had been abraded and the thickness of the skin had decreased due to erosion.

Testing Procedure and Results

Scanning Electron Fractography

The two tear surfaces shown as A and B in Fig. CH18.2 were examined in a SEM. One of them, A, was found corroded. The corrosion products and the cracks therein are shown in Fig. CH18.3. The other tear surface, B, appeared fresh. Dimples characteristic of ductile overload failure were seen on this surface (Fig. CH18.4). There was no evidence of fatigue failure on these fracture surfaces.

In another tail rotor blade from the same helicopter, a crack was noticed starting from the rivet hole A′ nearest to the leading edge and proceeding outboard to the edge of the tip. This crack was visible to the naked eye. The two rivets nearer to the leading edge had suffered more erosion than the skin.

The tip was sawed off from this blade and the rivets were removed carefully from the rib by drilling. The rib itself was removed in order to examine the inner side of the rivet holes.

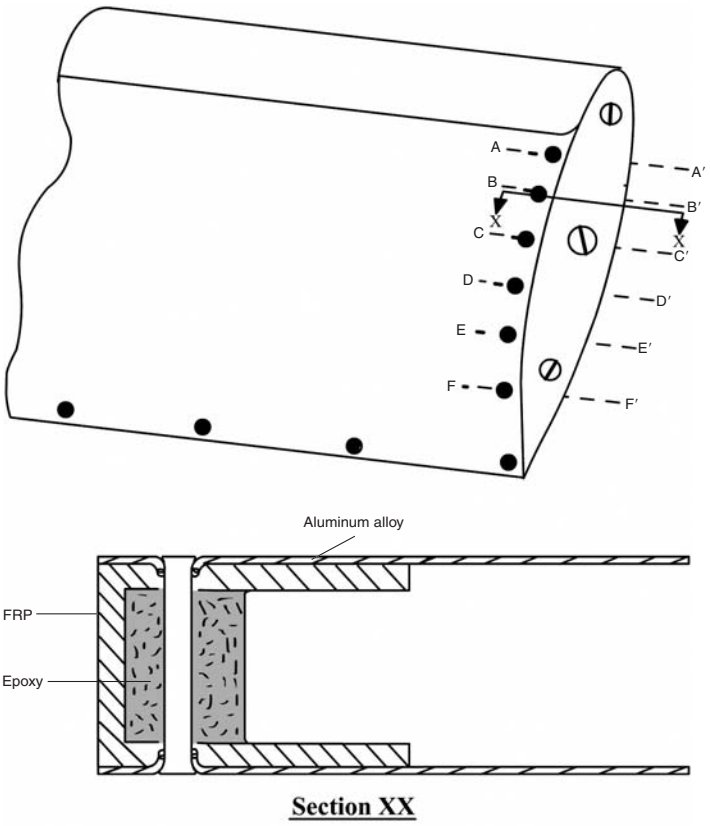

Fig. CH18.1 Sketch showing the fastening of the rib to the blade

The inner surface of the skin and the outer surface of the rib were found coated with soot. The crack emanating from the rivet hole A′, viewed from the inner side of the skin, is shown in Fig. CH18.5. Figure CH18.6 shows a magnified image of this crack. Secondary crack branching from the main crack can also be seen in this figure. In Fig. CH18.5, another small crack also emanating from the rivet hole can be seen.

Chemical Analysis

X-ray chemical analysis indicated that the skin was an aluminum-copper alloy and the rivets were made of an aluminum-magnesium alloy. The rib was made of a composite material and weighed about 55 g.

Microhardness

The microhardness of the skin was 124 HV and that of the rivet was 86 HV.

Discussion

The skin was made of an aluminum-copper alloy heat treated to high-strength condition. The rivet holes had been flared before driving the rivets. During flaring, further work hardening of this region took place. In this condition, the alloy is prone to SCC.

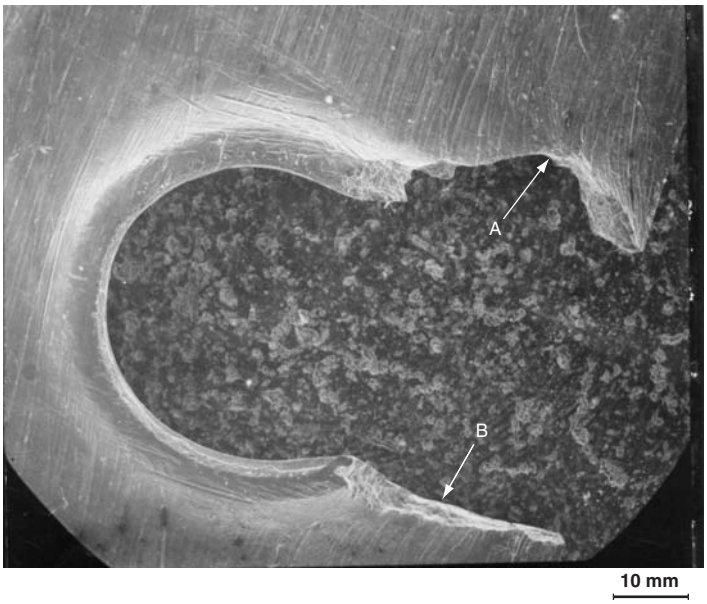

Fig. CH18.2 A typical tear in a rivet hole of a blade

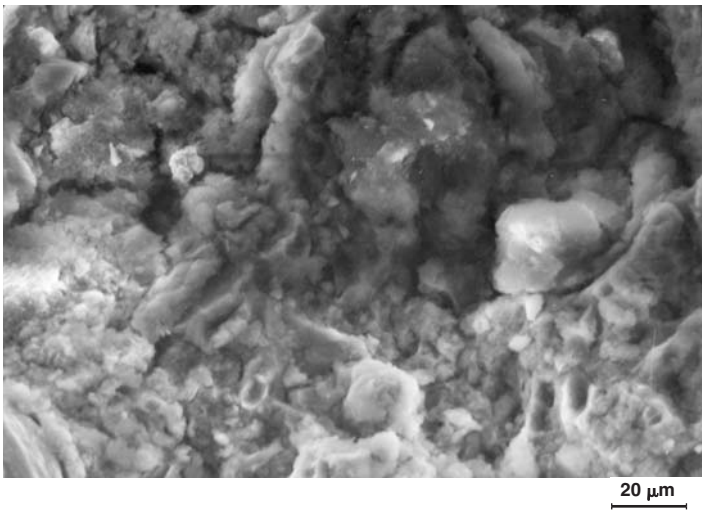

Fig. CH18.3 SEM fractograph showing corrosion products on the fracture surface A shown in Fig. CH18.2

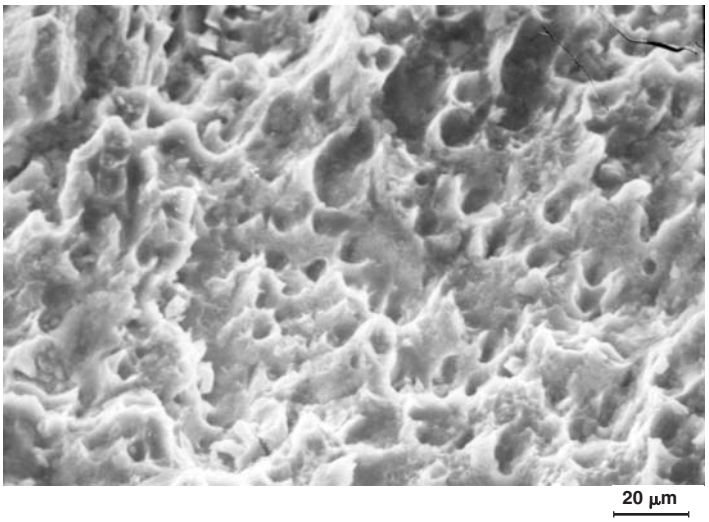

Fig. CH18.4 SEM fractograph showing ductile overload failure on the fracture surface B shown in Fig. CH18.2

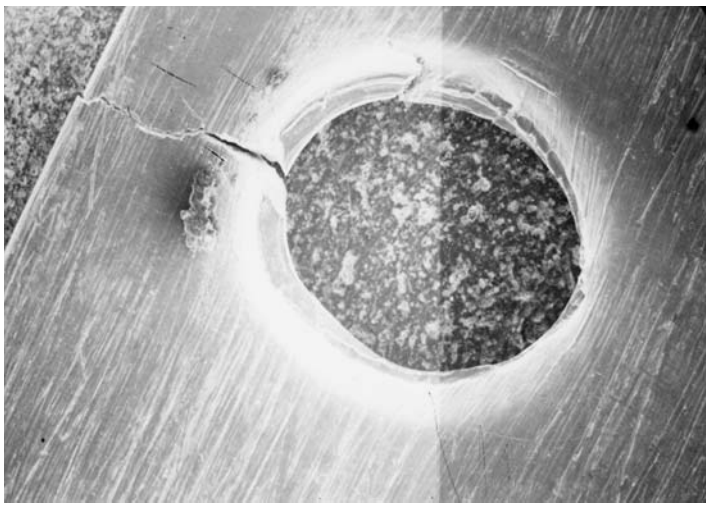

Fig. CH18.5 Cracks emanating from a rivet hole in a blade

The soot on the inner surface of the skin indicates that this region had been subjected to the action of corrosive exhaust gases from the engine.

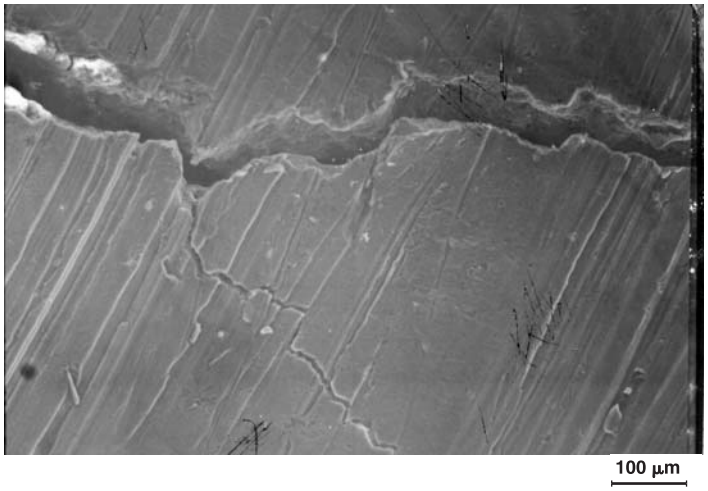

Fig. CH18.6 Magnified image of the larger crack in Fig. CH18.5

Due to erosion, the skin had thinned and the rivet heads had been reduced in size. The erosion on the rivet head was due more to lower hardness.

By a combination of these factors, SCC had set in on the skin near the rivet holes. This is evidenced by the intergranular nature of the crack. There was no evidence of fatigue failure. Due to the centrifugal forces and the already-cracked skin near the rivet holes, the outboard rib with the rivets had been pulled out of the skin.

Conclusions

The separation of the outboard rib was due to SCC in the regions adjacent to the rivets. Erosion could also have contributed. The exhaust gases from the engine provided the necessary corrosive environment.

Recommendation

Frequent inspection of the skin near the rivet holes is essential. Care should be taken to prevent formation of a gap between the skin and the rib. Upon development of a visible crack on the skin, the blade must be withdrawn from service.

Failure Analysis of Engineering Structures: Methodology and Case Histories
V. Ramachandran, A.C. Raghuram, R.V. Krishnan, S.K. Bhaumik, p110-112
DOI:10.1361/faes2005p110

CASE 19

Failure of the Body Structure in a Helicopter at the Mixing Unit Attachment

Summary

In one type of helicopter flying at high altitudes in mountainous regions, a few failures had been reported at the mixing unit attachment lug joint. The mixing unit is held through fasteners to four lugs, two on top and two at the bottom, welded to two horizontal members of a tubular frame. The tubular frame is charged with nitrogen gas. The tube had cracked below the lug, resulting in gas leakage. It was a fatigue fracture due to excessive flexural load.

Background

In one type of helicopter, a few failures were experienced at the lug joint of the mixing unit attachment. The mixing unit assembly is a critical part of the flight control system. It is attached through fasteners to four lugs, two on top and two at the bottom, which are welded to two horizontal members of a tubular frame. The tubular frame is charged with nitrogen at a pressure of 1.8 bars. Any leakage of gas from the tubular frame due to cracks is revealed by a telltale "VIDEOPT" indicator.

Out of ten incidents reported, there were eight cases of such gas leakage, and in the other two, the lug had fractured above the weldment. It was reported that in all these cases, the helicopters were flying at high altitudes in the mountainous regions. In one such incident, there was gas leakage at the welded joint of the bottom lug, on the port side.

Pertinent Specifications

The tubular frame and the lugs were made of a chromium-molybdenum-vanadium steel equivalent to French specification 15CDV6.

Visual Examination of General Physical Features

The tubular structure holding the two bottom lugs cut from the body structure of the helicopter is sketched in Fig. CH19.1. The tube was cut near the region of leakage to expose the interior. The inner surface was cleaned. A crack was observed on the tube wall, directly below the lug. The location of this crack is shown schematically in Fig. CH19.2.

The lug had been welded with a tack weld on one side and a continuous weld on the other side, penetrating the entire tube wall thickness. The crack had occurred in the heat-affected zone (HAZ) in between these two welds. This crack was opened. The features of this fracture surface were indicative of fatigue crack. The crack had originated on the inner surface of the tube and propagated through the wall thickness toward the lug. This indicates that the

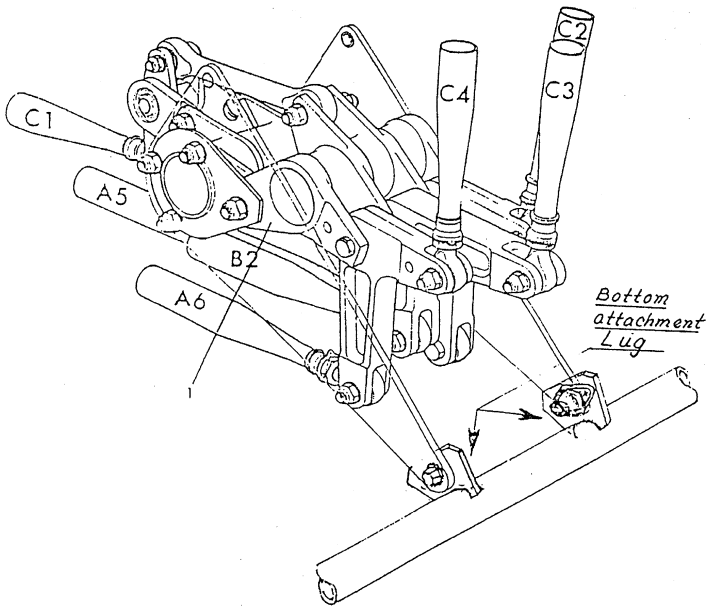

Fig. CH19.1 Tubular structure holding the two bottom lugs

tube had been subjected to upward flexure about the welded region.

Testing Procedure and Results

Scanning Electron Microscopy

The thickness side of this cut piece was polished and examined in a SEM. A number of other cracks parallel to the crack that was opened were observed. These are sketched in Fig. CH19.2 and shown in Fig. CH19.3 and CH19.4. These also confirm the flexure of the tube in this region.

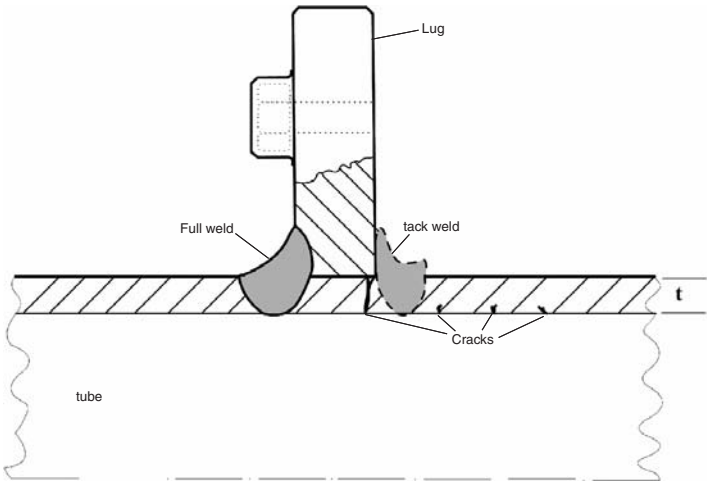

Fig. CH19.2 Sketch showing the location of the cracks on the tube

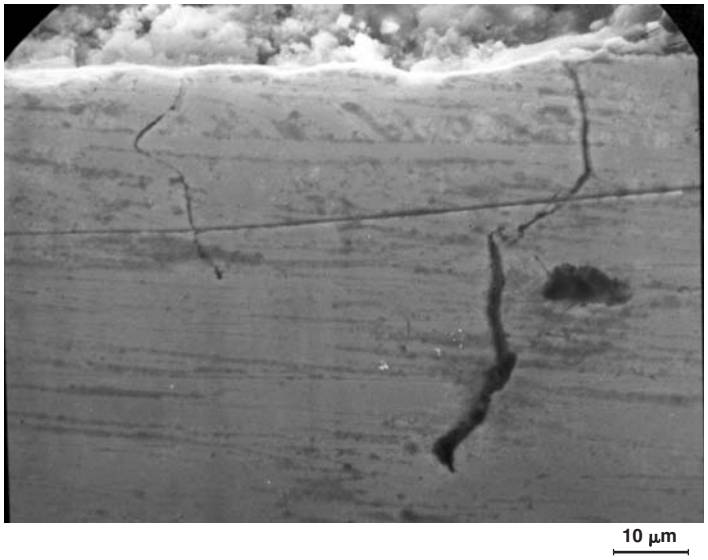

Fig. CH19.4 SEM photograph showing cracks in the tube wall

The leakage of gas from the tube was due to the crack at the port side lug attachment. In order to determine whether a similar situation had prevailed on the starboard side weldment, a cut was made in that region also and the tube wall examined. A crack was observed, emanating from the weld toe (Fig. CH19.5, CH19.6). This again confirms flexure of the tube.

Discussion

Presence of cracks below the lug clearly indicates the tube had been subjected to a two-point load at the two bottom attachment lugs, resulting in the flexure of the tube and subsequent cracking due to fatigue.

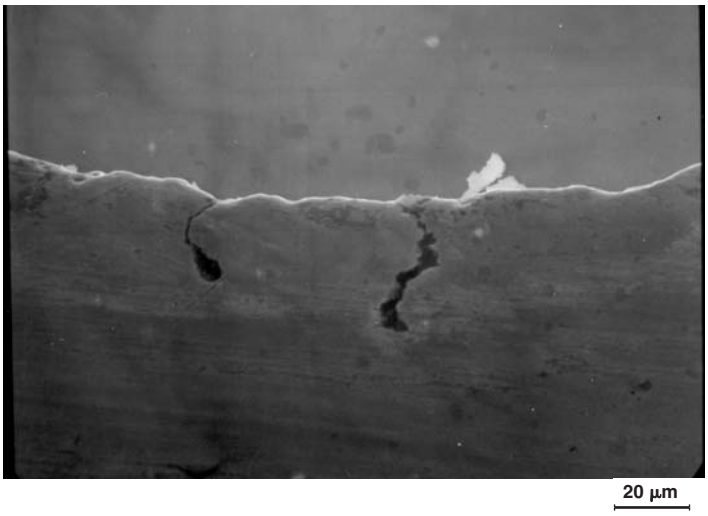

Fig. CH19.3 SEM photograph showing cracks in the tube wall

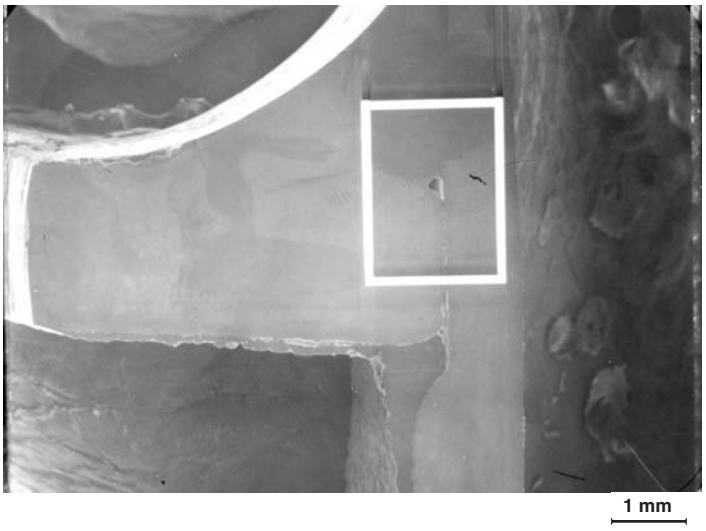

Fig. CH19.5 SEM photograph showing a crack emanating from the weld toe at the starboard lug

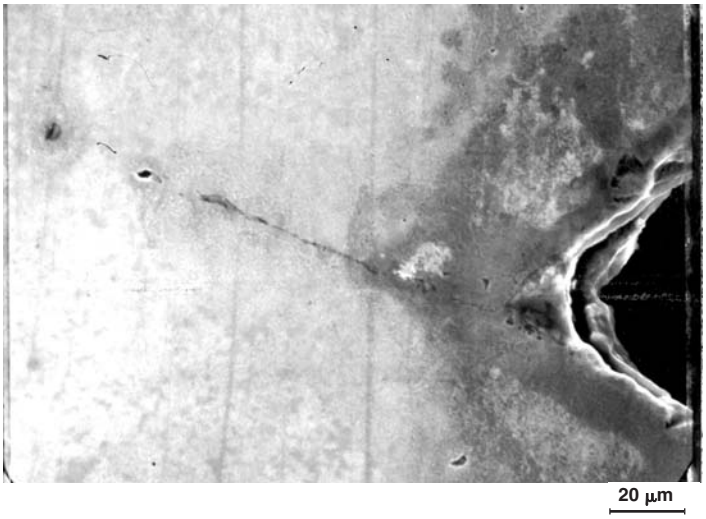

Fig. CH19.6 SEM photograph showing a crack emanating from the weld toe at the starboard lug

Conclusion

The tube cracked below the lug by fatigue due to excessive flexural load. The crack initiated on the inner surface of the tube below the lug and propagated through the tube thickness, causing leakage of gas and pressure drop.

Recommendation

It is necessary to redistribute the loads on the tube to avoid failures. However, before carrying out any modification, it is desirable to know the nature and magnitude of loads at this area under flying conditions. This is best done by instrumenting a helicopter and actually measuring the strains and loads experienced in the region.

Once the data are obtained, suitable modifications to redistribute the loads can be made. The modified designs should be rig tested under simulated loading conditions to select the most optimal design modification.

Failure Analysis of Engineering Structures: Methodology and Case Histories
V. Ramachandran, A.C. Raghuram, R.V. Krishnan, S.K. Bhaumik, p113-114
DOI:10.1361/faes2005p113

CASE 20

Failure of Elevator Hinge Pins in an Aircraft

Summary

In an aircraft that was retrieved from the sea, the hinge pins that join the elevator to a connecting flange were found fractured at the tack welded joint on both the port side and the starboard side. The failure of the pins was due to hydrogen embrittlement.

Background

An aircraft fell into the sea after a flight of 30 minutes. The aircraft was retrieved and the elevator linkage components were dismantled, cleaned, and reassembled with the elevator motor. When the elevator was moved, the hinge pin joining the elevator to a connecting flange was found fractured on the port side at the joint where it was tack welded to the flange. While removing this pin, the starboard side pin also gave way, fracturing at its tack welded joint.

Pertinent Specifications

As per specifications, the connecting flanges were made of EN 1A material, and the connecting pins were made of EN 19 "R" material. Subsequent to machining, these parts are to be cadmium plated. The flange and the hinge pin are connected by a taper pin, and to avoid further play and vibration, the two are welded partially.

Visual Examination of General Physical Features

A schematic diagram of the elevator-hinge pin-connecting flange assembly is shown in Fig. CH20.1. The failed regions close to the welded joints are indicated in the figure.

Testing Procedure and Results

Macroexamination and Scanning Electron Fractography

Through macroexamination, it was found that one of the fractures was fresh without any damage or corrosion and with shiny bright and dull gray areas (Fig. CH20.2). On further examination in the SEM, the dull gray area showed intergranular fracture (Fig. CH20.3). The brighter area showed typical brittle fracture features (Fig. CH20.4).

Chemical Analysis

A spot analysis of the materials used for the hinge pin and the connecting flange was carried out. From Fig. CH20.5 and CH20.6 showing the energy spectra, it is seen that both the components were made of the same steel. Specification requires that the hinge pin be made of EN 19 steel, which contains molybdenum; the hinge pin was not made of EN 19.

It was confirmed that the pins were cadmium plated. From the intergranular nature of the fracture, it is suspected that no "baking"

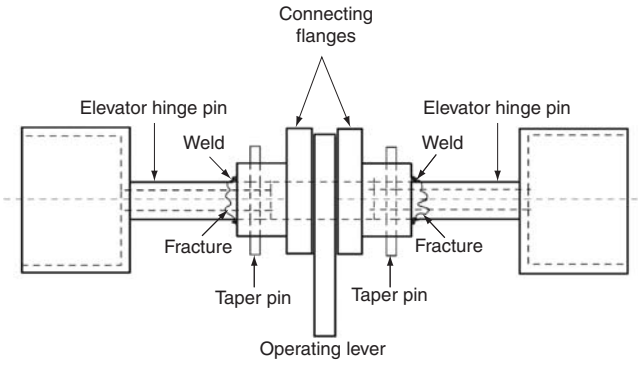

Fig. CH20.1 Schematic diagram of the elevator-hinge pin-connecting flange assembly

treatment was given to the pin after cadmium plating, and the failure occurred due to hydrogen embrittlement.

Further, welding of the hinge pin with the connecting flange is not a desirable engineering practice. This welding could have further aggravated the situation.

Conclusion

The failure of the pin was due to hydrogen embrittlement. The inferior grade of steel used and absence of a baking treatment after cadmium plating contributed to the failure.

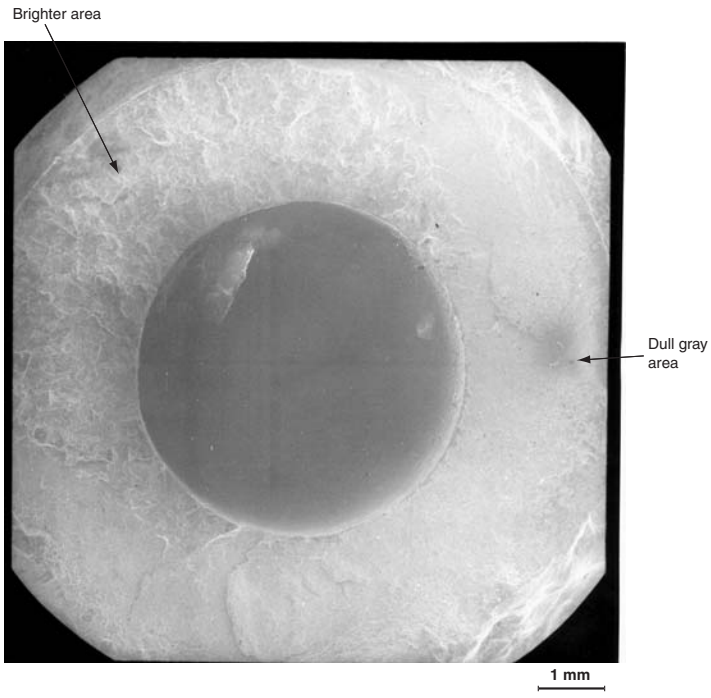

Fig. CH20.2 Fracture surface of the hinge pin

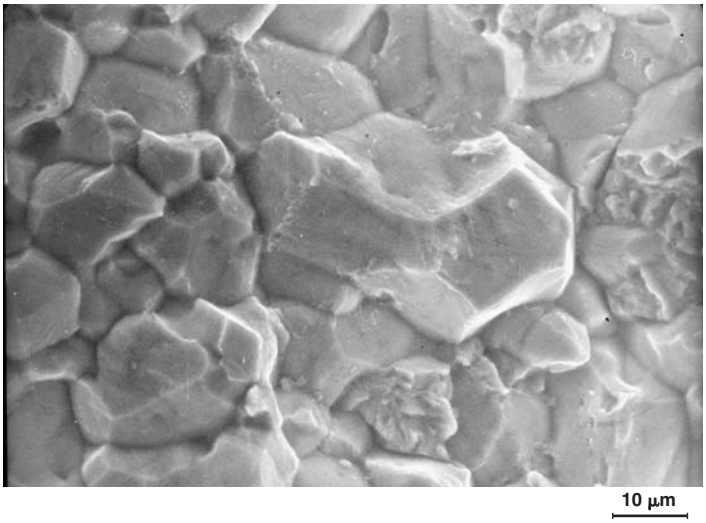

Fig. CH20.3 Intergranular fracture in the dull gray area shown in Fig. CH20.2

Recommendations

- Materials used should conform to the design specifications.
- Baking treatment as per ASTM standards must be carried out immediately after cadmium plating.
- To avoid vibration, instead of welding, alternative arrangements may be considered.

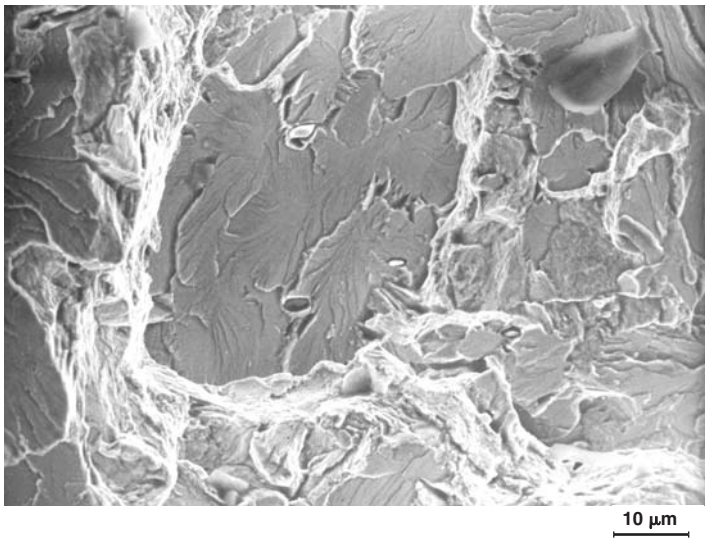

Fig. CH20.4 Brittle fracture features from the brighter area shown in Fig. CH20.2

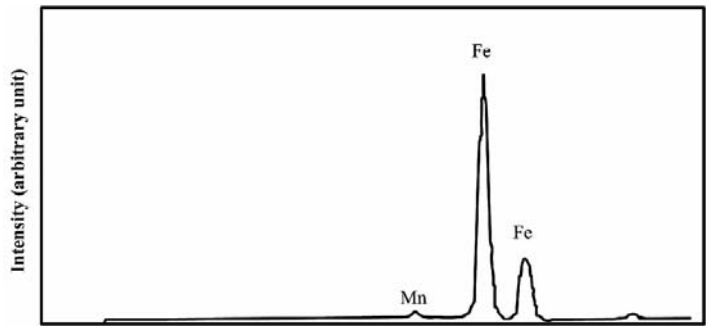

Fig. CH20.5 Energy spectrum and semiquantitative analysis of a failed hinge pin

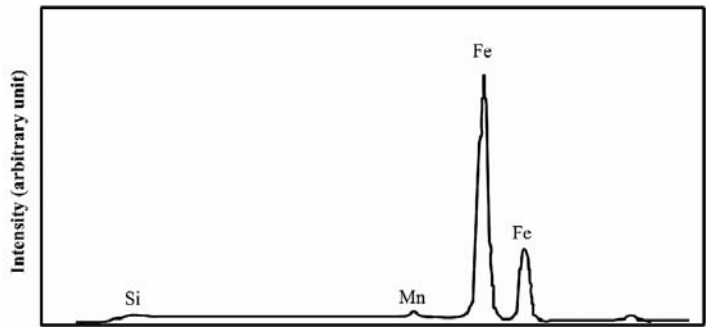

Fig. CH20.6 Energy spectrum and semiquantitative analysis of a connecting flange

Failure Analysis of Engineering Structures: Methodology and Case Histories
V. Ramachandran, A.C. Raghuram, R.V. Krishnan, S.K. Bhaumik, p115-117
DOI:10.1361/faes2005p115

CASE 21

Failure of Aircraft Engine Compressor Rotors

Summary

Two compressor rotors of an aircraft engine sustained severe damage during operation. In both rotors, several blades got sheared off with some blades lifted from the dovetail portion of the drum. Several mounting dovetails on the rotor drum had fractured. The severity of damage progressively decreased toward downstream. Detailed fractographic studies revealed that the damages on both the rotors were due to SCC of the dovetail mountings.

Background

Two compressor rotors of an aircraft engine, identified as "A" and "B," suffered serious damage during operation. Detailed analysis was carried out to find the cause of the damage.

Visual Examination of General Physical Features

Compressor Rotor A

It was observed in compressor rotor A that all the blades in the third and fourth stages had been sheared off, with some blades lifted from the dovetail portion of the drum (Fig. CH21.1). Most of the fracture surfaces except those at the dovetail on the drum were obliterated by rubbing. The first-stage blades were largely intact with minor damages. The second- and fifth-stage blades on either side of the sheared blades had suffered extensive damages in the form of denting and tip bending. From the fifth stage onward, the severity of damage had progressively decreased toward the 10th stage, where it was only minor.

Several mounting dovetails on the rotor drum that had fractured in the third and fourth stages showed two distinct regions: a half-moon-shaped region typical of progressive failure and a region of rapid fracture with clearly delineated chevron markings (Fig. CH21.2). The extent of the half-moon-shaped region varied among the fractured dovetails. The half-moon-shaped regions were considerably corroded and were dark brown in color compared with the light gray color of the rapid fracture region.

Compressor Rotor B

In this rotor, most of the blades on the first four stages had sheared off, with several blades lifted from the dovetail portion on the drum, particularly in the first two stages (Fig. CH21.3). The blades on the rest of the stages had suffered varying degrees of

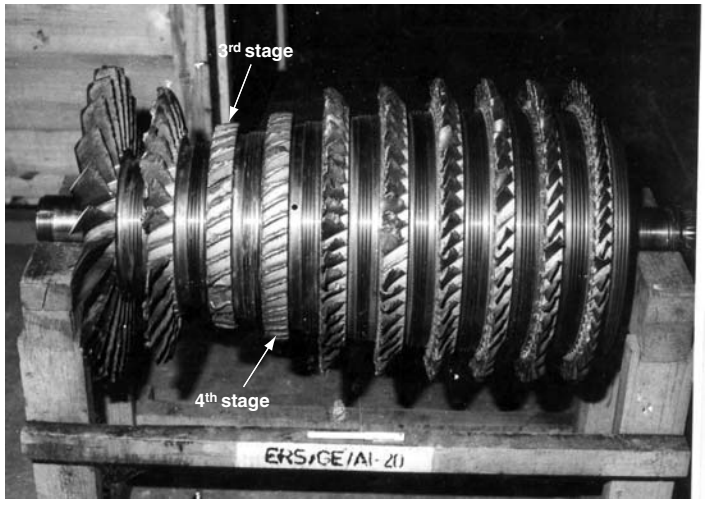

Fig. CH21.1 A view of the compressor rotor A showing the third- and fourth-stage blades sheared at their roots

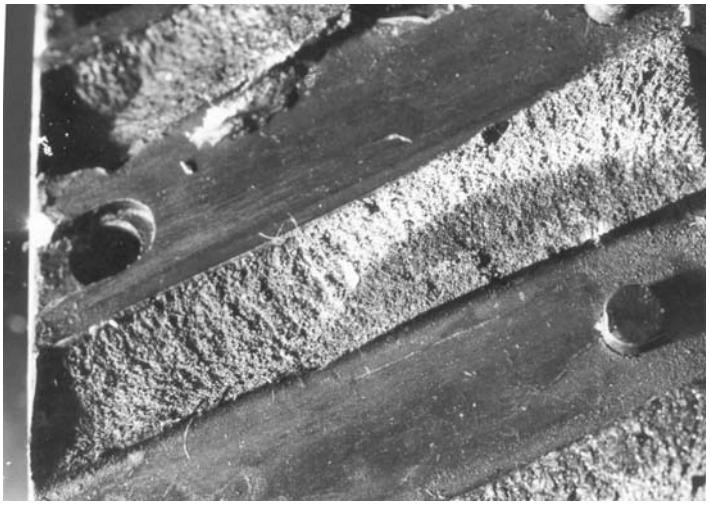

Fig. CH21.2 Close-up view of one of the fractured dovetails in rotor A showing regions of slow crack growth and rapid fracture

damage, the severity of damage decreasing progressively toward the 10th stage. The roots of a few sheared blades were relatively intact, and their fracture surfaces showed features typical of overload. On this rotor also, several mounting dovetails on the drum had fractured, particularly in the first two stages. The fractured dovetails exhibited the same two distinct regions that were observed on the broken dovetails in rotor A.

Testing Procedure and Results

Scanning Electron Fractography

A fractured dovetail containing the two regions was carefully cut from one of the rotors. After ultrasonic cleaning, the fracture surface was observed in a SEM. The discolored half-moon-shaped region showed extensive intergranular fracture (Fig. CH21.4), and the region of fast fracture showed ductile/brittle mode of fracture.

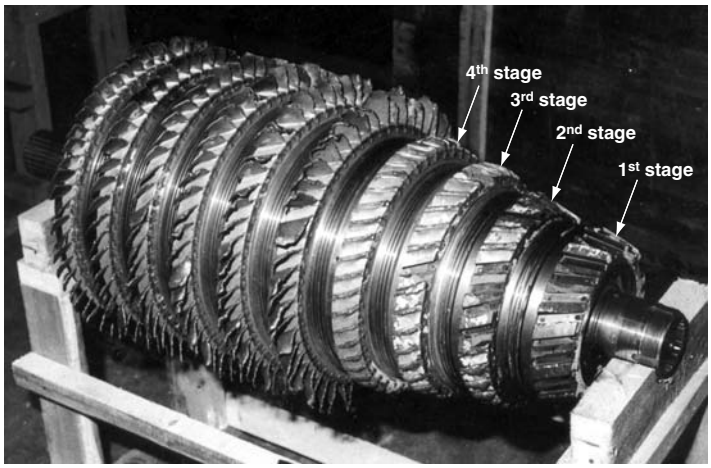

Fig. CH21.3 A view of compressor rotor B showing blades sheared in the first four stages

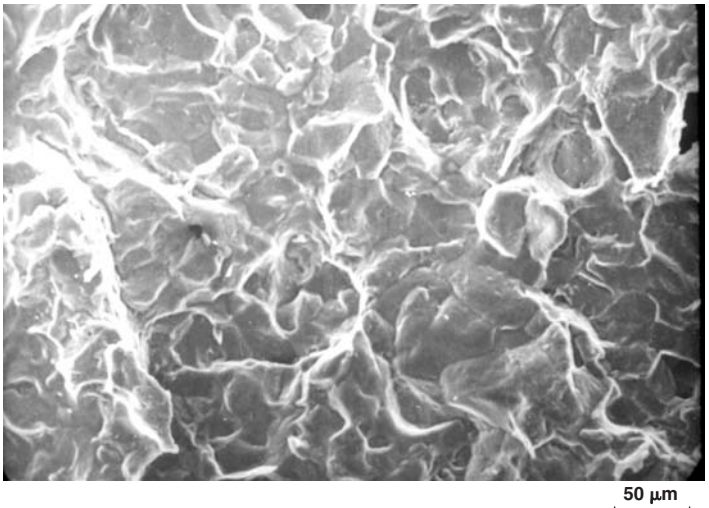

Fig. CH21.4 SEM fractograph showing intergranular fracture in the slow-crack-growth region

Chemical Analysis

Semiquantitative analysis of the blade and the drum showed that they were made of the same material, i.e., high-chromium steel.

Metallography

Metallographic examination was carried out on samples taken from a blade and a dovetail region, after etching with a solution containing 2.5 g ferric chloride, 5 g picric acid, 2 ml hydrochloric acid, and 90 ml ethyl alcohol. Both the blade and the dovetail portion showed tempered martensitic structure, with carbides distributed along the grain boundaries and in the interior of grains (Fig. CH21.5). The dovetail portion showed more carbides along the grain boundaries than the blade material. The dovetail material had a grain size between ASTM 5 and 6, while the blade had a finer grain size of ASTM 8. The dovetail portion showed a network of intergranular cracks (Fig. CH21.6).

Hardness

The blade as well as the dovetail material showed the same hardness of 310 HV.

Discussion

The presence of two distinct regions on the fracture surface of the broken dovetail clearly indicates delayed failure. The discol-

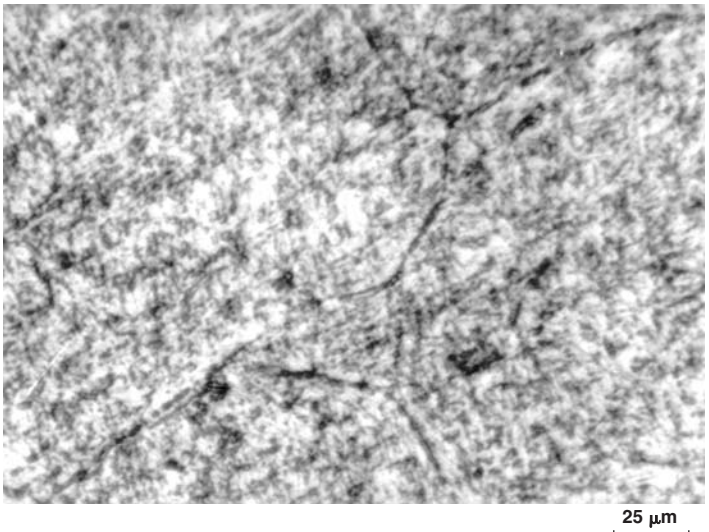

Fig. CH21.5 Microstructure of dovetail material showing tempered martensite with grain boundary carbide

Fig. CH21.6 Intergranular branching cracks in the dovetail region

ored half-moon-shaped regions represent slow, progressive crack growth, while the brighter regions with chevron marks represent rapid fracture. Intergranular fracture features on the half-moon-shaped region, as well as the network of branching intergranular cracks, is typical of SCC.

The way damages occurred on the rotors indicate that SCC had initiated and propagated simultaneously on several dovetail mountings on the drum (in the third and fourth stages on rotor A and in the first and second stages in rotor B). When one of the cracks had grown to critical dimensions, it would have led to fracture. Once the dovetail mounting cracks, it is easy for the blade mounted on its slot to get loose and fly off. Once a blade is detached, it can cause all the subsequent damages at the high speed of rotation.

In rotor A, the maximum secondary damage is seen in the second and fifth stages, which are adjacent to the third and fourth stages in which the blades are completely sheared. In this rotor, it is reasonable to suspect that a dovetail mounting on the second stage would have cracked first, leading to the loosening of a blade and the subsequent damages. In rotor B, it is probable that a dovetail mounting in the first stage would have cracked initially, leading to all other damages.

Because the blade and the dovetail mountings are made of the same material, it is reasonable to expect SCC on both. But it is possible that, while the blades are subjected to stress only during rotation, the dovetail mountings can experience constant sustained stress arising from the mounting even while on ground and hence can become potential sites for SCC. This stress acting simultaneously with the saline atmosphere while the aircraft is on the ground can cause SCC. Also, the damages are maximum in the first few stages on the suction side where the intensity of corrosion is expected to be maximum. It is possible that the finer grain size and less carbides in the grains in the blade material, compared with the dovetail material, can give it better stress-corrosion resistance.

Conclusion

The damages observed on both the rotors can be attributed to SCC of dovetail mountings.

Recommendations

The rotors should be subjected to fresh water compressor wash from time to time, and the engine intakes should be kept covered in coastal areas.

Failure Analysis of Engineering Structures: Methodology and Case Histories
V. Ramachandran, A.C. Raghuram, R.V. Krishnan, S.K. Bhaumik, p118-119
DOI:10.1361/faes2005p118

CASE 22

Failure of a First-Stage Compressor Blade in an Aircraft Engine

Summary

Premature service failure of a first-stage compressor blade of an aircraft engine was analyzed. The blade had failed by fatigue. The fatigue crack had originated from corrosion pits at the root transition region.

Background

One first-stage compressor blade of an aircraft engine that had failed in service was analyzed for determining the cause of its premature failure. The engine had performed a total of 467 hours since new and 130 hours since its last overhaul.

Visual Examination of General Physical Features

Visual examination indicated that the blade had failed at the midpoint of the root transition region on the convex side of the airfoil (Fig. CH22.1).

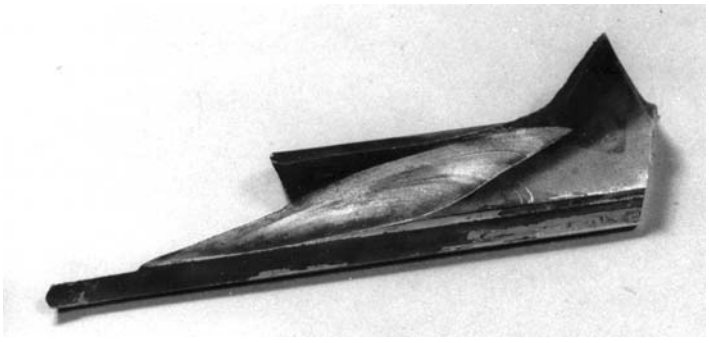

Fig. CH22.1 Failed compressor blade showing beach marks indicative of fatigue

Testing Procedure and Results

Microscopy and Scanning Electron Fractography

Stereobinocular microscopy revealed well-defined beach marks originating from the midpoint of the root transition region and propagating inward to a depth of about 80% of the blade cross section before final fracture. At the origin, deep corrosion pits were seen on the root flank. Several other pit marks were found close to the origin.

Under the SEM, striations typical of fatigue were seen on the fracture surface (Fig. CH22.2). At the origin and the surrounding area, deep corrosion pits were seen.

Fig. CH22.2 Striations typical of fatigue seen on the fracture surface

Discussion

Microscopic examination confirms that the blade failed due to fatigue, the crack originating from corrosion pits at the transition region of the root on the convex side of the airfoil and propagating inward. The pit acting as a stress concentrator would have given rise to the initiation of a crack.

Conclusion

The blade failed by fatigue, the fatigue crack initiating at surface corrosion pits at the root transition region on the convex side of the airfoil section.

Recommendation

Because the pits are confined only to the dovetail region, further investigations have to be carried out to find the cause of pitting.

Failure Analysis of Engineering Structures: Methodology and Case Histories
V. Ramachandran, A.C. Raghuram, R.V. Krishnan, S.K. Bhaumik, p120-121
DOI:10.1361/faes2005p120

CASE 23

Failure of Main Undercarriage Struts in an Aircraft

Summary

In an aircraft that met with an accident, it was found that the undercarriage struts of port side as well as starboard side had failed. The starboard oleo strut had failed by fatigue, the crack initiating at the outer periphery and propagating inward. The port side strut had failed by overload and its fracture was secondary.

Background

In an aircraft accident, it was found that the undercarriage oleo struts had fractured on both port and starboard sides. Investigation was carried out to find the nature of failures in the two struts.

Visual Examination of General Physical Features

Figure CH23.1 shows the fractured starboard strut. The fracture occurred at about 13 cm from the top end close to the underside of the wing surface. It was seen that there was a change in wall thickness at this location.

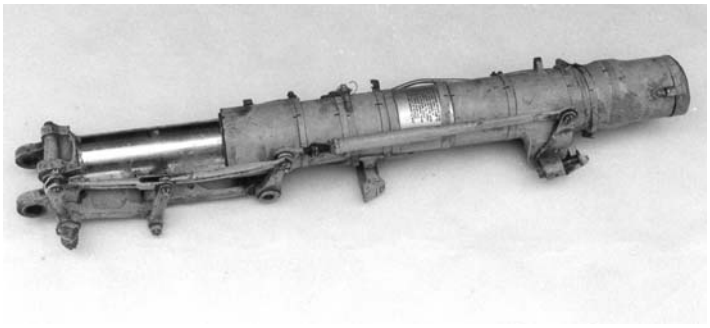

Fig. CH23.1 The fractured starboard strut

Testing Procedure and Results

Macroscopy and Scanning Electron Fractography

The fracture surfaces on the two struts were cleaned and examined visually as well as under microscopes. Figure CH23.2 shows the fracture surface of the starboard strut. On this fracture surface, there was a small flat region, marked "A," covering a length of about 25 mm along the circumference of the strut and a slant fracture region covering the remaining portion of the circumference. Region A showed evidence of delayed failure. The crack had initiated at the outer periphery of the strut in the region of transition and propagated inward before giving rise to the overload fracture.

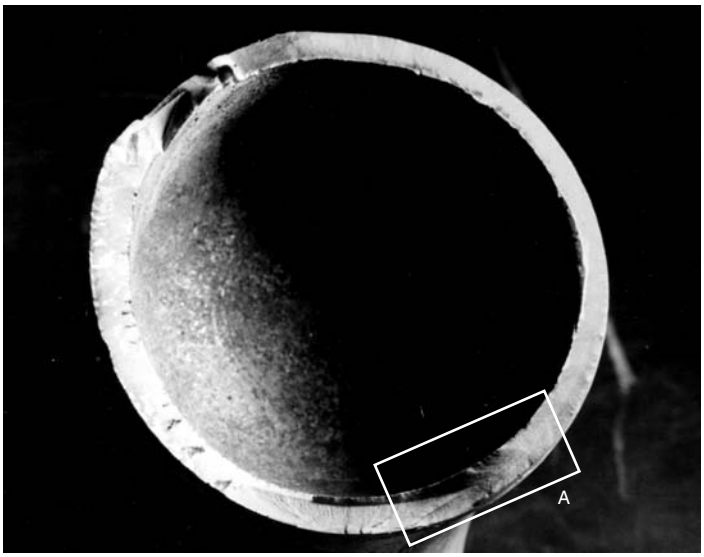

Fig. CH23.2 Fracture surface of the failed starboard strut

Figure CH23.3 shows three distinct zones in region A: (a), a half-moon-shaped region with beach marks typical of slow crack growth extending inward to a depth of 2 mm from the periphery; (b), a region of chevron marks emanating from the outer periphery of the half-moon-shaped zone representing fast crack propagation; and (c), a shear lip zone coinciding with the final rupture of the strut.

A portion of the strut containing the region A was cut, ultrasonically cleaned, and examined in a SEM. Striations typical of fatigue were seen in zone (a) (Fig. CH23.4). The other two zones, (b) and (c), showed dimpled rupture typical of tensile overload. The striations in zone (a) indicated crack propagation by low-cycle fatigue.

The fracture surface of the port side strut was of the slant type with features typical of shear overload (Fig. CH23.5). There were no regions of delayed failure.

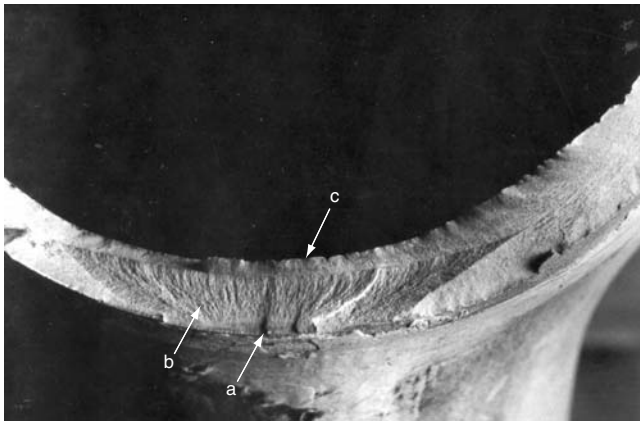

Fig. CH23.3 Close-up view of region A of Fig. CH23.2 showing three distinct zones: (a) half-moon-shaped region, (b) chevron marks, and (c) shear lip

Discussion

Visual and macroscopic observations did not reveal any mechanical damage at the point of crack initiation in the starboard strut. No material flaws were seen under the microscope in the region of crack initiation. This indicates that the fatigue crack initiation was due mainly to stress factors. It may be noted that the location of the origin of fatigue is almost in line with the axis about which the oleo is swiveled.

Conclusions

The starboard oleo strut failed by a fatigue crack originating on the outer periphery of the oleo near the top end and propagating inward to a depth of 2 mm before giving rise to a single overload failure. The port side strut failed by overload and the fracture is of a secondary nature.

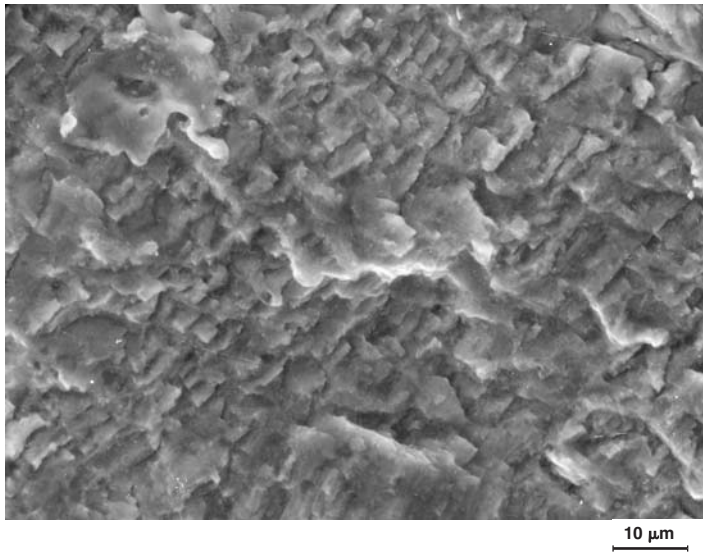

Fig. CH23.4 SEM fractograph showing striations typical of fatigue region (a) of Fig. CH23.3

Fig. CH23.5 Fracture surface of the port side strut

Failure Analysis of Engineering Structures: Methodology and Case Histories
V. Ramachandran, A.C. Raghuram, R.V. Krishnan, S.K. Bhaumik, p122-123
DOI:10.1361/faes2005p122

CASE 24

Failure of a Quill Shaft

Summary

In an aircraft that had a flameout, the quill shaft in the engine fractured. It was found that the shaft failed by torsional overload.

Background

An aircraft had a flame out. Following this incident, it was found that the quill shaft in the engine had broken.

Visual Examination of General Physical Features

The broken quill shaft is shown in Fig. CH24.1. It had fractured at about 50 mm from the spline at the HPT rotor end (driver end), and this portion of the shaft was straight and had no other damage. The remaining portion of the failed shaft toward the accessory gear box end (driven end) was found bent at two locations in the form of "S" (Fig. CH24.1). The sleeve covering the shaft was also damaged and jammed and it had to be cut open to remove the shaft.

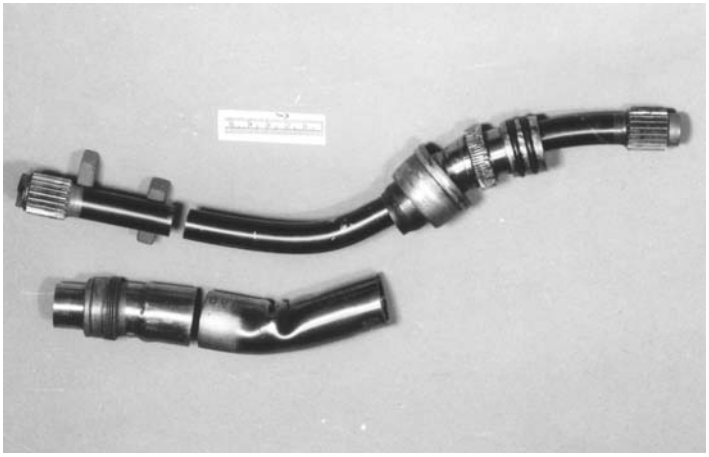

Fig. CH24.1 Broken quill shaft and damaged sleeve

Testing Procedure and Results

Macroscopy and Scanning Electron Fractography

A close-up view of the fracture surface of the shaft is shown in Fig. CH24.2. The fracture was typical of torsional overload type. The surface was flat and shiny with deformation marks. The periphery of the fracture surface (region A) had suffered considerable rubbing. The final fracture (region B) was close to the center of the shaft cross section.

In region A, elongated dimples were seen under the SEM (Fig. CH24.3). Equiaxed dimples were seen in region B, the region of final fracture (Fig. CH24.4).

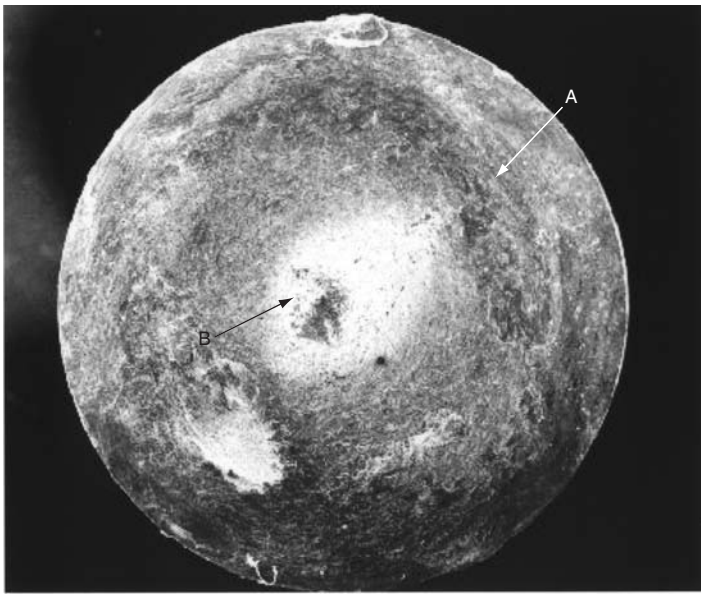

Fig. CH24.2 Fracture surface of the shaft

Chemical Analysis

Energy-dispersive x-ray analysis (EDAX) in the SEM showed that the shaft was made of steel with 3.5% Ni, 1.5% Cr, and 0.8% Mo.

Discussion

Fracture surface examination indicated that torsional overload caused the failure of the shaft. Elongated dimples in region A are to be expected because this region has undergone a considerable amount of shear deformation. Equiaxed dimples in region B are typical of final fracture. Also, rubbing on the periphery of the fracture surface indicates that there was relative rotary motion between the two surfaces after fracture.

The fact that the top end of the failed shaft suffered no bending and the fracture surfaces rubbed suggests the possibility that the torsional fracture preceded the bending of the shaft.

Conclusion

The quill shaft failed by torsional overload.

Recommendation

The source of the torsional load has to be explored.

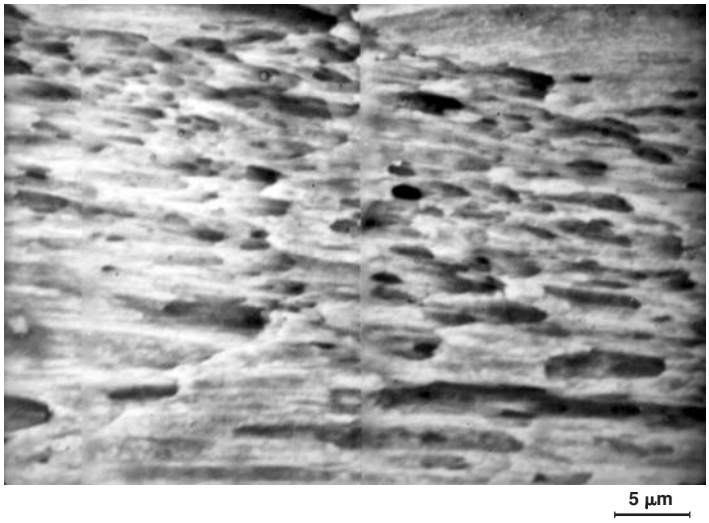

Fig. CH24.3 SEM fractograph showing elongated dimples in region A of Fig. CH24.2

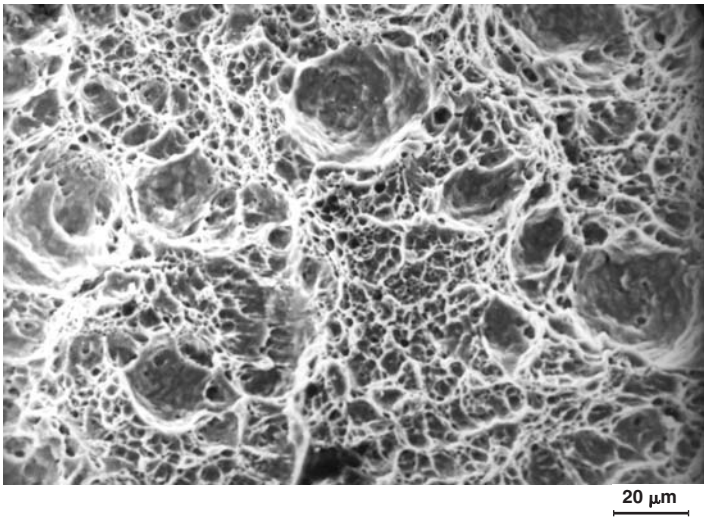

Fig. CH24.4 SEM fractograph showing equiaxed dimples in the final fracture region B of Fig. CH24.2

Failure Analysis of Engineering Structures: Methodology and Case Histories
V. Ramachandran, A.C. Raghuram, R.V. Krishnan, S.K. Bhaumik, p124-125
DOI:10.1361/faes2005p124

CASE 25

Failure of a Cardon Shaft

Summary

A cardon shaft in an aircraft engine failed in service. Investigations revealed that the shaft failed due to torsional overload.

Background

A failed cardon shaft from an aircraft engine was investigated to find the cause of its failure.

Visual Examination of General Physical Features

The failed shaft in the as-received condition is shown in Fig. CH25.1. The shaft fractured transversely at the location indicated by the arrow. The fracture surface was smooth, having undergone considerable rubbing subsequent to fracture.

Testing Procedure and Results

In spite of rubbing, certain macroscopic and microscopic features were discernible on the fracture surface when observed in a SEM. Figure CH25.2 is a SEM fractograph of the gross features on one of the fracture surfaces. The surface was flat with deformation marks with no shear lips. The region of final fracture was at the center point of the shaft cross section.

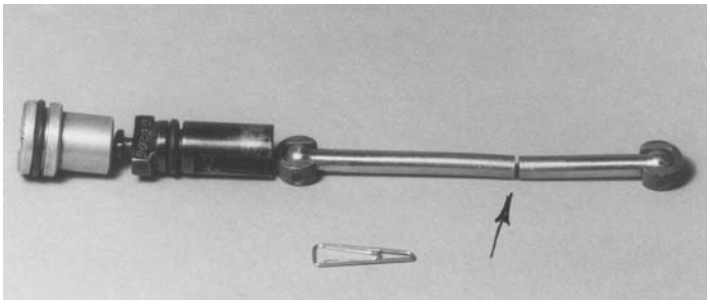

Fig. CH25.1 Failed shaft showing the location of fracture

In the SEM, elongated dimples, typical of shear overloads, with rub marks were seen on the periphery of the fracture surface (Fig. CH25.3). At the center, corresponding to the region of final fracture, equiaxed dimples were seen (Fig. CH25.4).

Chemical Analysis

EDAX analysis in the SEM indicated that the shaft was made of 12% Cr, 1.5% Ni steel.

Hardness

The hardness of the shaft was found to be 336 HV (34 HRC).

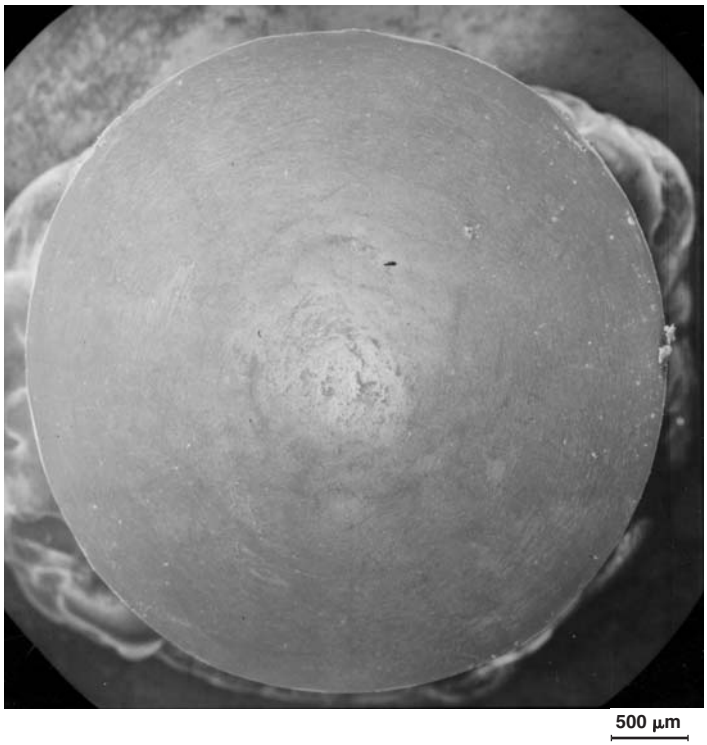

Fig. CH25.2 SEM fractograph showing features typical of torsional overload

Microstructure

The microstructure of the shaft material was tempered martensite.

Discussion

The fractographic features of the shaft are clear indications of torsional failure. The universal links at the ball ends showed wear marks as evidence of torsional loading in one direction.

Conclusion

From the damage features observed, it is concluded that the cardon shaft failed under torsional overload.

Recommendation

Because torsional overloading has been conclusively established, it is necessary to identify the reason for the overloading. It is necessary to examine the driven end of this shaft in detail.

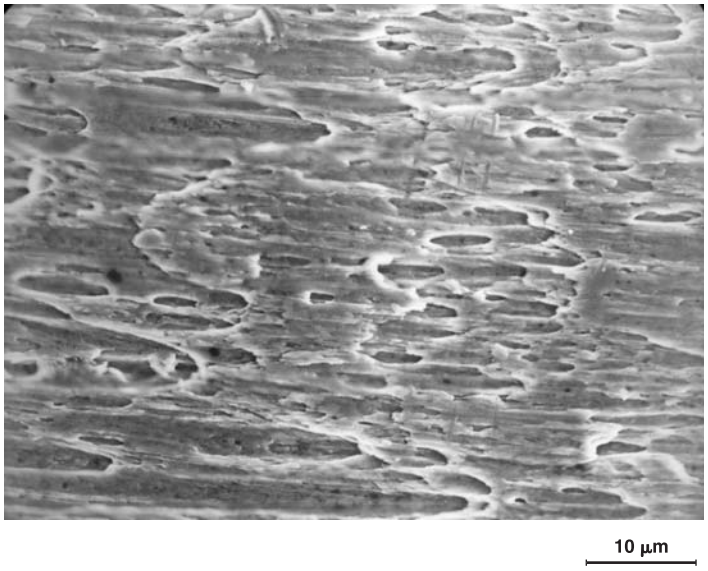

Fig. CH25.3 Elongated dimples with rub marks seen at the periphery of the fracture surface

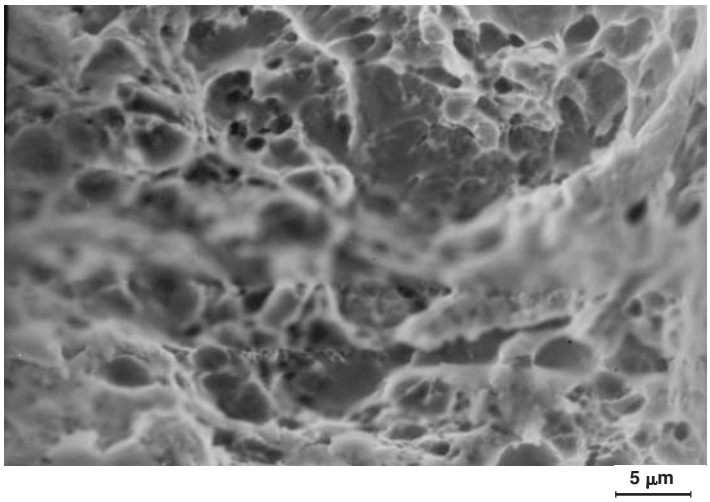

Fig. CH25.4 Equiaxed dimples seen at the center of the shaft corresponding with the region of final fracture

Failure Analysis of Engineering Structures: Methodology and Case Histories
V. Ramachandran, A.C. Raghuram, R.V. Krishnan, S.K. Bhaumik, p126-127
DOI:10.1361/faes2005p126

CASE 26

Failure of a Fuel Nozzle in an Aircraft Engine

Summary

A four-engine aircraft made a test flight after a number of rectifications and ground runs. After becoming airborne, a fire warning came on for one of the engines. Even after a three-engine landing, the fire warning continued. On strip examination of the engine, the hoses and rubber gaskets were found to be burnt. One of the bottom mounting bolts of the burner flange had melted and separated from the stem. The problem was traced to the burner being fitted the wrong way—facing the compressor end instead of the turbine end.

Background

An aircraft with four engines made a check flight after a number of rectifications and ground runs. Twelve minutes after being airborne, fire warning of the first engine came on. When onboard fire fighting exercises failed, a precautionary landing was made with three engines. The fire warning continued until the aircraft was switched off.

Visual Examination of General Physical Features

Strip examination of the engine revealed, among other things, burning of hoses and rubber gaskets. During the false start of the engine after rectifications, fuel was found leaking extensively from the base of the main fuel burner. When the burner was removed, it was found that it was fitted facing the compressor end, instead of the turbine end. One of the bottom mounting bolts of this burner flange had melted and separated from the stem. The sealing gasket was found burnt, and hard carbon deposit was found on the burner stem behind the nozzle along the nozzle body toward the flange end.

Figure CH26.1 shows the damaged nozzle. It had been exposed to flames resulting in burning and deposition of soot at the flange end and the atomizer end. At the atomizer end, the nozzle was found melted at the elbow bend and showed large blow holes formed during subsequent solidification of the molten metal. One of the fastening holes at the flange had burned and melted and was found elongated.

Testing Procedure and Results

Metallography and Hardness

To determine the extent of overheating/burning, microstructural studies and hardness measurements were made along the nozzle body from the stem end to the flange end. Figure CH26.2 shows a sketch of the nozzle body delineating zones of different microstructures and hardness. Analysis of the nozzle material in SEM indicated that it was made of chromium steel. The other atomizing parts found inside the nozzle had not suffered any damage due to heat. The Widmanstätten/basket weave microstructure seen near the flange and the stem is indicative of overheating above the transformation temperature (950 °C, or 1740 °F) followed by relatively fast cooling. This is also corroborated by the variation in hardness on the stem. The overheating was confined mostly to the two ends and had not affected the entire stem of the nozzle. This suggests that the stem had not been exposed to high temperature to the same extent as the ends. Thus, it can be concluded that the exposure to high temperature is very short; a "guess estimate" may be of the order of minutes.

Fig. CH26.1 Damaged fuel nozzle

Discussion

The damages observed on the nozzle were due to wrong mounting. By that, the primary and secondary manifolds also get interchanged. When the nozzle is mounted with the atomizer toward the compressor side, the fuel spray will be turned back to envelope this end over the stem. There is no way of igniting the fuel at this point. When the heat radiated from the turbine heats the diffuser parts to match the flash point of the fuel, it can become ignited, stabilizing a flame around the stem causing it to burn. This flame might be responsible for the overheating/melting of some areas on the nozzle.

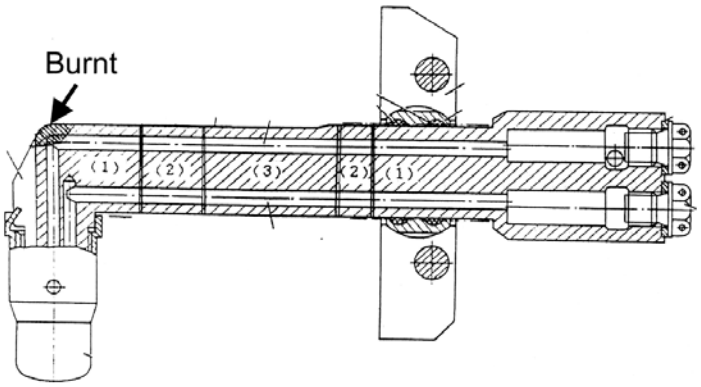

Fig. CH26.2 Sketch of the nozzle assembly showing zone 1, Widmanstätten/basket weave microstructure (hardness, 320 HV); zone 2, spheroidized microstructure (hardness, 410 HV); and zone 3, martensitic microstructure (hardness, 520 HV)

Conclusion

The variation in the microstructure on the stem of the nozzle indicated that the nozzle had been subjected to very high temperature close to the melting point of the nozzle material for a short duration. This was due to the reverse mounting of the nozzle in the combustor.

Recommendation

The end manifolds should be designed in such a way that the fuel nozzle can be fitted facing the turbine only.

Failure Analysis of Engineering Structures: Methodology and Case Histories
V. Ramachandran, A.C. Raghuram, R.V. Krishnan, S.K. Bhaumik, p128-129
DOI:10.1361/faes2005p128

CASE 27

Failure of a First-Stage Compressor Blade in an Aircraft Engine

Summary

The first-stage compressor blade of an aircraft engine failed. Investigations revealed that the failure was due to fatigue, the fatigue crack originating from corrosion pits at the root transition region on the convex side of the airfoil.

Background

A blade on the first stage of the compressor of an aircraft engine failed.

Pertinent Specifications

The blade was forged out of U961W material and heat treated as per schedule. It was Ni-Cd plated on the airfoil, silver plated on the dovetail area, and chromium plated on the bottom of the blade dovetail.

Visual Examination of General Physical Features

Figure CH27.1 shows the failed blade. It had failed at the root in the region of transition from the dovetail to the blade airfoil.

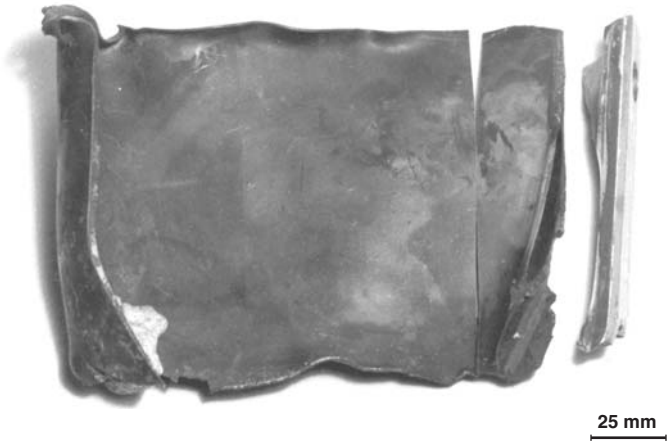

Fig. CH27.1 Failed first-stage compressor blade

The fracture surface showed two distinct regions: a smooth region extending inward from the surface to a depth of 50% of the cross section and a rough region extending over the remaining cross section at the root (Fig. CH27.2).

Testing Procedure and Results

Macroscopy

Under the stereobinocular microscope, a series of half-moon-shaped beach marks were seen in the smooth region (Fig. CH27.3). These marks are typical of fatigue crack propagation. The innermost mark was found to surround the midpoint of the root transition region on the convex side of the blade airfoil, indicating this to be the point of crack initiation. The width of the fatigue crack was 75 mm. The remaining cross section of the blade at the root was rough, typical of single overload fracture. At the point of crack initiation, presence of a corrosion pit was revealed (Fig. CH27.4). Pitting was also seen in the surrounding region including the root flank and the root landing where the blade fits into the dovetail.

Chemical Analysis

EDAX analysis in SEM showed that the blade was made of 12% Cr, 1.2% Ni steel.

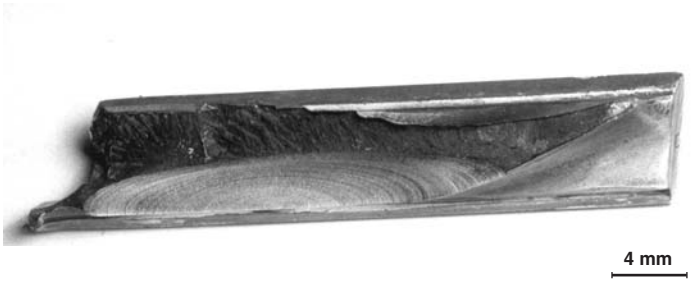

Fig. CH27.2 Fracture surface of the blade showing two distinct regions

Scanning Electron Fractography

In the SEM, poorly defined markings resembling fatigue striations were seen in the half-moon-shaped regions of the fracture surface. Corrosion pits were also seen at the point of crack origin and its surroundings. No foreign object damage or material flaw was seen.

Discussion

The presence of well-defined beach marks and their extent on the fracture surface indicates that the blade failed by a fatigue crack initiating at the root transition region on the convex side of the airfoil and propagating inward to a depth of 50% of the blade root cross section before giving rise to a single overload failure. The crack initiation can be traced to the corrosion pits. No tool mark or foreign object damage or flaw in the material is responsible for the initiation of the fatigue crack.

Conclusion

The compressor blade failed by a fatigue crack initiating from corrosion pits at the root transition region on the convex side of the airfoil and propagating to a depth of 50% of the blade cross section, before the final overload fracture. No foreign object damage or material flaw was responsible for the initiation of the fatigue crack.

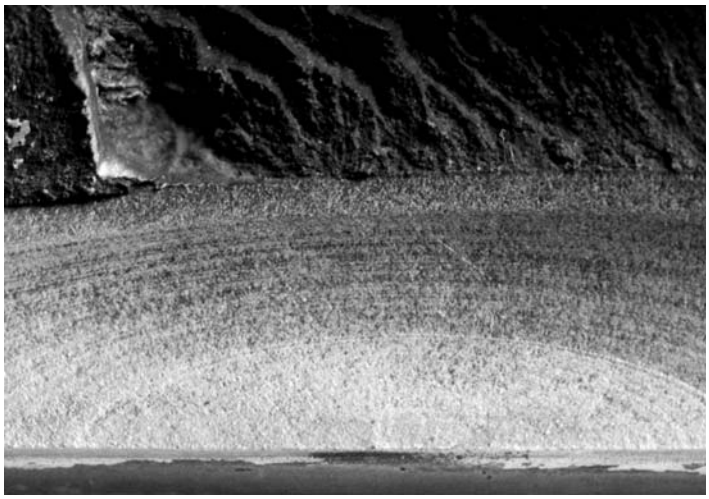

Fig. CH27.3 Beach marks in the smooth region, typical of fatigue

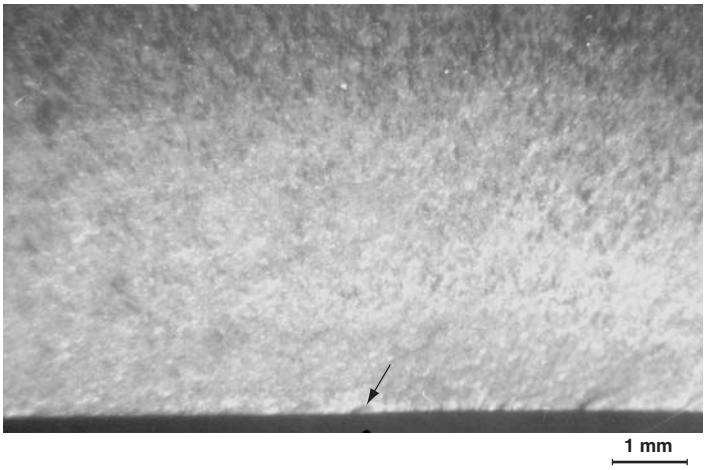

Fig. CH27.4 Corrosion pit seen at the region of fracture origin

Failure Analysis of Engineering Structures: Methodology and Case Histories
V. Ramachandran, A.C. Raghuram, R.V. Krishnan, S.K. Bhaumik, p130-132
DOI:10.1361/faes2005p130

CASE 28

Failure of Shutter Bolts in a Reaction Control Valve in an Aircraft

Summary

Following an aircraft accident, it was found that the shutter bolts on the reaction control valve had failed. During an inspection campaign, one bolt each on five shutters belonging to different aircraft were also found failed. Also, a new bolt had failed during fitment. Investigations revealed that the five bolts had failed by SCC and the new bolt by torsional overload due to excessive torque tightening.

Background

An aircraft crashed following loss of yaw control while in full airborne flight, due to failure of shutter bolts on the rear pitch reaction control valve. Following this accident, shutter bolts on all reaction control valves of similar aircraft were inspected. During inspection, one bolt each on five shutters belonging to different aircraft were found to be fractured. Further, one new bolt also failed during fitment. These six failed bolts were analyzed to determine the mode and cause of failure.

It was reported that these bolts were located in hot zones operating over a temperature range between 250 and 300 °C (480 and 570 °F).

Visual Examination of General Physical Features

Figure CH28.1 shows the failed bolts. The new bolt that failed during fitment is marked No. 6. Bolts 1 to 5 showed similar features. The fractures were of the brittle type. The fracture origin was generally at the thread root. In all the bolts, the fracture surfaces were found to be oxidized to varying degrees. They had also suffered considerable rubbing.

Fig. CH28.1 Failed bolts in the as-received condition, marked 1 to 6

Testing Procedure and Results

Macroscopy and Scanning Electron Fractography

All the bolts were ultrasonically cleaned and observed under the stereobinocular and SEM. Under the SEM, only a mud-crack pattern was seen on the fracture surface of the heavily oxidized bolts (e.g., bolt No. 2, Fig. CH28.2). The other bolts, 1, 4, and 5, showed a clear pattern of intergranular cracking, with a rock candy appearance. Figure CH28.3 is a typical SEM fractograph.

Bolt No. 6 showed clear indication of single torsional overload failure. Twisting deformation marks at the periphery, with the final region of fracture close to the center of the bolt, is typical of torsional overload failure (Fig. CH28.4a). Scanning electron micros-

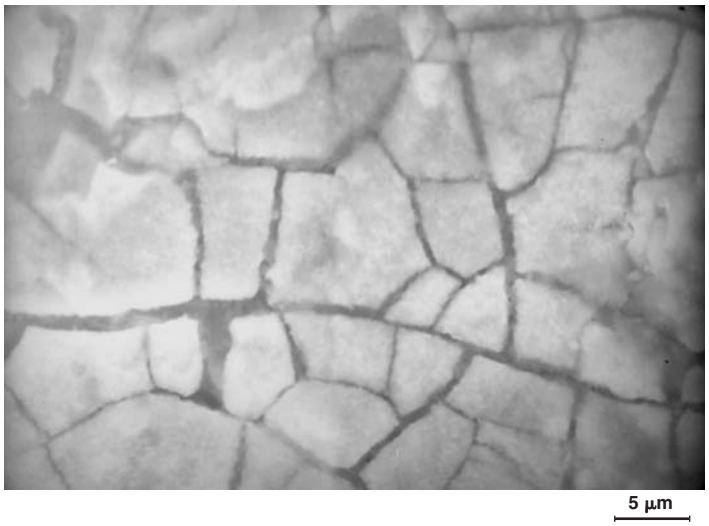

Fig. CH28.2 Fracture surface of bolt No. 2 showing mud cracks

copy showed elongated dimples typical of shear loads (Fig. CH28.4b).

Metallography

Metallographic examination was carried out on a longitudinal section cut from bolt No. 2, etched with alcoholic ferric chloride. Close to the fracture surface, branching cracks were observed (Fig. CH28.5). These cracks are typical of SCC. The microstructure was tempered martensite, with partial spheroidization (Fig. CH28.6).

Chemical Analysis

Semiquantitative analysis of one of the bolts by EDAX in a SEM showed the presence of 14% Cr, 5% Ni, and 1.76% Cu, apart from Fe, indicating that the steel can be classified into one of the precipitation hardenable grades.

Discussion

The network of intergranular cracks seen under the SEM and the branching cracks seen under the optical microscope clearly indicate SCC. Martensitic and precipitation hardening steels as a class are susceptible to SCC under a wide range of environmental conditions, and cracking is known to occur even under mild conditions. The fact that cracks were seen during inspection on five shutter bolts belonging to different aircraft indicates that these cracks were present and have propagated over a period that is characteristic of stress corrosion. Deposits found on the fracture surfaces of bolts 1 to 5 indicate that these have been subjected to corrosive attack.

Fig. CH28.3 Intergranular cracks seen on the fracture surface of bolt No. 4

Failure in bolt No. 6 is clearly of the torsional overload type and can be attributed to excessive torque tightening during fitting.

Conclusion

Bolts 1 to 5 failed by SCC, and the new bolt by torsional overload.

(a)

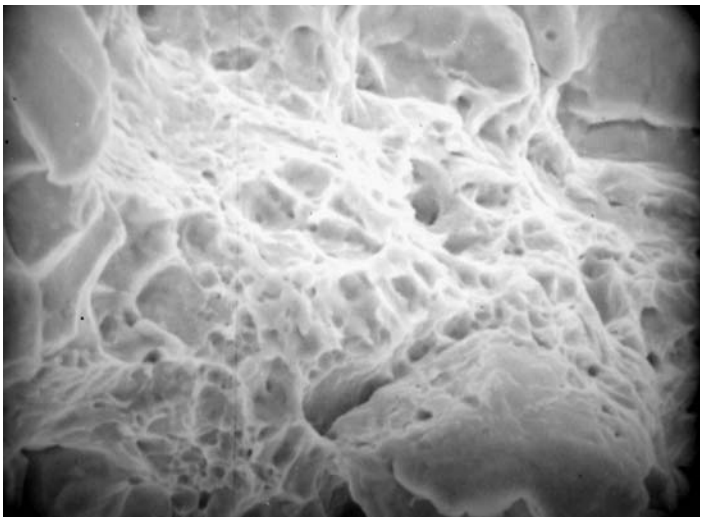

(b)

Fig. CH28.4 (a) Fracture surface of bolt No. 6, showing deformation marks and central region of fracture indicative of torsional loads. (b) Shear dimples on the fracture surface of bolt No. 6

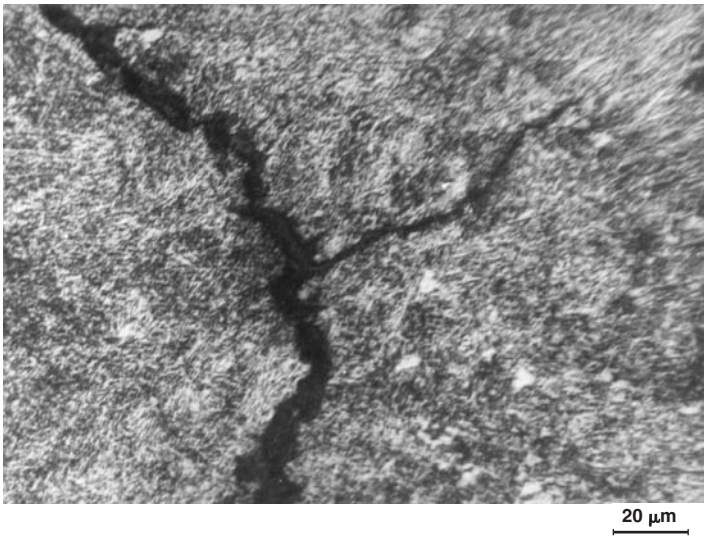

Fig. CH28.5 Branching cracks close to the fracture surface seen in bolt No. 2

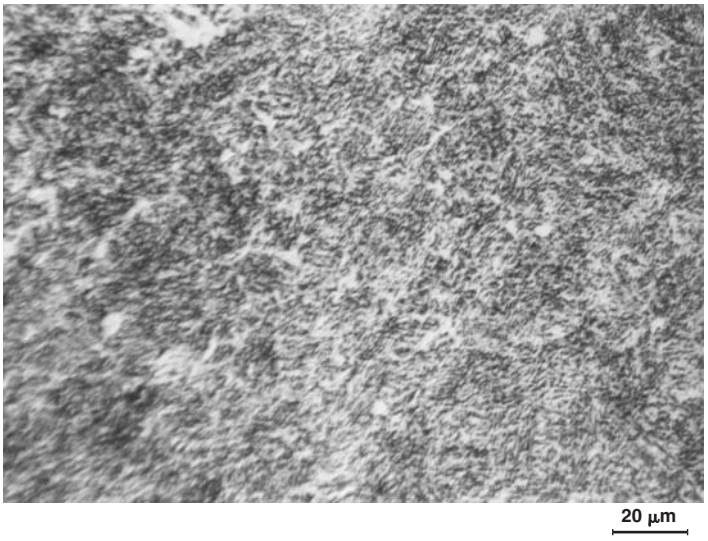

Fig. CH28.6 Microstructure of the bolt material showing tempered martensite with partial spheroidization

Failure Analysis of Engineering Structures: Methodology and Case Histories
V. Ramachandran, A.C. Raghuram, R.V. Krishnan, S.K. Bhaumik, p133-134
DOI:10.1361/faes2005p133

CASE 29

Failure of a Second-Stage Compressor Blade in an Aircraft Engine

Summary

A blade of the second-stage compressor in an engine fractured in service. The fracture was in brittle mode, with intergranular facets. The blade also had cracks in other regions. The blade had unusually high hardness, and the fracture was attributed to SCC.

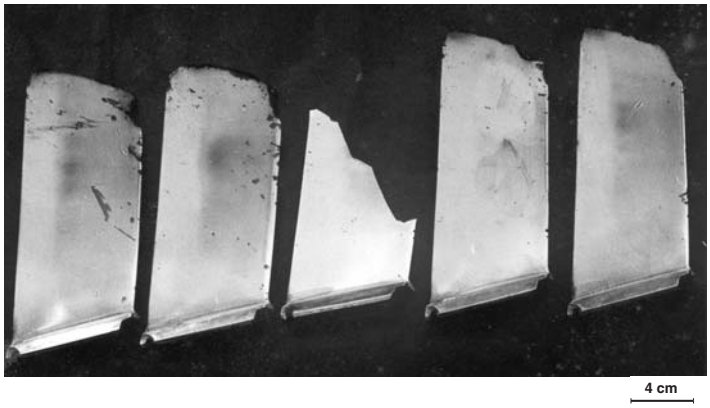

Fig. CH29.1 Second-stage compressor blade failed in an engine, along with the adjacent blades

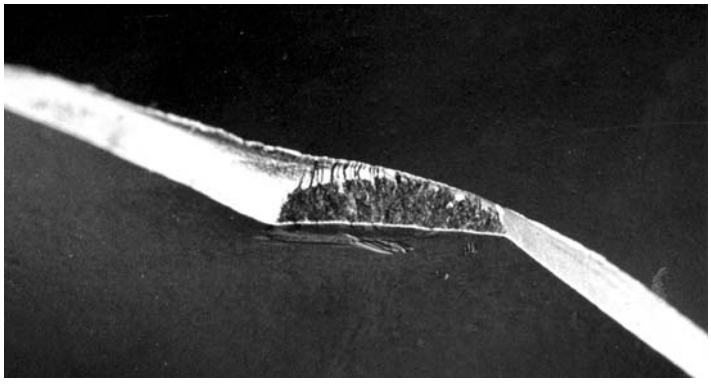

Fig. CH29.2 Close-up view of the discolored area on the fracture surface of the failed blade

Background

A blade of the second-stage compressor blade of an aircraft engine fractured after 21 hours and 19 minutes of service. The failed blade and its adjacent blades were examined.

Visual Examination of General Physical Features

The failed blade and its adjacent blades, two on either side, are shown in Fig. CH29.1. A close-up view of the fracture surface is shown in Fig. CH29.2. The fracture surface was generally light gray in color except for a flat region at the mid chord of the blade, where it was dark brown. Macroscopically, the fracture was brittle. Cracks were observed at the leading edge and the root of the blade (Fig. CH29.3).

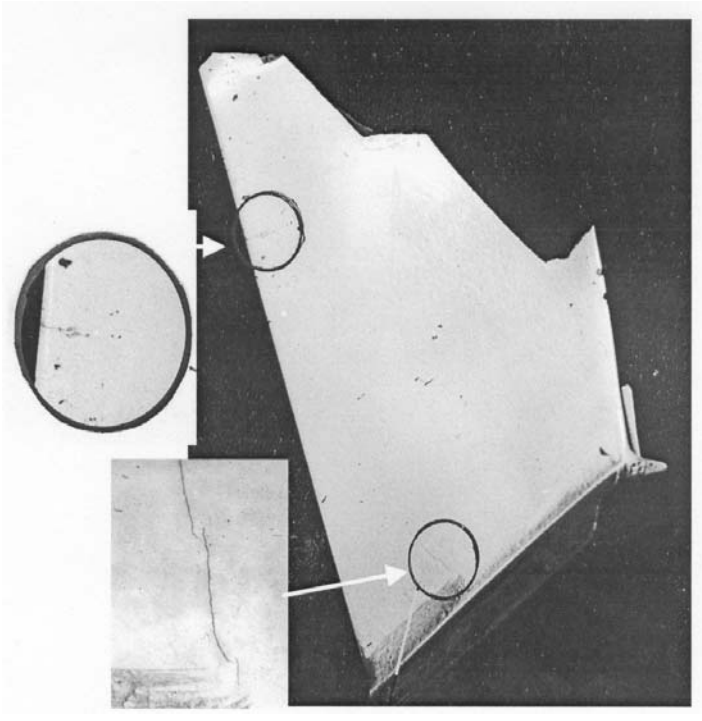

Fig. CH29.3 Cracks in other areas of the failed blade. Insets show enlarged areas of some of these cracks.

The longest crack was opened, and the resulting fracture surface also exhibited a dark brown color (Fig. CH29.4) similar to that on the fracture surface, suggesting that all the cracks could be of similar nature.

Testing Procedure and Results

Scanning Electron Fractography

Under the SEM, intergranular facets were observed on the dark brown region of the failed blade (Fig. CH29.5). Careful examination of the transition zone did not reveal the presence of fatigue striations.

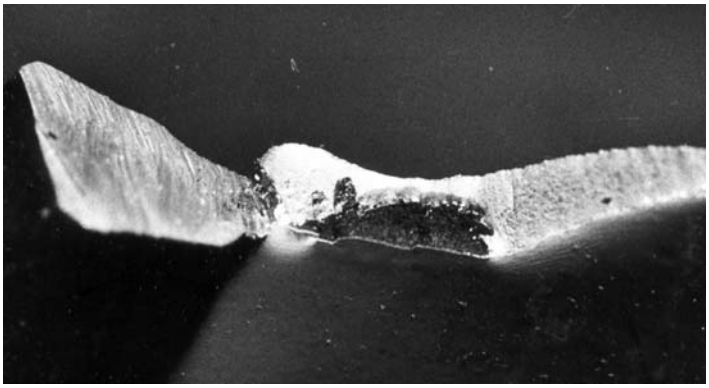

Fig. CH29.4 Crack shown in Fig. CH29.3 opened up. The discoloration is similar to that noticed on the fracture surface of the failed blade.

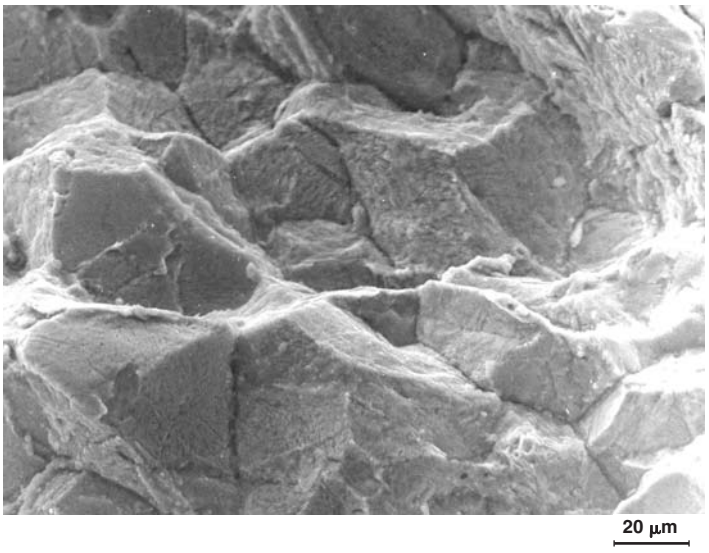

Fig. CH29.5 SEM fractograph showing the intergranular cracking in the dark brown region in the failed blade

Intergranular cracking was observed on the freshly opened up surface near the blade root area, further confirming that all the cracks were similar in nature.

Metallography and Hardness

The microstructure of the failed blade was tempered martensite. The hardness was 510 HV, which is unusually high compared with the specified value of 350 to 380 HV. The blades adjacent to the failed blade had a fully tempered martensite structure, with a hardness in the specified range. The crack on the surface with extensive branching is shown in Fig. CH29.6.

Discussion

The intergranular mode of fracture and the branching of cracks are typical of SCC. The high hardness due to inadequate tempering was conducive to such cracking. The other adjoining blades that showed hardness within the specified range showed no such cracking.

Conclusion

The blade failed due to SCC at the mid-chord region.

Recommendation

Care should be exercised to follow strictly the heat treatment schedule specified.

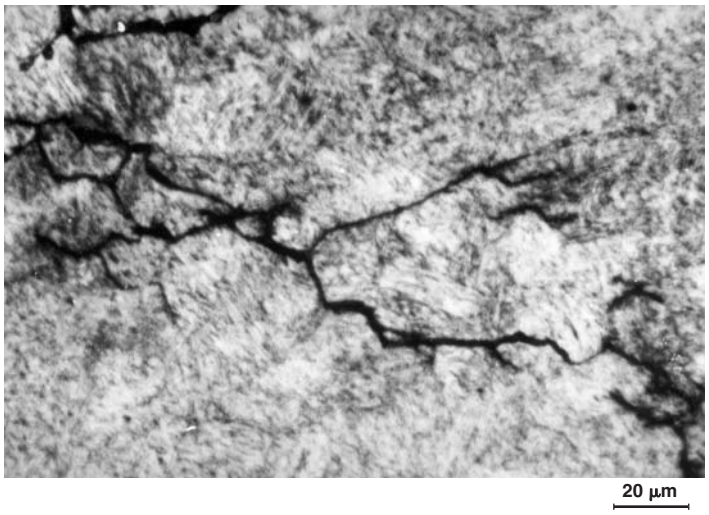

Fig. CH29.6 Optical micrograph of the cracks noticed on the blade surface

Failure Analysis of Engineering Structures: Methodology and Case Histories
V. Ramachandran, A.C. Raghuram, R.V. Krishnan, S.K. Bhaumik, p135-137
DOI:10.1361/faes2005p135

CASE 30

Failure of a Second-Stage Turbine Blade in an Aircraft Engine

Summary

A second-stage turbine blade in an aircraft engine fractured through the shroud hole, proceeding from the shroud hole during operation. The two adjacent blades had one crack each. Microscopic examination revealed that the failure and the cracking were due to fretting action of the shroud pins inside the shroud holes.

Background

A second-stage turbine blade failed in service, the fracture running through the shroud hole. The failed blade and its two adjacent blades were examined in detail.

Pertinent Specifications

The blades are made of the alloy AE 826.

Visual Examination of General Physical Features

The fracture surface of the failed blade is shown in Fig. CH30.1. The fracture surface showed two regions shown schematically in Fig. CH30.2. Region A near the leading edge was gray in color, while region B on the trailing edge was dark and oxidized.

Cracks were seen on the inner surface of the shroud hole, in region C. Deep rub marks were noticed on the cylindrical surface in region D. Region E of the surface perpendicular to the fracture surface had cracks and also evidence of deformation (Fig. CH30.3). Region F was free from cracks.

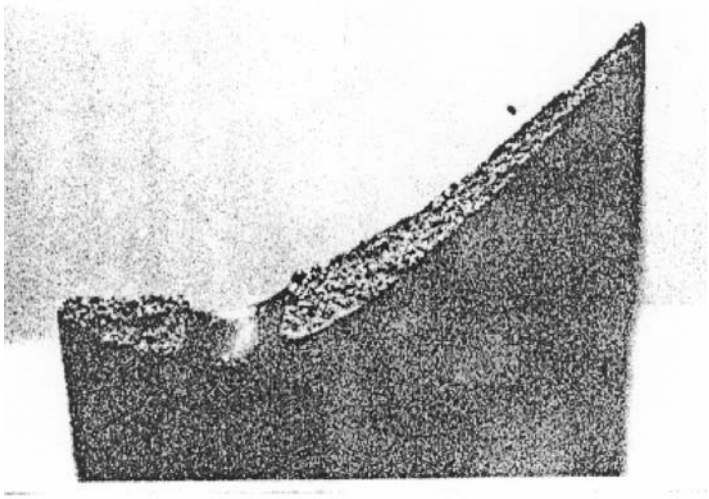

Fig. CH30.1 Fracture surface of failed blade

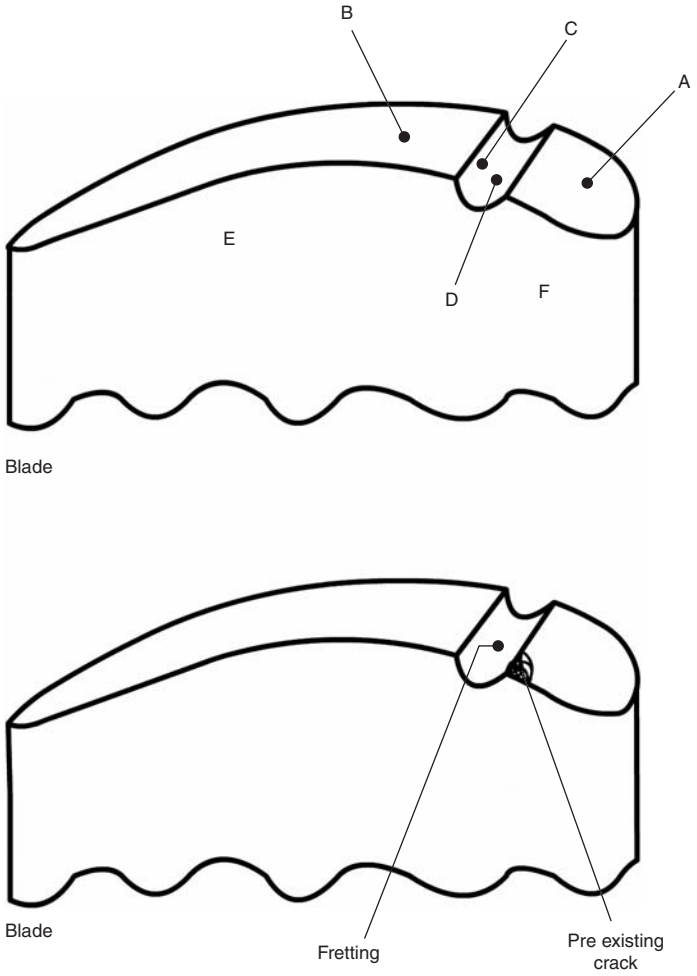

Fig. CH30.2 Schematic representation of fracture in the failed blade

Each of the adjacent blades had a crack, proceeding from the shroud hole toward the leading edge, on the concave side of the blade profile.

Testing Procedure and Results

Scanning Electron Fractography

Figure CH30.4 is a SEM fractograph of the failed blade. The fracture is intergranular. The crack in the blade was opened to expose the fracture surface. The dark region in one of the corners (Fig. CH30.5) shows that there was a preexisting crack that must have been oxidized. The SEM fractograph of this region also shows intergranular cracking (Fig. CH30.6). In this blade also, fretting marks were noticed on the surface of the shroud hole in the region of the crack. Such marks were also found in the other adjacent blade inside the shroud hole.

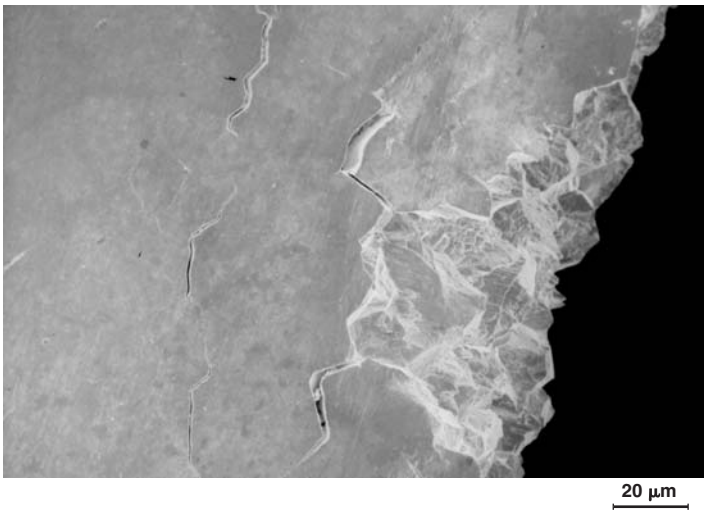

Fig. CH30.3 Cracks and deformation in region E (Fig. CH30.2)

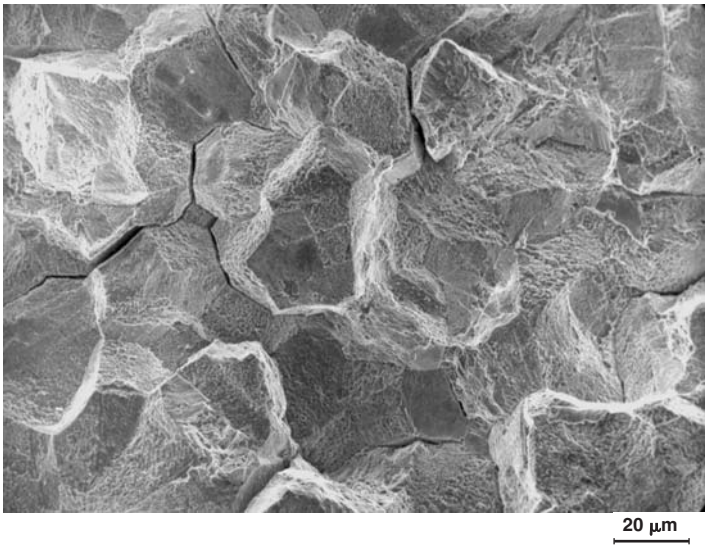

Fig. CH30.4 SEM fractograph of the failed blade, showing intergranular fracture

Discussion

These observations indicate the cracking of the blades is associated with fretting inside the shroud hole, possibly due to clearance between the shroud pin and the shroud hole. It is possible that the fretting action would have led to initiation of crack and its propagation by fatigue. Absence of striations does not rule out fatigue, particularly in materials prone to intergranular fracture.

Conclusion

The failure of the blade and the cracking of the adjacent blades are due to fretting action of the shroud pins inside the shroud holes.

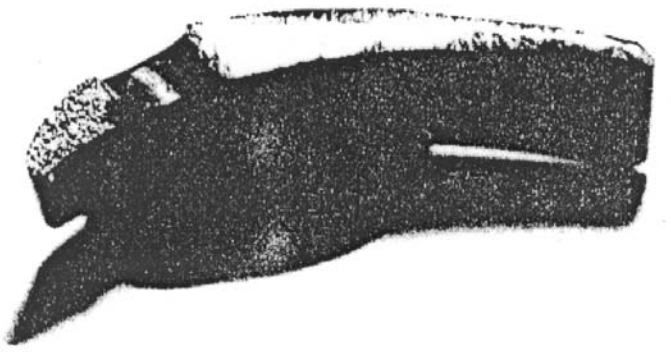

Fig. CH30.5 Preexisting crack (dark region) in one adjacent blade after opening

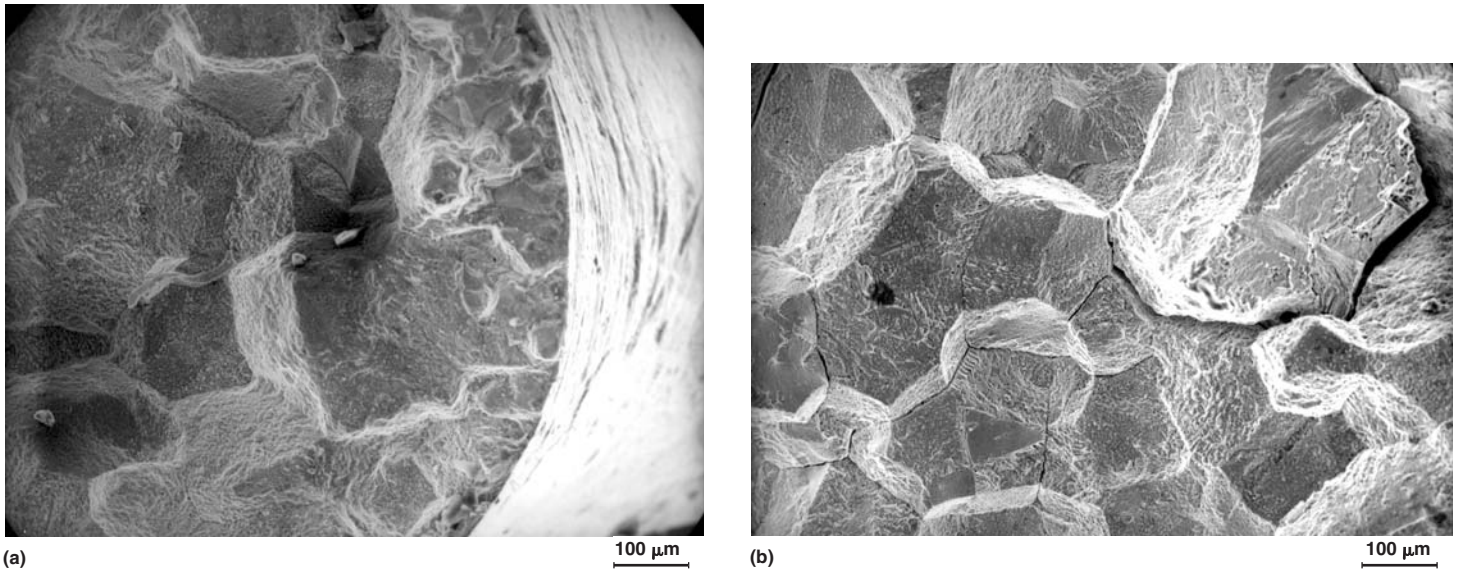

Fig. CH30.6 (a) SEM fractograph at the origin of the preexisting crack (dark region) shown in Fig. CH30.5. (b) SEM fractograph, taken slightly inward within the dark region

Failure Analysis of Engineering Structures: Methodology and Case Histories
V. Ramachandran, A.C. Raghuram, R.V. Krishnan, S.K. Bhaumik, p138-140
DOI:10.1361/faes2005p138

CASE 31

Failure of a High-Pressure Turbine Blade in an Aircraft Engine

Summary

A nimonic alloy turbine blade failed in service within 5 hours of total operation. Fractographic analysis indicated failure by low-cycle fatigue.

Background

A high-pressure turbine blade failed in service within 5 hours of total operation. Fractographic analysis was carried out to find the mode of failure.

Visual Examination of General Physical Features

The fracture occurred very close to the root of the blade. The fracture surface revealed three different zones (Fig. CH31.1). The small region near the trailing edge and a major portion toward the leading edge were dark gray in color, while the region in between was lighter. There was little or no evidence of plastic deformation in regions 1 and 2, whereas region 3 showed considerable plastic deformation.

Testing Procedure and Results

Scanning Electron Fractography

The SEM fractographs of the three zones are shown in Fig. CH31.2 to CH31.4. Zone 1 shows a mixed mode of fracture, consisting of cleavage and intergranular fracture (Fig. CH31.2). Zone 2 is characterized by striations and secondary fissures (Fig. CH31.3). The direction of crack growth is from the trailing edge to the leading edge. Zone 3 is marked by intergranular fracture typical of high-temperature tensile rupture (Fig. CH31.4).

Discussion

Striations and secondary fissures in zone 2 are typical of high-stress, low-cycle fatigue. The fatigue crack originated at the end of zone 1 rather than at the surface. It is probable that zone 1 came into existence during service due to the presence of a preexisting crack in the blade.

Conclusion

The blade failed by low-cycle fatigue, starting from a defective region already having cracks.

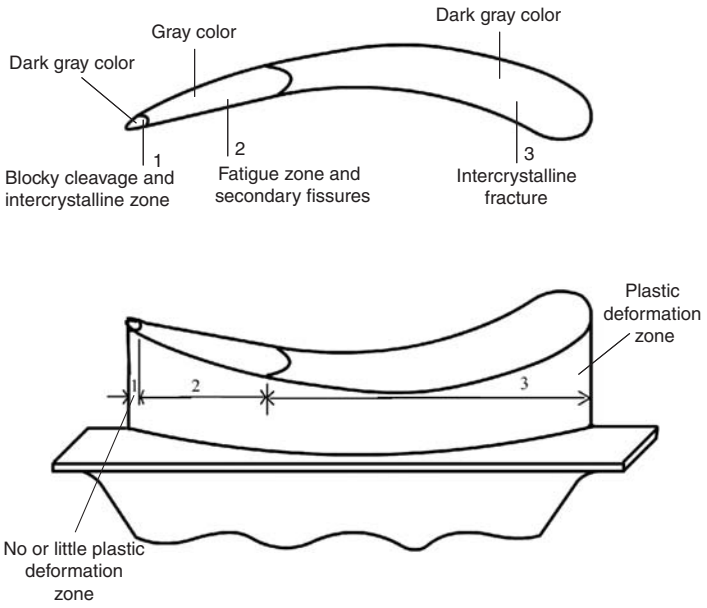

Fig. CH31.1 Sketch showing the zones in the failed turbine blade

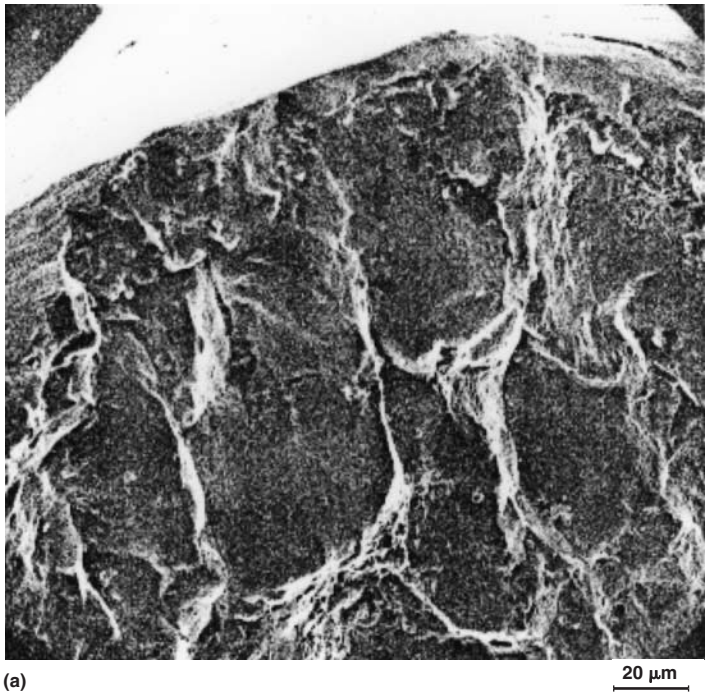

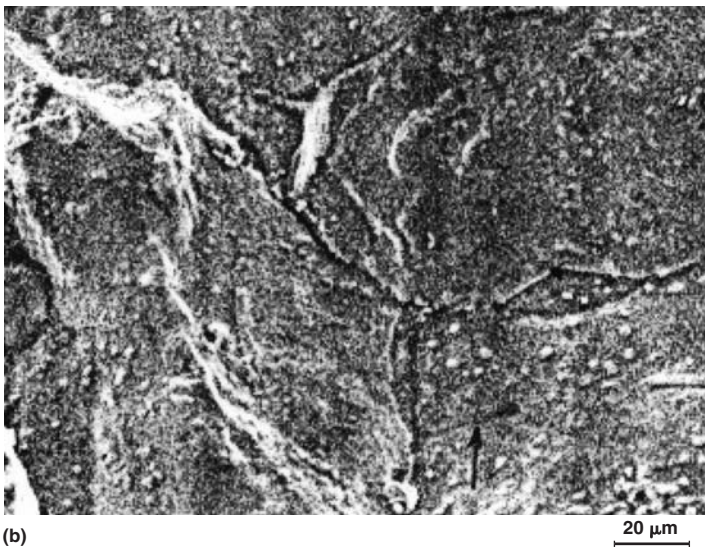

Fig. CH31.2 (a) SEM fractograph of trailing edge tip in region 1. (b) SEM fractograph showing crack within the blade, indicated by arrow

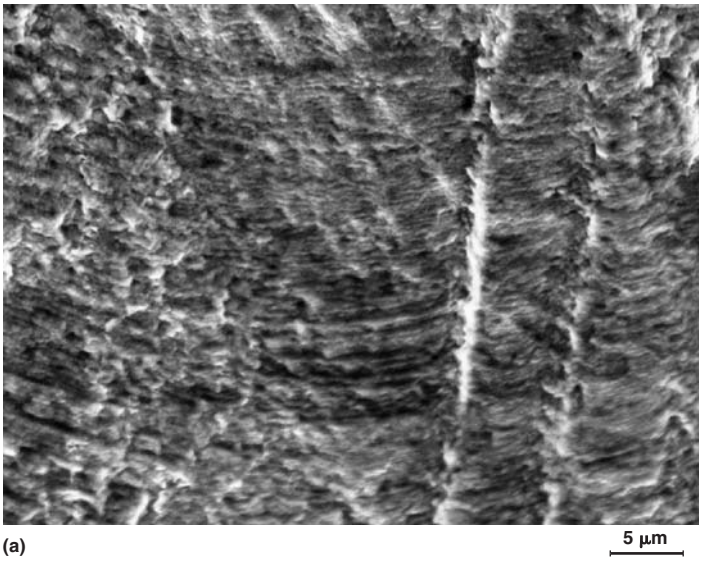

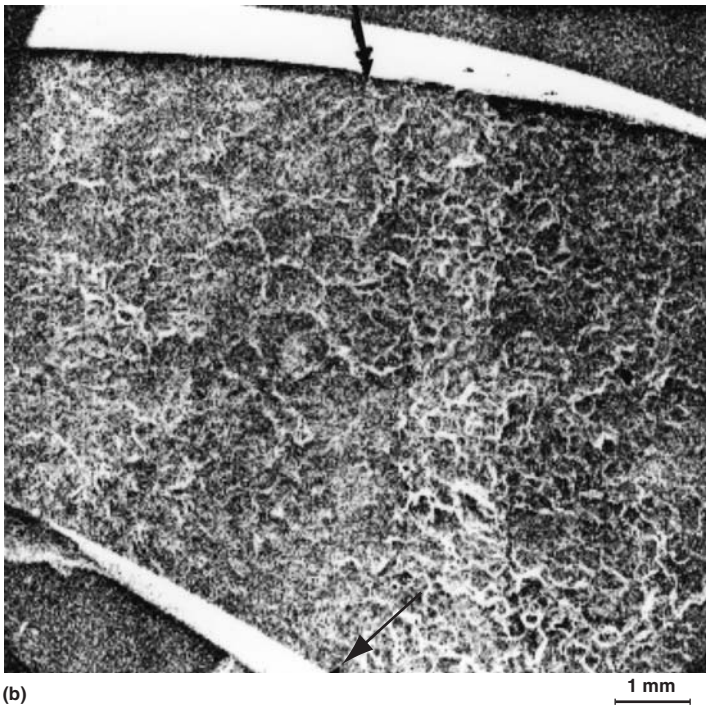

Fig. CH31.3 (a) SEM fractograph showing low-cycle fatigue striations in zone 2. (b) SEM fractograph showing the transition from fatigue to intercrystalline fracture. Arrows indicate the transition.

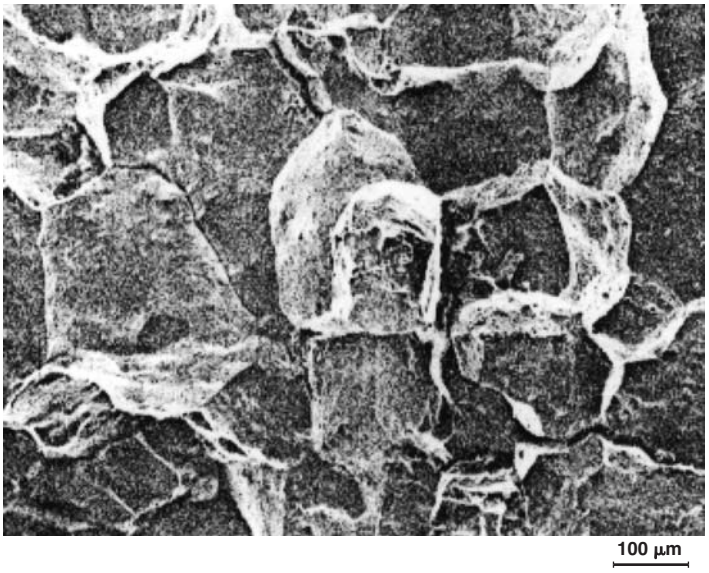

Fig. CH31.4 SEM fractograph of region 3 showing intercrystalline mode of fracture

Failure Analysis of Engineering Structures: Methodology and Case Histories
V. Ramachandran, A.C. Raghuram, R.V. Krishnan, S.K. Bhaumik, p141-142
DOI:10.1361/faes2005p141

CASE 32

Failure of a Compressor Blade in an Aircraft Engine

Summary

A compressor blade made of titanium alloy failed during testing of an aircraft engine. The blade material and the processing conditions of the blade were found to be satisfactory. Macro, micro, and electron fractographic investigations showed that the blade had failed by an impact load acting on its concave side.

Background

During the testing of an aircraft engine, a compressor blade fractured at the root. Tests were carried out to find the cause of fracture.

Visual Examination of General Physical Features

The fracture surface showed well-defined radial or chevron marks (Fig. CH32.1) originating on the concave side of the blade at two locations closer to the two edges and had propagated simultaneously before ending in a shear lip on the convex side.

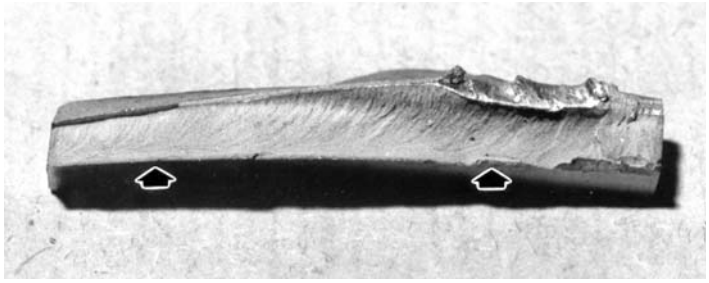

Fig. CH32.1 Fracture surface of the blade showing chevron marks

Testing Procedure and Results

Scanning Electron Fractography

A small section of the blade was cut in one of these regions and the fracture surface was observed in the SEM. Well-defined dimpled rupture was seen all over the cross section, indicating that the failure was due to overload (Fig. CH32.2).

Tensile Test

A miniature tensile specimen was machined from the root of the blade and tested in an Instron machine with the following results:

Mechanical properties of the compressor blade

Ultimate tensile strength, kg/mm^2	Yield strength, kg/mm^2	% elongation	% reduction of area
98.509	87.2	13.0	35.96

Microstructure

A sample from the root was polished, etched with Keller's reagent, and observed in a microscope. The microstructure showed well dispersed, duplex α and β structure with no abnormalities (Fig. CH32.3). No oxygen stabilized casing was observed, which rules out oxygen absorption during forming operations.

Discussion and Conclusion

The preceding observations show that the blade had an acceptable microstructure and that its strength and ductility were normal. It can, therefore, be concluded that the blade failed due to a sudden impact load acting on its concave side.

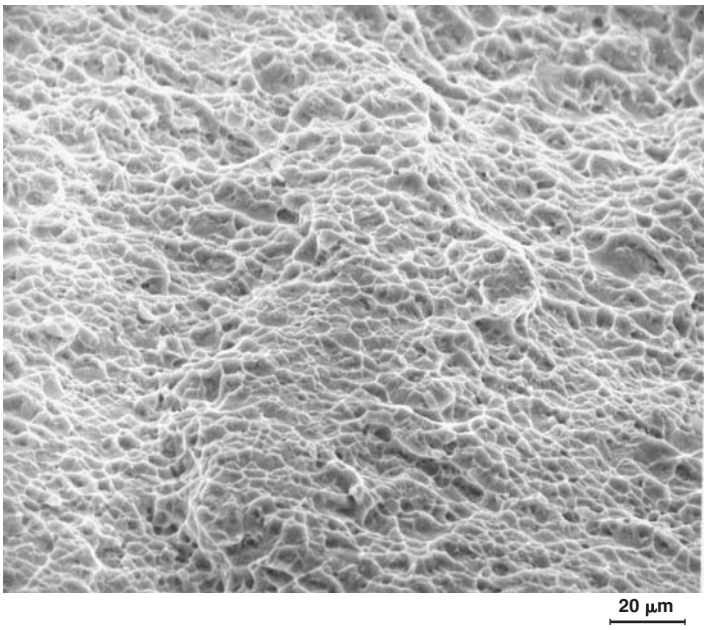

Fig. CH32.2 SEM fractograph of the fracture surface showing dimpled rupture

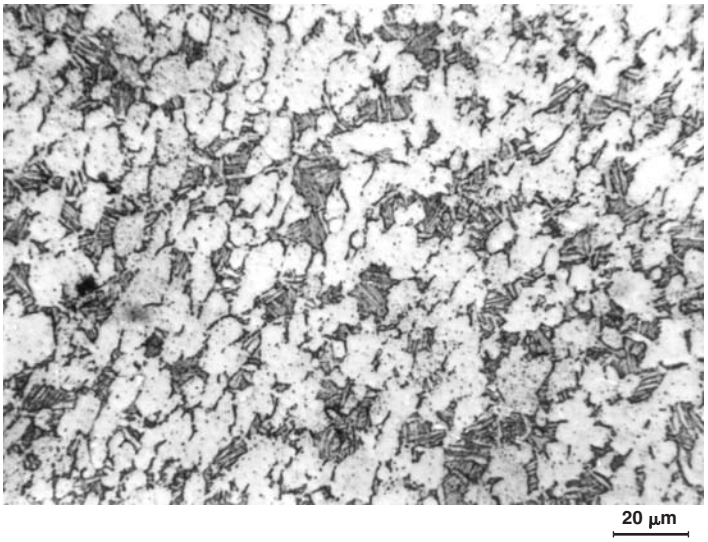

Fig. CH32.3 Microstructure of the blade material at the root showing well-dispersed α and β structure

Failure Analysis of Engineering Structures: Methodology and Case Histories
V. Ramachandran, A.C. Raghuram, R.V. Krishnan, S.K. Bhaumik, p143-145
DOI:10.1361/faes2005p143

CASE 33

Failure of a Low-Pressure Turbine Rotor (LPTR) Blade

Summary

A low-pressure turbine rotor (LPTR) blade failed during a test run causing damage to all the blades. The blade had failed by fatigue and the fatigue crack had initiated at surface coating cracks caused by mechanical damage.

Background

A low-pressure turbine rotor blade failed within hours of a test run causing extensive damage to the engine. Strip examination revealed that one of the LPTR blades had fractured near the blade root. The failed blade was examined for analyzing the cause of failure.

Pertinent Specifications

The LPTR blade was made of directionally solidified cast nickel-base superalloys with platinum aluminide surface coating.

Visual Examination of General Physical Features

Figure CH33.1 shows the failed blade. The blade had fractured above the blade root platform in the airfoil section. Macroscopically, the fracture surface showed two distinctive regions (Fig. CH33.2). In region I, the crack had propagated parallel to the blade root platform and the fracture surface was found discolored due to oxidation. The maximum oxidation was observed near the leading edge (LE), and the extent of oxidation decreased gradually toward the interior of the blade. The color changes could be noticed from dark blue at the LE to light yellow at the end of region I. This is indicative of progressive crack propagation. Under the stereobinocular microscope, a half-moon-shaped region consisting of beach marks, typical of fatigue, was observed on the fracture surface at the LE (Fig. CH33.3). The beach marks were found to have emanated from the LE, indicating that the crack initiation was at the LE. Detailed examination revealed two dent marks on the leading edge at the crack origin region (Fig. CH33.4).

The remaining portion of the fracture surface, region II (Fig. CH33.2), had a fresh and rough fracture surface and a coarse crystalline appearance. The gross fractographic features were typical of overload failure.

Fig. CH33.1 Photograph of the failed LPTR blade

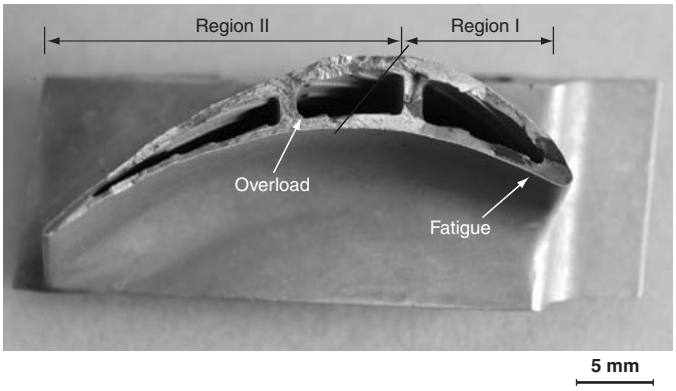

Fig. CH33.2 Fracture surface showing two fracture zones

Testing Procedure and Results

Scanning Electron Microscopy and Fractography

Figure CH33.5 shows a low-magnification fractograph of the fatigue-failed region. Beach marks, typical of progressive failure, can be seen. From the orientation of the beach marks, it was found that there were two fatigue crack origins (Fig. CH33.6). Both the fatigue cracks were found to have initiated at the mechanically damaged region, and they were separated by a distance of about 300 μm.

At higher magnifications, striations typical of fatigue were observed (Fig. CH33.7). Examination revealed wide variations in striation spacing as well as localized change in the direction of the crack front depending on the grain orientation. The coating thickness at the crack origin was measured to be about 73 μm, with no abnormalities in the coating.

The SEM photograph of the mechanically damaged regions (dents) is shown in Fig. CH33.8. Cracks were seen in the coating around the dent mark. Examination also revealed that the fatigue cracks had initiated from these coating cracks. The surface of the damaged regions was found oxidized and found to be similar to that observed elsewhere in the blade.

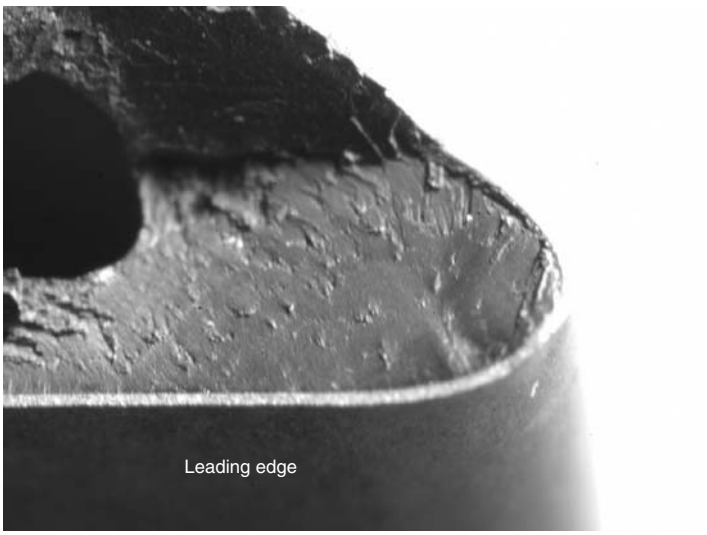

Fig. CH33.3 Photograph showing beach marks emanating from the leading edge of the blade

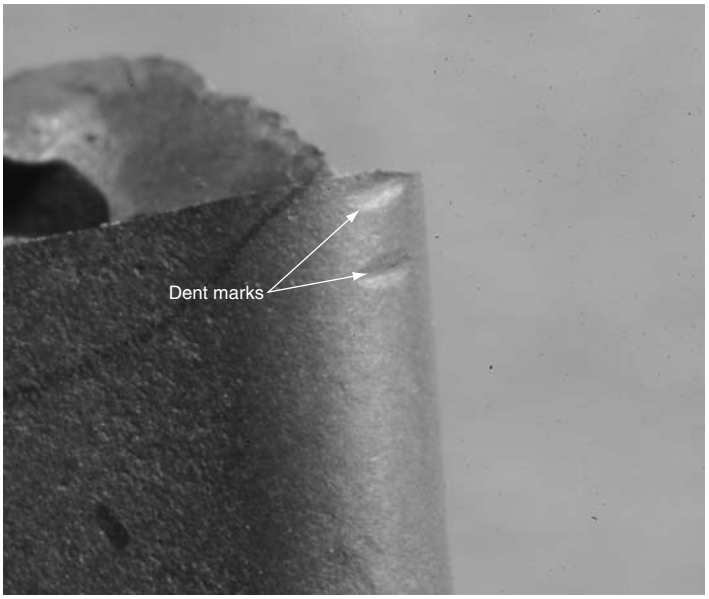

Fig. CH33.4 Photograph showing dent marks at the crack origin

Fig. CH33.5 SEM fractograph at the fatigue crack origin

Fig. CH33.6 SEM fractograph showing two fatigue cracks

Discussion

Fractographic examination suggests that the LPTR blade had failed by fatigue. The fatigue crack had initiated at the leading edge above the blade root platform and propagated progressively over a period of time before culminating in an overload fracture at the trailing edge. From the orientation of the beach marks, two fatigue crack origins were identified at the leading edge.

Examination revealed that there were two shallow dent marks on the leading edge of the blade at the fatigue crack origin region. A network of cracks was observed in the coating surrounding these dent marks. The surface of the dented regions was found oxidized similar to that seen elsewhere on the blade surface. This indicates that the dents were not caused freshly due to secondary damages, and they were present in the blade before the failure took place. This suggests that the cracks in the coating caused due to mechanical damage were responsible for the fatigue crack initiation in the blade.

Conclusion

The LPTR blade failed by fatigue due to the presence of coating cracks created as a result of mechanical damage.

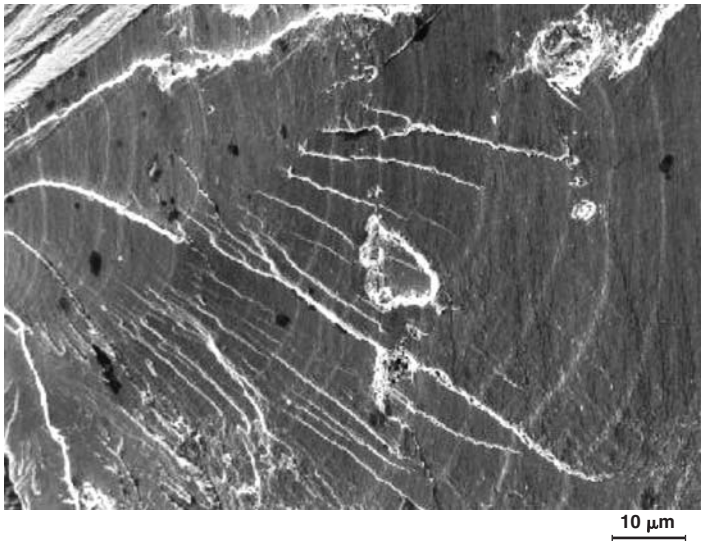

Fig. CH33.7 SEM fractograph showing fatigue striations at location A shown in Fig. CH33.6

Fig. CH33.8 SEM picture showing network of crack around the mechanical dent

Failure Analysis of Engineering Structures: Methodology and Case Histories
V. Ramachandran, A.C. Raghuram, R.V. Krishnan, S.K. Bhaumik, p146-147
DOI:10.1361/faes2005p146

CASE 34

Cracking in the Wing Root Fitting in an Aircraft

Summary

Cracking observed in the bottom wing root fitting of an aircraft discovered during major servicing was investigated. The cause was found to be stress corrosion.

Background

During a major servicing of an aircraft after 795.35 hours since its last overhaul, cracks were observed in the bottom wing root fitting. The aircraft had done 2587.1 hours of service.

Pertinent Specification

The fitting was made of aluminum alloy of DTD 5044 specification.

Visual Examination of General Physical Features

The bottom wing root fitting is shown in Fig. CH34.1. A crack 45 mm in length was noticed on one of the root radii, penetrating through the thickness. Dye-penetrant inspection revealed the crack more clearly (Fig. CH34.2).

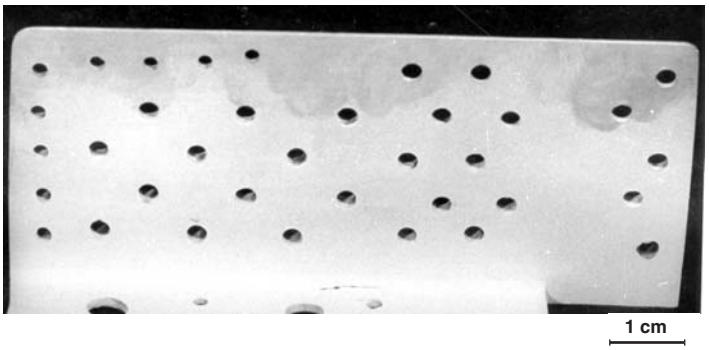

Fig. CH34.1 The bottom wing root joint

Testing Procedure and Results

A portion of the fitting was cut and the crack was opened to observe the fracture surface. The fracture surface showed dis-

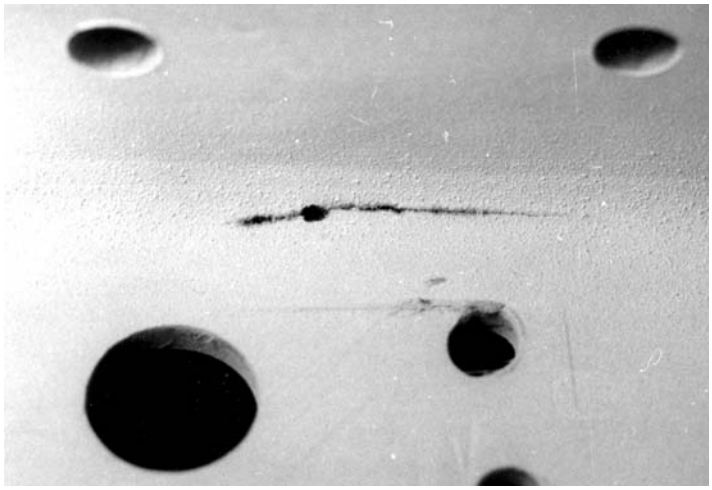

(a)

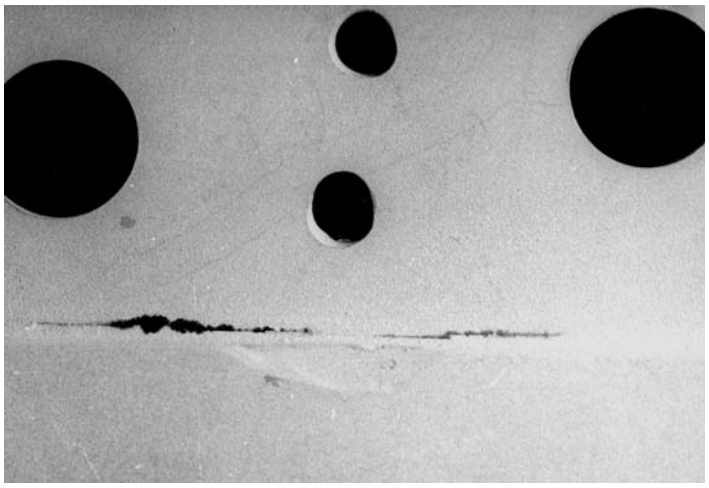

(b)

Fig. CH34.2 (a) and (b) Two views of the crack as revealed by dye-penetrant inspection

tinct crack front with discoloration characteristic of delayed failure.

Scanning Electron Fractography and EDAX

The fracture surface was examined in a SEM. The surface was covered with a deposit, with classical "mud-cracked" regions (Fig. CH34.3). In situ microanalysis of the deposit revealed presence of significant amounts of sulfur (Fig. CH34.4). In some places, deep secondary cracks were seen on the fracture surface.

In contrast, freshly fractured regions were clean, with dimple features (Fig. CH34.5).

To confirm the presence of secondary cracks, the specimen was sectioned across the fracture surface and metallographically polished and observed in the SEM. Clear secondary cracks were observed, propagating below the fracture surface (Fig. CH34.6).

From these observations, it is clear that the crack was due to stress corrosion.

Conclusion

The cracks in the bottom wing root fitting in the aircraft were due to stress corrosion.

Recommendations

Examine all other aircraft with similar fittings made of DTD 5044 alloy to determine presence of any cracks.

Aluminum alloy DTD 5044 is generally known to be prone to SCC. Hence, alternate material may be considered.

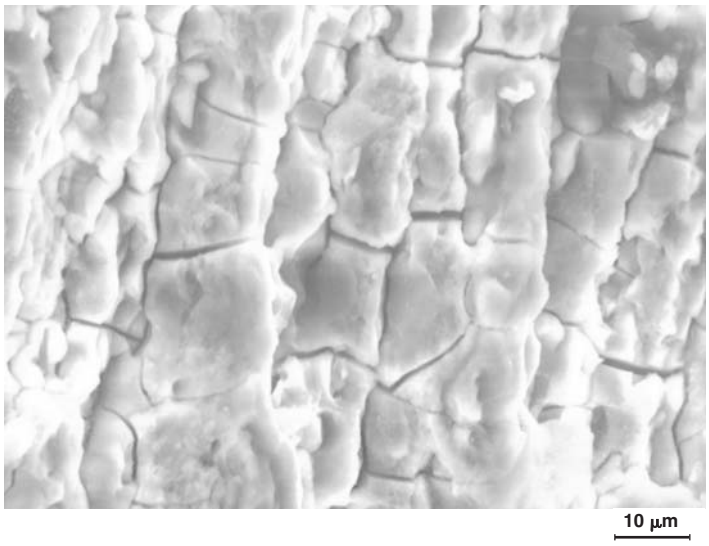

Fig. CH34.3 Mud cracking on the oxide layer of fracture surface

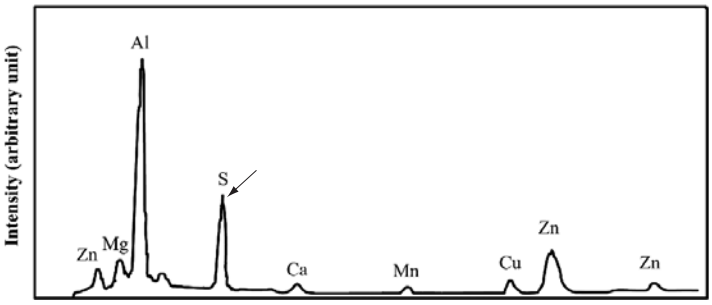

Fig. CH34.4 Energy-dispersive x-ray spectrum of the fracture surface. Note the presence of sulfur (arrow).

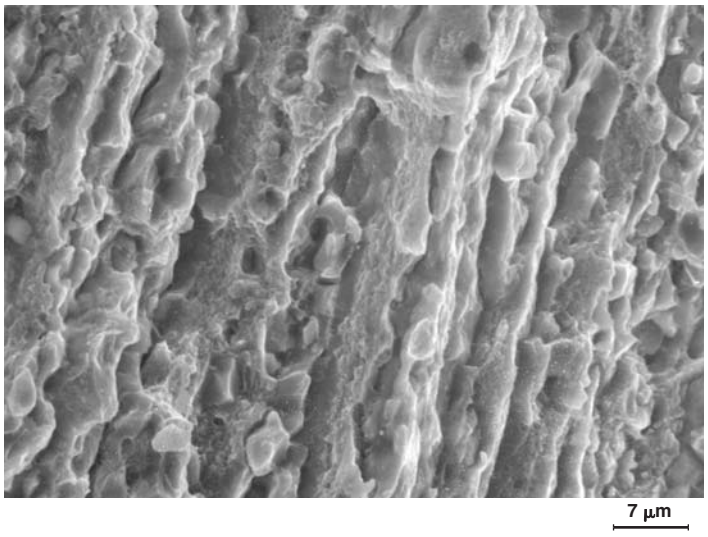

Fig. CH34.5 Freshly fractured surface showing dimpled features

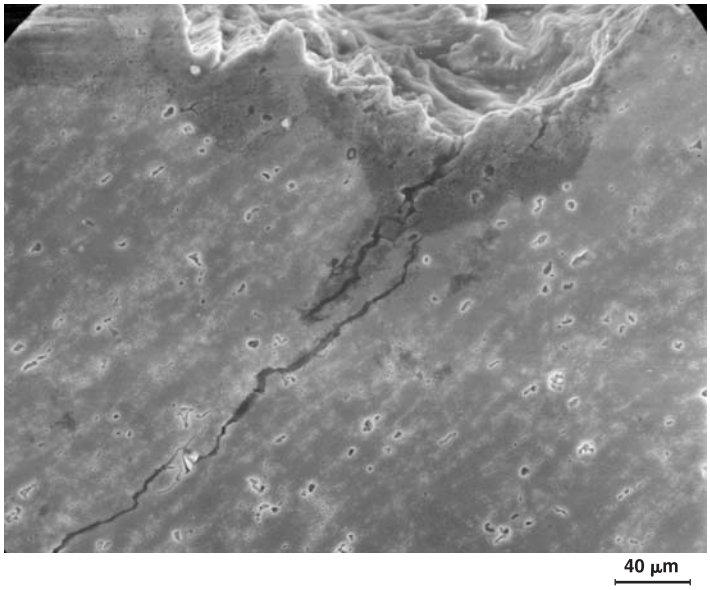

Fig. CH34.6 Secondary cracking below the fracture surface

Failure Analysis of Engineering Structures: Methodology and Case Histories
V. Ramachandran, A.C. Raghuram, R.V. Krishnan, S.K. Bhaumik, p148-149
DOI:10.1361/faes2005p148

CASE 35

Failure of Quill Shafts in the Accessory Gear Box in an Aircraft Engine

Summary

There have been a few cases of premature failure of quill shafts in the accessory gear boxes of aircraft engines. The failure was found to be due to gradual wear resulting from inadequate lubrication.

Background

It was reported that there have been a number of premature failures of quill shafts that transmit the drive from the engine accessory gear box to the oil unit. The failed quill shaft was not available for investigation. However, its mating splines in the splined bore were available.

Visual Examination of General Physical Features

The splines in the splined bore on the drive side were found covered with dry red powder. The splines were cleaned. They had an odd shape compared with the splines on other drives. The splines were cut open for detailed examination. They showed excessive wear. There was some blueing on the splines indicating heating effects.

Testing Procedure and Results

The reddish powder collected from the worn out splines was found to contain all the elements from the gear material. This powder is thus a result of wear of the splines. The reddish color is due to formation of iron oxide.

The profiles of the drive side spline and a good spline were examined in a contourograph and the profile traces are shown in Fig. CH35.1.

Scanning Electron Microscopy

The cross section of these splines was observed in a SEM. Figure CH35.2 shows the spline profiles in the worn spline and in a good spline. It was estimated that about 30% of the effective spline volume had become worn.

Metallography and Hardness

The cross sections of the splines were metallographically polished and observed in the microscope. The splines were found to be case hardened to a depth of 0.25 mm. The hardness of the case was 63 HRC and that of the core was 38 HRC. These values appeared to be within the normal spline specifications.

From these observations, it may be concluded that the failure of the spline in the spline bore resulted from wear due to inadequate lubrication.

Conclusion

The failure of the spline was due to gradual wear resulting from inadequate lubrication.

Recommendation

Adequate lubrication should be ensured at all times by periodic inspection.

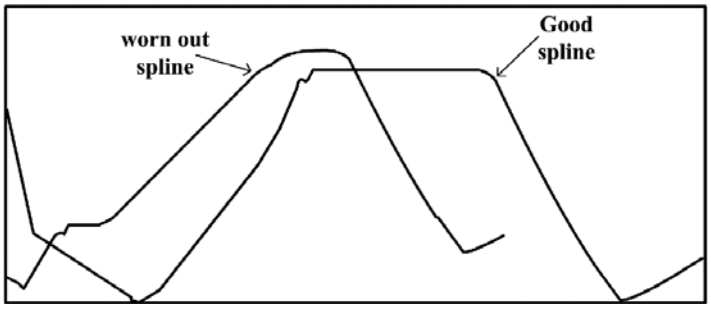

Fig. CH35.1 Traces of the profiles of the splines taken in a contourograph

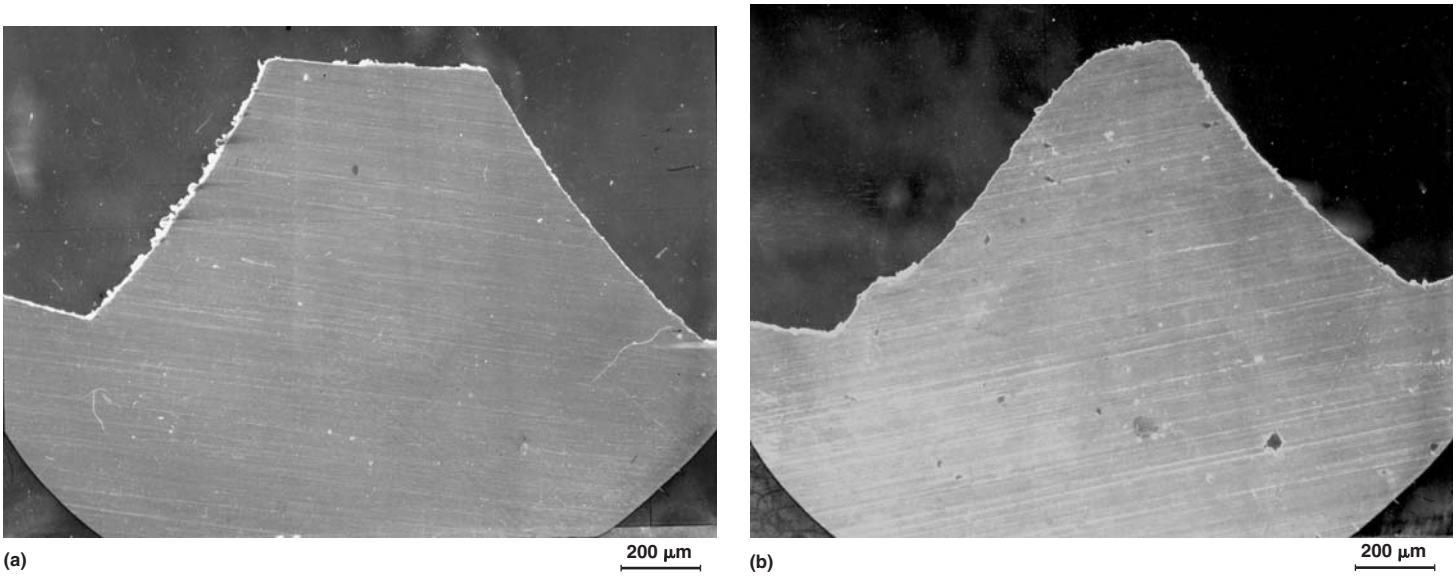

Fig. CH35.2 SEM photographs showing cross sections of (a) good and (b) worn splines

Failure Analysis of Engineering Structures: Methodology and Case Histories
V. Ramachandran, A.C. Raghuram, R.V. Krishnan, S.K. Bhaumik, p150-151
DOI:10.1361/faes2005p150

CASE 36

Failure of a Compressor Blade in an Aircraft Engine

Summary

A compressor blade in an aircraft engine failed in service. The failure was due to fatigue fracture originating from nonmetallic inclusions present at a critical location near the blade root.

Background

A compressor blade of an aircraft engine failed in service. One-half of the blade containing the root portion was available for investigation.

Visual Examination of General Physical Features

The blade had fractured at the root, with the fracture surface showing a conchoidal pattern indicating the delayed nature of fracture. The fracture had originated from the convex surface of the blade, almost from the middle portion, and progressed to about 80% of the cross section before final fracture, with a shear lip. Figure CH36.1 shows the macrograph near the origin. Well-delineated beach marks are present on the fracture surface (Fig. CH36.2).

Testing Procedure and Results

Scanning Electron Fractography and EDAX

Examination of the cleaned fracture surface in the SEM revealed coarsely spaced striations near the origin with cracks running parallel to the striations (Fig. CH36.3). Away from the origin but still within the region of beach marks, the striation appeared much finer and without cracks (Fig. 36.4). The rapid fracture region showed the presence of dimples.

Detailed examination of the fracture surface near the origin revealed the presence of inclusions (Fig. CH36.5). The inclusions

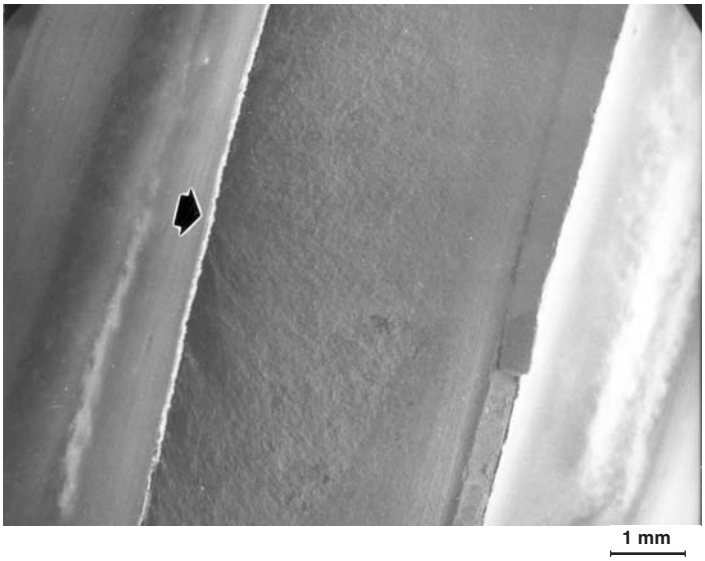

Fig. CH36.1 Fracture surface showing the fracture origin

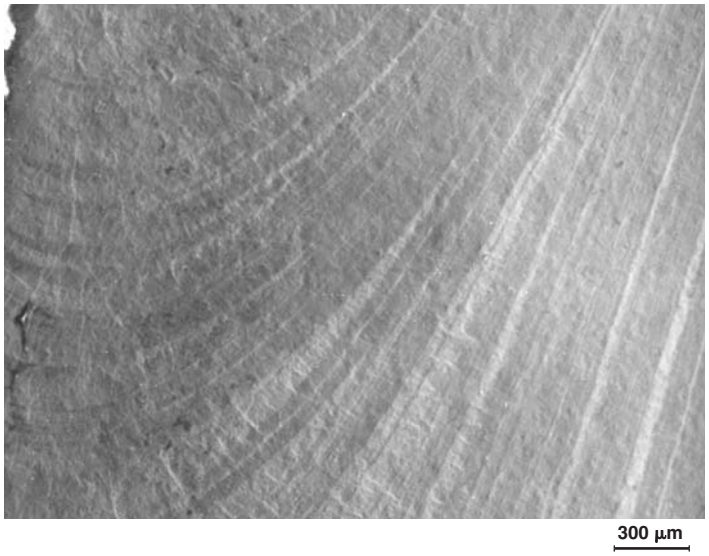

Fig. CH36.2 Well-defined beach marks on the fracture surface

by in situ EDAX were found to be rich in silicon. They are possibly silicates. Similar inclusions were seen on the fracture surface away from the origin also.

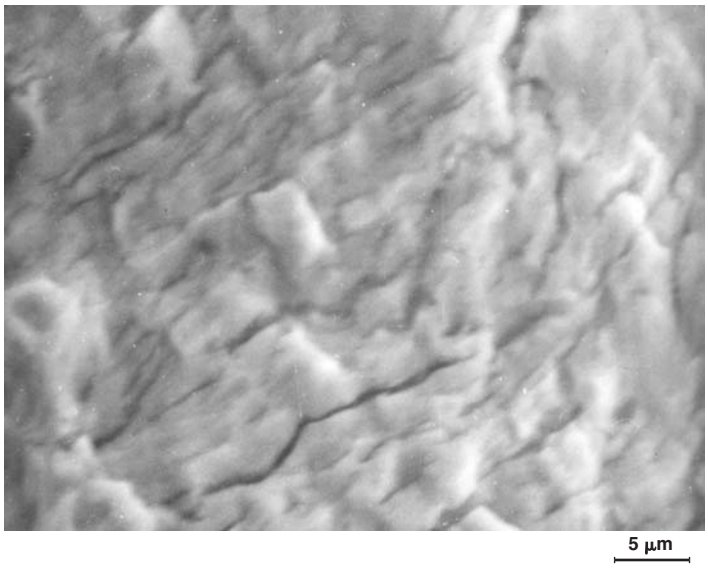

Fig. CH36.3 SEM fractograph near the origin showing fatigue striations along with cracking

Fig. CH36.4 SEM fractograph farther away from the origin showing very-fine fatigue striations

Metallography

A section from the root was cut and prepared for metallographic examination. It was found to contain a few large silicon-rich inclusions.

Discussion

It is obvious that the primary cause of fracture of the blade was fatigue, originating from inclusions present in a critical area. The change in the nature of striations could best be explained as due to a change from low-cycle fatigue condition in the initial stages to a high-cycle fatigue condition after the crack had grown to a critical length.

Conclusion

The failure of the compressor blade was due to fatigue fracture originating from inclusions present at critical location near the blade root on the convex side.

Recommendation

Blades manufactured from this batch of raw material should be reviewed.

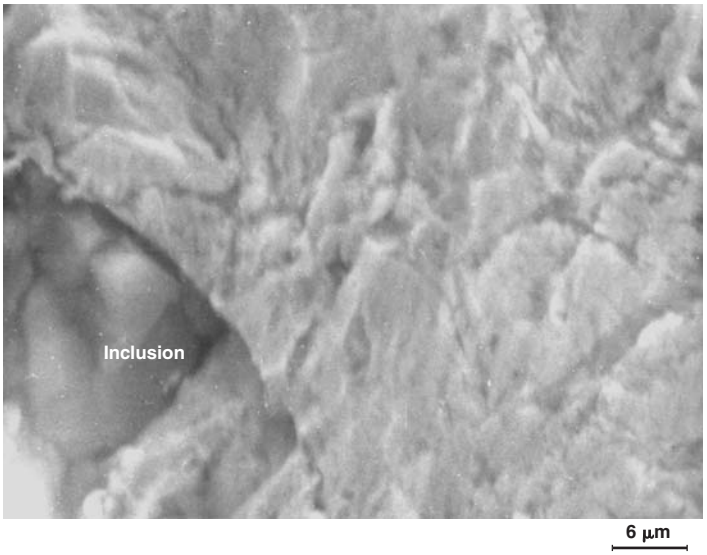

Fig. CH36.5 SEM fractograph of region close to the origin showing inclusions that were analyzed to be rich in silicon

Failure Analysis of Engineering Structures: Methodology and Case Histories
V. Ramachandran, A.C. Raghuram, R.V. Krishnan, S.K. Bhaumik, p152-153
DOI:10.1361/faes2005p152

CASE 37

Failure of an Aileron Control Cable in an Aircraft

Summary

The aileron control cable of an aircraft had failed. It was found damaged. Investigation revealed that the cable had been damaged by a shearing tool.

Background

The cable controlling the aileron movement in an aircraft had failed. The two mating portions of the cable were made available for the investigation to find the type of failure.

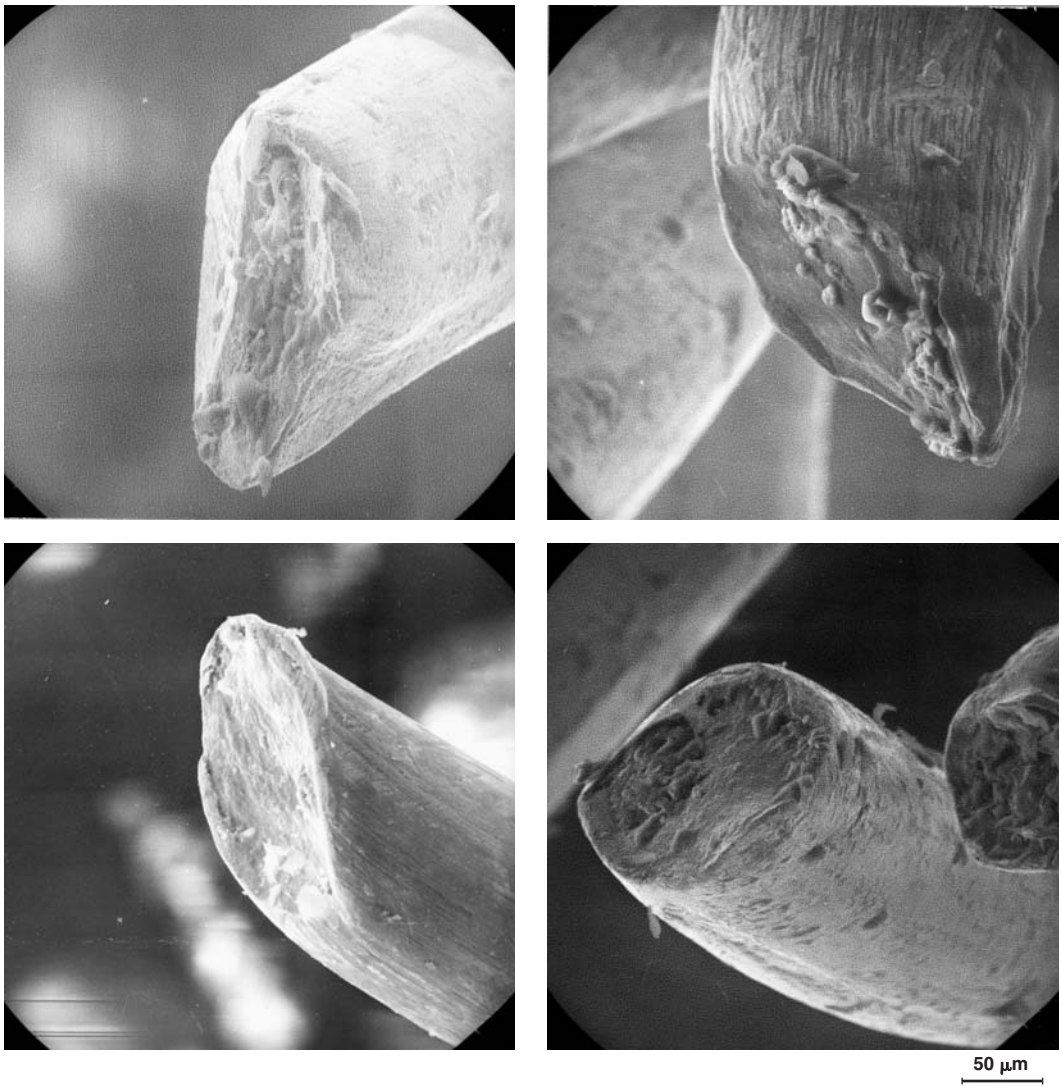

Fig. CH37.1 SEM photographs of broken ends of individual wires showing shear fracture

Visual Examination of General Physical Features

The control cable was made of galvanized plain carbon steel wires of diameter 0.23 to 0.25 mm. It contained seven strands of 19 wires in each strand.

Fig. CH37.2 SEM photograph of broken end of a wire showing tensile fracture preceded by necking (typical cup and cone fracture)

Testing Procedure and Results

Scanning Electron Fractography

The fractured ends of the strands of the cable were examined in a SEM. The majority of the wires showed sheared ends. Some of the sheared ends are shown in Fig. CH37.1. A few wires were found to have fractured after necking under a tensile load (Fig. CH37.2).

Discussion

The localized failure of the cable and the evidence that the majority of the wires showed sheared ends indicated that the cable had been damaged by a shearing tool. The general wear and tear and overload were not the cause of failure.

Conclusion

The aileron cable failed because of damages caused by a shearing tool.

Failure Analysis of Engineering Structures: Methodology and Case Histories
V. Ramachandran, A.C. Raghuram, R.V. Krishnan, S.K. Bhaumik, p154-155
DOI:10.1361/faes2005p154

CASE 38

Cracking of the Skin in the Main Rotor Blade in a Helicopter

Summary

The main rotor blade of a helicopter had developed cracks on the aluminum alloy skin. Visual and electron microscopic examination revealed that a fatigue crack had originated at the trailing edge of the blade on the sandwiched aluminum alloy center sheet on the underside of a rivet hole. Propagation of this crack through the outer skin had led to a sudden tearing off of the sheet metal.

Background

Cracks were observed on the aluminum alloy skin of the main rotor blade of a helicopter. The blade was constructed of aluminum alloy sheet 0.5 mm thick, wrapped around a foam with a forged aluminum leading edge (LE). At the trailing edge, an aluminum alloy sheet 1.0 mm thick was sandwiched and riveted.

Visual Examination of General Physical Features

The sandwiched aluminum alloy center sheet had cracked through its thickness, the crack propagating through the outer skin up to the forged LE. The crack had originated in the center sheet at a rivet hole and had progressed in both directions before the sheet metal fractured catastrophically with reverse slant fracture, toward the LE.

Testing Procedure and Results

Macrofractography

Examination of the fracture surface in the region of the rivet hole revealed half-moon-shaped beach marks, typical of fatigue

Fig. CH38.1 Fatigue striations on the sandwiched trailing edge center sheet near the rivet hole

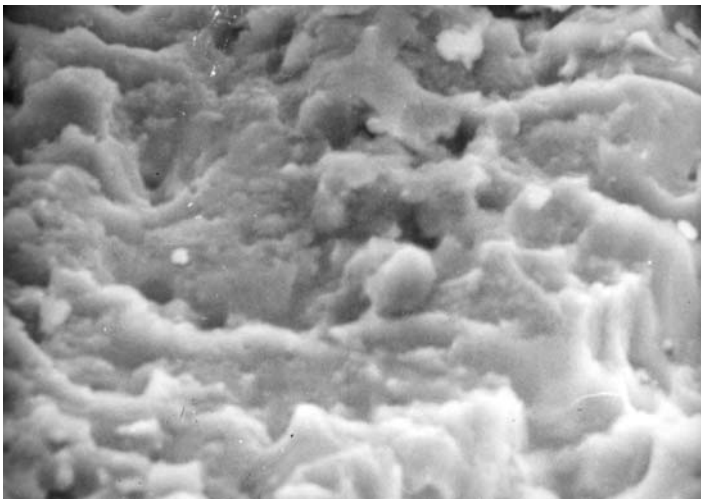

Fig. CH38.2 Shear dimples indicative of overload fracture on the outer skin region away from the rivet hole toward the leading edge

fracture, extending on either side of the rivet hole on the sandwiched center piece. From the orientation of the beach marks, it was concluded that the crack had initiated from the underside of the rivet hole.

Scanning Electron Fractography

A small piece of the sheet metal from this region was cut and examined in the SEM. Fatigue striations were clearly seen (Fig. CH38.1). The fracture on the outer skin region away from the rivet hole up to the leading edge showed reverse slant fracture edge and on the fracture surface, elongated dimples typical of shear overload were seen (Fig. CH38.2).

Discussion

The nature of the beach marks on the center piece indicated the sheet metal had been subjected to reverse bending stresses in this region. This stress led to crack initiation and propagation by fatigue in the trailing edge center piece. Once the center piece cracked fully, the outer skin was subjected to severe overload. The final overload fracture of one outer skin took place by the reverse slant mode, indicative of high strain rate fracture. Although full slant fracture may develop in thin sheets because through thickness stresses are relaxed by plastic deformation and a stress state approximating plane strain cannot develop, reverse slant rupture can occur only under very high strain rates. It can therefore be seen that once the fatigue crack progressed to a critical length, the rest of the sheet metal ripped apart catastrophically.

Conclusion

The helicopter rotor blade failed by fatigue crack in the trailing edge center sheet, the crack originating at the bottom of a rivet hole. The final fracture occurred catastrophically by a sudden tearing off of the sheet metal.

Failure Analysis of Engineering Structures: Methodology and Case Histories
V. Ramachandran, A.C. Raghuram, R.V. Krishnan, S.K. Bhaumik, p156-157
DOI:10.1361/faes2005p156

CASE 39

Cracking in a Tail Rotor Blade in a Helicopter

Summary

The tail rotor blade of a helicopter developed a crack on the skin. The cracking was due to local corrosion initiated from the inside surface. The local corrosion was due to excess burning of the resin used to bond the aluminum sheet at the trailing edge.

Background

The tail rotor blade of a helicopter developed a visible crack during service.

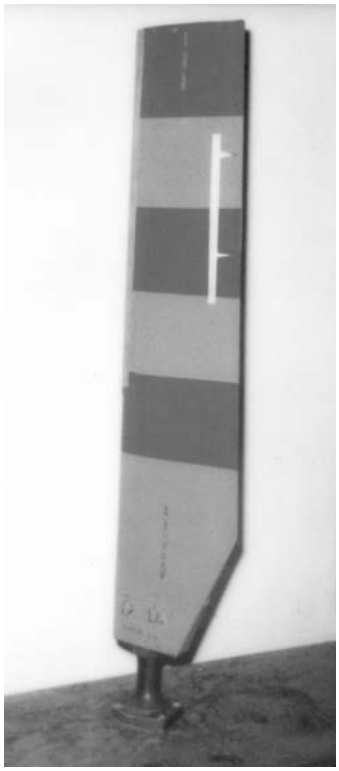

Fig. CH39.1 Tail rotor blade in the as-received condition

Visual Examination of General Physical Features

The crack was along the joggling at the trailing edge. It was about 11 cm long, located about 14 cm from the blade tip. Figure CH39.1 shows the cracked blade, and Fig. CH39.2, a close-up view of the crack. There were no other visible damages to the blade and the vent holes were free from any blockages.

Testing Procedure and Results

Scanning Electron Fractography

The blade was cut near the cracked region. After cleaning, the fracture surface was examined in a SEM. The inside surface of the

Fig. CH39.2 Tail rotor blade with cracking at the joggled line (arrow)

skin near the center of the crack showed shallow pitting very close to and at the fracture (Fig. CH39.3). The section thickness had reduced considerably at these locations.

Away from this region, the fracture surface showed striations, indicating crack propagation by fatigue (Fig. CH39.4). To find the extent of corrosion, other regions along the joggled and bonded end were examined, and those regions did not have any pitting. In the region of cracking, the resin used to bond the two skins at the trailing edge had burned excessively compared with other regions. This excessive burnt region left a dark residue that could have been responsible for the pitting corrosion locally in a humid environment.

Conclusion

Cracking of the tail rotor blade skin in the helicopter was due to a fatigue crack initiated from a corrosion pit on the inside surface. The local corrosion is due to excess burning of the resin used to bond the aluminum sheet at the trailing edge.

Recommendation

Care should be taken to avoid burning of epoxy during curing.

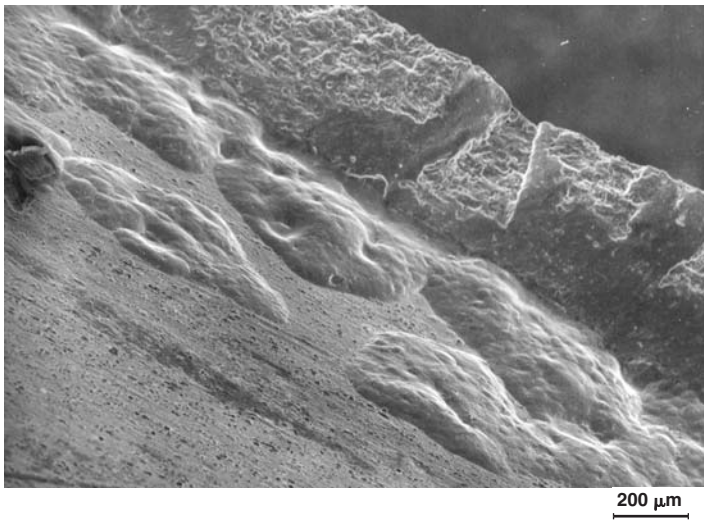

Fig. CH39.3 SEM of the inside surface of the skin at the cracked region showing localized pitting

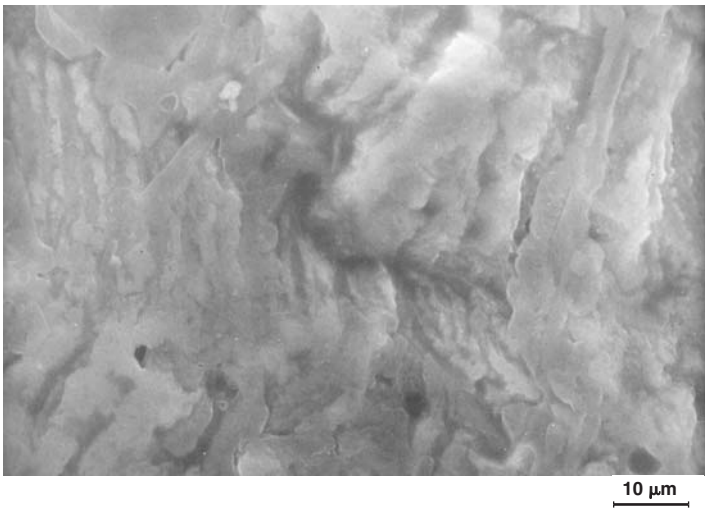

Fig. CH39.4 SEM fractograph showing fine fatigue striations

Failure Analysis of Engineering Structures: Methodology and Case Histories
V. Ramachandran, A.C. Raghuram, R.V. Krishnan, S.K. Bhaumik, p158-159
DOI:10.1361/faes2005p158

CASE 40

Failure of a Wing Control Cable in an Aircraft

Summary

A failed wing control cable of an aircraft was investigated. There was general degradation of the wire strands as evidenced by corrosion, pitting, small nicks, and rubbing. The wire rope had failed by tensile overload.

Background

The right wing control cable of an aircraft failed. The cable was made of seven strands of steel wire, each strand containing seven filaments.

Visual Examination of General Physical Features

All seven strands were found snapped. The separate wire strands are shown in Fig. CH40.1. Five of the strands had snapped in almost one location.

Testing Procedure and Results

Macro and Scanning Electron Fractography

After cleaning the wire rope ultrasonically, the strands and the filaments were observed in a stereobinocular microscope and a SEM. The fracture of individual filaments in any given strand was not in a single plane. In five of the strands, the fracture of all the individual filaments was of the cup-and-cone type with necking, indicating failure by tensile overload. In the other two strands, some of the individual filaments showed some variation in the mode of fracture. They were of the slant type. However, plastic deformation preceding fracture was observed in these filaments also. Under the SEM, the fracture surfaces of the filaments that had failed by cup-and-cone mode revealed dimples typical of tensile overload.

No sharp cut marks were seen on or near the fracture surfaces of the filaments or at any other location on the surface of the wire rope. General degradation of the strands was observed. These include corrosion and pitting, small nicks, and rubbing of the wires (Fig. CH40.2, CH40.3).

Conclusion

From the preceding observations, it was concluded that the failure of the wire rope was predominantly by tensile overload.

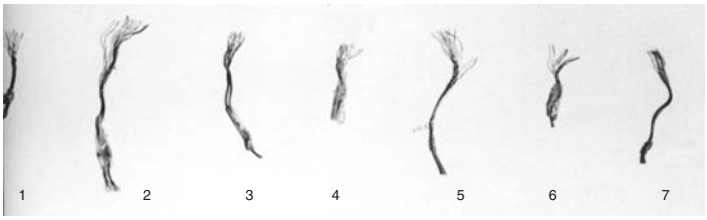

Fig. CH40.1 Strands of wires found snapped in a wing control cable

Fig. CH40.2 Corrosion observed on a failed strand from the general location of the fracture of the cable

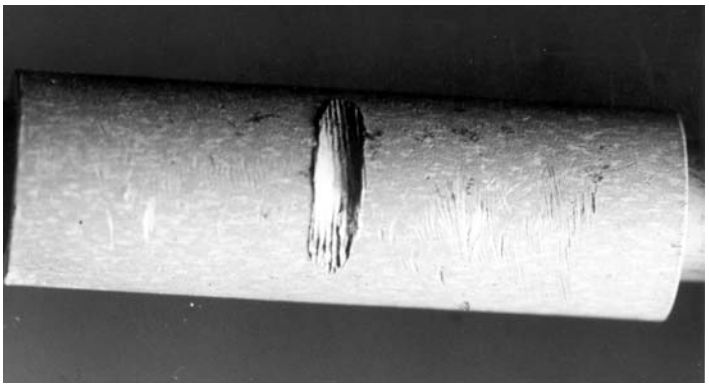

Fig. CH40.3 Wire rope impression imprinted on the spacer tube due to digging in of wire rope

Failure Analysis of Engineering Structures: Methodology and Case Histories
V. Ramachandran, A.C. Raghuram, R.V. Krishnan, S.K. Bhaumik, p160-161
DOI:10.1361/faes2005p160

CASE 41

Failure of the Nose Bullet in an Aircraft Engine

Summary

The nose bullet of an aircraft engine was found cracked. The bullet was of welded construction. The crack could be traced to a region of rework in the welded area.

Background

The nose bullet of an aircraft engine had developed a crack. The bullet was made of titanium alloy and was of welded construction.

Visual Examination of General Physical Features

Figure CH41.1 shows the cracked nose bullet. A close-up view of the crack is shown in Fig. CH41.2.

Testing Procedure and Results

Macroexamination

The cracked region was sectioned. Close examination of this region revealed an area of rework (rewelding) in the region of the original weld. The crack was found to originate in the reworked region and propagated on either side (Fig. CH41.3).

Discussion

Rework in a welded region without proper precaution can give rise to welding stresses or microstructurally transformed regions or stabilized, hardened casing, all of which can lead to cracking.

Conclusion

The crack in the nose bullet can be traced to a region of rework in the welded area.

Fig. CH41.1 The cracked nose bullet of the aircraft engine

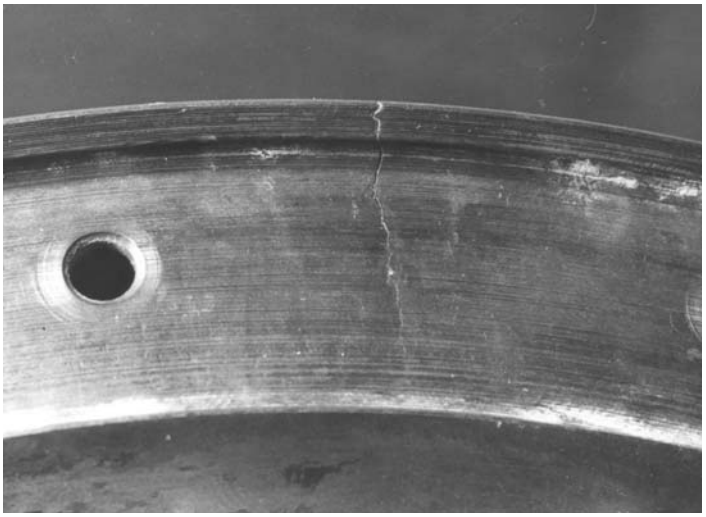

(a)

(b)

Fig. CH41.2 Close-up view of the crack (a) base and (b) conical surface

Fig. CH41.3 Rework in the welded region from where the crack had originated

Failure Analysis of Engineering Structures: Methodology and Case Histories
V. Ramachandran, A.C. Raghuram, R.V. Krishnan, S.K. Bhaumik, p162-164
DOI:10.1361/faes2005p162

CASE 42

Failure of Tail Boom Attachments in a Helicopter

Summary

A helicopter crashed. From the wreckage, certain components of the tail boom attachment were found fractured. Fractographic examination was carried out on these. They had failed by bending/overload.

Background

Following a helicopter crash, certain components from the tail boom attachment that were found fractured were recovered (Fig. CH42.1). Also, the snapped tail rotor pitch control cable shown in Fig. CH42.2 was recovered.

Visual Examination of General Physical Features

On both the left- and right-hand sides, there were clusters of tubular structures, welded to a 6 mm thick gusset plate on each side, with a hole for attaching the tail boom yoke. On both sides, the fracture had occurred on the gusset plate near the tail boom yoke attachment and close to the weldments (Fig. CH42.3, CH42.4). The bolts were intact with the split pin locking. The portion of the gusset plate in the yoke on the left side was tightly held in the original position, whereas the portion of the gusset plate on the right side had rotated clockwise looking from the top.

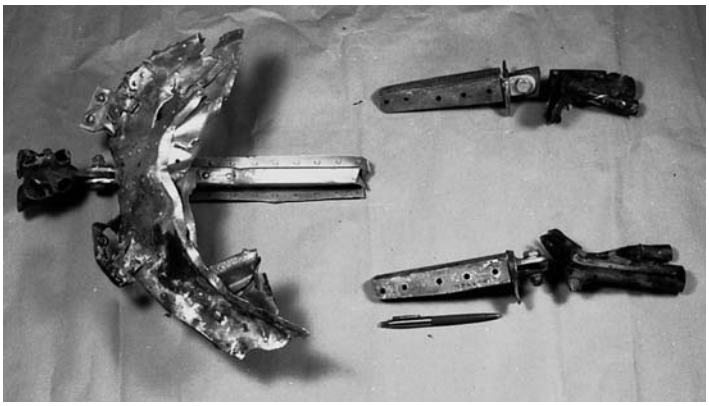

Fig. CH42.1 Failed components from the tail boom

Further examination of the fractured gusset plates in relation to the tube cluster indicated that the fracture had occurred due to a downward bending force. The bending feature was grossly visible when the two matching parts were joined together.

The snapped tail rotor pitch control cable is shown in Fig. CH42.5 The strands showed necking, indicating ductile fracture.

Testing Procedure and Results

Scanning Electron Fractography

The fracture surfaces of the gusset plates and the hat section near the yoke were examined in a SEM. The fractographs are shown in Fig. CH42.6 to CH42.8. The fracture surface on the left-side gusset plate indicated cleavage (Fig. CH42.6), while on the

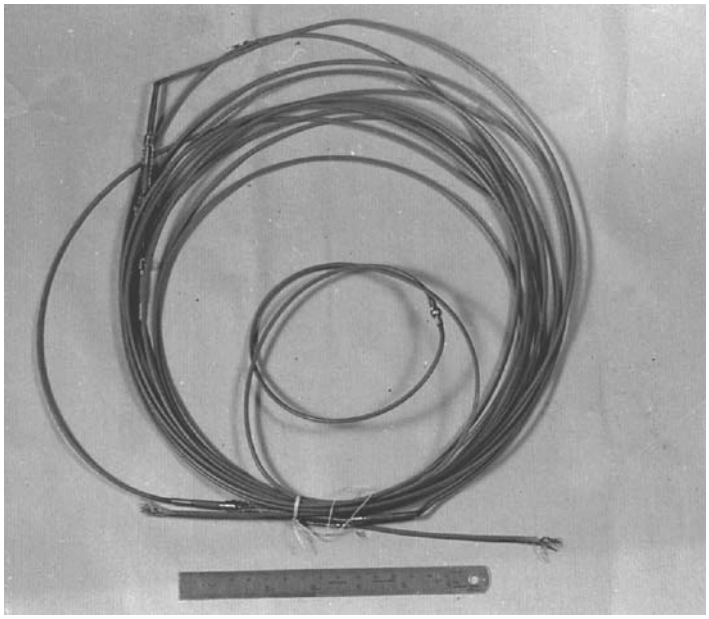

Fig. CH42.2 Snapped tail rotor pitch control cables

right side, dimpled rupture was observed (Fig. CH42.7). This also corresponded to a lower hardness and better ductility compared with the left side. The fracture surface of the hat section near the lower yoke indicated only ductile shear (Fig. CH42.8). There were no indications of delayed failure in any of the areas examined.

The fracture of the strands of the control cable indicated equiaxed dimples typical of tensile overload (Fig. CH42.9).

Discussion

Fractographic examination of the gusset plates indicated the failure was due to downward bending/overload in tension of the tail boom. The fact that the gusset plate on the left side was in the original position and the one on the right side had rotated indicated that the left-side plate must have failed first and, subsequently, the right-side plate failed after a slight rotation, at which point the bottom plate became twisted before final fracture of the longeron, thus separating the tail boom.

Conclusion

The gusset plates failed due to bending/overload in tension. The cable also snapped due to tensile overload.

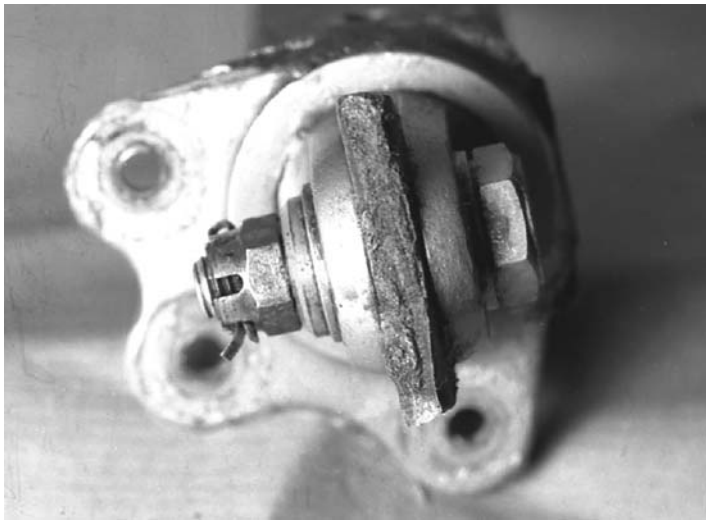

Fig. CH42.3 Fracture surface of the gusset plate, right-hand side

Fig. CH42.4 Fracture surface of the gusset plate, left-hand side

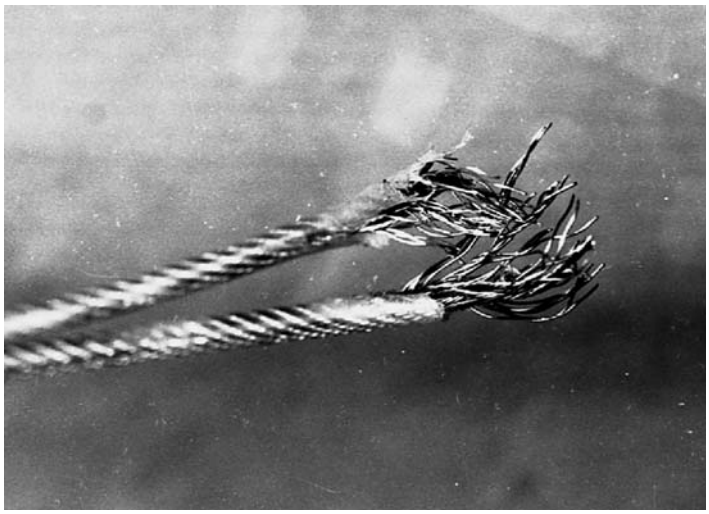

Fig. CH42.5 Broken strands of the tail rotor pitch control cable

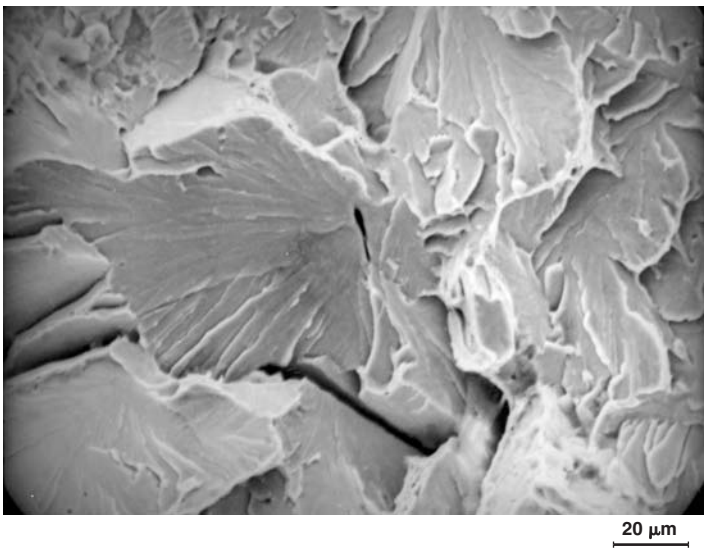

Fig. CH42.6 SEM fractograph of the failed gusset plate, left-hand side

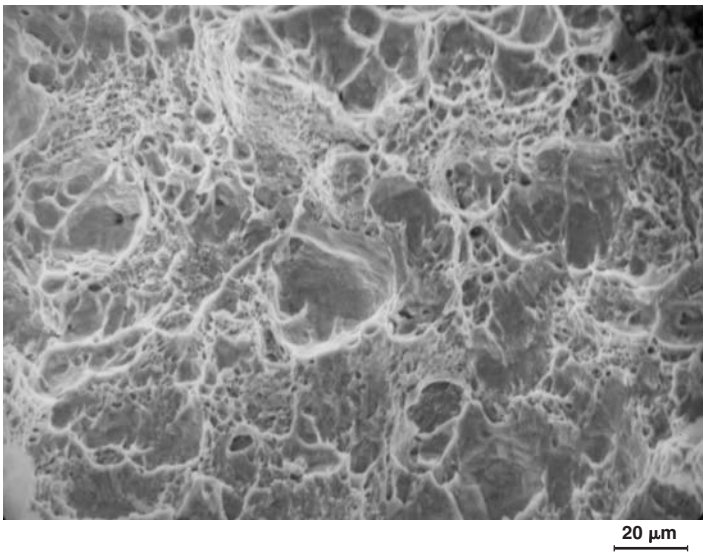

Fig. CH42.7 SEM fractograph of the failed gusset plate, right-hand side

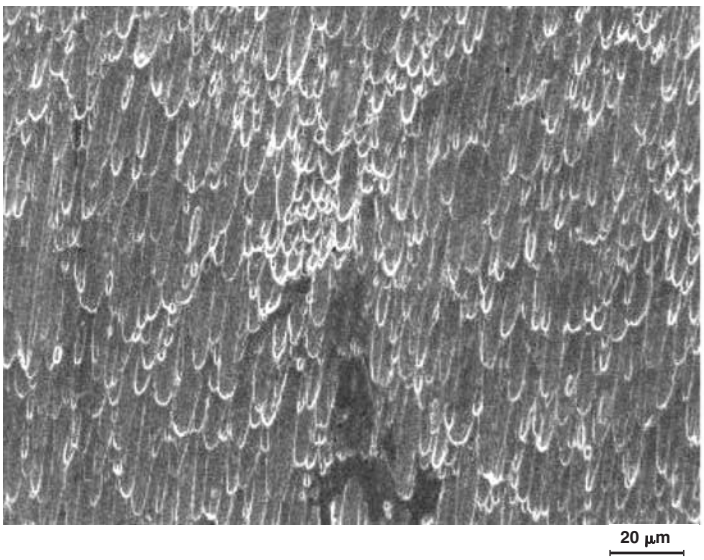

Fig. CH42.8 SEM fractograph of the hat section

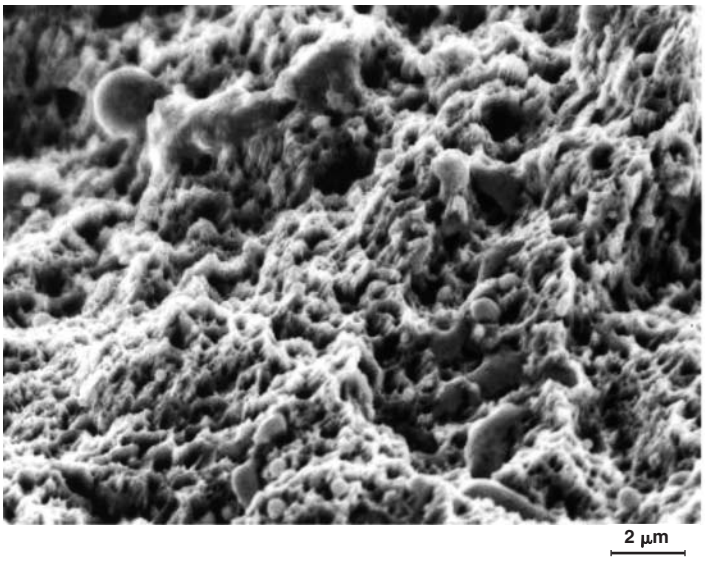

Fig. CH42.9 SEM fractograph of a broken strand

Failure Analysis of Engineering Structures: Methodology and Case Histories
V. Ramachandran, A.C. Raghuram, R.V. Krishnan, S.K. Bhaumik, p165-167
DOI:10.1361/faes2005p165

CASE 43

Cracking of Filter Components in an Aircraft

Summary

A high-pressure (HP) filter head and a low-pressure (LP) filter bowl, forming parts of the filter for an aircraft, cracked during pressure impulse testing. These parts were made of an aluminum alloy, solutionized and aged. The cracking in both of them was due to fatigue. In both cases, the crack initiated at the transition regions on the inner surface due to insufficient fillet radius and had progressed circumferentially outward.

Background

For a developmental aircraft, during impulse pressure testing, cracks developed in the LP filter bowl and the HP filter head.

Visual Examination of General Physical Features

Figure CH43.1 shows these parts. The bowl had a crack in the transition region at the head (Fig. CH43.2) and also radial cracks at the top, originating from the corners of the hexagon (Fig. CH43.3). The HP filter head had a circumferential crack about 45 mm in length, close to the outlet and in the region of transition. These components were made of the Al-Cu-Zn alloy, solutionized and aged.

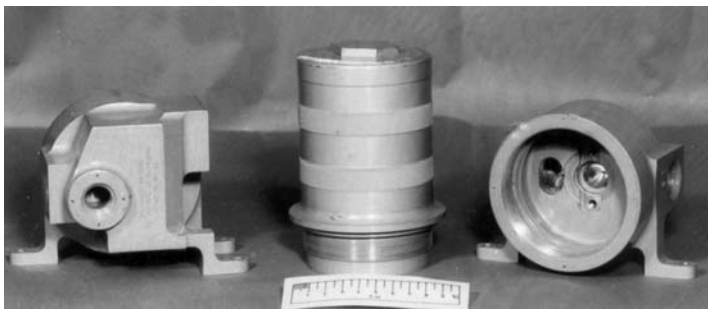

Fig. CH43.1 Low- and high-pressure filter heads and low-pressure bowl

Testing Procedure and Results

Macro and Scanning Electron Fractography

In the LP filter bowl, the circumferential crack was opened up for further examination. The crack surface showed a flat region extending to nearly half the section thickness and a slant region over the rest of the cross section (Fig. CH43.4). These features indicated progressive failure. Under the SEM, the flat region showed well-defined, uniformly spaced fatigue striations (Fig. CH43.5). The slant region showed dimple rupture (Fig. CH43.6).

The circumferential crack in the HP filter head was a through crack that was opened for further examination. The fracture surface showed a flat region extending to over 90% of the section thickness, emanating from the inner surface and a slant shear lip region over the rest of the cross section (Fig. CH43.7). Under the SEM, well-defined, uniformly spaced fatigue striations were seen in the flat region (Fig. CH43.8).

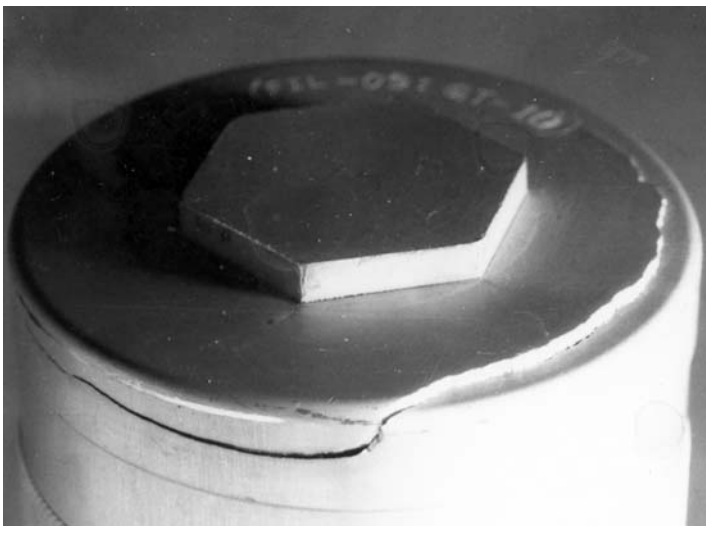

Fig. CH43.2 Cracking in the low-pressure bowl in the region of transition at the head

Metallography

A piece from the HP filter head close to the cracked region was prepared for metallography and examined after etching with Keller's reagent. The microstructure was typical of a wrought, heat treated aluminum alloy. No abnormality was seen in the microstructure.

Hardness

The hardness of the material was 145 to 150 HV.

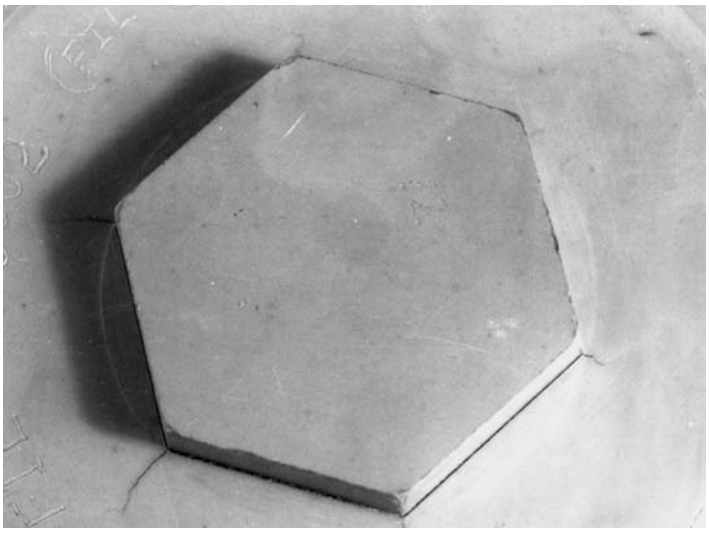

Fig. CH43.3 Radial cracks emanating from the sharp corners of the hexagon

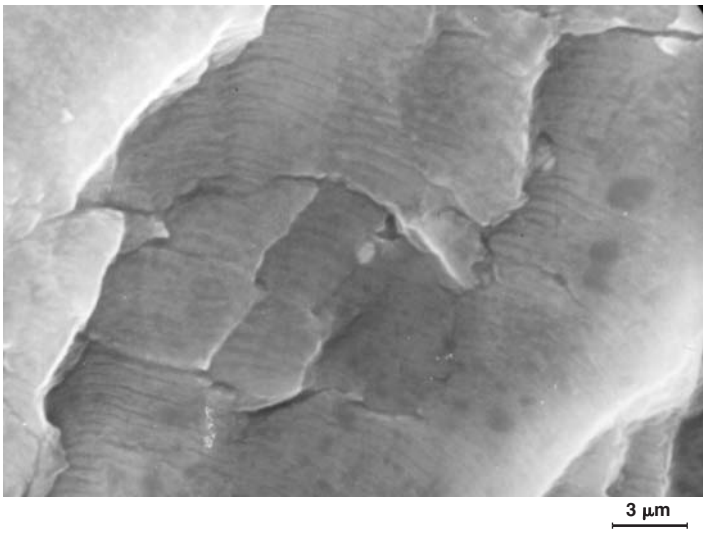

Fig. CH43.5 Well-defined, uniformly spaced striations in the slow crack growth region, typical of fatigue

Composition

Semiquantitative analysis in SEM showed that the material of the filter head was an Al-Cu-Zn alloy.

Dye-Penetrant Inspection

Fluorescent dye-penetrant inspection was carried out on the LP filter head, focusing attention on the inner surface of the transition zone. No crack was detected.

Discussion

The presence of well-defined striations on the fracture surfaces of the LP filter bowl and the HP filter head confirm fatigue as the

Fig. CH43.4 SEM fractograph showing the slow crack growth (flat) and overload (slant) regions

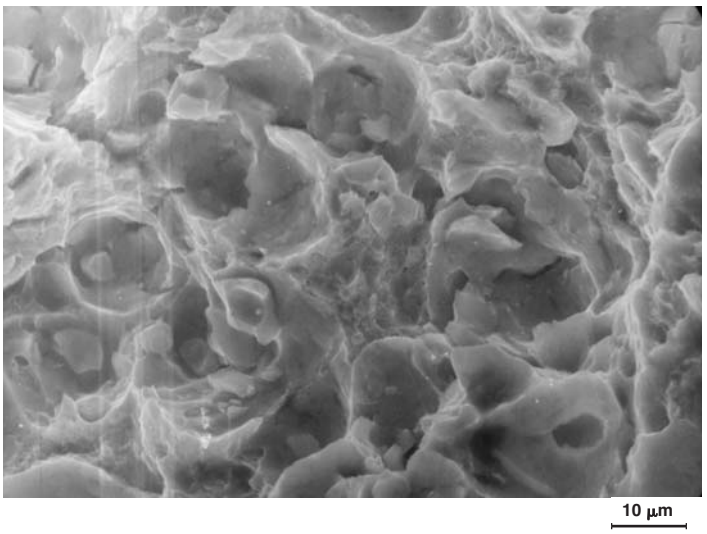

Fig. CH43.6 Dimple rupture in the overload (slant) region

cause of cracking of these components. The region of crack initiation did not show any metallurgical flaw. Microstructure and hardness measurements ruled out processing parameters as the cause for fatigue crack initiation and propagation. Therefore, the fatigue cracking was stress related. The fillet at the transition regions in both the components was sharp and did not conform to specifications. The sharp fillet acts as a stress raiser and lowers the threshold value of the stress-intensity factor for crack initiation.

Conclusion

The cracking of the LP filter bowl and the HP filter head was due to fatigue. The fatigue crack in both cases initiated at transition regions on the inner surface and progressed circumferentially outward. The fatigue crack can be traced to insufficient fillet radius at the transition zone.

Recommendation

The design specification regarding rounding off of corners and edges should be adhered to.

Calibration of the pressurizing system may also be checked for any possibility of overpressurizing.

Fig. CH43.7 Circumferential crack close to the bullet end in the high-pressure filter head

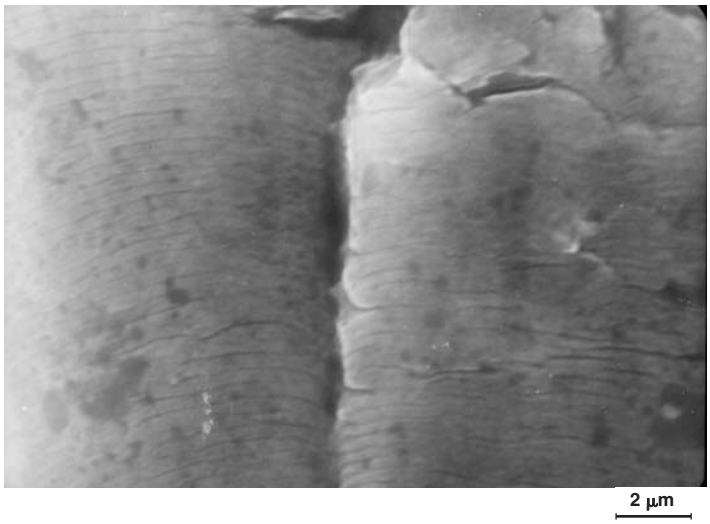

Fig. CH43.8 Fatigue striations in the slow crack growth (flat) region

Failure Analysis of Engineering Structures: Methodology and Case Histories
V. Ramachandran, A.C. Raghuram, R.V. Krishnan, S.K. Bhaumik, p168-171
DOI:10.1361/faes2005p168

CASE 44

Failure of an LP Turbine Disc in an Aircraft Engine

Summary

During cyclic spin tests on an LP turbine disc of an aircraft engine, several components of the turbine disc and fixtures fractured with a loud noise, followed by a fire. The LPT blade locking plate became dislodged due to the shearing of the screws holding it. The dislodgement could be attributed to nonadherence to design drawings and aggravation by the lower strength of the screws.

Background

In an aircraft engine under development, during cyclic spin tests on an LP turbine disc, a loud noise was heard when the turbine speed had reached around 12,000 rpm. This noise was followed by a fire. The drive motor was shut immediately and the fire extinguished. On strip examination of the engine, several components of the turbine disc and fixtures had fractured or damaged. The following damaged components were received for investigation: disc spinning drive shaft with seal carrier and splined coupling (1 No.), dummy blade roots of LPT disc (72 Nos.), LPT blade retaining plates (23 Nos.), LPT blade locking plate (1 No.), T-headed bolts (43 Nos.), Bihexagonal nuts (38 Nos.), damaged fir tree portions (38 Nos.), and LP turbine disc (1 No.).

All the parts were solvent cleaned and examined visually and under the microscope.

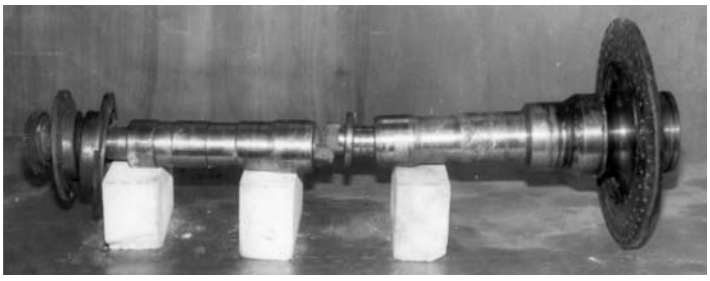

Fig. CH44.1 Fractured drive shaft with damaged seal carrier and coupling

Visual Examination of General Physical Features

Disc Spinning Drive Shaft

Figure CH44.1 shows the fractured drive shaft with the damaged seal carrier and spline coupling. The fracture surface is shown in Fig. CH44.2. The shaft fractured at about its midspan with slight bending close to the region of fracture (Fig. CH44.3). There was no evidence of delayed failure. The fracture surfaces were well preserved and showed no rubbing, indicating there was no relative motion between the mating fracture surfaces after failure. The teeth on the splined coupling were flattened and chipped and the splined teeth showed distortion. The seal carrier showed deformation. The damages to the seal carrier and splined coupling were secondary in nature.

LPT Blade Retaining Plates

The damaged retaining plates are shown in Fig. CH44.4. All the plates were found twisted, mangled and torn, and were covered with soot. The damages were secondary.

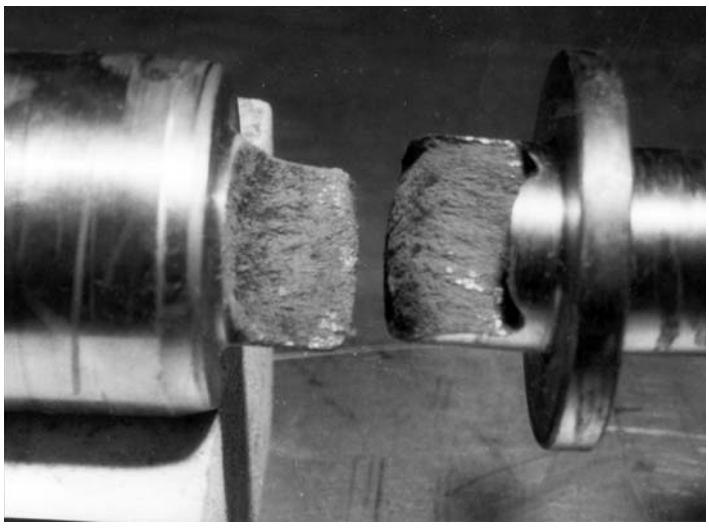

Fig. CH44.2 Close-up view of the fracture surface. The fracture features are typical of tensile/bending overloads.

LPT Locking Plate

Figure CH44.5 shows the damaged locking plate. This plate was also mangled and torn and the damage was secondary.

T-Headed Bolts, Bihexagonal Nuts, and Fir Tree Portions

Figure CH44.6 shows these parts. The fracture surfaces in some of the T-headed bolts are shown in Fig. CH44.7.

In the T-headed bolts, fractures had generally taken place at the first thread root below the bolt head. As the fracture surfaces show fire exposure with thick deposit of soot, no fractographic features were discernible. However, gross features indicate failure due to shear loads. The damages to the bihexagonal nuts were also similar. The fir tree portions disintegrated into pieces.

LP Turbine Disc

The damaged turbine disc is shown in Fig. CH44.8. All the dummy blades were found dislodged from the dovetail mountings and subjected to further damage. Some of the dovetail mounting regions were also found sheared. The region that had suffered minimum damage was the locking plate region. The two mounting studs were found pulled outward and sheared (Fig. CH44.9), along with the locking plate. The region showed no other damage.

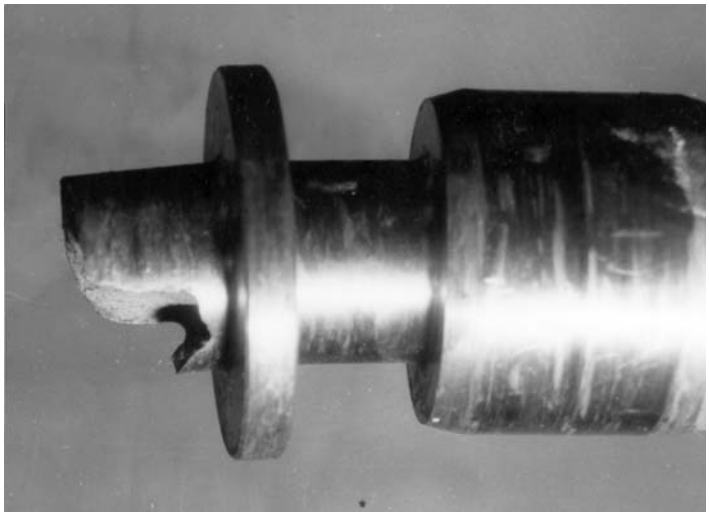

Fig. CH44.3 Location of fracture. Note the slight bending on the shaft close to the region of fracture.

Fig. CH44.5 Damaged locking plate. The damages are secondary in nature

Testing Procedure and Results

The two broken studs were extracted using spark erosion machining and studied.

Fig. CH44.4 Damaged retaining plates

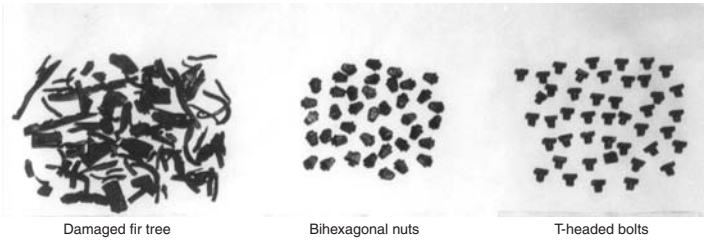

Fig. CH44.6 The damaged T-head bolts. Bihexagonal nuts and fir tree portions are also shown.

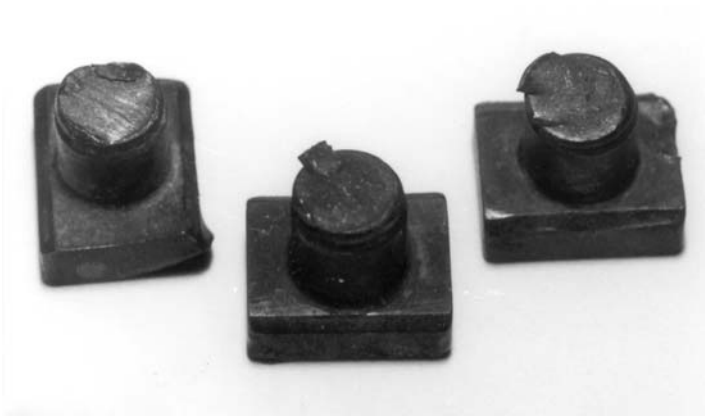

Fig. CH44.7 Fracture surfaces of some of the T-headed bolts. Gross features of fracture indicate shear loads.

Scanning Electron Fractography and EDAX

Under the SEM, elongated dimples were seen on the fracture surfaces of the studs (Fig. CH44.10), indicating fracture by shear loads. Energy-dispersive x-ray analysis of the stud material showed that it was made of Nimonic 718 alloy.

Hardness

Hardness of the damaged stud and damaged blade locking plate were measured and compared with those measured on an unused stud and unused locking plate of the same material:

	Hardness, HV (500 gms load)	
Part	**Unused**	**Damaged**
Stud	460	325
Blade locking plate	455	375

Discussion

These observations indicated the center of attention was the LPT blade locking plate region because fractures and damages in all other components appeared to be secondary. It is probable that the first event was the dislodgement of the LPT blade locking plate from its position because of the shearing of the screws holding it, under the centrifugal force of rotation. Once the locking plate is not in its position, it is possible for the adjacent dummy blades to slide out of the fir tree mounting and cause further damages, including jamming of the rotating mechanism, leading to the fracture of the shaft.

An insight into the probable reason for the failure of the locking plate can be obtained by considering the locking plate design and also the strength of the screw used to hold it in position. The locking plate in the present case is of uniform thickness of 1.8 mm, whereas the design specifies a thickness of 3 mm over a width of 19.8 mm and 1.8 mm over the rest of the width. The design also specifies countersinking on one side only while the actual plate was countersunk on both sides. The total length of the locking screw should be 10.5 mm. The length of the hole drilled in the disc to accommodate the screws is 6.6 mm. With this design, with a locking plate of 3 mm thickness and a tab washer of 0.914 mm thickness, it can be seen that the stud can be screwed in completely to hold the locking plate in position. However, when the locking plate is only 1.8 mm thick, as is the case presently, a gap of 1.2 mm is left. Because the screw is tightened completely, this gap is perhaps made up by grinding the bottom of the screw to this extent. The extracted screw (stud) did show grinding marks at its base. This means that the plate was held effectively, by a smaller length of screw. The locking plate of 1.8 mm thickness and countersunk on both sides had a bearing on the screws to a thickness only of 0.8 mm, which is also the pitch of the threads.

In addition, the hardness of the screw used is considerably less than that of a new screw, implying lower strength. Because the fire was supposed to be for a short time, and because the screw em-

Fig. CH44.8 Damaged low-pressure turbine disc. Arrow indicates the locking plates region that suffered practically no damage.

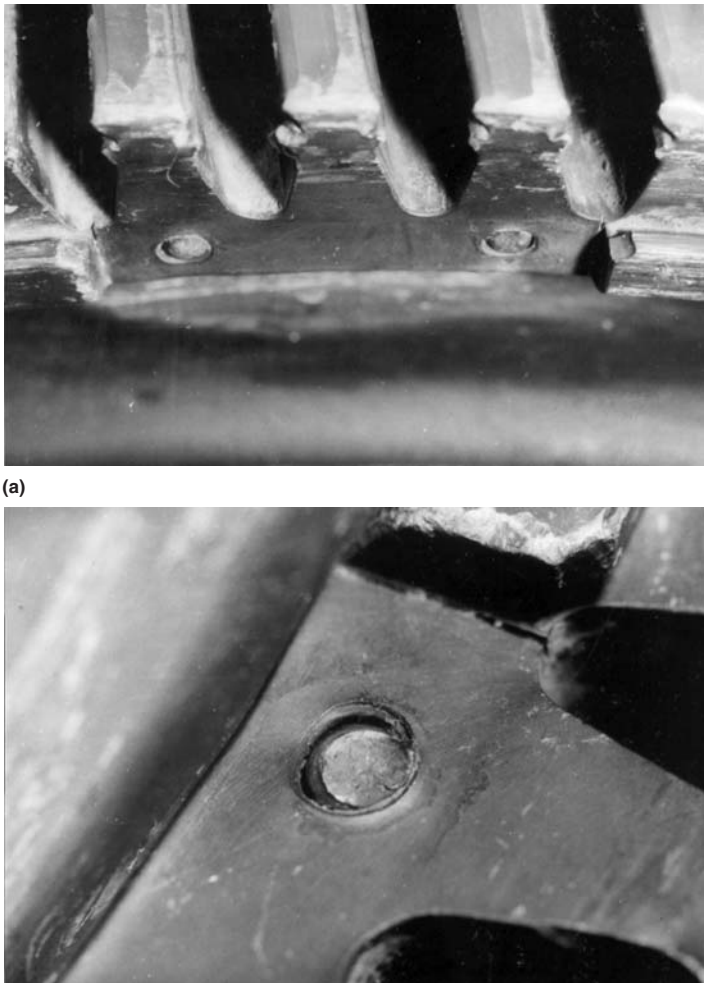

(a)

(b)

Fig. CH44.9 (a) Two sheared mounting studs. (b) Close-up view of one of the sheared studs. Note the direction of pulling of the studs.

bedded inside the disc would not have come into direct contact with the fire, the reduction in hardness of the screw is unlikely to have been caused by the fire, which was post failure.

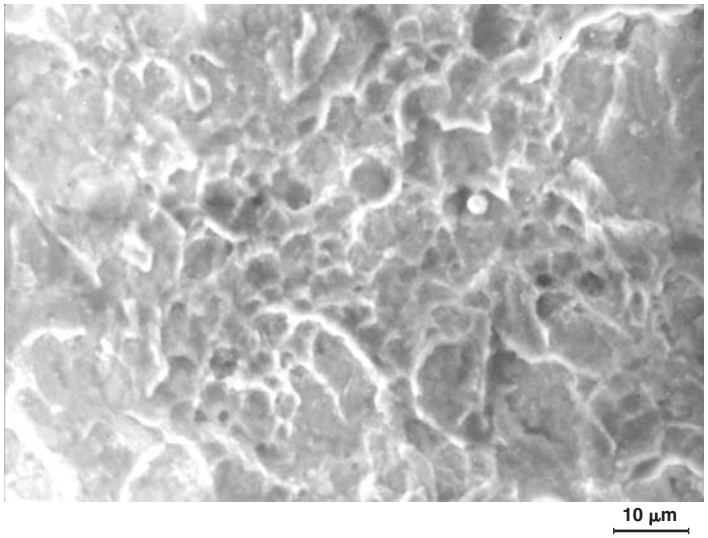

Fig. CH44.10 SEM fractograph of the stud. Elongated dimples indicate failure due to shear loads.

Conclusion

It is probable that the LPT blade locking plate would have come out due to the shearing of the screws holding it in the outward direction. The dislodgement of the locking plate would have led to further damages observed. The dislodgement of the locking plate can be attributed to factors related to nonadherence to design drawings. The problem was perhaps aggravated by the lower strength of the screw.

Recommendations

Use of an LPT blade locking plate of uniform thickness has to be reviewed in the light of the design specification, which recommends a locking plate of variable thickness. Confirm that the locking screws (studs) and the locking plates have been heat treated to the required specifications.

Failure Analysis of Engineering Structures: Methodology and Case Histories
V. Ramachandran, A.C. Raghuram, R.V. Krishnan, S.K. Bhaumik, p172
DOI:10.1361/faes2005p172

CASE 45

Failure of a Cooling Fin in an Aircraft Engine

Summary

The cylinder cooling fin of a piston engine was found broken off from the engine cylinder during routine inspection. The fin was made of an aluminum-silicon alloy. Investigations revealed that the fin had failed in a brittle manner by overload.

Background

During routine inspection of a piston engine prior to a run, a portion of the cylinder cooling fin was found broken off from the cylinder.

Testing Procedure and Results

The piece was cleaned ultrasonically and observed in a stereobinocular microscope and a SEM. The fracture surface was typically of the brittle, overload type, with very little plastic deformation. A SEM fractograph showed features resembling cleavage, with indications of isolated dimples, but the overall fracture feature was brittle (Fig. CH45.1). An EDAX in the SEM indicated that the piston was made of an aluminum-silicon alloy.

Conclusion

The engine cooling fin has undergone overload fracture, with very little ductility.

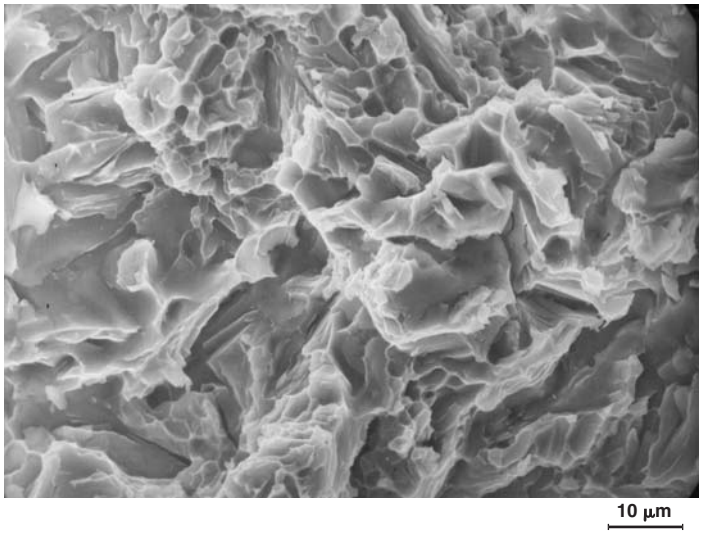

Fig. CH45.1 SEM fractograph of the fin showing cleavage-like features

Failure Analysis of Engineering Structures: Methodology and Case Histories
V. Ramachandran, A.C. Raghuram, R.V. Krishnan, S.K. Bhaumik, p173-174
DOI:10.1361/faes2005p173

CASE 46

Failure of a Fourth-Stage Compressor Disc in an Aircraft Engine

Summary

A fourth-stage disc in the LP compressor of an aircraft engine was found cracked. There were actually two cracks, one originating from the front side and the other from the rear side, propagating through the thickness. Fluctuating loads of high magnitude acted on both sides of the diaphragm, causing the two fatigue cracks.

Background

A titanium alloy disc fitted on the fourth stage of the compressor of an aircraft engine was found cracked when the engine was received for defect investigation. The disc had flown 212 hours out of an overhaul life of 550 hours.

Visual Examination of General Physical Features

The disc was found cracked close to the rim run-out radius, the crack penetrating through the thickness (Fig. CH46.1). The total length of the cracked region was about 110 mm and, viewed on the diaphragm surface, the crack appeared to branch (Fig. CH46.2).

Testing Procedure and Results

The crack was opened by pulling apart the cracked region, and the fracture surface was ultrasonically cleaned and examined. What appeared to be a branching crack turned out to be two different cracks, both showing features of delayed failure (Fig. CH46.3). Both showed regions of slow crack growth with beach marks covering nearly 90% of the thickness of the disc. One crack, about 30 mm in length, had originated on the front side of the disc. The other crack, about 80 mm, had originated on the rear side. Dye-penetrant inspection did not reveal any other crack. Besides the machining and dressing marks, no abnormalities were found at the origin.

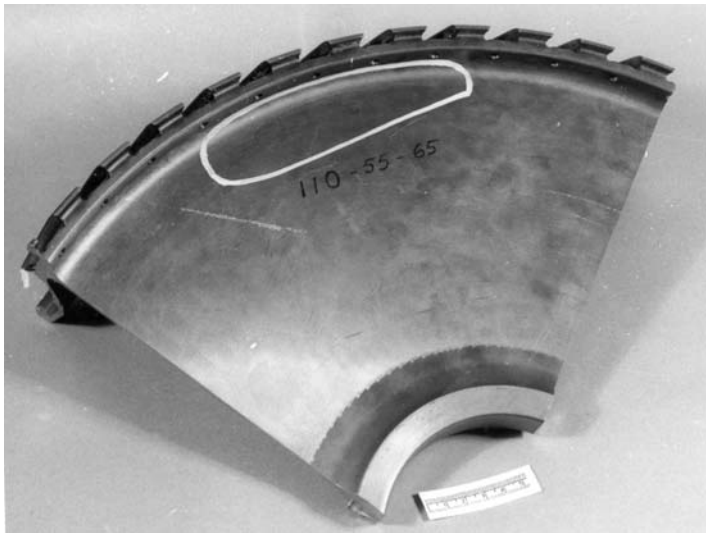

Fig. CH46.1 Disc segment containing the crack

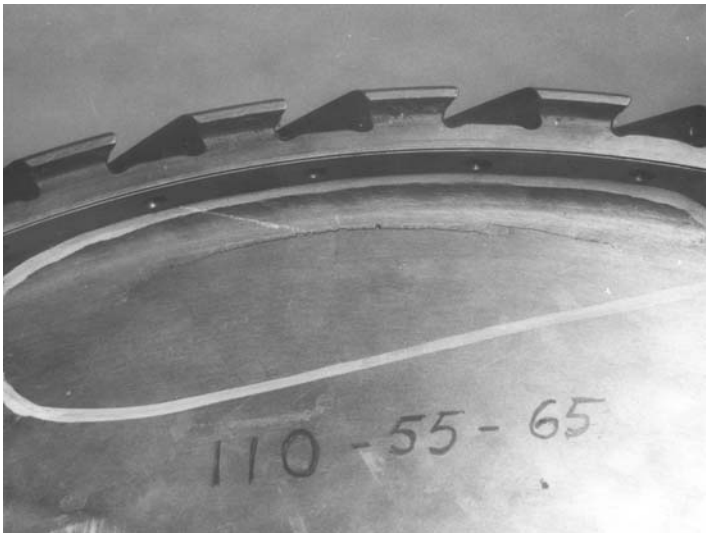

Fig. CH46.2 Close-up view of the cracked region

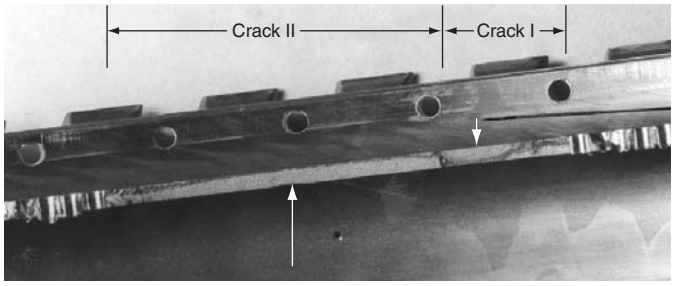

Fig. CH46.3 Fracture surface opened up for investigation, showing two fatigue cracks initiating on opposite sides of the disc diaphragm

Discussion

These observations point to the presence of two fatigue cracks originating from the opposite faces of the disc at the rim run-out radius and propagating through the thickness. The initiation of fatigue cracks on both sides point to the presence of fluctuating loads of high magnitude on both sides. It is necessary to investigate the source of the fluctuating load on the disc diaphragm.

Conclusion

The compressor disc had cracked at the rim run-out radius by fatigue, the cracks originating from the front and aft sides of the diaphragm and propagating through the thickness.

Failure Analysis of Engineering Structures: Methodology and Case Histories
V. Ramachandran, A.C. Raghuram, R.V. Krishnan, S.K. Bhaumik, p175-176
DOI:10.1361/faes2005p175

CASE 47

Failure of Plungers in Hydraulic Pumps

Summary

Failure of hydraulic pumps fitted in an aircraft was reported from some of the operating units. On disassembly, the plungers in the cylinders were found seized. The damage is attributed to cavitation erosive wear, with corrosion adding to the problem.

Background

Hydraulic pumps in one type of aircraft failed during service. The damage was severe and hydraulic testing was not possible. The pumps were disassembled and a set of seven plungers and cylinders was examined, after cleaning.

Visual Examination of General Physical Features

The plunger body showed surface damage. The extent and location of this damage varied from plunger to plunger. In some locations, galling, pitting, and scoring were also seen. Similar damages were seen also in the cylinders. No blueing was seen either on the plunger body or in the cylinders.

Testing Procedure and Results

Scanning Electron Microscopy and EDAX

A SEM examination of the damaged locations of the plunger showed cracking and corrosive attack (Fig. CH47.1). Spherical, loose particles were seen in some of the cavities in this region (Fig. CH47.2). In situ analysis of the particles by EDAX showed that they were of the same material as that of the plunger body, namely, Fe-Cr-Ni alloy. Electron-dispersive x-ray analysis of the corroded regions showed the presence of chlorine, calcium, and potassium.

Pitting was seen at the fork ends of three plungers. The fractures at the fork end were due to compressive/bending loads.

Dimensional measurements indicate discrepancies in the ovality between the failed and unfailed plungers. Ovality in the failed plunger was 5 μm, and in the unfailed plunger, 2 μm.

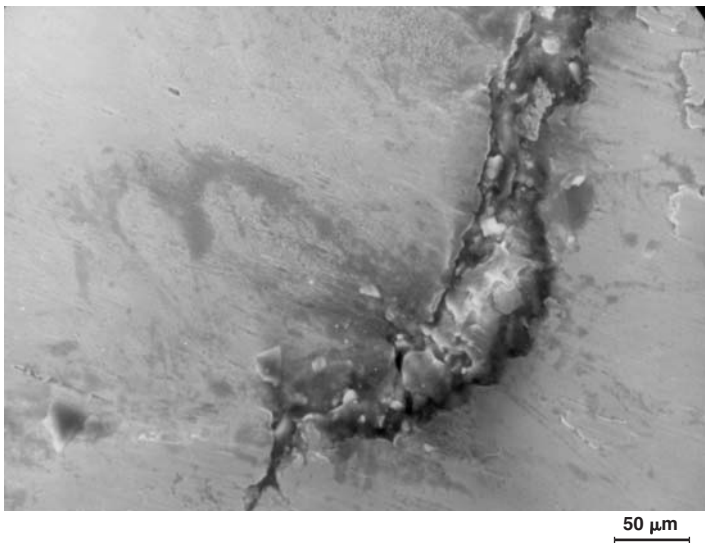

Fig. CH47.1 Cracking and corrosive damage seen on the body of the plunger

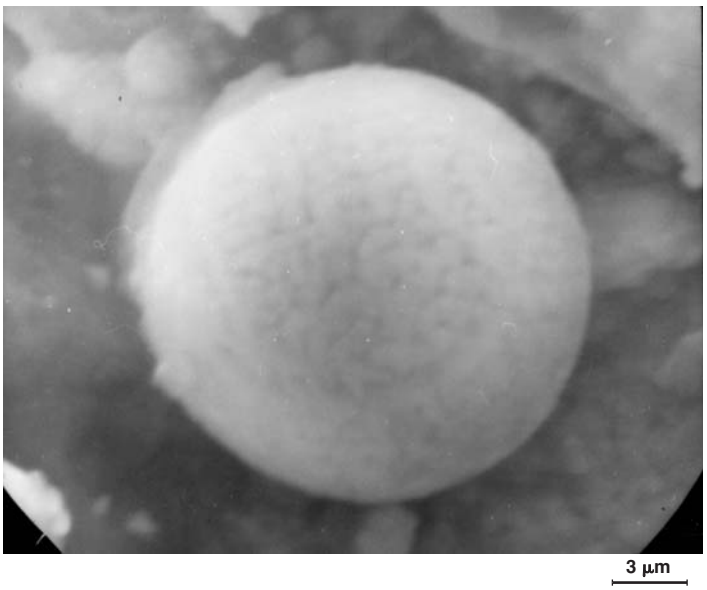

Fig. CH47.2 Loose spherical particles seen in the damaged region. Particles are of the same composition as the plunger material.

Discussion

There was no indication of overheating. This eliminates the possibility of the pump's having run dry. The damage observed on the plunger body is typical of cavitation erosive wear, with corrosion adding to the problem. There is also evidence of metal being dislodged and worked into the piece. The fork end fractures were secondary in nature and might have resulted due to the seizure of plungers.

Conclusion

The damage to the plungers was due to cavitation erosion. Failure of the pump was due to seizure of plungers.

Failure Analysis of Engineering Structures: Methodology and Case Histories
V. Ramachandran, A.C. Raghuram, R.V. Krishnan, S.K. Bhaumik, p177-179
DOI:10.1361/faes2005p177

CASE 48

Failure of a Gear in an Aircraft Engine

Summary

In an aircraft engine, the gear system failed after 40 hours of run. The driven gear had fractured, and a portion of it had fallen off. The remaining teeth of this gear, the teeth of the driving bevel gear, and the pinion of the shaft had been damaged. The primary cause for the fracture of the driven gear was a fatigue crack at the corner of the inner rim where a stringer of MnS inclusion was present.

Background

A driven gear in the gear box of an aircraft engine fractured after a total of 40 hours of test run. The driving gear and the shaft also had been damaged. The gear was made of S-157 steel and plasma nitrided.

Visual Examination of General Physical Features

The failed parts are shown in Fig. CH48.1. The fracture in the driven gear occurred over a segment of about 6 cm, and all the teeth in this segment were intact, indicating the piece had fallen away after fracture (Fig. CH48.2). The rest of the teeth on this gear, the teeth on the driving gear, and the pinion on the shaft had suffered extensive damage. These damages appeared secondary and were generally in the form of chewing and flattening of the teeth.

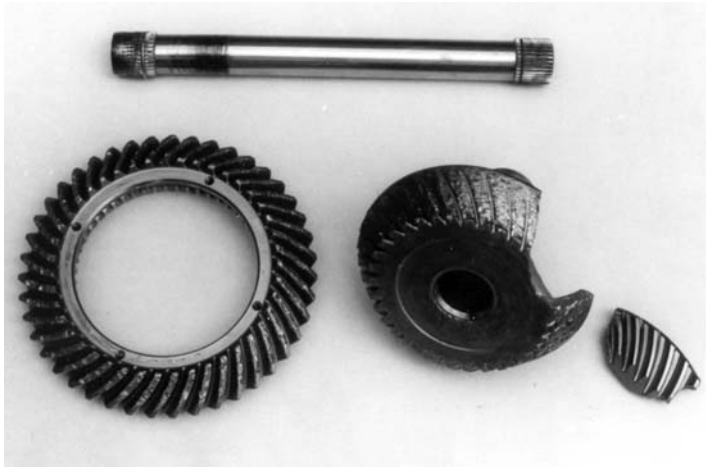

Fig. CH48.1 Damaged driving gear, damaged shaft, and fractured driven gear

Testing Procedure and Results

Fractography and EDAX

The fractured gear was ultrasonically cleaned and examined in a stereobinocular microscope. A series of concentric, half-moon-shaped rings were seen emanating from the inner corner of the rim and progressing through the section before giving rise to the final fracture and separation. These beach marks were typical of fatigue crack growth. The initiation site of the fatigue crack was badly damaged (Fig. CH48.3), precluding further observation of the initiation site. However, this region on the mating surface in the gear was intact (Fig. CH48.4), and no mechanical damage, such as nicks or dents, was seen at the crack origin.

The fracture surface was observed in a SEM. A stringer-like defect was seen in the region of fatigue origin (Fig. CH48.5).

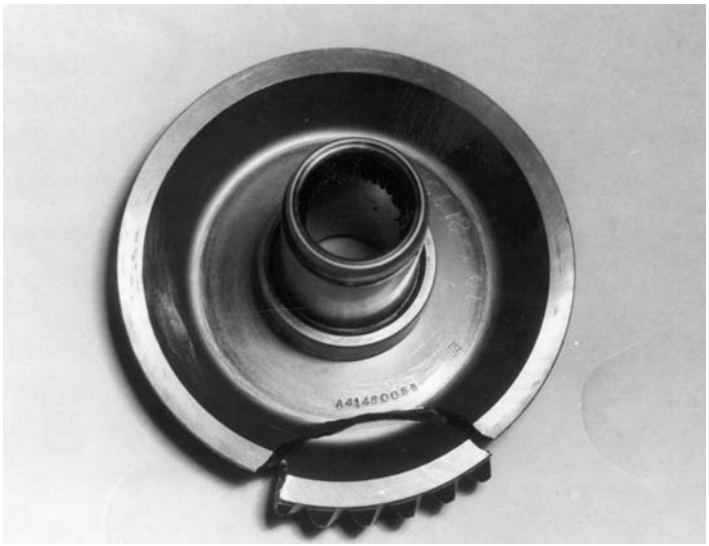

Fig. CH48.2 Failed driven gear showing the area of fracture

Semiquantitative analysis by EDAX on the defect showed the presence of manganese and sulfur, indicating a MnS inclusion (Fig. CH48.6). A few more inclusions of this type were also seen close to the origin of fracture. In the crack propagation zone, fatigue striations were not well defined.

Metallography

A sample sectioned from the fractured gear, parallel to the plane of fracture, was metallographically prepared and examined. Elongated inclusions, dove gray in color, typical of MnS, and a few globular oxide-type inclusions were found distributed in the material. The size of the MnS inclusions varied up to 35 μm in length. When etched with nital, it was found that the gear was case hardened on the inner surface of the rim also, where the fatigue crack had originated. The total case depth in this region was about 0.8 mm. The microstructure at the case and at the core showed no abnormality.

Hardness

Microhardness survey across the section showed a hardness equivalent of 59 to 62 HRC in the case and 36 to 37 HRC in the core.

Discussion

Fractographic features clearly indicated fatigue crack as the cause of fracture of the gear. The fatigue crack had initiated at the inner corner of the rim where an elongated MnS inclusion was present at the critical location near the surface. Elongated MnS inclusions act as stress raisers and are potential sites for crack initiation. The presence of a hardened case in this region would magnify the notch effects of the inclusion. Considering the mechanism of operation of the gear, it can be seen that the inner surface of the rim experiences tensile hoop stresses at each point as the gear teeth mesh. Because this stress continuously shifts along the circumference, any point can act as a potential site for crack initiation. The presence of an inclusion can render that region vulnerable for crack initiation.

Conclusion

The gear fractured by a fatigue crack initiating at the corner of the inner rim and propagating to critical dimension before giving rise to final fracture. A stringer-like MnS inclusion was seen in the region of fatigue crack origin.

Recommendations

Use a cleaner material. Avoid case hardening the entire exposed surface of the gear blank and verify whether specification provides for case hardening in the rim surface.

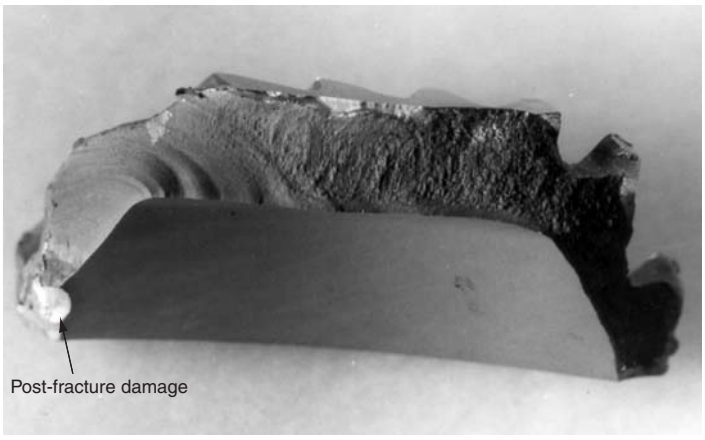

Fig. CH48.3 Fractured segment. Note the secondary (post-fracture) damage at the fracture origin.

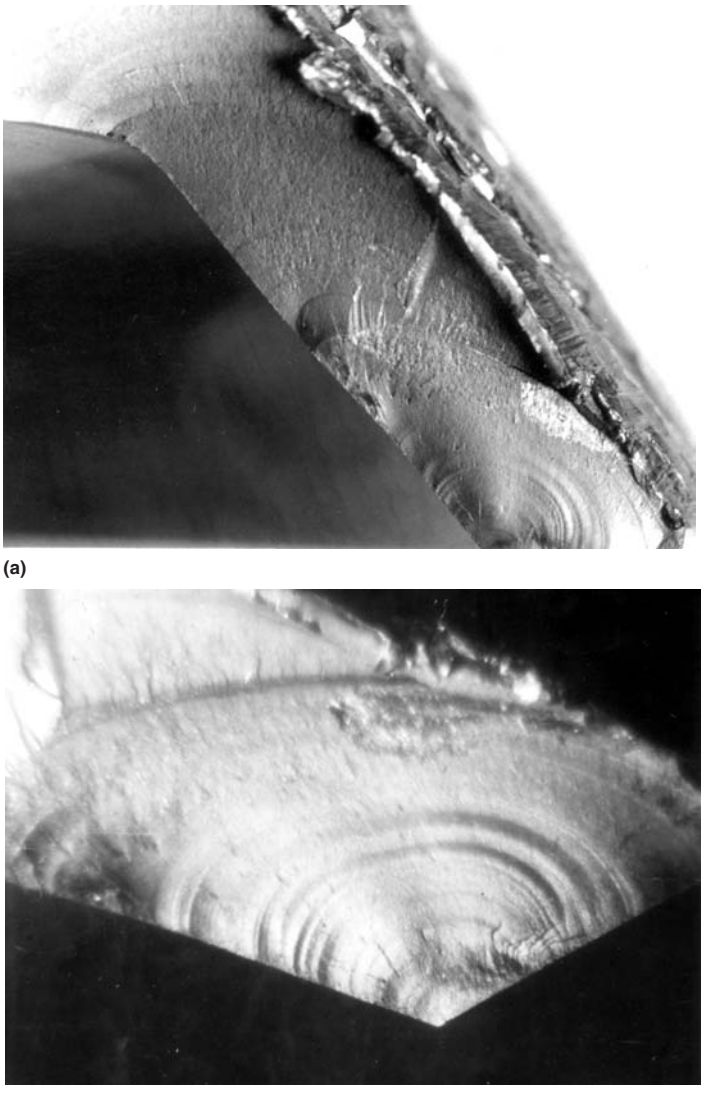

Fig. CH48.4 (a) and (b) mating fracture surfaces in the gear

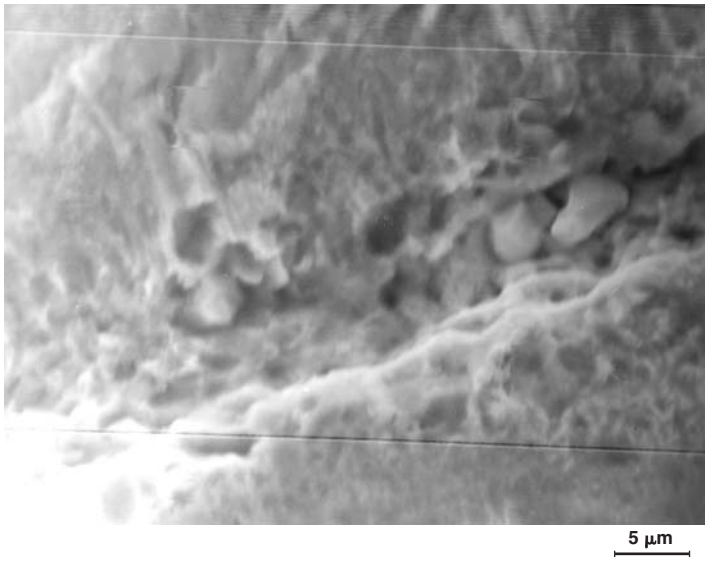

Fig. CH48.5 The region near the origin of fatigue crack. A stringer-like inclusion can be seen close to the origin.

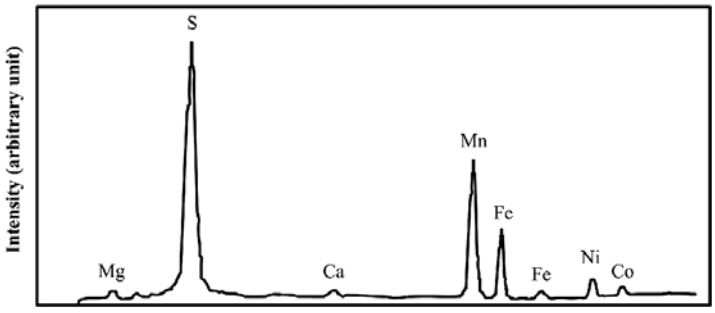

Fig. CH48.6 Energy-dispersive spectrum showing the presence of MnS inclusion

Failure Analysis of Engineering Structures: Methodology and Case Histories
V. Ramachandran, A.C. Raghuram, R.V. Krishnan, S.K. Bhaumik, p180-181
DOI:10.1361/faes2005p180

CASE 49

Failure of a Nose Undercarriage Retraction Jack Support Beam

Summary

An aircraft had an incident when the nose landing gear got retracted on landing roll. Two studs of the nose undercarriage retraction jack support were found fractured. The studs had failed by fatigue. Because of the way they were mounted, they were vulnerable to fatigue crack initiation and propagation.

Background

During landing roll, the nose landing gear of an aircraft got retracted. It was found that two studs of the nose undercarriage retraction jack support beam had fractured. The studs were in use for about 5955 landings, and their expected full life was 7000 landings.

Testing Procedure and Results

Fractography

The support beam was sectioned in order to remove one of the broken studs. The stud was thoroughly cleaned and examined in a stereobinocular microscope and a SEM. The threads were found to be intact. There was no evidence of outward pulling of the threads. Beach marks, characterizing the fatigue zone, were found on the fracture surface (Fig. CH49.1), the crack initiating at a thread root and extending to about 20% of the cross section.

Under the SEM, fatigue striations were seen in the region of beach marks (Fig. CH49.2). The rest of the fracture surface showed dimples (Fig. CH49.3).

Fig. CH49.1 Fracture surface of the failed stud showing the fatigue zone

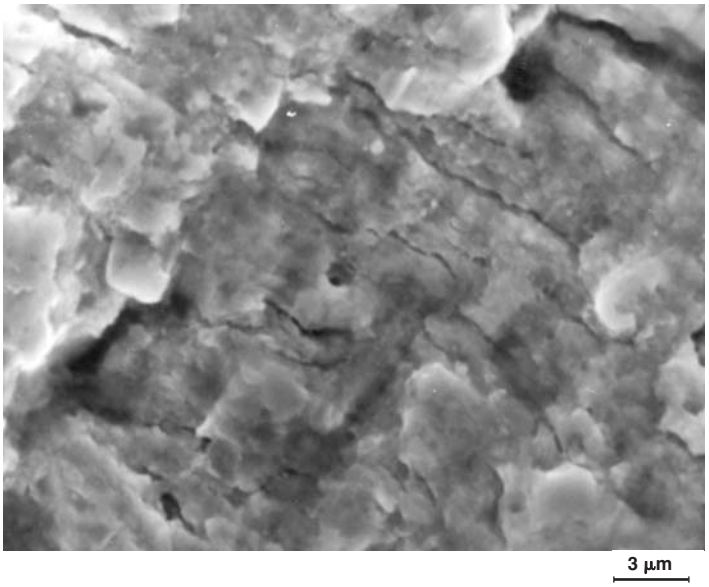

Fig. CH49.2 Striations in the fatigue region

Discussion

The studs failed due to fatigue crack initiation and progression during each loading cycle. It was noticed that in the jack support beam, the two holes where the studs were fixed had no threads machined for an initial depth equal to about three threads. The leading thread in the stud was thus well inside and not at the shear region (Fig. CH49.4). With this kind of free, unrestricted length of the stud, every time the load is applied, a fluctuating bending load on the leading thread of the stud results. Thus, fatigue crack initiates and propagates on every landing cycle. This is an incorrect design.

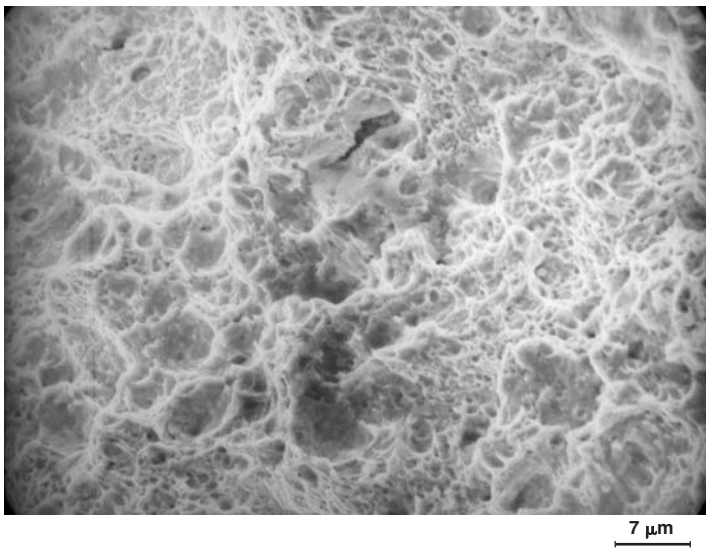

Fig. CH49.3 Final fracture region showing dimpled rupture

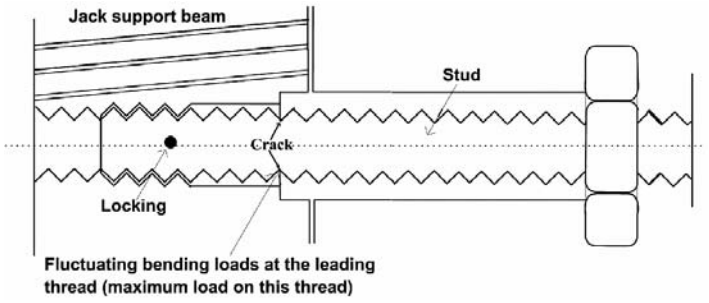

Fig. CH49.4 Sketch showing the location of leading thread in the stud

Conclusion

A correct engineering design for such studs subjected to shear and tensile loads is shown in Fig. CH49.5. The studs failed due to fatigue. The way the studs were mounted, they were vulnerable to fatigue crack initiation and propagation. Failure of the studs led to the retraction of the landing gear on landing roll.

Recommendation

Check all similar studs in the same vintage aircraft. Modify the stud design as suggested.

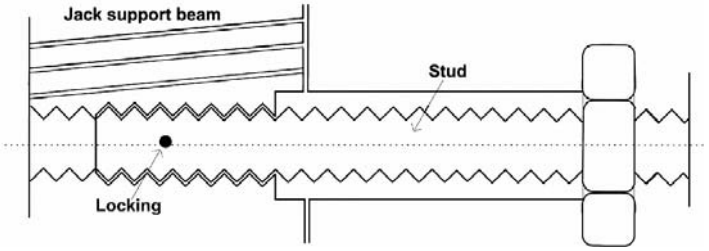

Fig. CH49.5 Sketch showing correct engineering design

Failure Analysis of Engineering Structures: Methodology and Case Histories
V. Ramachandran, A.C. Raghuram, R.V. Krishnan, S.K. Bhaumik, p182-184
DOI:10.1361/faes2005p182

CASE 50

Failure of a Rotor Blade in a Turbine in a Fertilizer Plant

Summary

On experiencing heavy vibration in a turbine unit of a fertilizer plant, it was found that one of the blades of the first stage of rotor had fractured. The blade had fractured at the tenon due to high hardness of the base material. Fracture of the tenon led to vibration of the blade and its failure by fatigue.

Background

In the turbine unit of a fertilizer plant, heavy vibration was experienced. On strip examination, one of the blades of the first stage rotor was found fractured. After site examination, the remaining part of the fractured blade, two blades on either side of the fractured blade, and two diametrically opposite blades were collected for further laboratory examination. These parts are shown in Fig. CH50.1, along with a sketch indicating their location.

Visual Examination of General Physical Features

The damaged rotor is shown in Fig. CH50.2. The blade had fractured at the outer pin location. About nine blades following the fractured blade had suffered severe buckling. The shroud was found missing on three blades (Fig. CH50.3). It was reported that a small quantity of severely deformed material presumably belonging to the shroud plate was recovered during stripping.

Testing Procedure and Results

Metallography

Metallography was carried out on the root portion of the fractured blade. The microstructure was tempered martensite (Fig. CH50.4), typical for this type of material. No abnormalities were noticed.

Hardness

A hardness survey was carried out on blades D, E, and F and the values were as follows:

Blade No.	Location	Hardness, HRC	Location	Hardness, HRC
D	Blade surface	27.8	Tenon	34.4
E	Blade surface	27.8	Tenon	37.7
F	Blade surface	27.1	Tenon	34.4

The hardness value for the base material was 28 HRC, and at the tenon head, 34 to 38 HRC.

Macrofractography

A close-up view of the fracture surface of the blade is shown in Fig. CH50.5. The fracture shows macroevidence of fatigue.

The blade G was sectioned in the tenon region to observe the material flow during the peening operation. There is a gap between the shroud hole and the tenon (Fig. CH50.6).

Discussion

The hardness of the base material is high. According to the manufacturer's report, it is desirable to have a hardness around 22 HRC for the base material. The high hardness of the blade will prevent proper forming of the tenon. This is further increased during the peening operation. As seen in Fig. CH50.6, in the case of blade G, a gap between the tenon and the shroud plate could have also existed in the failed blade. Ideally, the curvature at the root of the tenon should match the curvature of the hole in the shroud plate. During service, the blade might have fractured the tenon. This causes the blade to vibrate and fail by fatigue at the outer pin. The fatigue at the outer pin location could not occur if the tenon were intact. The other damages were subsequent to these events.

Conclusion

The tenon failure could be due to the high hardness of the base material, which was further increased by peening. The fracture of the tenon led to vibration of the blade, which failed at the outer hole by fatigue.

Recommendations

The base material should have a hardness of 22 HRC as specified. At the tenon root, the curvatures of the shroud plate hole and the tenon should match.

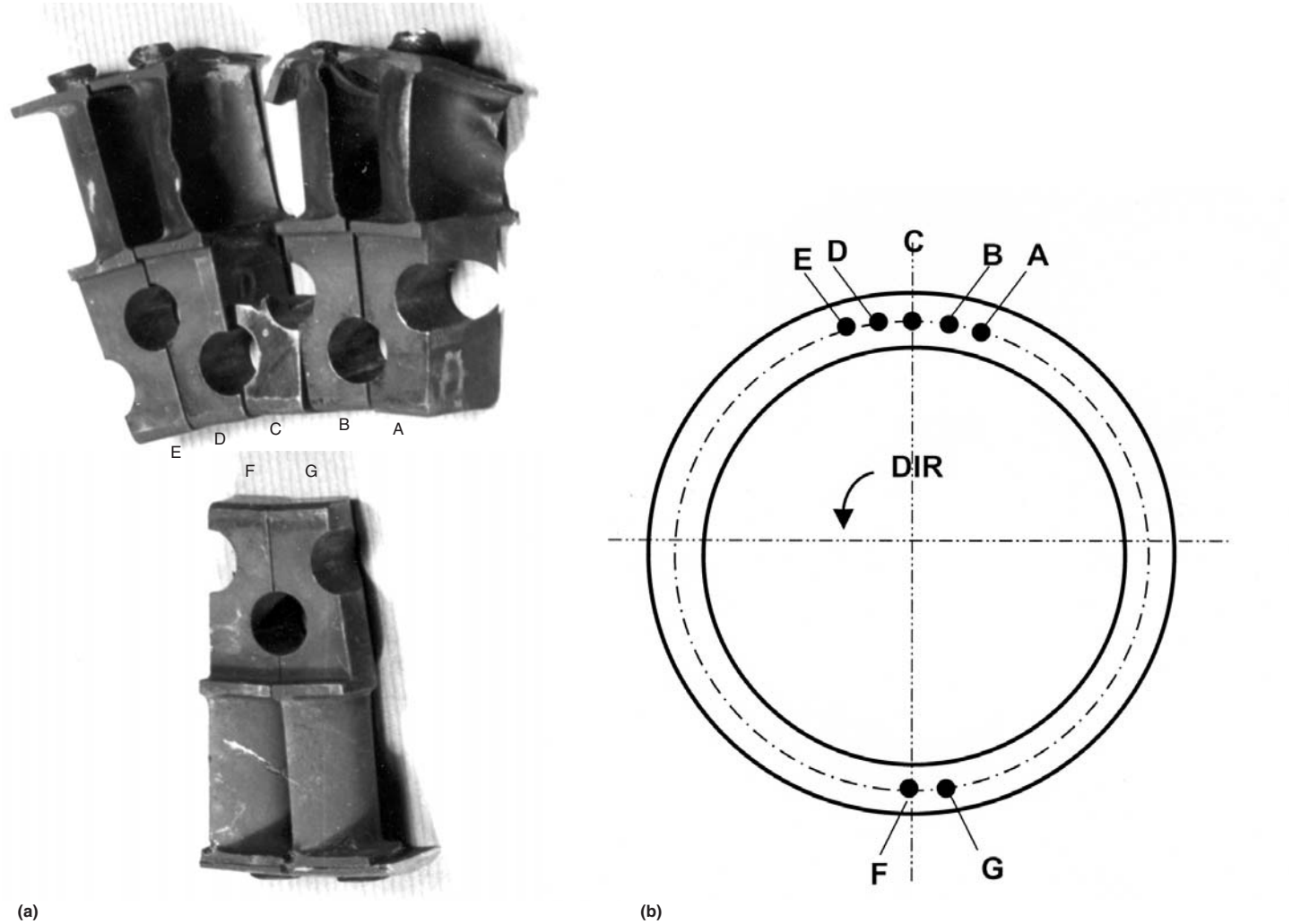

Fig. CH50.1 (a) Root portion of the failed blade, C; neighboring blades, A, B, D, E; blades diametrically opposite, F, G. (b) Sketch showing the location of blades

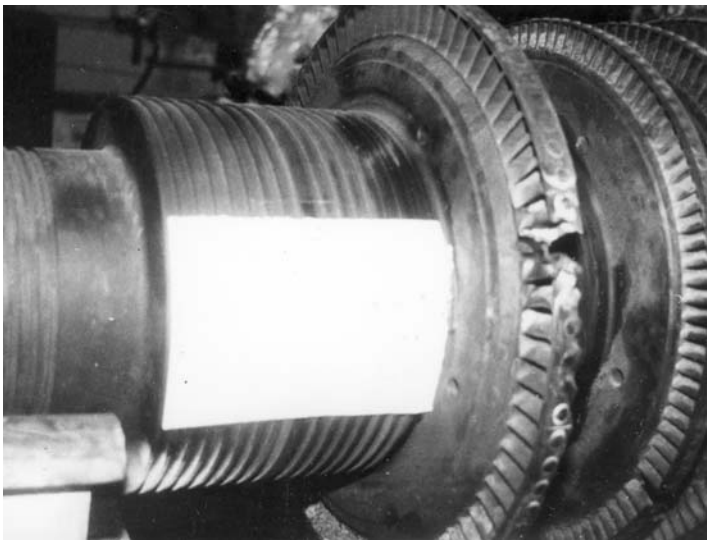

Fig. CH50.2 Damaged rotor C

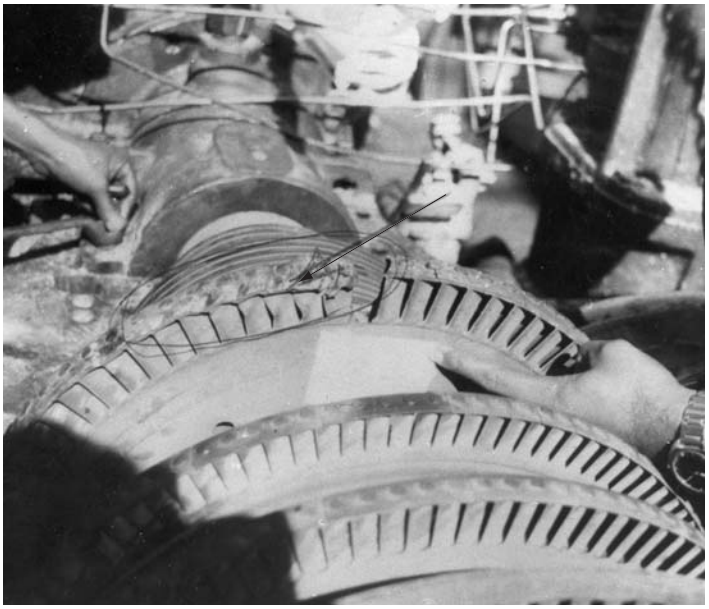

Fig. CH50.3 Close-up view of the damage to the first-stage disc

Fig. CH50.4 Microstructure from the root of blade C showing tempered martensite

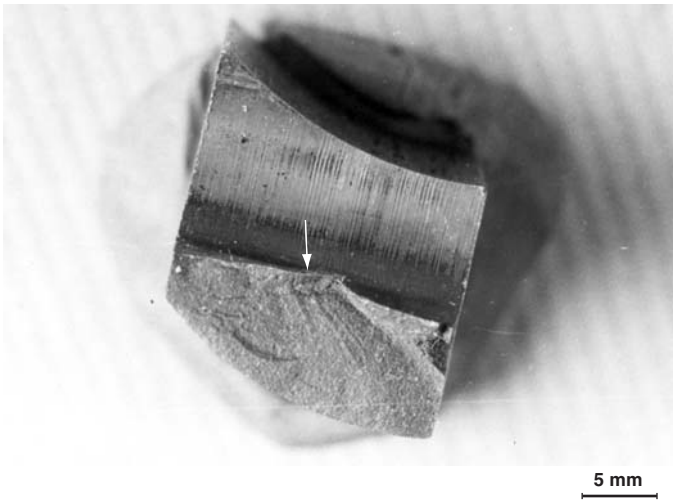

Fig. CH50.5 Fracture surface in the failed blade C. Arrow indicates the crack initiation site.

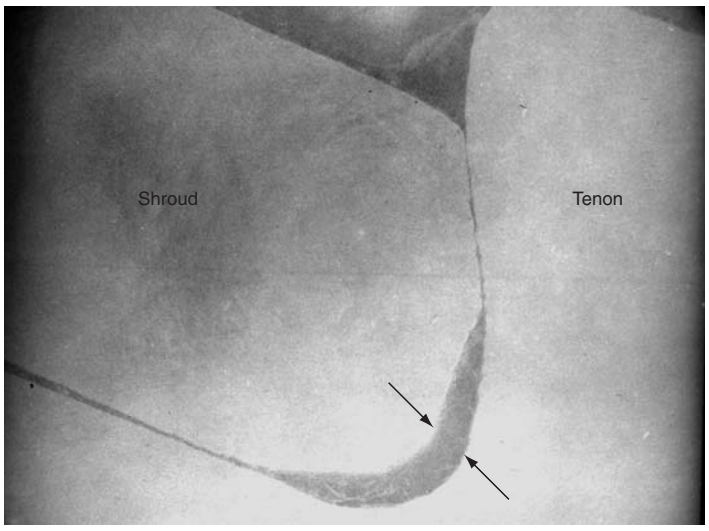

Fig. CH50.6 A section view of blade G at the tenon end showing the gap between the tenon and shroud plate

Failure Analysis of Engineering Structures: Methodology and Case Histories
V. Ramachandran, A.C. Raghuram, R.V. Krishnan, S.K. Bhaumik, p185-188
DOI:10.1361/faes2005p185

CASE 51

Failure of Connecting Rod Bolts in a Ground-Based Engine

Summary

In a prototype land-based engine, a pair of bolts of one of the connecting rods failed during a test run. The bolts were made of En 24 steel. They failed by excessive tensile overload. They were then replaced by bolts made of maraging steel, which also failed during test run, one of them by fatigue and the other by tensile overload. The bolts were experiencing loads in excess of the design loads. The design of the connecting rod system needs to be reviewed.

Background

During a test run of a prototype engine, two bolts of one of the connecting rods failed. The bolts were made of En 24 steel in the W condition. Subsequently, the material of the bolts was changed to maraging steel MDN 250. They were hardened to about 48–50 HRC and fitted in a single-cylinder engine, which was run at 2600 rpm, to study the effect of inertial load on all components. These bolts failed after about 1.5 hours of test run.

Visual Examination of General Physical Features

The failed En 24 steel bolts are shown in Fig. CH51.1. Pieces marked 1 and 2 are from one bolt and those marked 3 and 4 are from the other. The fracture surfaces of pieces 1 and 4 are shown in Fig. CH51.2. General observations indicated the bolts had experienced excessive tensile loads coupled with bending.

The failed maraging steel bolts marked M-1 and M-2 are shown in Fig. CH51.3 and their fracture surfaces in Fig. CH51.4. In bolt M-1, beach marks are seen, suggesting failure by fatigue. In bolt M-2, the fracture surface is rough and indicative of tensile overload failure.

Testing Procedure and Results

Scanning Electron Fractography

The SEM fractographs of pieces 1 and 4 of the En 24 steel bolts are shown in Fig. CH51.5. They show well-defined dimples characteristic of failure by tensile overload. There was no evidence of any delayed failure.

In bolt M-1, in the region showing beach marks, distinct striations were revealed in the SEM (Fig. CH51.6a), confirming failure by fatigue. The fatigue crack had propagated to approximately one-third of the cross section. Final failure of the bolt had occurred by tensile overload as shown by the dimples in the fractograph Fig. CH51.6b. The core of the bolt M-2 shows equiaxed dimples, and the edge shows elongated dimples (Fig. CH51.7a, b). From the SEM fractographs, it is clear that bolts 1, 2, and M-2 failed by tensile overload. Change of the bolt material has not helped to solve the problem. Whereas the bolts made of En 24 steel failed predominantly in tension, one of the bolts made of maraging steel failed under fatigue/tensile loads. This indicated the bolts had experienced loads far in excess of the design loads.

Conclusion

The bolts failed predominantly by tensile overload.

Recommendation

There is a need to reassess the design of the connecting rod system.

Fig. CH51.1 Failed En 24 steel bolts

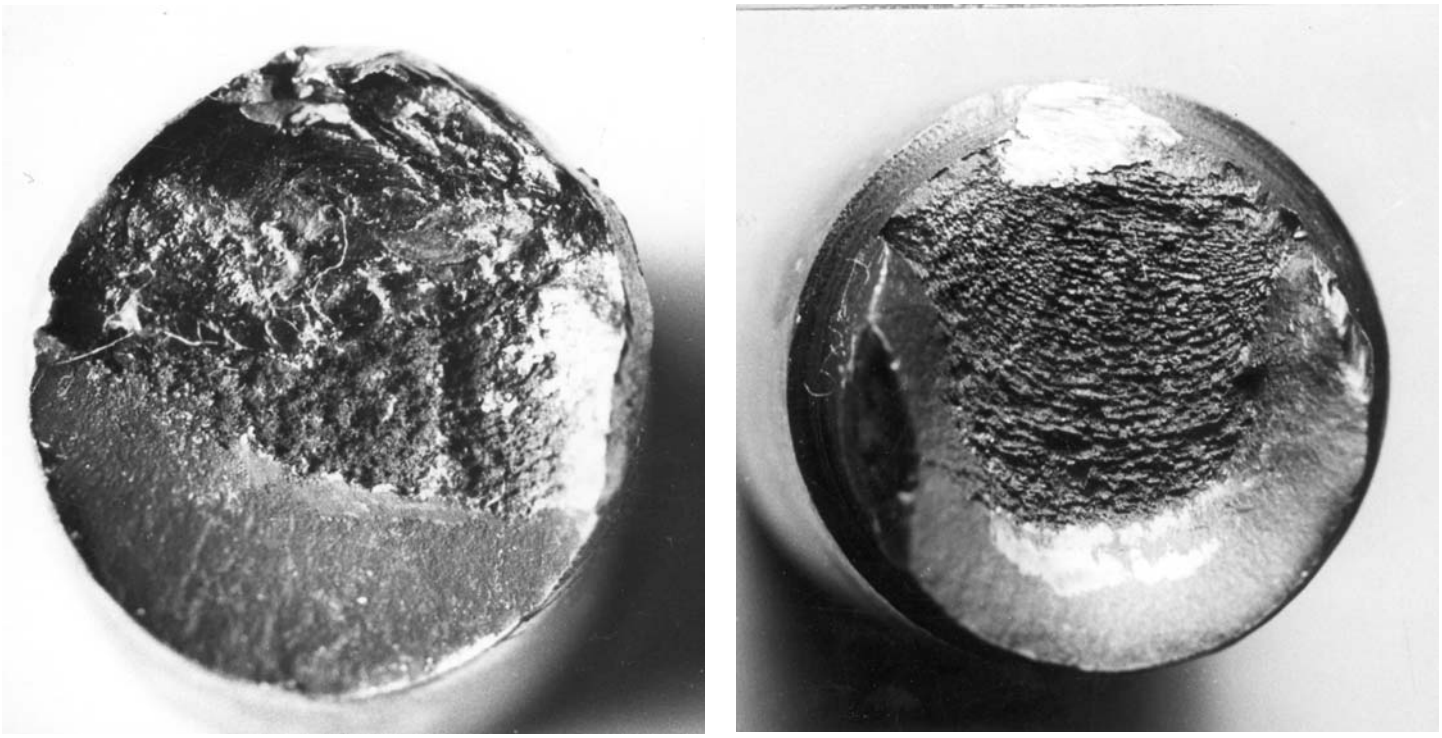

(a) (b)

Fig. CH51.2 (a) Fracture surface of bolt piece 1. (b) Fracture surface of bolt piece 4

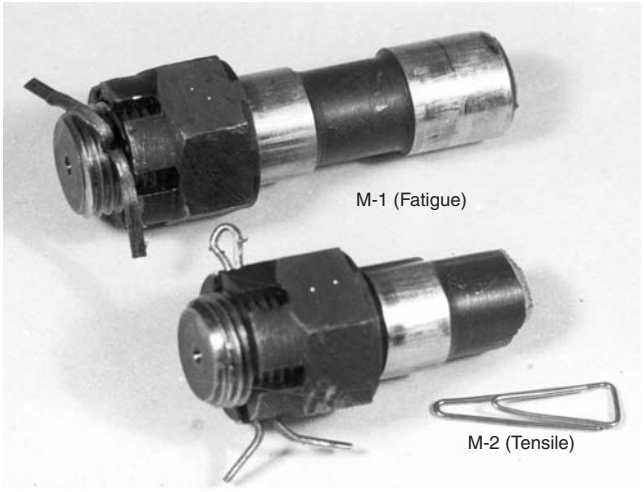

Fig. CH51.3 Failed maraging steel bolts

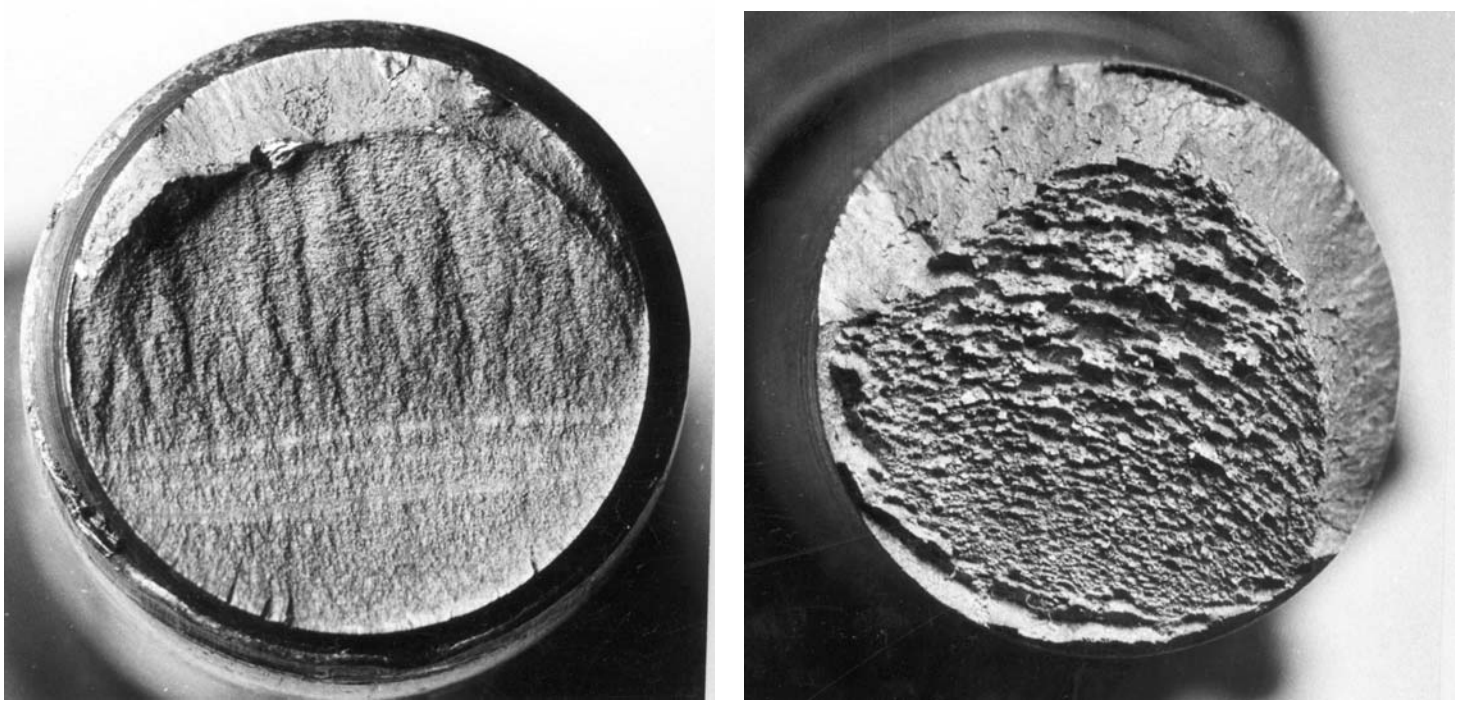

(a) (b)

Fig. CH51.4 (a) Fracture surface of bolt M-1. (b) Fracture surface of bolt M-2

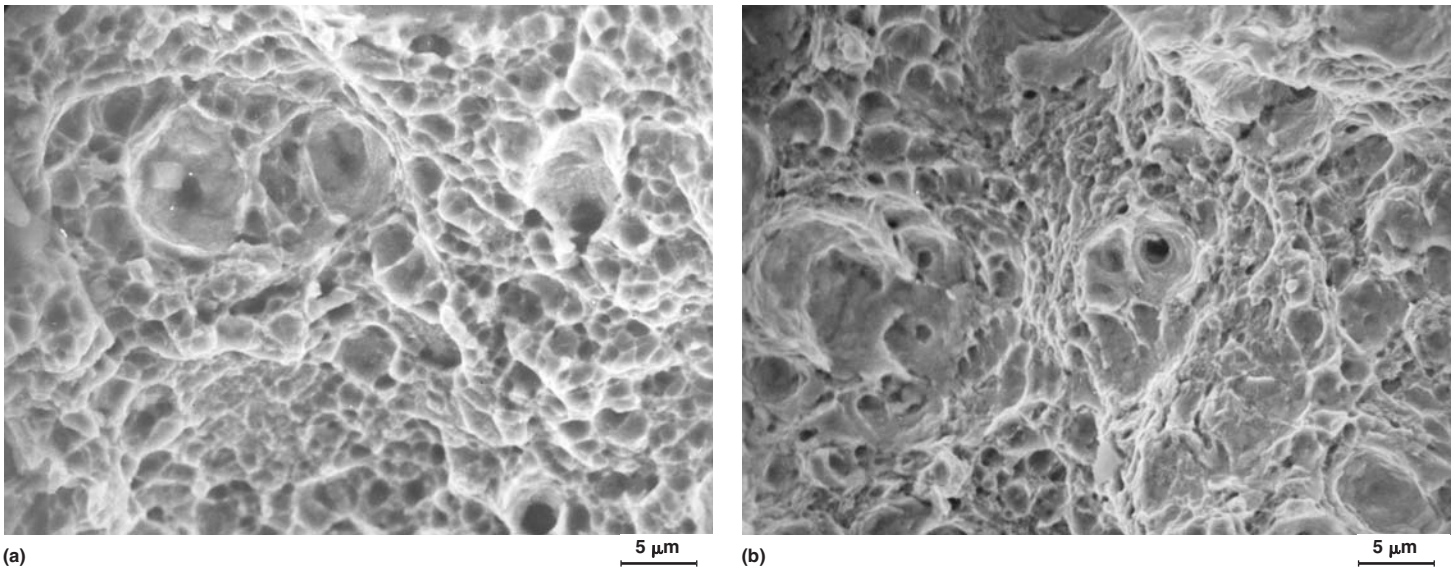

(a) (b)

Fig. CH51.5 SEM fractographs of the bolts shown in Fig. CH51.2. (a) Piece 1. (b) Piece 4

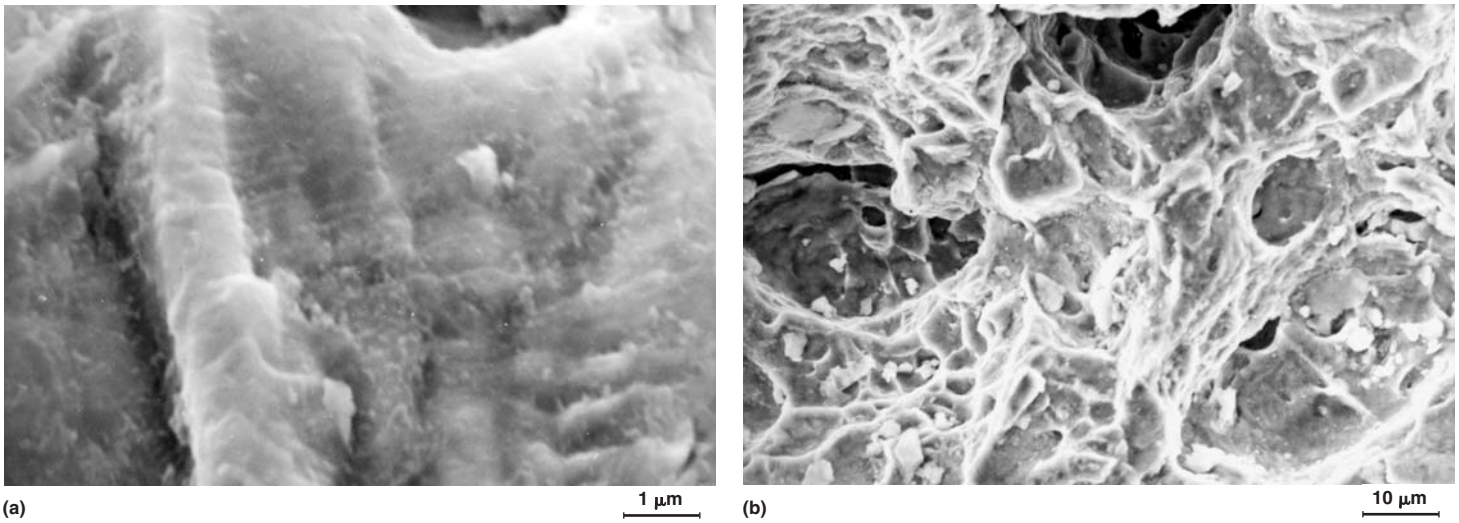

Fig. CH51.6 (a) SEM fractograph of bolt M-1 showing fatigue striations. (b) SEM fractograph of bolt M-1 showing dimples in the fast-fracture region

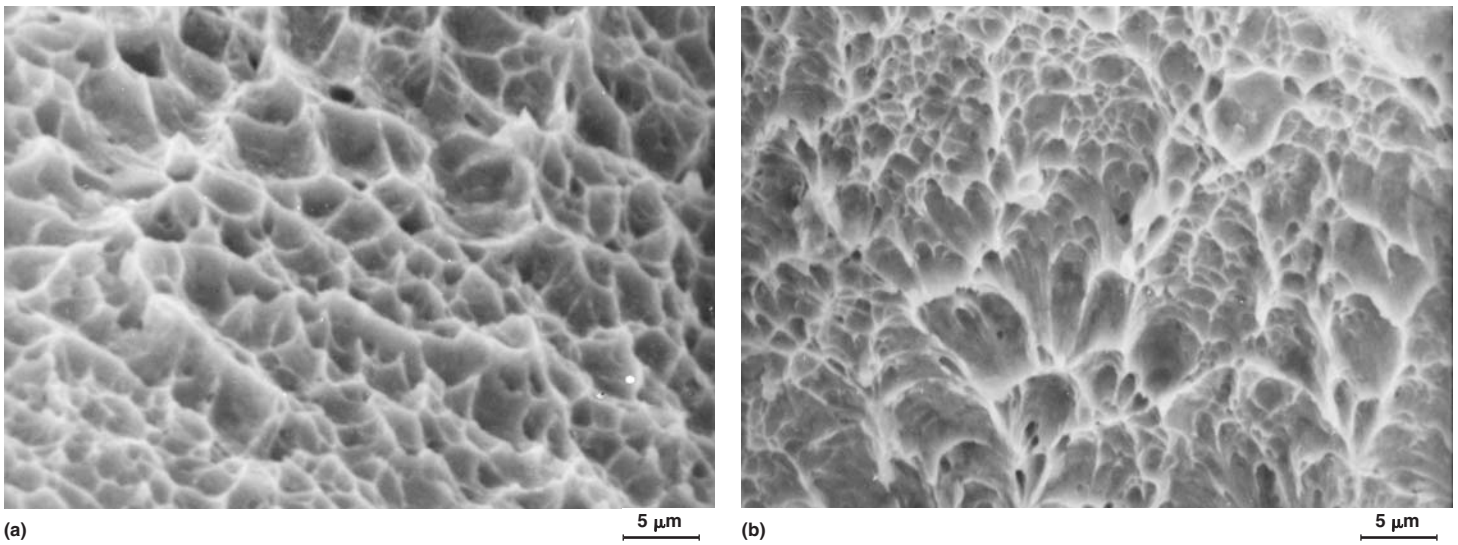

Fig. CH51.7 (a) SEM fractograph of bolt M-2 showing equiaxed dimples at the core. (b) SEM fractograph of bolt showing elongated dimples close to the edge

Failure Analysis of Engineering Structures: Methodology and Case Histories
V. Ramachandran, A.C. Raghuram, R.V. Krishnan, S.K. Bhaumik, p189-190
DOI:10.1361/faes2005p189

CASE 52

Failure of a Turbine Vane in a Hydroelectric Power Plant

Summary

The runner of a hydroelectric turbine failed by breakage of one of the vanes. The crack originated at a corner near the boss and fractured the cantilever portion of the vane. The diametrically opposite vane had developed a very similar crack. From the gross features, it was concluded that the vane failed due to a fatigue crack, initiated at a highly stress-concentrated region.

Background

In a 9 MW unit of a hydroelectric power plant, the runner of a 12,500 BHP turbine failed by way of breakage of one of the vanes. The failure occurred when abnormal sounds were heard from the unit. After shutting off the unit and strip examination, it was found that one of the vanes of the runner had broken. The broken piece was recovered from the tail race.

Visual Examination of General Physical Features

The runner had six adjustable vanes, fixed on the hub through a boss. In the broken vane, the crack initiated at a corner near the boss and fractured the cantilever portion of the vane (Fig. CH52.1). This fracture surface showed clear beach marks, indicative of delayed failure. Further, it was observed on the same runner, the vane diametrically opposite the fractured vane had developed a similar crack, about 3 in. in length, which was repair welded during the previous inspection. From the records of the manufacturer, it was discovered that the vanes had been cast into their shapes.

Fig. CH52.1 Failed runner showing the broken vane. Arrow indicates the origin of fatigue.

Testing Procedure and Results

Chemical Analysis

Semiquantitative analysis of the vane material indicated that it corresponded to a high-chromium steel of Swiss specification SIS 14-2303, equivalent to En 56C.

Fractography

Fracture surface examination indicated presence of two regions: an initial fracture region with well-defined beach marks typical of fatigue, which had progressed to about one-third of the vane width; and a final fracture region with tensile overload features (Fig. CH52.2). Examination of replicas of the fracture surface in the SEM did not show fatigue striations.

Fig. CH52.2 Fracture surface showing the fatigue and rapid-fracture zones

Discussion

From the gross observations of the beach markings, initiation of the crack at a highly stress-concentrated region, and a similar crack on a vane diametrically opposite this vane, it can be concluded that the vane failed due to a fatigue crack. Clear fatigue striations were not seen in this case probably due to two reasons: fatigue striations are not well defined in the case of high-strength materials, and long delay periods under hostile environments might have obliterated them.

Conclusion

The vane failed in fatigue after long service.

Failure Analysis of Engineering Structures: Methodology and Case Histories
V. Ramachandran, A.C. Raghuram, R.V. Krishnan, S.K. Bhaumik, p191-195
DOI:10.1361/faes2005p191

CASE 53

Failure of Compressor Blades in a Power Plant

Summary

A gas turbine unit tripped following the failure of the turbine rotor. The damage was maximum in the 18th/19th-stage seal land region of the compressor, with the 19th-stage blades sheared off. Metallurgical investigations were carried out on the roots and airfoil sections of the damaged blades. The blade roots had suffered excessive overheating due to heavy rubbing between the 18th-stage stator and the 19th-stage rotor blades and disc during the early stages of starting and final stages of stopping. This led to the subsequent damages to the turbine before final damage. The failure was attributed to inadequate clearances in the 18th–19th-stage seal land region.

Background

In a combined-cycle power plant, during the initial stages of operation, the main rotor developed problems. The compressor part of the rotor had 19 stages and the turbine portion had four stages. The major damage was confined to the area between the 18th and 19th stages. Farther down on the rotor, the damage was minimal.

Visual Examination of General Physical Features

On strip examination of the engine, it was found that all the 19th-stage compressor blades had been sheared off at the root. The first 17 stages of the compressor rotor blades and discs were intact with no external damage. However, the 14th-stage rotor blades had suffered slight tip rubbing, without affecting the blade geometry, and one 17th-stage blade tip was slightly damaged. There was slight rubbing on the 18th-stage compressor disc on the 17th-stage side.

The trailing edges of all the 18th-stage blades had suffered mechanical damage. The gap between the 18th- and 19th-stage discs showed excessive metal burning and melting at the seal land and the gap, which should normally be in the range 6 to 8 mm.

The gap had increased to about 30 mm, with deposits of burnt/molten metal. Farther down on the first-stage turbine blades, some deposits of molten metal were found, similar to those between the 18th and 19th stages.

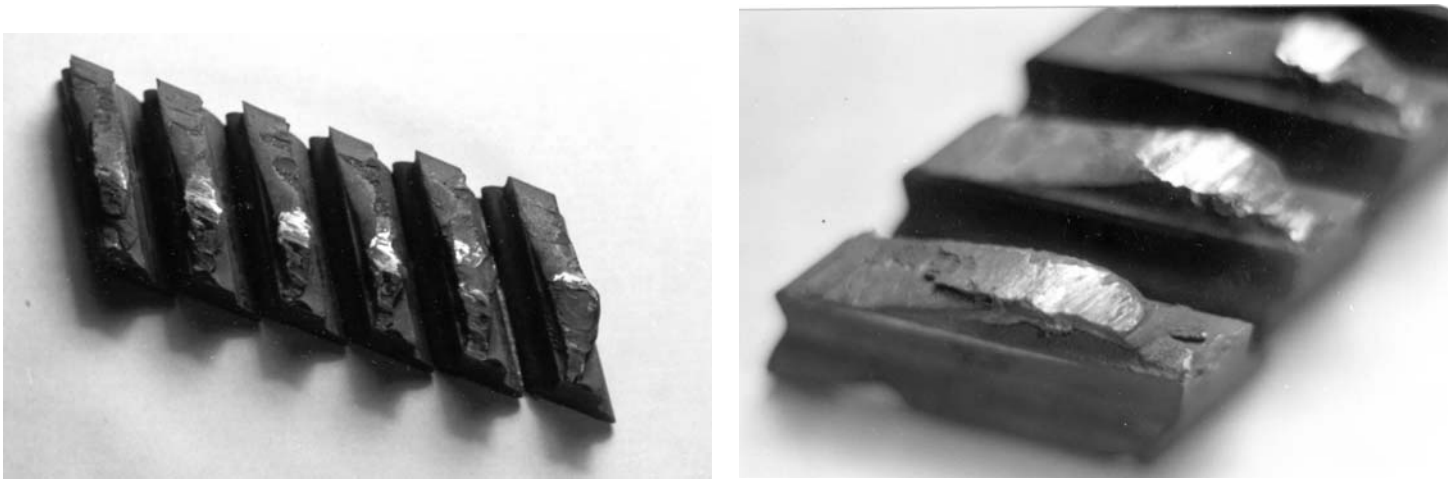

(a) (b)

Fig. CH53.1 (a) Fractured blade roots. (b) Close-up view of a few fractured blade roots

Testing Procedure and Results

Metallurgical investigations were carried out on six fractured blade roots and six fractured airfoil sections from the 19th-stage compressor rotor (Fig. CH53.1, CH53.2). The blades were found to conform to 12% Cr steel by semiquantitative analysis carried out in a SEM. The fracture surfaces were too obliterated to reveal any fractographic features.

Metallography and Hardness

Two blades were mounted on their cross sections at the root, polished, etched in picric acid, and examined in an optical microscope. The blades showed heat-affected zones (HAZs) at the inlet tip as shown by the difference in etching behavior. This zone had a width of about 10 mm and showed considerably higher hardness than the rest of the section. The HAZ showed undertempered or untempered martensite, compared with a region farther away, which showed well-tempered martensite. The hardness profiles and the corresponding microstructures of the blades are given in Fig. CH53.3, CH53.4.

Two of the airfoil regions were sectioned along the blade length and examined. The HAZ in these sections was much smaller com-

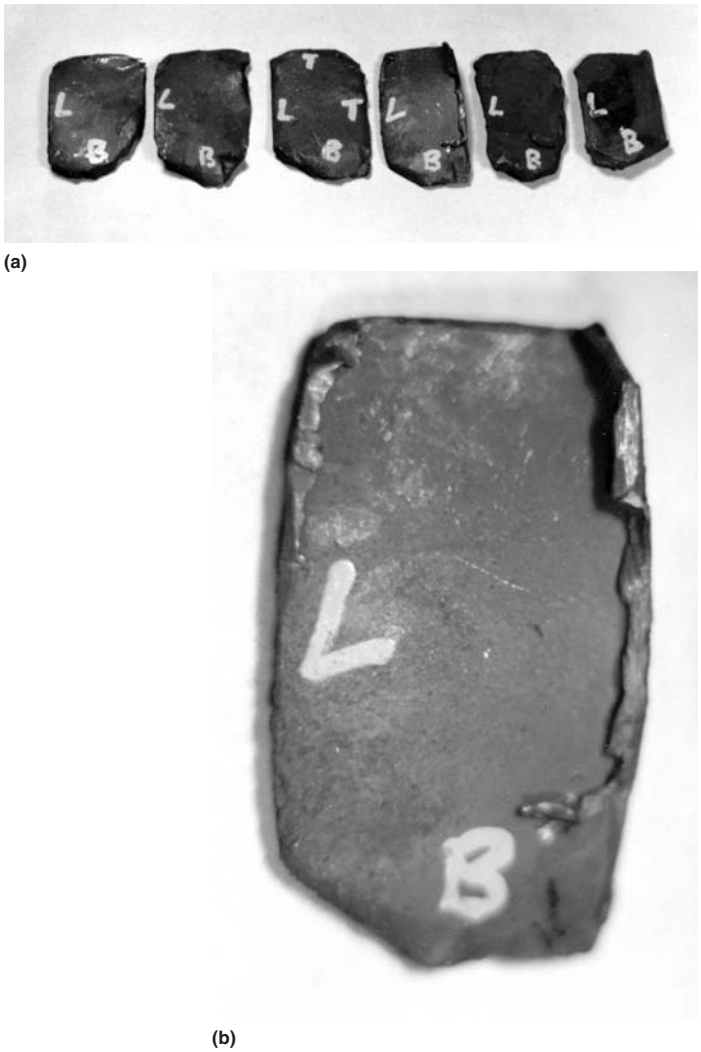

Fig. CH53.2 (a) Fractured airfoil sections. (b) Close-up view of one of the sections

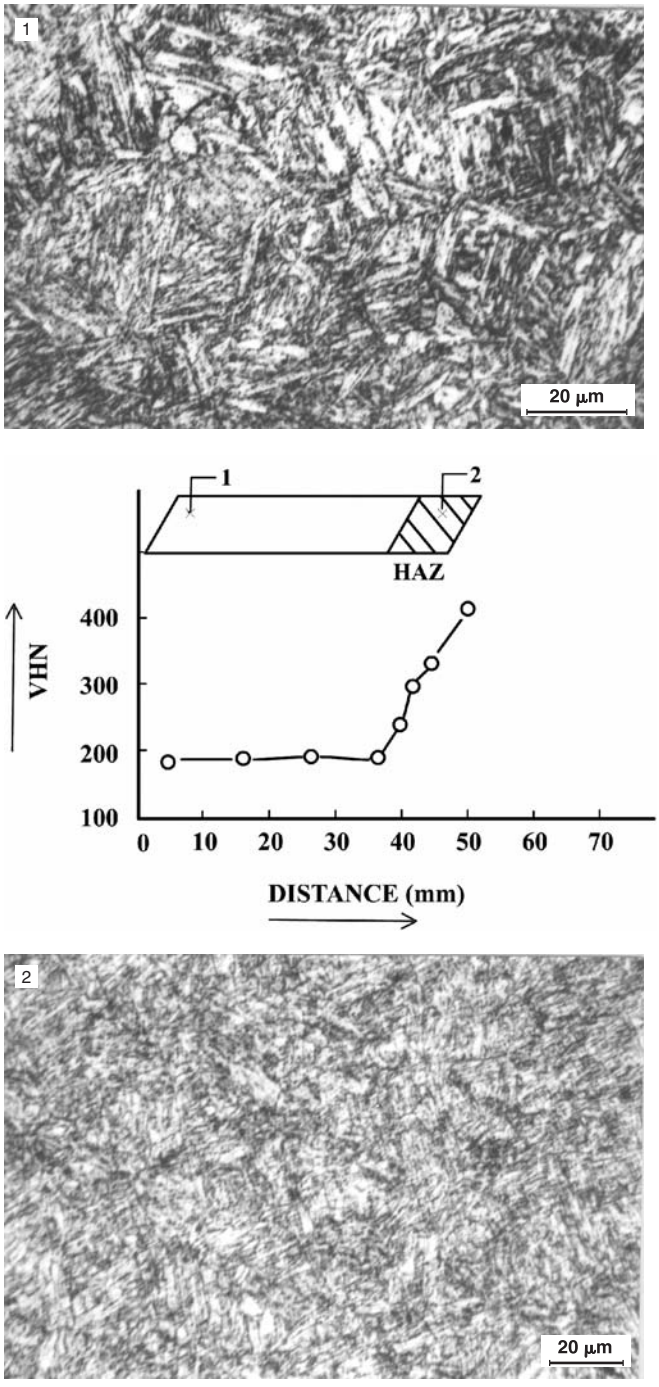

Fig. CH53.3 Hardness profile and microstructures across the transverse section at the root of a blade of 19th stage

pared with that at the root and was confined to less than 4 mm. The microstructure was similar, showing undertempered and untempered martensite in the HAZ and well-tempered martensite farther away. The hardness profiles and the microstructures are shown in Fig. CH53.5, CH53.6. Examination of the blades with differential etching and microhardness measurements in the suspected regions did not reveal any delta ferrite.

The blade material showed globular oxide-type inclusions and isolated elongated inclusions of the sulfide type. The inclusions were well within limits and conformed to ASTHMA D, Thin Series 2 for the oxides and ASTHMA A, Thin Series 1 for the sulfides.

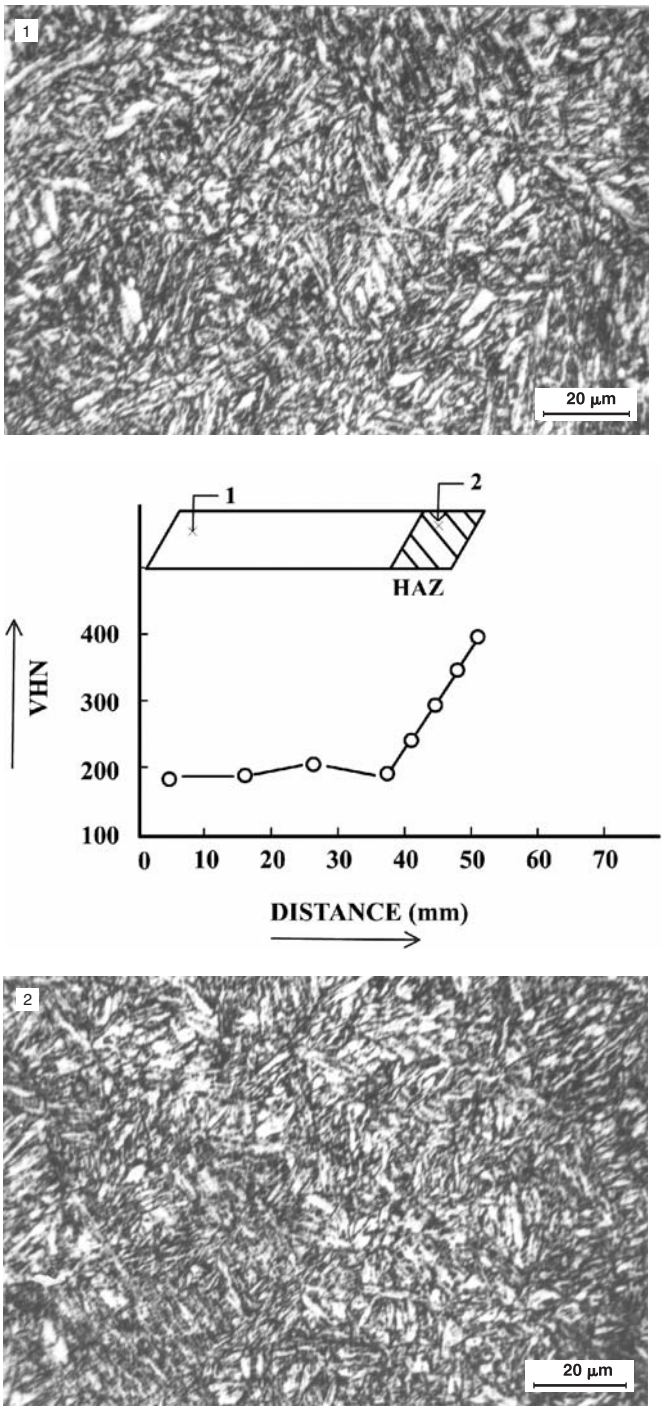

Fig. CH53.4 Hardness profile and microstructures across the transverse section at the root of another blade of 19th stage

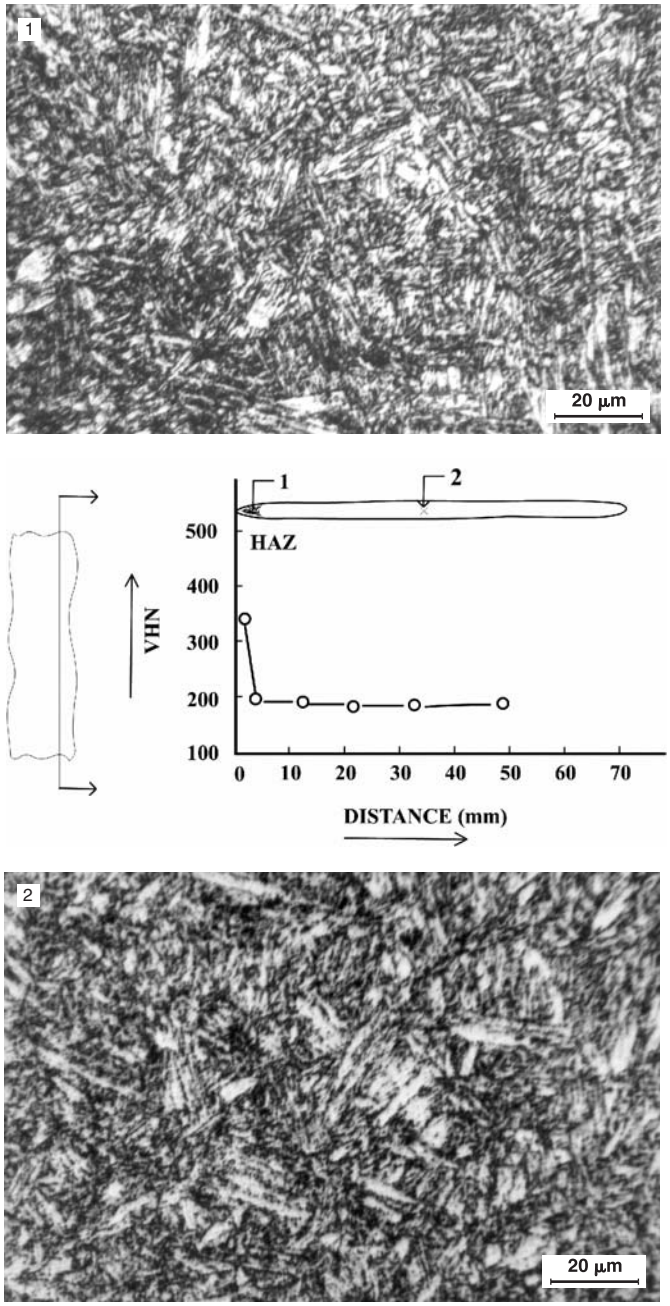

Fig. CH53.5 Hardness profile and microstructures along the longitudinal section of the airfoil region of a blade

Tensile Tests

Tensile tests were conducted on miniature tensile test specimens machined from the roots of the blades, with a gage length of 16 mm and diameter of 5 mm. Mechanical properties of the blade material are as follows:

Specimen No.	0.2% yield strength, kg/mm² (MPa)	Ultimate tensile strength, kg/mm² (MPa)	Elongation, %	Reduction in area, %
1	57.56 (563.8)	74.22 (727)	24.9	64.8
2	59.1 (578.9)	74.43 (729)	25.0	65.2

These values compare very well with the values reported in literature for this class of steels.

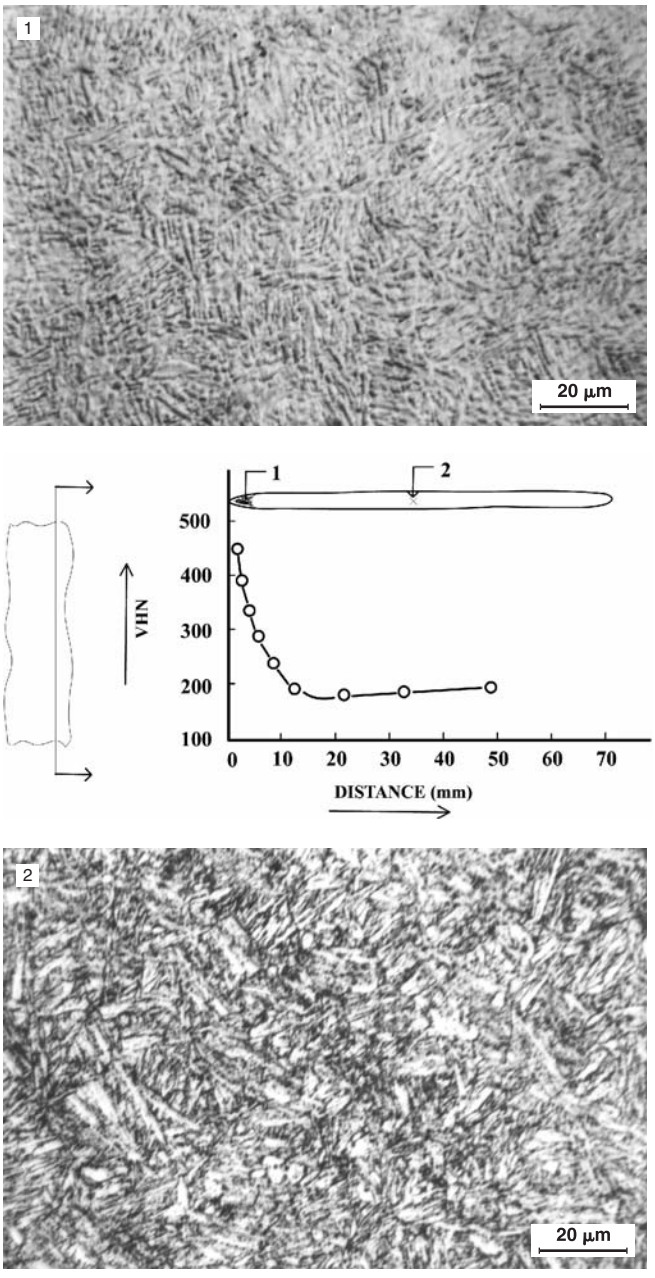

Fig. CH53.6 Hardness profile and microstructures along the longitudinal section of the airfoil region of a blade

Discussion

The blade roots had suffered excessive overheating due to rubbing on the inlet end, i.e., on the 18th-stage side. The cause for the seal land burning/melting could be that there was insufficient clearance between the 18th-stage stator seal box and the seal land below which is the rotating part. During operation, these two surfaces must have been rubbing and over a period of time, this rubbing must have caused sufficient damage, such that some pieces from this region became separated and caused the shearing off of the 19th-stage rotor blades and other damages downstream.

It is to be noted that the rotor is a heavy and long mass, supported at the two ends with bearings. Under stationary conditions, the deflection of the rotor would be maximum at the midspan of the shaft. In this rotor, the region of 18th/19th stage or near happens to be the midpoint, and that is where the clearances between the rotating and stator parts become critical, especially at the very early stages of starting and the final stage of stopping of the rotor.

The clearances data were checked on a new rotor. The minimum was at the 18th and 19th stages, and the minimum, 0.06 mm, was at the bottom side under stationary conditions. The minimum clearances were defined over the diameter and not over the radius. A near-zero clearance at one end and a larger clearance at the diametrically opposite end could still satisfy the requirement. This could lead to serious consequences during operation, as in the present case.

Another factor to consider are the large fluctuations in the ambient temperature during the year at the plant. The assembly was done during November and December and the clearances were checked then. Subsequently, in April and May, due to thermal expansion, the clearances can get reduced in the critical locations leading to rubbing during the starting and stopping of the engine.

The possible cause for the seal land burning and melting could be that the 18th-stage stator blade seal box fell and broke during normal operation and this, during rotation, could have rubbed on the seal land, creating excessive frictional heat and burning and melting at that portion. In this process, some of the 18th-stage stator blades must have hit the trailing edges of the 18th-stage rotor blades, causing damage upstream. The upstream side of the 18th-stage disc might have rubbed against the downstream side of the 17th-stage seal box.

The fracture of any parts from this region could have broken the blades of the 19th stage and caused further damages downstream.

Conclusion

The failure of the rotor could be attributed to inadequate clearances in the 18th/19th-stage seal land region, which resulted in heavy rubbing during the early stages of starting and final stage of stopping the engine. This resulted in subsequent damages to the turbine.

Recommendation

The specified clearances in this region should be redefined with respect to the radius and the actual clearances checked against these values and maintained.

Failure Analysis of Engineering Structures: Methodology and Case Histories
V. Ramachandran, A.C. Raghuram, R.V. Krishnan, S.K. Bhaumik, p196
DOI:10.1361/faes2005p196

CASE 54

Failure of Max Screws in Fuel-Injection Pumps

Summary

Max screws used in fuel-injection pumps failed during assembly. The fracture initiated at the thread roots. Fractography indicated brittle intergranular failure. The most probable cause of the failure was hydrogen embrittlement.

Background

Max screws failed during assembly in fuel-injection pumps. Their specified heat treatment was hardening and tempering to 33 to 39 HRC, to be followed by zinc plating, passivation, and tempering again at 180 °C (360 °F).

Visual Examination of General Physical Features

The fracture in the screws had initiated at thread roots and progressed inward. Secondary circumferential cracks at thread roots below the main fracture were observed in one of the screws. Gross fracture features were typical of brittle failure with limited ductility.

Testing Procedure and Results

Scanning Electron Fractography

Under the SEM, close to the thread root, intergranular fracture with partially formed dimples on the fracture facets was predominantly seen (Fig. CH54.1).

Hardness

The hardness of the material was measured and was found to correspond to an equivalent of 43 to 45 HRC.

Discussion

Intergranular fracture with partially formed dimples on the fracture facets is a characteristic of hydrogen embrittlement in steels. Embrittled steel components generally exhibit secondary cracking. High-strength steels of the type under investigation are susceptible to hydrogen embrittlement. Hydrogen enters the steel during pickling and subsequent plating. As per specification, the hardness of the screws should be 33 to 39 HRC, whereas the measured hardness was in the region of 43 to 45 HRC. This higher hardness increases the susceptibility of the steel to hydrogen embrittlement. It must be noted that some material requirements even specify allowable hardness values for use under hydrogen environments.

Conclusion

Hydrogen embrittlement seems to be the most probable cause of failure of the screws.

Recommendations

The screws should be baked immediately after plating according to ASTM specifications, i.e., 2 to 3 hours at 205 °C (400 °F). The steel should be heat treated to the lowest permissible hardness level.

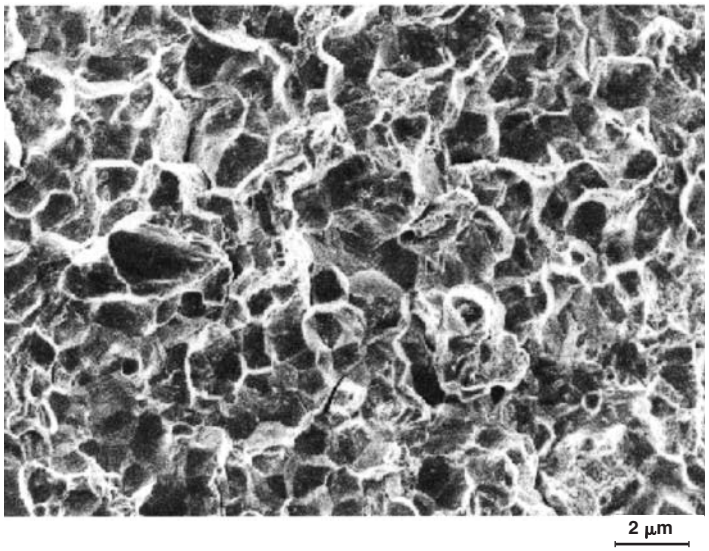

Fig. CH54.1 SEM fractograph of the failed screw showing intergranular fracture facets with partially formed dimples

Failure Analysis of Engineering Structures: Methodology and Case Histories
V. Ramachandran, A.C. Raghuram, R.V. Krishnan, S.K. Bhaumik, p197-198
DOI:10.1361/faes2005p197

CASE 55

Failure of a Sealed Ball Bearing

Summary

A grease-packed sealed ball bearing in an electric motor failed, causing severe vibration of the rotor. Excessive damage was seen on the inner ring raceway and on the surface of the balls, in the form of craters and bruises. There was evidence of melting and burning of metal. The failure was associated with electrical pitting due to static electric discharge, and detachment of metal particles leading to seizure of the bearing.

Background

The ball bearing in an electric motor failed after it had run for 552 hours after commissioning. The normal speed of the rotor was between 1500 and 2100 rpm. The failure was indicated by excessive vibration of the rotor.

Visual Examination of General Physical Features

Figure CH55.1 shows the failed bearing and Fig. CH55.2 shows the inner and outer ring raceways, the split bearing cage and the balls, after dismantling.

It was noticed that the grease was contaminated and turned black. After dissolving it in solvent and filtering, metallic slivers were recovered from the contaminated grease. The outer ring raceway was relatively intact with slight discoloration on its raceway. Extensive damage was seen on the inner ring raceway over a portion, in the form of wide craters and extensive bruising (Fig. CH55.3). The split bearing cage was intact. Some of the ball surfaces also showed the presence of small craters (Fig. CH55.4).

Fig. CH55.1 Failed bearing

Testing Procedure and Results

Scanning Electron Microscopy

Observation of the crater areas, both on the inner ring raceway and the bearing balls, in the SEM, showed loose spherical particles sticking to the craters (Fig. CH55.5). Figure CH55.6 shows detached metal particles having worked into the raceway due to continued operation of the bearing, producing excessive metal flow.

Energy-Dispersive X-ray Analysis

EDAX showed that the slivers recovered from the grease had the same composition (Fe-Cr-Ni alloy) as that of the bearing raceway material or the bearing ball material. The spherical particles sticking to the craters had the same composition as that of the parent metal.

Fig. CH55.2 The bearing in the dismantled condition showing the inner and outer ring raceways, the split cage, and the bearing balls

Discussion

The presence of burned craters on the inner ring raceway and the ball surfaces is typical of electrical arcing with local melting of the metal. Due to the heat of the arc, the metal melts and is pulled apart by the force of rotation of the balls and the inner raceway. This can lead to bruising of the raceway with continued operation. Electrical pitting is produced by the passage of current between two surfaces. In applications such as electric motor, there is a possibility of the current passing through the bearings. When the current is broken at the contact surfaces between raceways and rolling elements, arcing or sparking occurs, producing high temperatures and localized damage.

It is known that electrical discharges result from the use of an electrically nonconductive lubricant in the bearings, which permits a static charge to be accumulated and discharged. In this case, the lubricant grease used was tested by measuring the resistance across two copper plates with the grease as the separator, and it was found that the grease was a poor conductor of electricity.

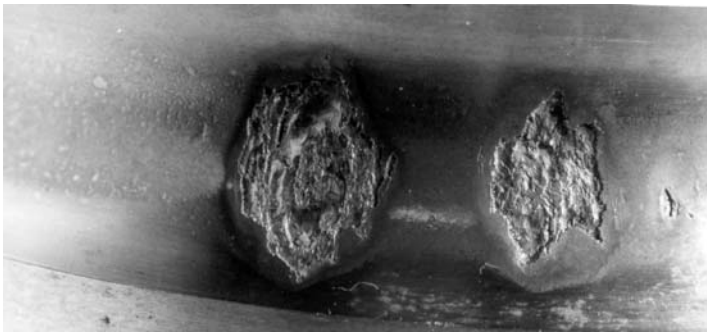

Fig. CH55.3 Craters and metal bruising seen on the inner ring raceway

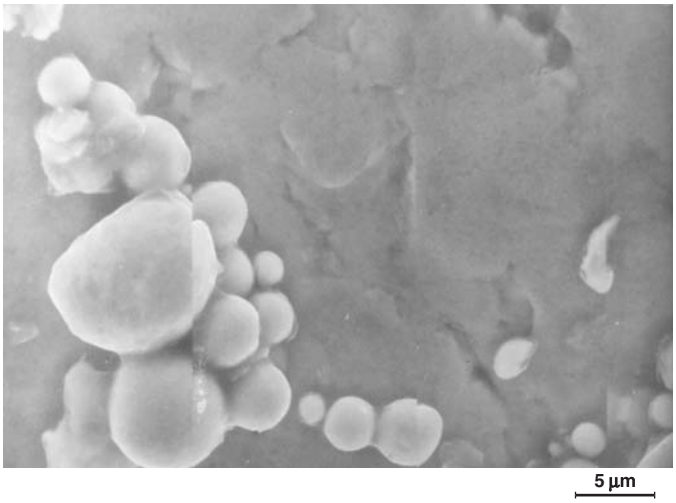

Fig. CH55.5 Spherical metal particles sticking to the craters

Conclusion

The bearing failed because of electrical pitting of the inner raceway and the ball bearing due to static discharge and consequent melting and detachment of metal particles. The detached metal particles would have caused further damage leading to seizure of the bearing. Use of a nonconductive lubricant is a probable cause for the electrical discharge.

Recommendation

Replacement of the lubricant by an electrically conductive grease would permit proper grounding of the rotor and eliminate welding between the balls and the raceways.

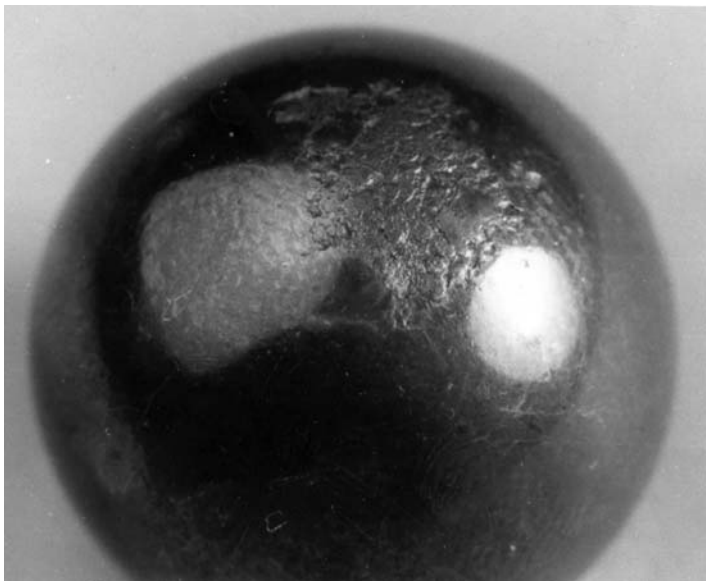

Fig. CH55.4 Craters seen on one of the bearing balls

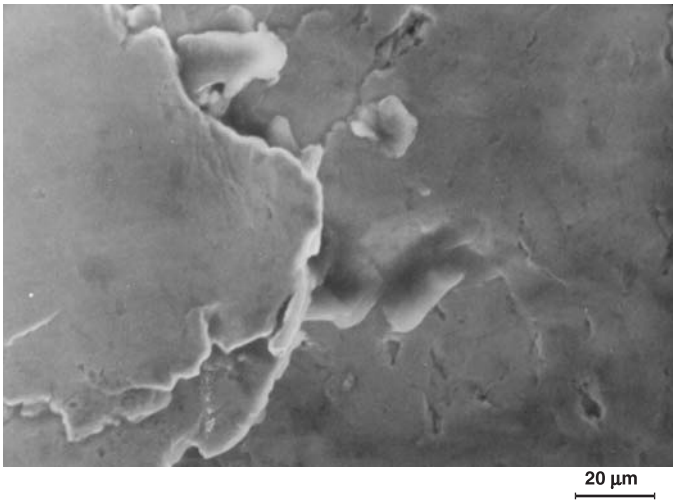

Fig. CH55.6 Detached metal particles having worked into the inner ring raceway

Index

C

G

H

T

U

V

W

X

ASM International is the society for materials engineers and scientists, a worldwide network dedicated to advancing industry, technology, and applications of metals and materials.

ASM International, Materials Park, Ohio, USA
www.asminternational.org

Publication title	Product code
Failure Analysis of Engineering Structures: Methodology and Case Histories	05127G

To order products from ASM International:

Online Visit www.asminternational.org/bookstore

Telephone 1-800-336-5152 (US) or 1-440-338-5151 (Outside US)

Fax 1-440-338-4634

Mail Customer Service, ASM International
9639 Kinsman Rd, Materials Park, Ohio 44073, USA

Email CustomerService@asminternational.org

In Europe American Technical Publishers Ltd.
27-29 Knowl Piece, Wilbury Way, Hitchin Hertfordshire SG4 0SX, United Kingdom
Telephone: 01462 437933 (account holders), 01462 431525 (credit card)
www.ameritech.co.uk

In Japan Neutrino Inc.
Takahashi Bldg., 44-3 Fuda 1-chome, Chofu-Shi, Tokyo 182 Japan
Telephone: 81 (0) 424 84 5550